Investigation of Operating Parameters Influencing Electrostatic Charge Generation in Gas-Solid Fluidized Beds

by

Amanda Giffin

Thesis submitted to the
Faculty of Graduate and Postdoctoral Studies
In partial fulfillment of the requirements
For the M.A.Sc. degree in Chemical Engineering

Department of Chemical and Biological Engineering
Faculty of Engineering
University of Ottawa

Abstract

Electrostatic charge generation in gas-solid fluidized beds is a significant industrial problem. Associated problems include particle agglomeration and particle wall fouling. In the polymerization industry this may result in “sheets” of fused polymer, due to exothermic reaction causing the melting of the polymer, which can fall off and block the distributor plate disrupting fluidizing gas flow. Additionally, blockage of the catalyst feed or the polymer removal system can take place or the product can become non-uniform. All of these problems require shut-down of the reactor which results in lost production time. While this phenomena has been identified for many years, the mechanisms involved are not well understood, especially wall fouling and the distribution of charge within the bed. Isolation of individual parameters such as hydrodynamics, operating conditions, and material involved is necessary to evaluate how each parameter impacts charge generation during fluidization.

In this thesis, the fluidization system consisted of a stainless steel column, two online Faraday cups, and a retractable distributor plate. This system allowed for the simultaneous measurement of charge within different regions of the bed: the entrained fine particles, the particles adhered to the column wall, and the bulk of the bed. Additionally, mass and particle size distributions were measured and images of the layer of particles adhered to the column wall were taken for comparison. This allowed for a charge distribution comparison and evaluation of wall fouling.

Three different parameters were investigated: duration of fluidization, column wall material, and relative humidity of fluidizing gas. Fluidization time was studied for 15, 30, 60, 120, 180, and 360 min; relative humidity was investigated for 0%, 20%, 40%, 60%, and 80% relative humidity. Both fluidization time and relative humidity were evaluated at four different fluidization gas velocities, two each in the bubbling and slugging flow regimes. Column wall material was evaluated for a stainless steel and carbon steel column at two gas velocities, one each in the bubbling and slugging flow regimes.

Fluidization time was found to influence wall fouling in the bubbling flow regime as the particle layer continued to build as fluidization progressed. In the slugging flow regime, the particle layer developed within 15 minutes of the onset of fluidization. The bubbling flow regime was shown to have a greater capacity for charge generation than the slugging flow regime. This was due to the vigorous mixing in the bubbling flow regime resulting in more particle-particle interactions.

Column wall material was shown to influence wall fouling in the slugging flow regime due to the differences in surface roughness of the columns. This was due to the particle-wall contacts resulting in frictional charging which is the predominant charging mechanism in this flow regime. Charge was also impacted in the bubbling flow regime in those particles that were adhered to the column wall.

Relative humidity was found to influence wall fouling at the lowest gas velocity tested. However, variations in generation of charge occurred at all fluidization gas velocities tested; the charge-to-mass ratios for the particles adhered to the column wall in the slugging flow regime decreased with high relative humidities. This was due to either the formation of a water film layer on the column wall or instantaneous surface water films on the particles throughout fluidization.

Table of Contents

Abstract……i
Table of Contents……ii
List of Tables……viii
List of Figures……x
Nomenclature……..xvii
Acknowledgements……..viii
Dedication……xix

Chapter 1. Introduction 1
1.1. Background Information 2
1.1.1. Gas-Solid Fluidization 2
1.1.1.1. Fluidization Flow Regime 3
1.1.1.2. Classification of Particles 4
1.1.2. Electrostatics 5
1.1.2.1. Charging Mechanisms 6
1.1.2.2. Work Function 7
1.1.2.3. Triboelectric series 8
1.1.3. Electrostatic Charge Generation in Gas-Solid Fluidized Beds 8
1.1.4. Electrostatic Charge Measurement Techniques 11
1.1.4.1. Electrostatic Probe 11
1.1.4.2. Faraday Cup 12
1.1.5. Parameters Influencing Electrostatic Phenomenon in Gas-Solid Fluidized Beds 15
1.1.5.1. Fluidization Time 15
1.1.5.2. Fluidization Column Material 18
1.1.5.3. Fluidizing Gas Relative Humidity (RH) 20
1.2. Thesis Objectives 27
1.3. Thesis Outline 29

Chapter 2. Experimental Apparatus and Method 31

2.1. Experimental Apparatus 31

2.1.1. Humidification system 36

2.2. Fluidizing Gas 40

2.3. Fluidizing Particles 40

2.4. Experimental Method 50

Chapter 3. Effect of Fluidization Time on Bed Electrification in Bubbling and Slugging Flow Regimes 56

3.1. Bubbling Flow Regime 57

3.1.1. 1.5 U_{mf} Gas Velocity Results and Discussion 57

3.1.1.1. Mass Collected (m%) 57

3.1.1.2. Charge-to-Mass Ratio (q/m) 59

3.1.1.3. Wall Particle Layer 62

3.1.1.4. Particle Size Distribution (PSD) 63

3.1.2. 1.75 U_{mf} Gas Velocity Results and Discussion 68

3.1.2.1. Mass Collected (m%) 68

3.1.2.2. Charge-to-Mass Ratio (q/m) 69

3.1.2.3. Wall Particle Layer 72

3.1.2.4. Particle Size Distribution (PSD) 73

3.1.3. Bubbling Flow Regime Comparison 77

3.1.3.1. Mass Collected (m%) 77

3.1.3.2. Charge-to-Mass Ratio (q/m) 79

3.1.3.3. Particle Size Distribution (PSD) 80

3.1.4. Bubbling Flow Regime Summary 81

3.2. Slugging Flow Regime 82

3.2.1. 3.5 U_{mf} Gas Velocity Results and Discussion 82

3.2.1.1. Mass Collected (m%) 82

3.2.1.2. Charge-to-Mass Ratio (q/m) 84

3.2.1.3. Wall Particle Layer 86

3.2.1.4. Particle Size Distribution (PSD) 87

3.2.2. 4 U_{mf} Gas Velocity Results and Discussion 91
3.2.2.1. Mass Collected (m%) 91
3.2.2.2. Charge-to-Mass Ratio (q/m) 92
3.2.2.3. Wall Particle Layer 94
3.2.2.4. Particle Size Distribution (PSD) 95
3.2.3. Slugging Flow Regime Comparison 99
3.2.3.1. Mass Collected (m%) 99
3.2.3.2. Charge-to-Mass Ratio (q/m) 100
3.2.3.3. Particle Size Distribution (PSD) 102
3.2.4. Slugging Flow Regime Summary 103
3.3. Comparison of Results of the Two Flow Regimes 104
3.3.1. Mass Collected (m%) 104
3.3.2. Charge-to-Mass Ratio (q/m) 106
3.3.3. Particle size distribution (PSD) 108
3.4. Charge Saturation 112
3.5. Conclusion 113

Chapter 4. Effect of Column Wall Material on Bed Electrification 115
4.1. Results…… 117
4.1.1. Mass Collected (m%) 117
4.1.2. Charge-to-Mass Ratio (q/m) 118
4.1.3. Wall Particle Layer 121
4.1.4. Particle Size Distribution (PSD) 122
4.1.4.1. 1.5 U_{mf} Gas Velocity 123
4.1.4.2. 4 U_{mf} Gas Velocity 124
4.2. Discussion 125
4.3. Conclusion 129

Chapter 5. Effect of Fluidizing Gas Relative Humidity on Bed Electrification in Bubbling and Slugging Flow Regimes 130
5.1. Bubbling Flow Regime 131

5.1.1. 1.5 U_{mf} Gas Velocity Results and Discussion 131
5.1.1.1. Mass Collected (m%) 131
5.1.1.2. Charge-to-Mass Ratio (q/m) 133
5.1.1.3. Wall Particle Layer 136
5.1.1.4. Particle Size Distribution (PSD) 137
5.1.2. 1.75 U_{mf} Gas Velocity Results and Discussion 140
5.1.2.1. Mass Collected (m%) 140
5.1.2.2. Charge-to-Mass Ratio (q/m) 141
5.1.2.3. Wall Particle Layer 143
5.1.2.4. Particle Size Distribution (PSD) 144
5.1.3. Bubbling Flow Regime Comparison 146
5.1.3.1. Mass Collected (m%) 146
5.1.3.2. Charge-to-Mass Ratio (q/m) 147
5.1.3.3. Particle Size Distribution (PSD) 148
5.1.4. Bubbling Flow Summary 150
5.2. Slugging Flow Regime 150
5.2.1. 3.5 U_{mf} Gas Velocity Results and Discussions 150
5.2.1.1. Mass Collected (m%) 150
5.2.1.2. Charge-to-Mass Ratio (q/m) 152
5.2.1.3. Wall Particle Layer 153
5.2.1.4. Particle Size Distribution (PSD) 154
5.2.2. 4 U_{mf} Gas Velocity Results and Discussion 157
5.2.2.1. Mass Collected (m%) 157
5.2.2.2. Charge-to-Mass ratio (q/m) 158
5.2.2.3. Wall Particle Layer 159
5.2.2.4. Particle Size Distribution (PSD) 160
5.2.3. Slugging Flow Regime Comparison 163
5.2.3.1. Mass Collected (m%) 163
5.2.3.2. Charge-to-Mass Ratio (q/m) 164
5.2.3.3. Particle Size Distribution (PSD) 166
5.2.4. Slugging Flow Regime Summary 168

5.3. Comparison of Results of the Two Flow Regimes 168
5.3.1. Mass Collected (m%).....169
5.3.2. Charge-to-Mass Ratio (q/m) 169
5.3.3. Normalized Mean Particle Diameter 170
5.4. Overall Summary 172
5.4.1. Additional Experiments 174
5.4.1.1. Bench-scale water adsorption tests.....174
5.4.1.2. Differential pressure fluctuations 175
5.4.1.3. Humidity probe data 176
5.4.1.4. Thermogravimetric analysis (TGA) 177
5.5. Conclusions 179

Chapter 6. Conclusions and Future Work 180
6.1. Conclusions 180
6.1.1. Charging Mechanisms 181
6.1.2. Fluidization Time.....184
6.1.3. Column Material 185
6.1.4. Relative Humidity.....185
6.2. Recommendations for Future Work 186

Bibliography……187
Appendix A: Preliminary Parameters……193
Appendix B: Fluidization Times Experimental Data and Additional Graphs……197
Appendix C: Experimental Data and Additional Graphs……..224

List of Tables

Table 1-1: Work functions of various materials (Adapted from Tanoue and Masuda, 2006). 7

Table 1-2: Examples of Triboelectric series (Adapted from Adams, 1987 and Hersh and Montgomery, 1955). 8

Table 1-3: Previous studies on the effect of fluidization time on electrostatic charge generation in fluidized beds. 16

Table 1-4: Previous studies on the effect of column wall material on electrostatic charge generation in fluidized beds. 18

Table 1-5: Previous studies on the effect of relative humidity on electrostatic charge generation in fluidized beds. 21

Table 2-1: Fluidizing particles (i.e., Polyethylene resins) properties. 40

Table 2-2: Comparison of U_{mf} values 43

Table 3-1: Comparison of m% for all regions for different fluidization times and gas velocities. 105

Table 3-2: Particle wall layer height with respect to fluidization time and gas velocity. 106

Table 3-3: Comparison of net q/m for all regions of the bed for different fluidization times and gas velocities. 107

Table 3-4: Normalized $D_{P\ 0.5}$ for all regions for different fluidization times and gas velocities. 109

Table 3-5: Average experimental q/m and theoretical $|q/m|_{max}$ with respect to fluidization time and gas velocity. 113

Table 4-1: Materials surface conductivity. 126

Table 4-2: Surface roughness of column wall materials. 127

Table 5-1: Comparison of m% for all gas velocities and relative humidities. 169

Table 5-2: Comparison of q/m for all gas velocities and relative humidities. 170

Table 5-3: Normalized mean particle diameters ($D_{P\ 0.5}$) for all fluidization gas velocities at different relative humidities. 171

Table 5-4: Contact angles of stainless steel, polyethylene, and glass surfaces 173

Table 5-5: Water adsorption test results. 175

Table 5-6: Standard deviation (σ) of differential pressure fluctuations in psi at different relative humidities for different gas velocities. 176

Table B - 1: Normalized values for $D_{P\,0.1}$, $D_{P\,0.5}$, and $D_{P\,0.9}$ at 1.5 U_{mf} for all fluidization times 198
Table B - 2: Normalized values for $D_{P\,0.1}$, $D_{P\,0.5}$, and $D_{P\,0.9}$ at 1.75 U_{mf} for all fluidization times 205
Table B - 3: Normalized values for $D_{P\,0.1}$, $D_{P\,0.5}$, and $D_{P\,0.9}$ at 3.5 U_{mf} for all fluidization times 212
Table B - 4: Normalized values for $D_{P\,0.1}$, $D_{P\,0.5}$, and $D_{P\,0.9}$ at 4 U_{mf} for all fluidization times 219

Table C-1: Normalized values for $D_{P\,0.1}$, $D_{P\,0.5}$, and $D_{P\,0.9}$ at 1.5 U_{mf} for all relative humidities. 227
Table C-2: Normalized values for $D_{P\,0.1}$, $D_{P\,0.5}$, and $D_{P\,0.9}$ at 1.75 U_{mf} for all relative humidities. 233
Table C-3: Normalized values for $D_{P\,0.1}$, $D_{P\,0.5}$, and $D_{P\,0.9}$ at 3.5 U_{mf} for all relative humidities. 239
Table C-4: Normalized values for $D_{P\,0.1}$, $D_{P\,0.5}$, and $D_{P\,0.9}$ at 4 U_{mf} for all relative humidities. 246

List of Figures

Figure 1-1: Fluidization flow regimes (Adapted from Kunii and Levenspiel, 1991). 3

Figure 1-2: Geldart classification of powders for air at ambient conditions (Adapted from Geldart, 1973). 4

Figure 1-3: Triboelectric charging mechanism. 6

Figure 1-4: Frictional charging mechanism. 7

Figure 1-5: Schematic of a polyolefin gas-solid fluidized bed reactor (Adapted from Chirillo et al., 1989). 9

Figure 1-6: Electrostatic probe: (a) Electric field measurement, (b) Types of probe insertion into a fluidized bed. 11

Figure 1-7: Application of electrostatic probe in gas-solid fluidized beds: (a) Contacting probe (Adapted from Cibrowski and Woldarski, 1962), and (b) Non-contacting probe (Adapted from Boland and Geldart, 1971/1972). 12

Figure 1-8: Schematic of Faraday cup operation. 13

Figure 1-9: Applications of a Faraday cup in gas-solid fluidized beds. 14

Figure 1-10: Characteristic curve for the variation in charge on capacitance plates due to relative humidity (Adapted from Guardiola et al., 1996). 23

Figure 2-1: Experimental set-up: (a) Overall system schematic, and (b) Fluidization column with Faraday cups. 33

Figure 2-2: Image of the complete experimental system. 34

Figure 2-3: Humidifier system schematic. 38

Figure 2-4: (a) Picture of the Humidification system. (b) Cooling Coil. 39

Figure 2-5: SEM image of polyethylene resin. 44

Figure 2-6: Normalized distribution within initial particle sample by m%. 46

Figure 2-7: Measurement of charge distribution: (a) picture, and (b) schematic. 48

Figure 2-8: Charge separation experiments (a) charge-to-mass distribution of initial particle sample, and (b) $D_{P\ 0.1}$, $D_{P\ 0.5}$, $D_{P\ 0.9}$ of particles in each plate. 49

Figure 2-9: Measurement points: (a) Charge, mass, & PSD, (b) Additional PSD points. 51

Figure 2-10: Typical data collection during an experimental run: (a) Initial, (b) Dropped, (c) Wall, and (d) Initial. 54

Figure 3-1: Mean m% at 1.5 U_{mf} for different fluidization times: (a) Dropped, (b) Wall, (c) Fines, and (d) Irretrievable. 59

Figure 3-2: Mean net q/m at 1.5 U_{mf} for different fluidization times: (a) Initial, (b) Dropped, (c) Wall, and (d) Fines. 62

Figure 3-3: Images of particle layer on the column wall at 1.5 U_{mf} for different fluidization times: (a) 15 min, (b) 30 min, (c) 60 min, (d) 120 min, (e) 180 min, and (f) 360 min. 63

Figure 3-4: Normalized PSDs at 1.5 U_{mf} for different regions of the bed: (a) Initial, (b) Dropped, (c) Fines, (d) Wall, (e) Bottom Column, and (f) Intermediate Wall. 65

Figure 3-5: Example PSDs at 1.5 U_{mf} for all regions of the bed for different fluidization times: (a) 15 min, (b) 30 min, (c) 60 min, (d) 120 min, (e) 180 min, and (f) 360 min. 67

Figure 3-6: Mean m% of particles collected at 1.75 U_{mf} for different fluidization times: (a) Dropped, (b) Wall, (c) Fines, and (d) Irretrievable. 69

Figure 3-7: Mean net q/m at 1.75 U_{mf} for different fluidization times: (a) Initial, (b) Dropped, (c) Wall, and (d) Fines. 71

Figure 3-8: Images of particle layer on the column wall at 1.75 U_{mf} for different fluidization times: (a) 15 min, (b) 30 min, (c) 60 min, (d) 120 min, (e) 180 min, and (f) 360 min. 72

Figure 3-9: Normalized PSDs at 1.75 U_{mf} for different regions of the bed: (a) Initial, (b) Dropped, (c) Fines, (d)Wall, (e) Bottom Column, and (f) Intermediate Wall. 74

Figure 3-10: Example PSDs at 1.75 U_{mf} for all regions of the bed for different fluidization times: (a) 15 min, (b) 30 min, (c) 60 min, (d) 120 min, (e) 180 min, and (f) 360 min. 76

Figure 3-11: Comparison of m% for two velocities in bubbling flow regime: (a) Dropped, (b) Wall, (c) Fines, and (d) Irretrievable. 78

Figure 3-12: Comparison of mean net q/m for two velocities in bubbling flow regime: (a) Initial, (b) Dropped, (c) Wall, and (d) Fines. 80

Figure 3-13: Comparison of normalized PSDs for two velocities in bubbling flow regime: (a) Dropped, (b) Wall, and (c) Fines. 81

Figure 3-14: Mean m% at 3.5 U_{mf} for different fluidization times: (a) Dropped, (b) Wall, (c) Fines, and (d) Irretrievable. 83

Figure 3-15: Mean net q/m at 3.5 U_{mf} for different fluidization times: (a) Initial, (b) Dropped, (c) Wall, and (d) Fines. 84

Figure 3-16: Images of particle layer on the column wall at 3.5 U_{mf} for different fluidization times: (a) 15 min, (b) 30 min, (c) 60 min, (d) 120 min, (e) 180 min, and (f) 360 min. 86

Figure 3-17: Normalized PSDs at 3.5 U_{mf} for different regions of the bed: (a) Initial, (b) Dropped, (c) Fines, (d) Wall, (e) Bottom Column, and (f) Top Column. 88

Figure 3-18: Example PSDs at 3.5 U_{mf} for all regions of the bed for different fluidization times: (a) 15 min, (b) 30 min, (c) 60 min, (d) 120 min, (e) 180 min, and (f) 360 min. 90

Figure 3-19: Mean m% at 4 U_{mf} for different fluidization times: (a) Dropped, (b) Wall, (c) Fines), and (d) Irretrievable. 92

Figure 3-20: Mean net q/m at 4 U_{mf} for different fluidization times: (a) Initial, (b) Dropped, (c) Wall, and (d) Fines. 93

Figure 3-21: Images of particle layer on the column wall at 4 U_{mf} for different fluidization times: (a) 15 min, (b) 30 min, (c) 60 min, (d) 120 min, (e) 180 min, and (f) 360 min. 95

Figure 3-22: Normalized PSDs at 4 U_{mf} for different fluidization times: (a) Initial, (b) Dropped, (c) Fines, (d) Wall, (e) Column Bottom, and (f) Column Top. 97

Figure 3-23: Example PSDs at 4 U_{mf} for all regions of the bed for different fluidization times: (a) 15 min, (b) 30 min, (c) 60 min, (d) 120 min, (e) 180 min, and (f) 360 min. 98

Figure 3-24: Comparison of m% for two velocities in slugging flow regime: (a) Dropped, (b) Wall, (c) Fines, and (d) Irretrievable. 100

Figure 3-25: Comparison of net q/m for two velocities in slugging flow regime: (a) Initial, (b) Dropped, (c) Wall, and (d) Fines. 101

Figure 3-26: Comparison of Normalized PSDs for two gas velocities in slugging flow regime: (a) Dropped, (b) Wall, and (c) Fines. 103

Figure 3-27: Normalized PSDs for all regions of the bed at a fluidization time of 120 minutes: (a) 1.5 U_{mf}, (b) 1.75 U_{mf}, (c) 3.5 U_{mf}, and (d) 4 U_{mf}....111

Figure 4-1: Mean m% collected for different column materials: (a) Dropped, (b) Wall, (c) Fines, and (d) Irretrievable....118

Figure 4-2: Mean net q/m for different column materials: (a) Initial, (b) Dropped, (c) Wall, and (d) Fines. 119

Figure 4-3: Images of particle wall layer: (a) Carbon Steel 1.5 U_{mf}, (b) Stainless Steel 1.5 U_{mf}, (c) Carbon Steel 4 U_{mf}, and (d) Carbon Steel 4 U_{mf}....121

Figure 4-4: Example PSDs at 1.5 U_{mf} for all regions of the bed for different column materials: (a) Carbon steel column, (b) Stainless steel column. 123

Figure 4-5: Example PSDs at 4 U_{mf} for all regions of the bed for different column materials: (a) Carbon steel column, (b) Stainless steel column. 124

Figure 5-1: Mean m% at 1.5 U_{mf} for different relative humidities: (a) Dropped, (b) Wall, (c) Fines, and (d) Irretrievable....133

Figure 5-2: Mean net q/m at 1.5 U_{mf} for different relative humidities: (a) Initial, (b) Dropped, (c) Wall, and (d) Fines. 134

Figure 5-3: Images of particle layer on the column wall at 1.5 U_{mf} for different relative humidities: (a) 0%, (b) 20%, (c) 40%, (d) 60%, and (e) 80%. 136

Figure 5-4: Normalized PSDs at 1.5 U_{mf} for different regions of the bed: (a) Initial, (b) Dropped, (c) Wall, (d) Fines, and (e) Bottom Column. 139

Figure 5-5: Mean m% at 1.75 U_{mf} for different relative humidities: (a) Dropped, (b) Wall, (c) Fines, and (d) Irretrievable. 141

Figure 5-6: Mean net q/m at 1.75 U_{mf} for different relative humidities: (a) Initial, (b) Dropped, (c) Wall, and (d) Fines. 142

Figure 5-7: Images of particle layer on the inner column wall at 1.75 U_{mf} for different relative humidities: (a) 0%, (b) 20%, (c) 40%, (d) 60%, and (e) 80%. 143

Figure 5-8: Normalized PSDs at 1.75 U_{mf} for different regions of the bed: (a) Initial, (b) Dropped, (c) Wall, (d) Fines, and (e) Bottom Column. 145

Figure 5-9: Comparison of m% for two velocities in bubbling flow regime: (a) Dropped, (b) Wall, (c) Fines, and (d) Irretrievable. 147

Figure 5-10: Comparison of mean net q/m for two velocities in bubbling flow regime: (a) Initial, (b) Dropped, (c) Wall, and (d) Fines. 148

Figure 5-11: Comparison of normalized PSDs for two velocities in bubbling flow regime: (a) Dropped, (b) Wall, and (c) Fines. 149

Figure 5-12: Mean m% at 3.5 U_{mf} for different relative humidities: (a) Dropped, (b) Wall, (c) Fines, and (d) Irretrievable. 151

Figure 5-13: Mean net q/m at 3.5 U_{mf} for different relative humidities: (a) Initial, (b) Dropped, (c) Wall, and (d) Fines. 152

Figure 5-14: Images taken from the particle layer on the column wall at 3.5 U_{mf} for different relative humidities: (a) 0%, (b) 20%, (c) 40%, (d) 60%, and (e) 80%. 154

Figure 5-15: Normalized PSDs at 3.5 U_{mf} for different regions of the bed: (a) Initial, (b) Dropped, (c) Wall, (d) Fines, (e) Bottom Column, and (f) Top Column. 156

Figure 5-16: Mean m% at 4 U_{mf} for different relative humidities: (a) Dropped, (b) Wall, (c) Fines), and (d) Irretrievable. 157

Figure 5-17: Mean q/m at 4 U_{mf} for different relative humidities: (a) Initial, (b) Dropped, (c) Wall, and (d) Fines. 158

Figure 5-18: Images of particle layer on the column wall at 4 U_{mf} for different relative humidities: (a) 0%, (b) 20%, (c) 40%, (d) 60%, and (e) 80%. 160

Figure 5-19: Normalized PSDs at 4 U_{mf} for different regions of the bed: (a) Initial, (b) Dropped, (c) Wall, (d) Fines, (e) Bottom Column, and (f) Top Column. 162

Figure 5-20: Comparison of m% for two velocities in slugging flow regime: (a) Dropped, (b) Wall, (c) Fines, and (d) Irretrievable. 164

Figure 5-21: Comparison of net q/m for two velocities in the slugging flow regime: (a) Initial, (b) Dropped, (c) Wall, and (d) Fines. 165

Figure 5-22: Comparison of PSDs for two gas velocities in slugging flow regime: (a) Dropped, (b) Wall, and (c) Fines. 167

Figure 5-23: Amount of RH (%) lost between inlet and outlet of fluidization column for trials at 1.75 or 3.5 U_{mf}. 177

Figure 5-24: Thermogravimetric analysis for m% loss with temperature: (a) & (b) Initial Sample (repetition 1 & 2); (c) & (d) Humidified Sample (repetition 1 & 2).....178

Figure 6-1: Charging mechanisms in stainless steel column with polyethylene particle: (a) Particle-particle contacts, and (b) Particle-wall contacts. 183

Figure 6-2: Particles movement due to electrostatic forces. 184

Figure 6-3: Particle wall fouling. 184

Figure A-1: Typical initial particle size distribution. 194

Figure A-2: Experimental determination of U_{mf}. 194

Figure A-3: Mass distribution of initial particles as evaluated by PSD given in $D_{P\,0.1}$, $D_{P\,0.5,}$ and $D_{P\,0.9}$. 195

Figure A-4: Average PSDs for charge distribution tests. 195

Figure A-5: Humidity reference chart – approximate MFC 2 input values for desired fluidization gas relative humidity and velocity.. 196

Figure B-1: Normalized PSDs at 1.5 U_{mf} for Initial region for different fluidization times. 199

Figure B-2: Normalized PSDs at 1.5 U_{mf} for Dropped region for different fluidization times.....200

Figure B-3: Normalized PSDs at 1.5 U_{mf} for Wall region for different fluidization times. 201

Figure B-4: Normalized PSDs at 1.5 U_{mf} for Fines region for different fluidization times. 202

Figure B-5: Normalized PSDs at 1.5 U_{mf} for Bottom Column region for different fluidization times.....203

Figure B-6: Normalized PSDs at 1.5 U_{mf} for Intermediate Wall region for different fluidization times.....204

Figure B-7: Normalized PSDs at 1.75 U_{mf} for Initial region for different fluidization times.....206

Figure B-8: Normalized PSDs at 1.75 U_{mf} for Dropped region for different fluidization times.....207
Figure B-9: Normalized PSDs at 1.75 U_{mf} for Wall region for different fluidization times. 208
Figure B-10: Normalized PSDs at 1.75 U_{mf} for Fines region for different fluidization times.....209
Figure B-11: Normalized PSDs at 1.75 U_{mf} for Bottom Column region for different fluidization times.....210
Figure B-12: Normalized PSDs at 1.75 U_{mf} for Intermediate Column region for different fluidization times. 211
Figure B-13: Normalized PSDs at 3.5 U_{mf} for Initial region for different fluidization times. 213
Figure B-14: Normalized PSDs at 3.5 U_{mf} for Dropped region for different fluidization times.....214
Figure B-15: Normalized PSDs at 3.5 U_{mf} for Wall region for different fluidization times. 215
Figure B-16: Normalized PSDs at 3.5 U_{mf} for Fines region for different fluidization times. 216
Figure B-17: Normalized PSDs at 3.5 U_{mf} for Bottom Column region for different fluidization times.....217
Figure B-18: Normalized PSDs at 3.5 U_{mf} for Top Column region for different fluidization times.....218
Figure B-19: Normalized PSDs at 4 U_{mf} for Initial region for different fluidization times. 220
Figure B-20: Normalized PSDs at 4 U_{mf} for Dropped region for different fluidization times.....221
Figure B-21: Normalized PSDs at 4 U_{mf} for Wall region for different fluidization times. 222
Figure B-22: Normalized PSDs at 4 U_{mf} for Fines region for different fluidization times. 223
Figure B-23: Normalized PSDs at 4 U_{mf} for Bottom Column region for different fluidization times.....224
Figure B-24: Normalized PSDs at 4 U_{mf} for Top Column region for different fluidization times.....225

Figure C-1: Normalized PSD at 1.5 U_{mf} in the Initial region for different relative humidity. 228
Figure C-2: Normalized PSD at 1.5 U_{mf} in the Dropped region for different relative humidity. 229

Figure C-3: Normalized PSD at 1.5 U_{mf} in the Wall region for different relative humidity. 230
Figure C-4: Normalized PSD at 1.5 U_{mf} in the Fines region for different relative humidity. 231
Figure C-5: Normalized PSD at 1.5 U_{mf} in the Bottom Column region for different relative humidity. 232
Figure C-6: Normalized PSD at 1.75 U_{mf} in the Initial region for different relative humidity. 234
Figure C-7: Normalized PSD at 1.75 U_{mf} in the Dropped region for different relative humidity. 235
Figure C-8: Normalized PSD at 1.75 U_{mf} in the Wall region for different relative humidity. 236
Figure C-9: Normalized PSD at 1.75 U_{mf} in the Fines region for different relative humidity. 237
Figure C-10: Normalized PSD at 1.75 U_{mf} in the Bottom Column region for different relative humidity. 238
Figure C-11: Normalized PSD at 3.5 U_{mf} in the Initial region for different relative humidity. 240
Figure C-12: Normalized PSD at 3.5 U_{mf} in the Dropped region for different relative humidity. 241
Figure C-13: Normalized PSD at 3.5 U_{mf} in the Wall region for different relative humidity. 242
Figure C-14: Normalized PSD at 3.5 U_{mf} in the Fines region for different relative humidity. 243
Figure C-15: Normalized PSD at 3.5 U_{mf} in the Bottom Column region for different relative humidity. 244
Figure C-16: Normalized PSD at 3.5 U_{mf} in the Top Column region for different relative humidity. 245
Figure C-17: Normalized PSD at 4 U_{mf} in the Initial region for different relative humidity. 247
Figure C-18: Normalized PSD at 4 U_{mf} in the Dropped region for different relative humidity. 248
Figure C-19: Normalized PSD at 4 U_{mf} in the Wall region for different relative humidity. 249
Figure C-20: Normalized PSD at 4 U_{mf} in the Fines region for different relative humidity. 250
Figure C-21: Normalized PSD at 4 U_{mf} in the Bottom Column region for different relative humidity. 251
Figure C-22: Normalized PSD at 4 U_{mf} in the Top Column region for different relative humidity. 252

Acknowledgements

First, I would like to convey my gratitude to my supervisor Dr. Poupak Mehrani for both providing me the opportunity to participate in her research group and for all the support and encouragement throughout the process. Her guidance and input on all aspects of the project were greatly appreciated.

I would also like to sincerely thank my fellow group member Andrew Sowinski for being my walking encyclopaedia. A constant source of information, he was always ready to listen to ideas, problems, or anything else that I might need and made the thesis process much more enjoyable.

I would like to acknowledge the staff of the Chemical Engineering Department at the University of Ottawa: Franco Ziroldo, Gérard Nina, Louis Tremblay, Francine Pértrin and Sylvie Saindon for their help and expertise. Especially Franco Ziroldo who was available for help with any and all mechanical problems with the column.

I would like to thank Dr. Michael Muhle and Dr. F. David Hussein for their comments and recommendations. Additionally, thanks to Univation Technologies, Inc. for providing all the resins used in this work.

I would like to thank NSERC and OGS for financial contributions.

To my fellow grad students, I wish to thank you for keeping the last two years entertaining and making school a pleasant place to come to everyday. To Sarah Patterson and Christopher Simon, my roommates, thanks for making coming home from school even better and for always being there when I needed you. To my friends, thanks for everything, especially Leon Sutherland who took me on many adventures to keep school in perspective.

Finally, I wish to thank my family for all the love and encouragement. Thanks to my parents for instilling the importance of education, my sisters for pushing me to be better, and my brother and grandmother for always believing in me.

Dedication

This thesis is dedicated to my grandparents: Ralph and Helen MacKichan and Bob and Adrienne Giffin. It is also dedicated to my parents Gregory and Shirley Giffin.

Nomenclature

Ar	Archimedes number	dimensionless
D_C	Column diameter	m
D_P	Particle diameter	μm
$D_{P\,0.1}$	Particle diameter of 10^{th} percentile	dimensionless
$D_{P\,0.5}$	Mean particle diameter	dimensionless
$D_{P\,0.9}$	Particle diameter of 90^{th} percentile	dimensionless
E_d	Electrical breakdown field of air	V/m
L	Fixed bed height	m
M	Mass of particles	kg
PSD	Particle size distribution	μm
$(Re)_{mf}$	Reynold's number at minimum fluidization	dimensionless
RH	Relative humidity	%
U	Fluidization gas velocity	m/s
U_{mf}	Minimum fluidization velocity	m/s
d_P	Particle diameter	μm
g	Gravitational acceleration	m/s^2
m_i	Initial mass	g
m%	Mass percent	%
q/m	Charge-to-mass ratio	μC/kg
q	Charge	μC

Greek Letters

ΔP	Differential pressure	Pa
ε	Permittivity	F/m
ε_{fb}	Fixed bed voidage	dimensionless
ε_{mf}	Minimum fluidization voidage	dimensionless
ε_0	Permittivity of free space	F/m
κ	Conductivity	S/m
μ	Fluid viscosity	m^2/s
ρ_B	Bulk particle density	kg/m^3
ρ_f	Fluid density	kg/m^3
ρ_P	Particle density	kg/m^3
σ	Standard deviation	variable
ϕ	Sphericity	dimensionless
φ	Work function	eV
θ_a	Contact angle	°

Chapter 1. Introduction

Gas-solid fluidization is the process by which solid particles are forced to behave like a fluid by suspension of particles in a gas. The state of fluidization is achieved when the gas is at a high enough velocity that the particles become suspended within the gas. Industrial applications of gas-solid fluidized beds are numerous and can be found over a wide range of commercial operations such as physical operations (e.g., heat exchange, applying coatings, drying, etc.), synthesis reactions (e.g., Fischer-Tropsch, acrylonitrile, maleic anhydride), hydrocarbon cracking, combustion and incineration, gasification, biofluidization, to just name a few. Fluidization has been used by these industries for many years; for example, Dow Chemicals (Union Carbide at the time) commercialized the first gas phase fluidized bed reactor for polymer production before 1970 (Jazayeri, 2003).

Electrostatic charge generation in some gas-solid fluidized beds has been identified as a problem for over 50 years (Miller and Logwinuk, 1951). Electrostatic charges can be generated through triboelectrification and frictional charging when the fluidizing particles come in contact with other particles or the fluidization column wall. These particle-particle or particle-equipment interactions lead to particle agglomeration or particle wall fouling due to particle adhesion to the reactor wall. This phenomenon may require reactor shutdown to remove the agglomerates and adhesions resulting in reduced production and economic loss. Although such significant problems have been identified for many years, the mechanisms of charge generation in such reactors are still not well understood. Understanding the factors contributing to electrostatic charge generation and their involvement in reactor wall fouling is an important step in developing methods to reduce or prevent this phenomenon. The focus of this thesis is to understand the influence of three different parameters on electrostatic charge generation within gas-solid fluidized bed reactors: duration of fluidization, column wall material, and relative humidity of fluidizing gas.

1.1. Background Information

This thesis focuses on the merging of two main areas of study: gas-solid fluidization and electrostatic charge generation. This section details what each subject matter is and how they relate to each other and to the research.

1.1.1. Gas-Solid Fluidization

The fluid-like state of solid particles movement produced during gas-solid fluidization allows for a variety of equipment configurations for particle contacting. Kunii and Levenspiel (1991) state that the "fluidlike behaviour of solids with its rapid, easy transport and its intimate gas contacting is often the most important property recommending fluidization for industrial operations." There are many advantages to fluidized bed operations, however there are also some disadvantages.

Gas-solid fluidization reactors provide an environment that is compatible with wide size ranges of solid particles with the ability to continuously produce a uniform product. Due to the vigorous motion of particles, the heat and mass transfer properties within a fluidized bed provide almost uniform temperatures and concentrations within the bed. Additionally, rapid changes in temperature are resisted due to slow response to operating condition changes. The design of fluidized beds is suitable to large-scale operations. However, due to the complex nature of the flow, particle contacting is difficult to predict. Due to the rapid mixing occurring inside such reactors, the residence time for particles within the bed may be non-uniform resulting in potential inconsistencies in product. Attrition of particles and entrainment can be an issue as these particles must be captured and replaced within the bed. Agglomeration and wall fouling can present additional problems leading to non-uniform operation and reactor shutdown.

1.1.1.1. Fluidization Flow Regime

The fluidization gas velocity dictates the hydrodynamics within the bed (Figure 1-1). At low gas velocities, the gas passes over the particles, making its way through the gaps between particles (i.e. fixed bed). As fluidization gas velocity increases, the particles are suspended in the gas; this is the point of minimum fluidization. Beyond this point, the particles begin to move like a fluid. As the gas velocity continues to increase, voids are created within the bed where no particles exist, this is called bubbling fluidization. With additional gas flowing through the bed, bubbles begin to coalesce and as they grow they may take up the full diameter of the bed, forming slugging fluidization. Axial slugging takes place with finer particles where they are able to flow down the side of the bed. Beyond slugging, turbulent fluidization is reached when the fluidization gas velocity is substantial enough that the top boundary of the bed disappears and fines entrainment becomes significant.

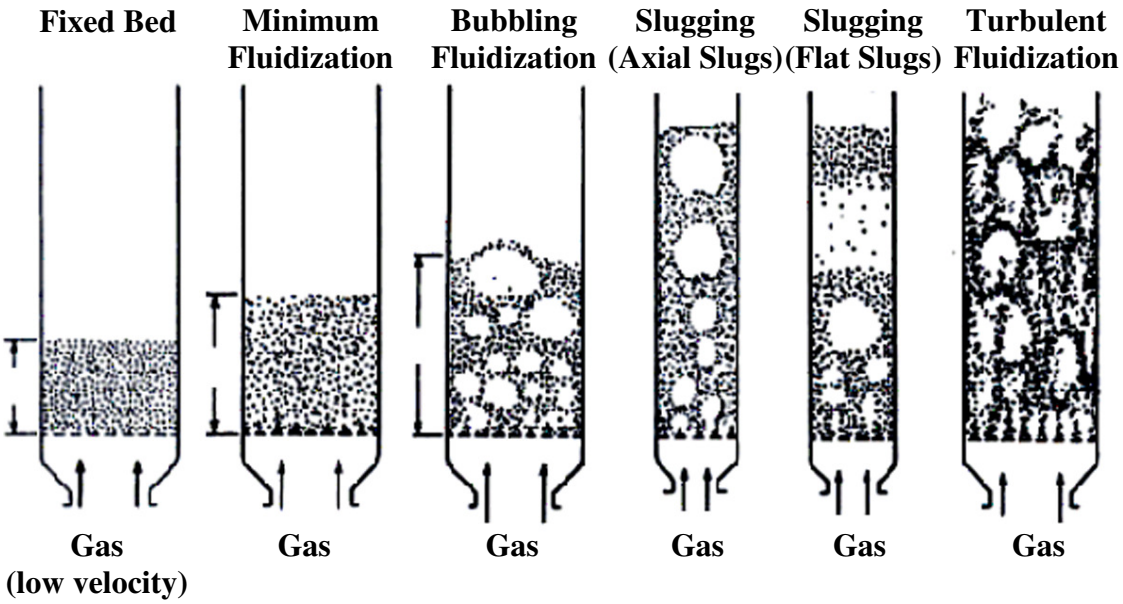

Figure 1-1: Fluidization flow regimes (Adapted from Kunii and Levenspiel, 1991).

Of main focus in this thesis were the bubbling and slugging (flat slugs) flow regimes. The hydrodynamics of these two regimes are important in understanding the particles movement throughout the bed. Within the bubbling flow regime, particles are vigorously mixed together (Kunii and Levenspiel, 1991). This results in particle movement in both the radial and axial directions. In the slugging flow regime, the particle motion is more similar to plug flow (van Putten et al., 2007) resulting in mainly axial mixing. As the slug formation is due

to the coalescence of bubbles, the locations of fully formed slugs are a function of bed height and column diameter (De Luca et al., 1992).

1.1.1.2. Classification of Particles

Due to the complex nature of fluidization, it can be difficult to predict the features of fluidization prior to experimentation. Geldart (1973) carefully observed different types and sizes of solids during fluidization and was able to divide particle behaviour into four separate groups (Figure 1-2).

- **Group A:** These particles are aeratable, or have a small mean particle size and/or low density (< ~1.4 g/cm^3) and fluidize easily.
- **Group B:** These particles are sandlike, or have particles sizes in the range of 40 μm < D_P < 500 and densities 1.4 < ρ_s < 4 g/cm^3. These particles fluidize easily.
- **Group C:** These particles are cohesive, or are very fine, and difficult to fluidize due to interparticle forces higher than those forces generated by the gas.
- **Group D:** These particles are spoutable, or are large and/or dense. These particles are difficult to fluidize in deep beds. Severe channelling and/or spouting may be observed due to uneven gas distribution (Kunii and Levenspiel, 1991).

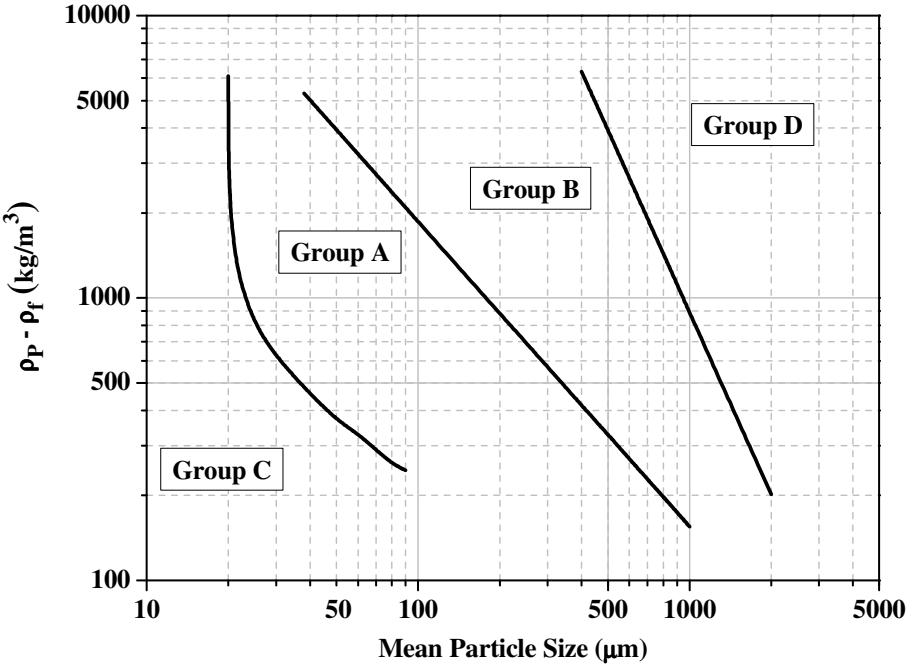

Figure 1-2: Geldart classification of powders for air at ambient conditions (Adapted from Geldart, 1973).

1.1.2. Electrostatics

Electrostatics is the area of physics that deals with static electricity or charge build-up on materials either due to an excess or deficit of electrons. In the case of conductors with a negative charge, the electrons are mobile and normal to the surface; in the case of insulators with a negative charge, the electrons are bound in place by lattice or molecular structure (Harper, 1967). With positive charges, the protons do not move but the electrons are free to move to neutralize positive charge elsewhere on the material, leaving a positive charge behind (Harper, 1967). Charge transfer is based on the movement of either electrons or ions from one material to another.

In the case of solid particles charging, various factors impact their charging properties as they come into contact with other surfaces including particle size and shape, surface chemical composition and work function, area and frequency of contacts, and environmental conditions (e.g., temperature, humidity, etc.) (Cross, 1987; Thomas et al., 2009). Due to the quantity of influencing factors and all their possible variations, certain prediction of charge magnitude and polarity is nearly impossible. Additionally, due to possible presence of contaminates on material surfaces, the ensuring repeatability of charge measurements is difficult.

The ability of a particle to gain both positive and negative charges, when contact is made with different materials, is based on particle size and surface composition, and is termed bipolar charging. In some cases this means that a single particle may have both positive and negative charges on its surface (Wolny and Kazmierczak, 1989). However, more commonly it refers to having some particles charged positively and some charged negatively in the same system when all particles have the same composition (Ali et al., 1998). During particle-particle contacting, charge exchange tendencies are greatest when a small particle and a relatively large particle come into contact (Gallo and Lama, 1985). For systems consisting of the same type of particles but having different sizes, some studies have found that finer particles become negatively charged while coarser particles gain positive charges (Cartwright et al., 1985; Zhao et al., 2002). However, another study done by Ali et al. (1998) reported that for some materials, the fines would become negatively charged, but with other

materials they become positively charged suggesting that the nature of the material influences how particles of different sizes would charge during particle-particle contacting.

1.1.2.1. Charging Mechanisms

There are several different mechanisms involved in electrostatic charge generation when surfaces of solids come into contact: triboelectrification, frictional charging, induction, and thermionic emission. In this work, the focus will be on triboelectrification and frictional charging.

Triboelectrification

Triboelectrification occurs when two materials come in contact with one another, due to differences in their surface energy of electrons and ions, electrons and/or ions are transferred from one material to the other until an equilibrium is reached (Harper, 1967; Piontek and Wypych, 2007). This mechanism is pictured in Figure 1-3. Upon separation, the surface which has lost electrons will become positively charged and the other which has gained electrons becomes negatively charged. This type of charging may also be identified as 'contact charging' or 'contact electrification'. The magnitude of charging with this mechanism is based on the surface conditions at the point of contact such as purity, roughness, and work function.

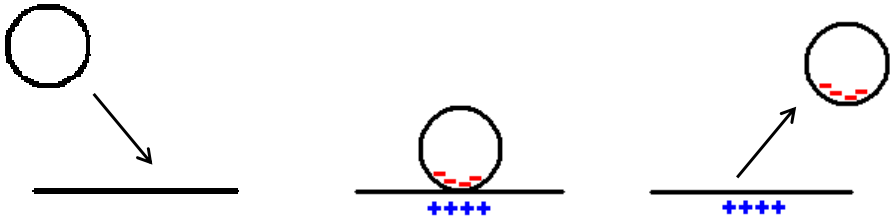

Figure 1-3: Triboelectric charging mechanism.

Frictional Charging

Frictional charging is when two materials rub against each other (Figure 1-4). The polarity of charge depends on the type of contact between the two materials, such as which material

is doing the rubbing and which material is getting rubbed (Cross, 1987). The amount of charge generated is based on the energy produced during rubbing. This energy can be based on rubbing velocity and temperature (Ohara, 1979). Additionally, due to non-uniformity of most surfaces, different amounts of charge can be generated on different locations on the materials being rubbed together.

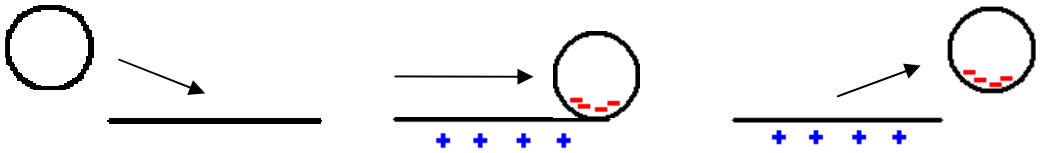

Figure 1-4: Frictional charging mechanism.

1.1.2.2. Work Function

Work function is the amount of energy required to remove an electron from the top energy distribution to infinity; for most metals this amount of energy is approximately equal to 4 eV (Cross, 1987). In comparison, the work function of polymers is hard to determine. This is because energetic electrons in insulators have different levels of energy throughout the material as electron energy is a function of surface impurities, atomic structure, and location (Cross, 1987). Examples of work function values for different materials are presented in Table 1-1. When two materials with different work functions come in contact, electrons will transfer from one material to the other. This is dependent on the relative work functions of the material; electrons will travel from the material with the lower work function leaving a positive charge behind, to the material with the higher work function, providing a negative charge (Blythe and Bloor, 2005; Cross, 1987).

Table 1-1: Work functions of various materials (Adapted from Tanoue and Masuda, 2006).

Material	Work Function (eV)	Material	Work Function (eV)	Material	Work Function (eV)
Zn	3.63	Ag	4.52 – 4.74	Polyethylene	5.23 ± 0.24
C	4	Si	4.60 – 4.91	Polypropylene	5.49 ± 0.34
Al	4.06 – 4.26	Fe	4.67 – 4.81	Polystyrene	4.77 ± 0.20
Cu	4.25	Co	5	PMMA	4.30 ± 0.29
Ti	4.33	Ni	5.04 – 5.35	Polyimide	4.36 ± 0.06
Pt	5.12 – 5.93	Au	5.31 – 5.47	Pylex7740	4.84 ± 0.21

1.1.2.3. Triboelectric series

The triboelectric series is a qualitative ranking system based on the amount of charge transferred from the materials. Such series allow for the prediction of charge polarity when two materials come in contact with one another. Materials higher on the list, charge positively when in contact with materials lower on the list. However, it is important to note that there is some variance between authors with respect to the order of materials in such series. Examples of triboelectric series are presented in Table 1-2; in these two series wool, nylon, cotton and silk are in different orders within the ranking system.

Table 1-2: Examples of Triboelectric series (Adapted from Adams, 1987 and Hersh and Montgomery, 1955).

Charge Polarity	Adams	Hersh and Montgomery
+	Glass	Wool
	Nylon	Nylon
	Wool	Viscose
	Lead	Cotton
	Silk	Silk
	Aluminum	Acetate
	Cotton	Lucite
	Steel	Polyvinyl alcohol
	Nickel, Copper	Dacron
	Brass, Silver	Orlon
	Polyester	Polyvinyl chloride
	Polyurethane	Dynel
	Polyethylene	Velon
	Vinyl (PVC)	Polyethylene
–	Teflon	Teflon

1.1.3. Electrostatic Charge Generation in Gas-Solid Fluidized Beds

During gas-solid fluidization, due to vigorous mixing of fluidizing particles electrostatic charges can be generated during particle-particle and particle-reactor wall contacting. Some significant consequences of charge generation are particle agglomeration and particle build-up on the reactor inner wall (Pfeffer and Quevedo, 2009).

For instance in polymerization reactors, due to the generation of electrostatic charges, polymer layers ("sheets") can be formed on the reactor wall when active catalyst becomes embedded in the particle layer, resulting in the polymer melting and fusing together due to the exothermic polymerization reaction (Hendrickson, 2006). These "sheets" can potentially dislodge from the column wall and fall on the distributor plate, blocking gas flow and requiring reactor shut down and clean up, and resulting in loss of production. Additional problems include interruption of the catalyst feed, plugging of the product discharge system, and the presence of agglomerates in the product (Agapiou et al., 2010). A typical schematic of a polyolefin production set-up is pictured in Figure 1-5 with a particle fouling appearing on the reactor walls.

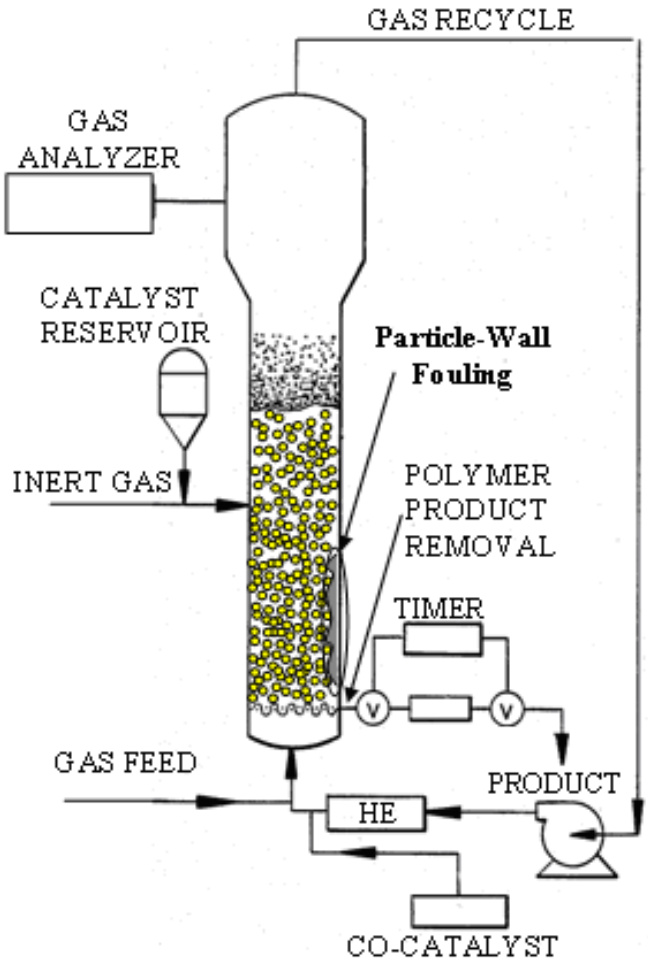

Figure 1-5: Schematic of a polyolefin gas-solid fluidized bed reactor (Adapted from Chirillo et al., 1989).

Factors contributing to the quantity and the polarity of charge on solid particles in fluidized beds include: frequency of contact between particles, and those with the reactor wall, particle size, shape and surface chemistry, and environmental conditions (e.g., temperature, pressure, relative humidity, etc.). With so many factors influencing charge generation, it is important to isolate each parameter to identify individual effects. After parameters have been quantified, the relationship between parameters can be investigated to determine whether charge generation factors are in competition (i.e., less charge generated) or working together (i.e., more charge generated). Electrostatic charging is more prominent in fluidized beds containing particles that are of materials which are electrically non-conductive (Tardos and Pfeffer, 1980).

Particle-particle interactions would likely result in almost equal quantities of positively and negatively charged particles within a fluidized bed; thus, resulting in a net zero charge. However, particle-wall interactions likely result in one polarity predominately being gained by the particles, and the opposite resulting on the column wall (Mountain et al., 2001). Likely wall effects contribute to a net charge observed on particles of consistently the same polarity.

During fluidization two main types of contacting contribute to the charge generation within the bed: particle-particle and particle-wall. While both triboelectrification and frictional charging can take place with either type of contacting, typically one is the dominant mechanism during each type of interaction. During particle-particle contacts triboelectrification is predominant, while frictional charging is the prime mechanism during particle-wall contacts. This can also be related to the fluidization flow regime. During bubbling flow, with its vigorous mixing, many particle-particle contacts take place, while particle-wall contacts do still take place in this regime it is at a smaller frequency in comparison to the quantity of particle-particle contacts. Thus in the bubbling flow regime triboelectrification is the predominant charging mechanism. During slugging flow, the majority of movement is in the axial direction as the slugs move up through the column. This results in more particle-wall contacts than particle-particle contacts; thus frictional charging is the predominant mechanism in this flow regime.

1.1.4. Electrostatic Charge Measurement Techniques

There are two main methods of measuring electrostatic charge: electrostatic probes and Faraday cups. This section will detail how both methods work and how they can be applied to fluidized beds.

1.1.4.1. Electrostatic Probe

Electrostatic probes are an indirect method of measuring electrostatic charge. The probe consists of a conductive metallic interior, surrounded by an insulator which is then covered by a metallic sheath. The metallic interior is connected to an electrometer while the metallic exterior is connected to ground, to act as a shield to prevent the measurement of additional electric fields. The measurement of electrostatic charge takes place when the tip of the probe detects an electric field generated by a passing charged object (Figure 1-6a). The real charge, transmitted by the electric field, induces an image of itself on the conducting surface. This allows for measurement of the real charge by the electrometer.

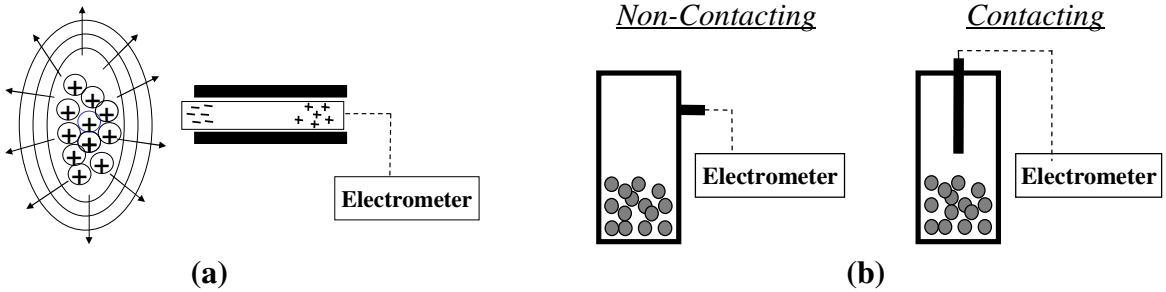

Figure 1-6: Electrostatic probe: (a) Electric field measurement, (b) Types of probe insertion into a fluidized bed.

This type of probe has been used within fluidized beds as either a contacting, or a non-contacting probe (Figure 1-6b). Contacting probes are generally placed inside the column by hanging in the middle or mounted on the reactor wall. In this case, the fluidizing particles within the reactor can contact the probe; thus, the probe measures charge by both induction and contact charging. Non-contacting probes are typically located on the fluidization column wall where the tip of the probe is covered by the wall material. This prevents actual particle-

probe contacts. Examples of both applications are presented in Figure 1-7: a contacting probe used by Cibrowski and Woldarski (1962) and a non-contacting probe used by Boland and Geldart (1971/1972).

Electrostatic probes typically measure either current or voltage, and provide a cumulative measurement of potential throughout fluidization. Since such probes can only measure charges near the probe tip, they only provide a local measurement within the bed. This provides a picture of what is happening only at that one location. Additionally, as electrostatic charges build-up within the bed, particles begin adhering to the tip of the probe, reducing the accuracy of the measurement (Fujino et al., 1985).

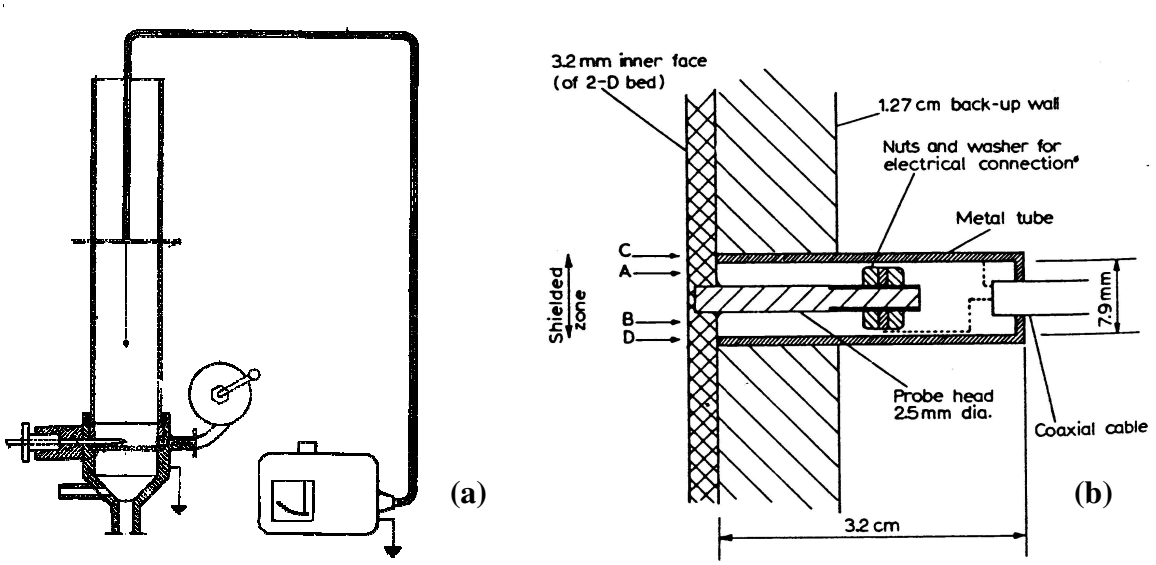

Figure 1-7: Application of electrostatic probe in gas-solid fluidized beds: (a) Contacting probe (Adapted from Cibrowski and Woldarski, 1962)**, and (b) Non-contacting probe** (Adapted from Boland and Geldart, 1971/1972)**.**

1.1.4.2. Faraday Cup

Faraday cups are a method of directly measuring charge. A Faraday cup consist of two concentric cups made of a conducting material (Figure 1-8). The outer cup is slightly larger, and is grounded to act as an electrical shield preventing any extraneous electric fields from affecting the measurement. The inner cup is directly attached to an electrometer for charge

measurement. The two cups are separated from each other by an insulator. When a charged object, such as a powder, is lowered into the inner Faraday cup, the field due to the charge on the particle redistributes the electrons on the wall of the inner cup by either attracting or repulsing the electrons, resulting in equal and opposite charges induced on the inner Faraday cup as seen in Figure 1-8. The induced charge is then measured by the electrometer providing the net charge on the object.

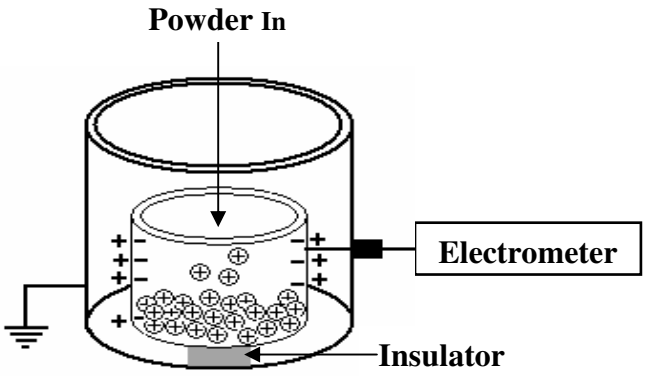

Figure 1-8: Schematic of Faraday cup operation.

Some typical applications of Faraday cups in gas-solid fluidized reactors for measuring charge are presented in Figure 1-9. Fasso et al. (1982) had a sampling port on the side of the reactor that allowed for measurement of charges on individual particles or small quantities of particles forced out of the column and into the Faraday cup. Bartilucci et al. (2003) converted the product discharge tank of the reactor into a Faraday drum to measure the charge of particles as they reached the desired production conditions. Ali et al. (1998) poured particles removed from the fluidized bed into a network of Faraday cups (Figure 1-9 c1) using a specially designed scooper (Figure 1-9 c2) that would remove repeatable quantities of particles from the bed. Overall, with most methods involving Faraday cups previously reported in literature (Ali et al., 1998; Bartilucci et al., 1982; Fasso et al., 1982; Tardos and Pfeffer, 1980; Wolny and Opaliński, 1983), the applications resulted in a local measurement of net charge since they only measured the charge of particles in a specific location. Additionally, as can be seen with examples shown in Figure 1-9, and others, due to handling of particles in piping or tubing prior to their arrival into the Faraday cup for the

charge measurement, additional charges can be generated or dissipated, affecting the actual charge that would be found on particles inside the fluidized bed.

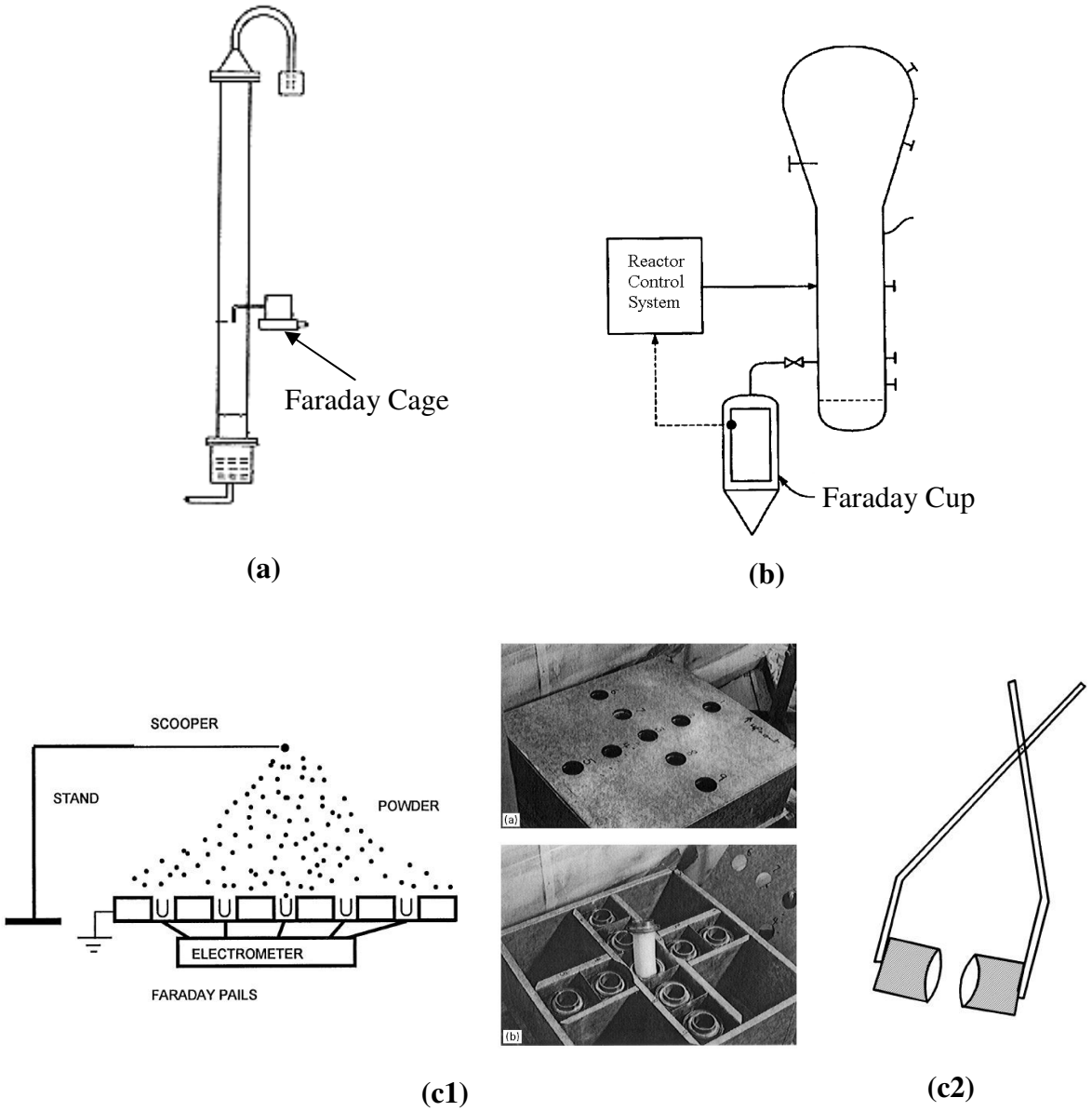

Figure 1-9: Applications of a Faraday cup in gas-solid fluidized beds.
(a) Adapted from Fasso et al. (1982) **(b)** Adapted from Bartilucci et al. (1982) **(c)** Adapted from Ali et al. (1998): 1. Faraday cup grid; 2. Scopper.

1.1.5. Parameters Influencing Electrostatic Phenomenon in Gas-Solid Fluidized Beds

In gas-solid fluidized beds, various parameters may contribute to the generation or dissipation of electrostatic charges and influence the dominating mechanisms involved. They include: **(a)** bed hydrodynamics (fluidizing gas velocity and particle size); **(b)** system operating conditions (fluidization time period, fluidizing gas relative humidity, pressure and temperature); and **(c)** materials involved (fluidizing particle type and column material). In order to develop a novel approach and to understand some of the theories that have been postulated to explain charge generation in gas-solid fluidized beds, a literature review was conducted. The following sections provide background on previous work that has been carried out in relation to three main operating conditions that are a focus of this thesis: fluidization time, column wall material, and fluidizing gas relative humidity.

1.1.5.1. Fluidization Time

Of particular interest is the effect of extending the residence time of particles within the reactor by increasing the duration of fluidization. With extended fluidization times, particle-particle and particle-wall contacts increase, which could influence the electrostatic charge generation. It is possible that a limit of charge generation exists but what causes such charge saturation or the effects it would have on the rest of the bed is unknown. Additionally in the case of sheeting, increased fluidization time may influence the formation and the growth of the particle layer that builds on the reactor wall. It is still unknown as to when particle sheets form following the onset of fluidization, how they change during the fluidization period (e.g., particle layer growth over time), and what the charging mechanism is behind layer formation.

Table 1-3 summarizes the previous studies that have reported on the relationship between electrostatic charge generation and fluidization time. Charge saturation has been observed in all of the previous studies over a range of times for different measurement techniques, fluidization particles, and fluidization column wall materials. Both Ali et al. (1999), using

polyamide in a steel column and Murtomaa et al. (2003), using glass beads in a glass column, observed the shortest times required to reach charge saturation of about 2-5 min. In contrast, Rojo et al. (1986) observed that in an acrylic column with glass beads charge saturation could take anywhere from 10 to 100 min, which was the longest time reported to reach charge saturation. Other studies measured saturation times of between 5 to 20 min (Guardiola et al. 1992; Kisel'nikov et al., 1967; Wolny and Kazmierczak), 20 to 40 min (Ciborowski and Wlodarski, 1962), and 40 to 60 min (Fujino et al., 1985). Two studies measured charge saturation at 60 min: Revel et al. (2003) with polyethylene particles in an acrylic column and Wolny and Opalinski (1983) with polystyrene particles in an acrylic column.

Table 1-3: Previous studies on the effect of fluidization time on electrostatic charge generation in fluidized beds.

Authors	Year	Measurement Technique	Particle Type	Particle Size (μm)	Column Material	Charge Saturation Time (min)
Ali et al.	1999	Faraday Cup	Polyamide	98	Steel	2-5
Ciborowski and Wlodarski	1962	Electrostatic Probe	Sand, Polystyrol, Vinyl Polyacetate	490-750	Glass	20-40
Fujino et al.	1985	Electrostatic Probe	Glass Beads	200, 250, 400-500	Acrylic	40-60
Guardiola et al.	1992	Electrostatic Probe	Glass Beads	500-590	Acrylic	5-20
Kisel'nikov et al.	1967	Electrostatic Probe	Polymeric Resins, Polyacrylonitrile, Ammonium Sulfate	n/a	Metal	20
Murtomaa et al.	2003	Ring Probe	Glass Beads	1130	Glass	5
Revel et al.	2003	Faraday Cup	Polyethylene	801	Acrylic	60
Rojo et al.	1986	Electrostatic Probe	Glass Beads	350-420	Acrylic	10-100
Wolny and Kazmierczak	1989	Capacitor	Polystrene	475	Glass	15
Wolny and Opalinski	1983	Faraday Cup	Polystrene	1020-1200	Acrylic	60

Two main techniques were used in previous work for measuring electrostatic charge: electrostatic probes and Faraday cups. Electrostatic probes were used in some of the studies to monitor the electrical potential within the bed. These studies found, through investigation of other parameters, that charge stabilization occurred within the bed with fluidization times ranging from 5 to 60 minutes. However, the use of an electrostatic probe is known to have reduced accuracy due to particle adhesion on the tip of the probe, causing potentials lower

than the true potential to be measured (Fujino et al., 1985). Moreover, the configuration of the probe connection to the voltmeter and the placement of the probe in the bed affect the length of fluidization time required to reach charge saturation (Rojo et al., 1986). In comparison, other works have used Faraday cups to measure charge during fluidization and have measured charge stabilization in a range of 2-5 minutes, and up to 60 minutes. In these studies the particles were removed from the bed during fluidization for charge measurement, which could have resulted in additional charging due to particle handling. As well, all studies, whether using the electrostatic probe or a Faraday cup, only took local measurements of the charge, which may not be representative of the net bulk charge of the bed.

In the majority of the previous studies, fluidization was conducted in columns made of glass or acrylic. These materials are far removed from those of industry which uses carbon steel reactors (or stainless steel in pilot scale operations); thus the mechanism of charge generation may differ. Few studies have been performed in metallic columns. Ali et al. (1999) used a steel column of a square geometry and found that the charge reached saturation within a few minutes and stayed stable for 72 hours. Kisel'nikov et al. (1967) provided neither column dimensions nor the type of metal used but found electrostatic potential levelled out in 20 minutes. Studies summarized in Table 1-3 utilized a variety of fluidizing particles of different sizes in their investigation. In only one study, conducted by Revel et al. (2003) using an acrylic column, were polyethylene particles used. They determined that charge saturation occurred at 60 minutes and that the particle layer began to develop shortly after the onset of fluidization.

Only a limited number of studies have been reported in literature that specifically investigate the fluidization period. Murtomaa et al. (2003) investigated the effect of fluidization time on electrostatic charge generation using a small acrylic column (outer diameter of 30 mm, height of 240 mm) with glass beads ($dp_{0.5}$ = 1130 μm). A ring probe was used to measure the induced charge in the column, 85 mm from the bottom of the bed. It was determined that a charge plateau was reached after 5 minutes. Ciboroswki and Wlodarski (1962) measured electrode potential within a Rasotherm glass fluidized bed (inner diameter of 60 mm, height of 555 mm) using particles of three different materials (Vinyl Polyacetate, Polystyrol, and

Sand) with size ranges of 49-75μm. The electrode potential was measured with a platinum wire ending in a small ball suspended in the centre of the fluidized bed. After the stabilization of gas velocity and humidity, the electrode potential reached a plateau after approximately 20-30 minutes of fluidization. These works suggest that an "equilibrium" of charge may be reached at some time during fluidization. However, all of these previously mentioned works measured the charge of the particles within the bed during fluidization and did not delve into the effect of time on the charge distribution within different regions of the bed and more importantly the formation of reactor wall fouling.

1.1.5.2. Fluidization Column Material

Collisions between particles and the reactor wall has been identified as a source of charge generation within gas-solid fluidized beds, and the amount of charge generated seems to be dependent on particle velocity, angle of contact, and the amount of pre-charging on both the particle and the column wall (Bi, 2005). Different materials tend to charge differently, suggesting that by altering the material of the reactor wall, the amount or polarity of charge generated may change. However, few studies have been performed to compare the results (Table 1-4).

Table 1-4: Previous studies on the effect of column wall material on electrostatic charge generation in fluidized beds.

Authors	Year	Electrostatic Measurement	Particle Type	Particle Size (μm)	Column Material
Boland & Geldart	1971/ 1972	Electrostatic Probe	Lead glass ballotini	100-800	Perspex Glass "Protectafilm"-lined walls
Ally & Klinzing	1985	Nickel Electrodes	Copper, Glass, Plexiglas	196; 75, 150, 314; 145	Copper Plexiglas Glass
Matsusaka et al.	2006	E-SPART	Alumina	3.3	Stainless Steel (316 & 304), Aluminum, Copper, Brass

Boland and Geldart (1971/1972) compared glass, Perspex, and "Protectafilm" lined columns; they found that the glass and "Protectafilm" resulted in less particle-wall attraction than the Perspex column. As the charging that each system endured was similar, it was suggested that the difference in attraction was due to surface conductivity. Perspex had the lowest surface conductivity and it experienced the least charge leakage. Additionally, it was suggested that the humid fluidization gas used in the experiments also influenced attraction due to differences in water affinity between column materials. The higher affinity of glass and "Protectafilm" for water may have lead to sufficient deposition of water molecules to promote charge dissipation.

The other two studies investigated charge generation during pneumatic charging. Ally and Klinzing (1985) looked at three different types of tubes (i.e., Copper, Glass, and Plexiglas) with copper, glass and Plexiglas particles. A base point pressure drop was evaluated at a fluidizing gas relative humidity where no electrostatic effects were observed ($\underset{\sim}{}$75%). At lower humidities any additional pressure drop was assumed to be due to electrostatic effects, which was indicative of overall energy consumption. The pressure drop in the system suggested that the glass/copper systems, where if the particles were glass and the tube was copper or vice versa, had the largest electrostatic effects while Plexiglas/copper systems experienced the least effects; a copper/copper system was not tested. It was suggested that these interactions were based on the ability of the material to release electrons where copper had the greatest ability and glass had the least. The charge-to-mass ratio (q/m) for each system was measured; however, the authors suggested that since the fluidization gas in each trial had different moisture contents, the charge results may not have been comparable. It was noted that pressure drop followed the same pattern as the q/m with the exception of the crushed glass particles in the copper tube likely due to the irregular shape of the crushed particles that may have prevented full drainage of charge from the particles.

Matsusaka et al. (2006) was able to measure charge with their system of five different pipes (i.e., Stainless steel 306, Stainless steel 316, Brass, Copper, and Aluminum) and alumina particles. They found that the stainless steel pipes, both 306 and 316, charged the alumina positively while the brass, copper, and aluminum resulted in negatively charged alumina. They also found that as the pipe length increased, charge saturation was reached, which

suggested that there was a maximum charge that could be transferred between the pipe and the particles. The lowest magnitude of charge on the particles was measured for the aluminum tube while similar quantities were measured with the rest of the materials.

There is little data on how the fluidization column material influences charge generation throughout the bed or how it impacts the development of particle wall fouling in a gas-solid fluidized bed. Thus, a comprehensive study in this area is required.

1.1.5.3. Fluidizing Gas Relative Humidity (RH)

In previous works reported in literature, high relative humidity of the fluidizing gas has been studied as a technique to control bed electrification (Table 1-5). In these studies, a variety of particle sizes, particle types, and column materials were used with respect to different fluidizing gas humidity. Additionally, all of these studies evaluated the effect of relative humidity in different terms, making comparison between studies very difficult.

Table 1-5: Previous studies on the effect of relative humidity on electrostatic charge generation in fluidized beds.

Authors	Year	Electrostatic Measurement	Particle Type	Particle Size (μm)	Column Material	Relative Humidity (%)
Bafrnec and Bena	1972	Ball Probe	Glass ballotini	170-210	Metal	30-65
Baron et al.	1987	No direct measurement of electrostatic charge.	Silica Sand	82	Carbon steel	7-60
Boland and Geldart	1971/ 1972	Electrostatic Probe	Lead glass ballotini	100-800	Perspex or Glass	15-80
Chen et al.	2003	Ball Probe	Glass Beads	321	Plexiglas	6-98
Ciborowski and Wlodarski	1962	Ball Probe	Vinylpolyacetate polystyrol, sand	490-750 400-490 300-400	Glass	0-12*
Fujino et al.	1985	Ball Probe	Glass beads, neobeads, PMMA	200 250 540	Perspex or Steel	10-65
Guardiola et al.	1992	Ball Probe	Glass ballotini, steel	500-590 420-500	Perspex	5-40
Guardiola et al.	1996	Ball Probe	Glass Ballotini	250-297 297-350 350-420	Perspex	5-70
Katz and Sears	1969	Upper electrode	Glass Beads	250-297	Plastic or Glass	0-25
Kisel'nikov et al.	1967	Ball Probe	Hydroquinone, polyarcylonitrile, ammonium sulfate	-	Plexiglas	4-11.51
Mehrani et al.	2007	Faraday Cup	Glass Beads, Polyethylene	450-752 500-600 38-876	Copper	0-60
Park et al.	2002	Ball Probe	Glass Beads, Polyethylene	321, 378	Plexiglas	6-98
Tardos and Pfeffer	1980	Ball Probe & Faraday Cup	Porcelain	2000	Plastic	20-42
Wolny and Kazmierczak	1989	Capacitor	Polystrene (Fines: aluminium (0.1-15um); NaCl (1-60um))	475	Glass	0-70
Yao et al.	2002	Ball Probe	Polyethylene	378, 318	Plexiglas	6-98

* g of water /kg of particles

Several studies used voltage potential to measure the effect of relative humidity. Bafrnec and Bena (1972) found that at relative humidities of 60 or 65%, the voltage potential reached a minimum which was explained by a higher surface conductivity. Ciborowski and Wlodarski (1962) measured the bed potential as the gas relative humidity was decreased from a maximum value. The electrode potential increased with decreasing relative humidity until a certain point and then a rapid decrease in potential was observed with continuous decreasing in relative humidity. The point of change was different for different particle materials. When the relative humidity was at the maximum electrode potential, particles began to form a non-uniform layer on the column wall; however as the relative humidity decreased the layer became more uniform and more stable. Water vapour was theorized to absorb on the column wall lowering its surface resistance (or increasing the surface conductivity) which would have in turn lowered the bed potential.

Fujino et al. (1985) used glass beads and PMMA particles in a Perspex column. They observed that as relative humidity increased, the potential in the centre of the bed decreased for glass beads, assuming that the rates of formation and dissipation of the charge also increased. If there was more charge dissipated than generated, the potential would have decreased with increasing relative humidity. However, with PMMA particles, the potential increased with increasing RH. Therefore, it was concluded that the effect of relative humidity was dependent on the type of particles involved. For both sets of particles, there was no dependence of q/m on relative humidity.

Guardiola et al. (1996) broke up the response of potential within the bed to relative humidity into five zones (Figure 1-10). For low values of relative humidity up to a critical value (RH_C) particles adhered to the column wall and the probe, hindering accurate measurement of electric potential. After that critical relative humidity, increasing relative humidities produced little or no effect on charge, and no particles were adhered to the column wall or the probe. At a certain point, the degree of bed electrification was again affected by relative humidity resulting in declines in measured charge and no particle layer observed on the column wall. For relative humidities greater than RH_{MAX}, there was no observed charge generation. Finally, above RH_T, the highest relative humidities (>85% for this system), the

high water content prevented particles from fluidizing due to increased cohesion between particles. This break up in zone resulted in a characteristic curve that could possibly be used for other materials with different relative humidity values (i.e., different values of RH_C, $RH_{MAX,}$ and RH_T) signalling the change between zones. However, it was postulated that this type of result may only be valid for hydrophilic materials and may not be true for hydrophobic material such as polyethylene. The authors did not indicate the RH values except that of the $RH_T = 85\%$.

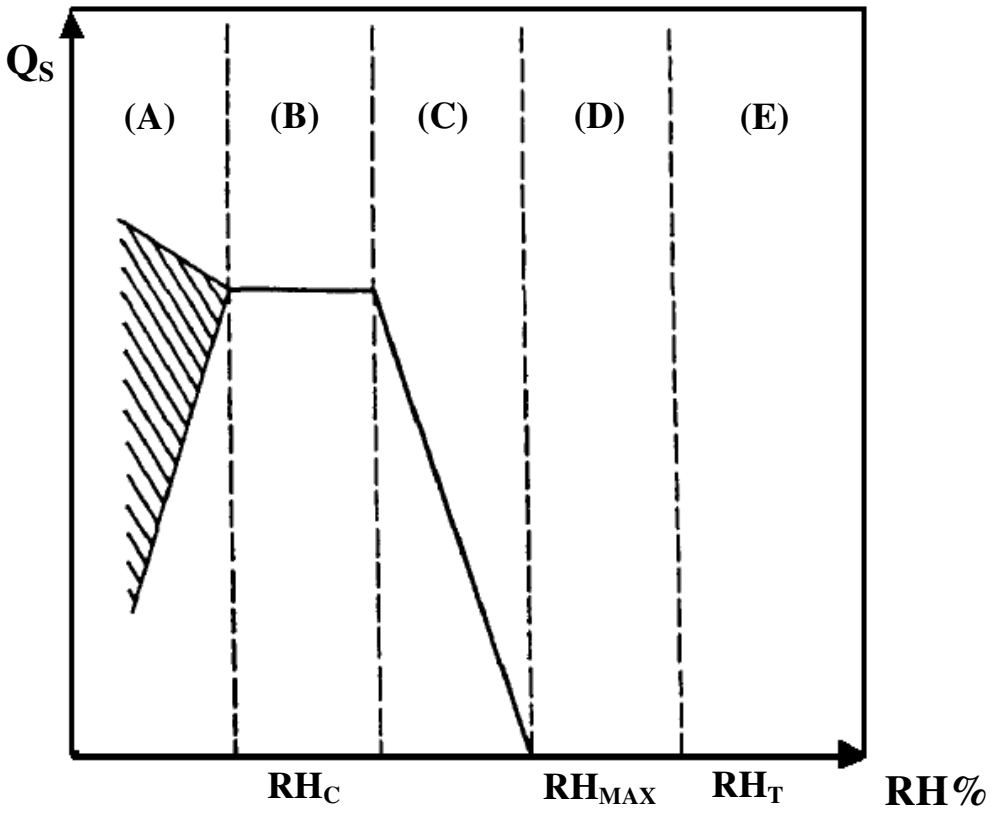

Figure 1-10: Characteristic curve for the variation in charge on capacitance plates due to relative humidity (Adapted from Guardiola et al., 1996).

Kisel'nikov et al. (1967), using a Plexiglas column, found that higher gas relative humidity resulted in a greater measured electrode potential and more deviation in measured charge from the bottom and top of the bed to the middle of the bed. Results were presented for ammonium sulfate and no mention was made whether this observation was solely for these particles or for all particles tested.

Voltage potential and charge measurements by a ball probe were used in conjunction in Park et al. (2002b) where glass beads (321 μm) and polyethylene (378 μm) were used in a glass column. In their 2-D bed the overall trend due to increasing relative humidity was a decrease in maximum voltage, maximum charge, and transferred charge. In their 3-D bed the increase in relative humidity resulted in a decrease in the magnitudes of recorded maximum and minimum voltages as well as a decrease in the magnitudes of charge transfer and maximum charge. As for the difference between the glass beads and polyethylene particles, they indicated that the porous structure of polyethylene may have been responsible for the higher reduction in magnitude of the measured variables than the glass beads with increasing relative humidity.

In several studies, charge was measured and presented either as charge, charge-to-mass ratio, or specific charge in the evaluation of the effect of relative humidity. Boland and Geldart (1971/1972) studied relative humidity in Perspex or Glass columns with lead ballotini particles. It was found that as relative humidity increased from 15 to 60% the charge measured by the electrostatic probe increased; however further increases from 60 to 80% resulted in a decrease in the measurement. Relative humidity did not affect charge generation between 60 and 70%, but did promote charge dissipation due to a decrease in bed resistivity which occurred around 60% RH. Resistivity was measured using a conductivity cell immersed in the bed and measurements of current flow were taken as the fluidization gas relative humidity was increased.

Chen et al. (2003) simulated the effect of relative humidity on charge transfer and charge induction in a Plexiglas column with glass beads. At relative humidities less than 80%, the permittivity (i.e., the speed at which an electric signal can be transmitted through a material) and conductivity of the beads increased slightly; however at humidities greater than 80% the permittivity and conductivity increased significantly due to a water film formed on the particles. These conclusions were based on data for conductivity and permittivity obtained from Boland and Geldart (1971/1972) and Chen and Jin (1992), respectively. At relative humidities less than 50%, the specific charge and specific charge-to-permittivity decreased with increasing relative humidities due to enhanced charge dissipation as relative humidity increases.

Mehrani et al. (2007) used large glass beads and polyethylene particles (~ 500 μm) with smaller particles (~ 40 μm) to create binary mixtures of coarse and fine particles. In their study, with increased relative humidity the cumulative charge measured on the entrained fines decreased in the system with glass beads mixture. With the polyethylene mixture, the q/m of the entrained fine decreased, while the number of particles adhered to the column wall also decreased as relative humidity increased.

Tardos and Pfeffer (1980) used porcelain particles in a glass column. Their work concluded that the relative humidities of 20-25% resulted in lower surface charges (q/surface area) than those measured between 36-42%. Additionally, lower current was measured at the higher relative humidity values.

Wolny and Kazmierczak (1989) used polystyrene and NaCl particles in a glass column. As relative humidity increased, elutriation of finer particles was easier and interparticle attraction decreased. The distribution of q/m shifted towards zero as relative humidity increased. Therefore, it was found that 70% relative humidity was best for reducing electrostatic charge as particle agglomeration and hydrodynamic disturbances were eliminated.

Katz and Sears (1969) used a plastic or glass column with fluidization particles of glass beads. Stabilization, or non-movement of particles at high gas flow rates, of the bed was achieved with an electric field. As moisture was introduced, the amount of stabilization decreased which suggested that the moisture disrupted the electric field within the bed.

Other methods of measuring the effect of relative humidity have been used such as the flux of elutriated fines, deviation of pressure fluctuations, and stabilization of particles. Baron et al. (1987) studied how relative humidity influenced the entrainment of finer particles. Silica sand particles were fluidized in a carbon steel column with three Plexiglas freeboard sections and two carbon steel sections above the transport disengagement height. The flux of particles out of the bed increased by a factor of 2 between 7 to 30% RH, after this point there was a plateau and no further increase in flux was observed with the continuous increase in relative humidity.

Yao et al. (2002) used polyethylene particles in a Plexiglas column. Standard deviations of voltage measurements and pressure fluctuations decreased with increasing relative humidity indicating that charge induction/transfer properties and hydrodynamics were changing. The decrease in standard deviation of pressure fluctuations with increasing relative humidity indicated that bubble size may have decreased with increasing relative humidity leading to smaller standard deviations of voltage.

The particle sizes tested previously mostly had narrow size distributions. However, in industrial reactors, particles of wide size range may be present which may affect the magnitude and polarity of net charges generated. Bipolar charging due to differences in particle size has been previously observed in fluidized beds (Ali et al., 1998; Cartwright et al. 1985; Inculet et al., 2006; Park et al., 2002a; Singh and Hearn, 1985; Zhao, 2002). As a result in commercial reactors containing particles of the wide size range bipolar charging may be more prevalent, affecting the net charge within the bed and the development of agglomerates or wall fouling.

The types of particles used in previous research have been wide-ranging; however, most authors have focused on glass beads and only a few have looked at polyethylene. The nature of a certain material may influence how it reacts with moisture. A common theory is that a film of moisture may surround a particle resulting in an increased surface conductivity leading to reduced charge generation (Bafrnec and Bena, 1972; Boland and Geldart, 1971/1972; Chen et al., 2003; Ciborowski and Wlodarski, 1962). However, whether the material is hydrophobic or hydrophilic would dictate how readily a water film is formed. For example, glass beads are hydrophilic and polyethylene is hydrophobic (Güleç et al., 2006) so each material has a different affinity for water vapour leading to different capabilities for water film formation. Additionally, the difference in particles structure, porosity and sphericity, may also impact the magnitude of charge generation and or dissipation (Park et al., 2002b).

In addition, the majority of previous studies have been conducted in Plexiglas or Glass columns with only a few using metallic reactors. Only one of the previous works combined polyethylene and a metallic column made of copper (Mehrani et al., 2007), but their

experimental trials were conducted with a binary bed with finer materials of different composition, and their system was only able to measure the charge on entrained fines rather than the net charge generated inside the bed. Since the column wall also interacts with the humid fluidization gas and the fluidizing particles during particle-wall contacting, the material composition of the column could influence the effect of relative humidity on the charge within the bed. A high or low affinity for water may result in different charge dissipation rates along the wall if a moisture layer were to form on either the column wall or the particles surface. Thus, it is important to study how a metallic column reacts to changes in relative humidity as it more closely mimics industrial conditions.

None of these previous studies have investigated how relative humidity affects the charging behaviour of different regions of the bed simultaneously. Most of the previous work was conducted as local measurements on either the bulk particles or fines elutriated from the bed, but none have investigated both regions concurrently and their relationship with one another.

A comprehensive study of how relative humidity affects charge generation is essential to understand the role of moisture as a possible charge reduction technique. By investigating the impact of changing fluidizing gas relative humidity on the particles charging behaviour throughout different regions of the bed, a full picture of the system can be developed. Furthermore, how relative humidity influences wall fouling in a metallic column is a significant aspect to be studied since the development of sheets within polymerization reactors is one of the major problems of electrostatic phenomena.

1.2. Thesis Objectives

Ultimately, research into electrostatic charge generation in gas-solid fluidized beds has one main purpose: identify a technique to either reduce or eliminate this phenomenon. However, a reliable technique cannot be developed until the mechanisms, and the influencing parameters are fully understood. By developing an understanding of contributing factors and possible reduction techniques, novel methods can be targeted specifically to reduce or eliminate those factors that contribute the most towards charge generation.

Previously in this research group, a novel online electrostatic charge measurement technique has been developed, which is first of its type as it is able to determine the charge distribution in different regions of the fluidized bed simultaneously. Most importantly it can help provide insight into the particle reactor wall fouling that is of great importance to industries such as petrochemical, suffering from such phenomenon for many years. The measurement technique is specifically capable of concurrently measuring the electrostatic charge on particles in the bulk of the bed, those adhered to the column wall and those entrained throughout the fluidization period. This novel technique has been successfully implemented in an atmospheric pilot-scale system (Sowinski et al., 2009, 2010). Therefore, it is of great interest to examine some of the parameters that affect the bed electrification by using this system with an overall focus related to the petrochemical industry. By isolating specific parameters, an intensive investigation of the effects of each parameter can be conducted. Charge distribution in various areas of the fluidization column can be measured and related to the particles residence time inside the bed. In particular, this will provide insightful information about the effect of each parameter on particle charging and the amount of particle-wall adhesion. Particle wall fouling is a significant problem in the polymerization industry, but the parameters influencing its buildup have not been previously isolated and investigated with respect to charge distribution within the reactor.

The goal of this thesis was to investigate the effects of three specific parameters chosen for focus with respect to charge generation in gas-solid fluidized beds. They include:

- Fluidization time
- Fluidization column wall material
- Fluidizing gas relative humidity

Fluidization time was chosen to investigate the progress of, (a) charge generation and distribution, as well as whether a maximum amount of charge could be generated inside the fluidized bed, and (b) reactor wall fouling. The impact of column wall material was chosen since the majority of academic research is focused on Plexiglas or glass columns while industry uses stainless steel for pilot-scale units and carbon steel for commercial reactors. Understanding the similarities and differences between these materials is essential for effective development and testing of the reduction and elimination techniques developed in

lab or pilot scale reactors. Finally, the fluidizing gas relative humidity was chosen since it has been identified as a possible charge reduction technique, but its direct influence on the reduction of reactor wall fouling has not been directly investigated and is not well understood.

All experimental work was conducted with specific reference to a polymerization process. Polyethylene resins, received directly from commercial reactors, were fluidized in a metal fluidization column, to more closely replicate industrial conditions, in a non-polymerizing environment. An online Faraday cup measurement technique was applied so no additional contact between particles and equipment through handling was experienced. Overall, the effect of fluidization time, column wall material, and gas relative humidity on charge generation and distribution was investigated in both the bubbling and the slugging fluidization flow regimes. The particles charge, mass and size distribution were measured in three key areas of the bed: the bulk particles, elutriated fines, and particles adhered to the column wall. Finally, it is important to note that no previous study, except those recently conducted in this research group, have investigated the effect of above mentioned parameters in different fluidization flow regimes. As indicated in previous sections, different charging mechanisms are predominant in different regimes; thus, bed hydrodynamics affects the bed electrification behaviour and should be considered while examining the effect of different operating parameters. Overall, this work is the first of its type in this area.

1.3. Thesis Outline

The following chapters will cover the experimental procedure and apparatus, parameters investigated, resulting conclusions, and proposed future work. Charge generation during fluidization was investigated for three parameters: fluidization time, fluidization column material, and fluidization gas relative humidity.

The second chapter describes the experimental apparatus, materials and measurement equipments that were used to conduct the experimental trials. This chapter's focus will be on

the fluidization system along with its operating procedure, and the fluidization gas and particles with their relevant properties.

The third chapter presents the results of the effect of fluidization time. This chapter details the results from six different fluidization times for four different gas velocities in two different flow regimes (bubbling and slugging). Results comparison is made based on fluidization times within each gas velocity, flow regime and overall.

The fourth chapter focuses on results obtained for the effect of fluidization column wall material. Results are presented for two different column materials for two gas velocities in the bubbling and slugging flow regimes. Comparison is made between column materials for each gas velocity.

The fifth chapter details experimental results from the effect of fluidization gas relative humidity. Five different relative humidities were evaluated for four different gas velocities in the bubbling and slugging flow regimes. Comparison of results is made for each individual velocity, for each flow regime, and overall.

The final chapter of this thesis focuses on the conclusions that resulted from each parameter tested and overall conclusions on how charging occurs in gas-solid fluidized beds. It also discusses future recommendations to expand knowledge of this phenomenon. Additional information and experimental results can be found in the appendices.

Chapter 2. Experimental Apparatus and Method

This chapter describes the experimental apparatus and procedure, and materials used in this work.

2.1. Experimental Apparatus

The overall schematic of the experimental setup is presented in Figure 2-1a, with a picture of the complete system shown in Figure 2-2. The system consisted of a 3-D fluidization column equipped with an online electrostatic charge measurement technique, a humidification system, a dryer, and a number of different measurement instruments. The fluidization system itself, as shown in Figure 2-1b, consisted of a cylindrical stainless steel column, two copper Faraday cups, located at the top and the bottom of the column, and a retractable distributor plate.

The fluidization column was 0.1 m in diameter and 1.27 m in height. On the side of the column were 5 instrumentation ports, with 11 additional plugged ports for future use if desired. For the majority of trials in this work a stainless steel 316 column was used. For the experiments comparing column material, an additional column fabricated of carbon steel was evaluated.

The same electrostatic charge measurement technique that was previously developed in this research group (Sowinski et al., 2009, 2010) was utilized in this work. The method was an online Faraday cup technique where the fluidization column was fitted with two Faraday cups; one at the top and one at the bottom. Both Faraday cups consisted of two concentric cups made of highly electrically conductive material (copper) with the outer cups grounded and acting as an electrical shield and the inner cups connected to a digital electrometer to measure the charge of the particles placed inside the cups. The inner cups of both the top and bottom cups, which were isolated from the outer cups using Teflon connectors, were

attached to a Keithley digital electrometer (Ohio, USA; Model 6514) for charge measurement. The outer cup of the bottom Faraday cup also acted as the windbox for the fluidization column.

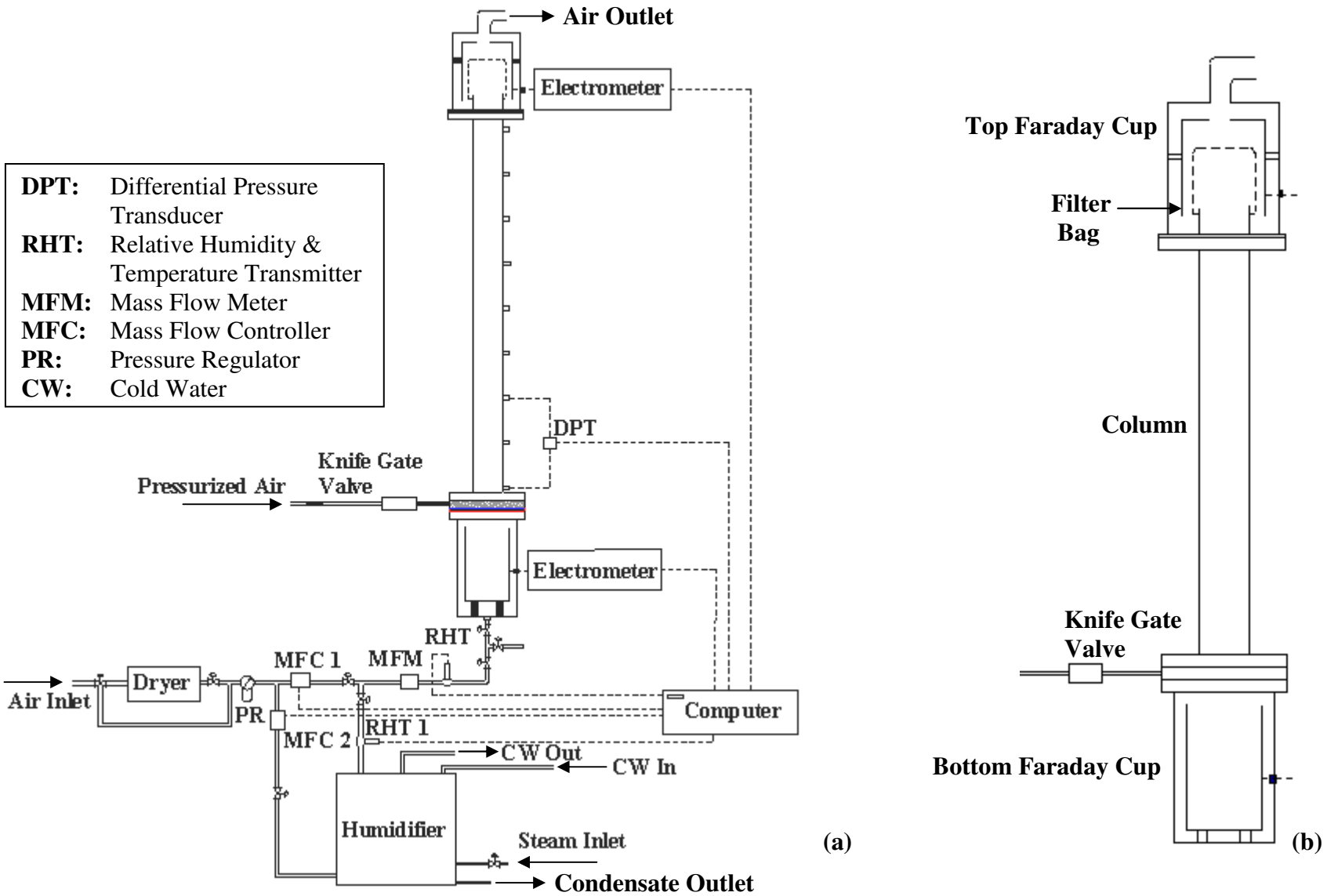

Figure 2-1: Experimental set-up: (a) Overall system schematic, and (b) Fluidization column with Faraday cups.

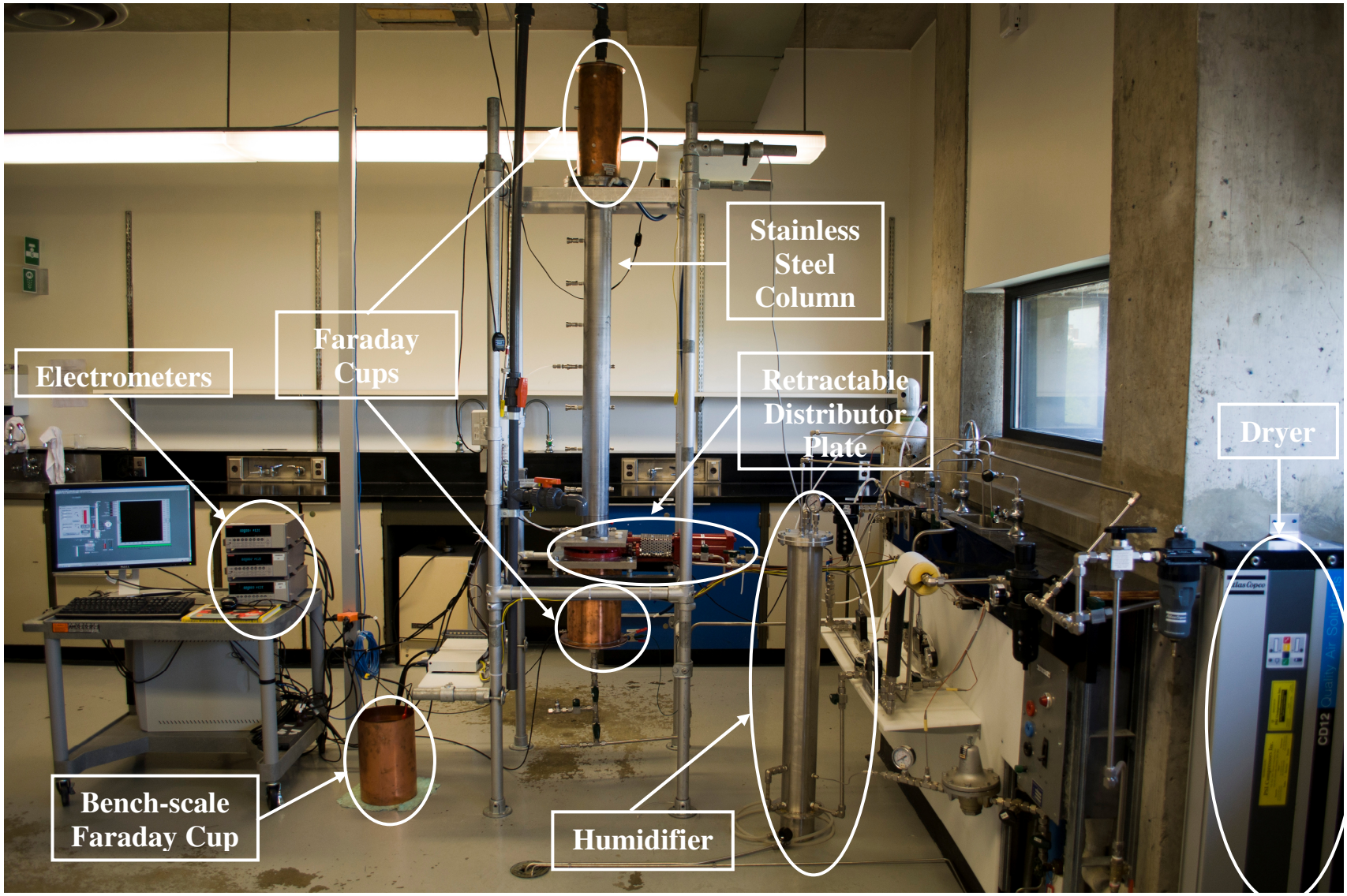

Figure 2-2: Image of the complete experimental system.

For the bottom Faraday cup, the outer cup was 0.2 m in diameter and 0.38 m in height, while the inner cup was 0.15 m in diameter and 0.25 m in height. For the top Faraday cup, the outer cup was 0.15 m in diameter and 0.41 m in height, and the inner cup was 0.13 m in diameter and 0.36 m in height. The top Faraday cup was inverted and placed on the top of the column to measure the cumulative charge of the finer particles that were elutriated during fluidization. In order to capture the entrained particles within the Faraday cup for charge measurement, a filter bag filled with dust-luck filters (provided by BC Air Filter with 26-30% dust capture efficiency of 1 μm particulates) was placed inside the inner cup. This also allowed for the measurement of the fine particles mass as the mass of the filter bag and its contents were recorded before and after fluidization.

Electrostatic charge measurements were conducted by a Keithley digital electrometer (Model 6514). Four different measurement ranges were available with this unit: 20 nC, 200 nC, 2 μC, 20 μC; for most charge measurements, a range of 2 μC was used. However, when large quantities of mass were collected inside Faraday cups a range of 20 μC was used. Both the 2 and 20 μC ranges had an accuracy of ±1 + 50 (%rdg + counts), where error was a combination of gain error (1) and offset error (50) which was defined as counts of the least significant digit.

The distributor plate was a modified knife gate valve (Red Valve Company, Inc.; Series G). The blade of the valve was perforated with 2 mm holes to create a porous distributor plate. To prevent particles with diameters less than 2 mm from falling through the pores, a 32 μm mesh was fitted from the bottom side, between the valve blade and another circular plate having the same number of holes but, 4 mm in diameter. Following fluidization the gate valve/distributor plate could be opened allowing the fluidizing particles to fall into the bottom Faraday cup for charge measurement. The valve opening was controlled by a pneumatic actuator and it took approximately 1 second to go from fully closed to fully opened.

Through out all experimental runs, particles mass was measured using a variety of Denver Instruments Balances. For the high precision measurements, such as those of the entrained particles collected in the filter bag inside the top Faraday cup, a SI-114 balance was used with a maximum value of 110g and an accuracy of ±0.0001g. For the rest of the measurements, other

balances were used, either the SI-6002 or the SI-2002, both with an accuracy of ±0.01g and a maximum capacity of 6kg and 2kg, respectively.

For the majority of experimental trials, the fluidization gas was dried with an Atlas Copco dryer (Model: CD12) to reduce its relative humidity to 0% ±0.02. Two mass flow controllers: MFC 1 and MFC 2 (MKS Instruments; Model: 1599A), and one mass flow meter (MKS Instruments; 1500 Series) worked in conjunction with one another to regulate the volumetric flow of fluidizing gas that entered the column. These controllers had a full range of 200 SLPM (standard litres per minute) with an accuracy of ±2 SLPM. The temperature and relative humidity of the gas stream was monitored by two Vaisala humidity transmitters (Model: HMT338) with an accuracy of ±1% between 0-90% relative humidity, and ±1.7% between 90-100%.

All instruments were connected to a computer with LabView (Version 8.5) data collection software.

2.1.1. Humidification system

For the experimental trials involving changing the fluidizing gas relative humidity (RH), the gas had to contain a desired level of moisture. To accomplish this, a humidification system was designed and built in-house at the Chemical and Biological Engineering Department of the University of Ottawa. A schematic diagram and a picture of the apparatus are shown in Figure 2-3 and Figure 2-4a, respectively. The humidifier was designed based on the injection of steam into a dry gas stream.

The humidifier was a three-dimensional stainless steel 316 column of 0.102 m in diameter and 0.914 m in height. As shown in Figure 2-4b, a cooling coil, which extended ¾ of the way down the unit and used cold tap water, was placed inside the unit to cool down the gas to create condensation ensuring that the gas leaving the column was 100% saturated with water vapour. A set of stainless steel 316 baffles were placed in the middle of the humidifier to enhance the air/steam mixing. The cooling coil also contributed to the mixing. A pack of industrial stainless steel 316 demister pads was placed at the top of the column, where the 100% saturated gas exited

the unit, to prevent any water droplets from leaving the humidifier and entering the piping system. The humidifier was also equipped with a liquid level gauge and a drain at the bottom to allow monitoring of the amount of water condensate in the unit, and to drain the water build-up due to condensation. It was important for the level of condensate to remain below the gas inlet as it was found that instability in the relative humidity occurred if the gas was allowed to bubble through the condensate.

Operation of the humidifier was based on the premise that mixing nearly dry gas (approximately 3% RH) with gas that was 100% saturated with water vapour would provide the ability to obtain a desired relative humidity at any flow rate within operational range. The gas used was the building air which was inputted into the system and directed through the pressure regulator, mentioned previously. The air was then split into two streams by the two mass flow controllers (MFC 1 and MFC 2) with one stream, with a relative humidity of approximately 3%, sent directly to the mixer unit and the other sent to the humidifier. Within the humidifier the building air (at approximately 23 ˚C) and steam (at approximately 112 ºC and 150 kPa absolute pressure), both injected close to the bottom of the unit, were then mixed and travelled to the top of the column.

After leaving the humidifier, the air passed through two filters in series to prevent any system contamination from particulates or foreign droplets that may have entered through the steam line, or any water droplets that might have passed through the demister pad. The first filter (Parker Hannifin Corp; Model: 07F32BC) had a filter rating of 5 μm, while the second filter (Parker Hannifin Corp; Model: 11F32EC) had a filter rating of 0.1 μm.

The relative humidity and the temperature of the air stream leaving the humidifier unit at the top was monitored to ensure that this stream was at 100% RH. This stream was then proportionally mixed with the un-humidified stream, which came directly from the air supply, to give the desired relative humidity for the fluidization trials. The flow was monitored by a flow meter (MKS Instruments; 1500 Series), and a second RH transmitter to ensure that both the desired flow rate and relative humidity were achieved. The air was then directed to the column for fluidization.

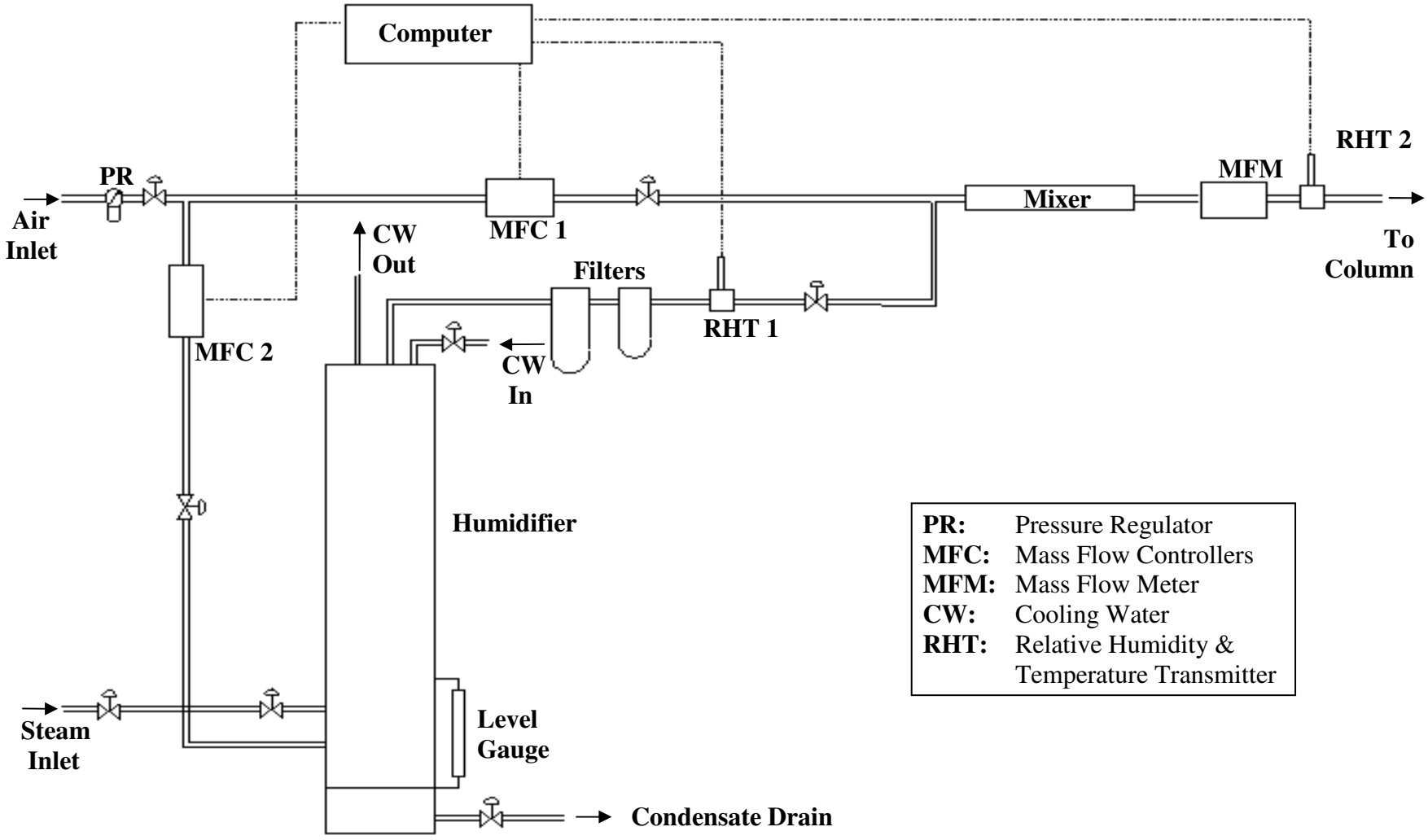

Figure 2-3: Humidifier system schematic.

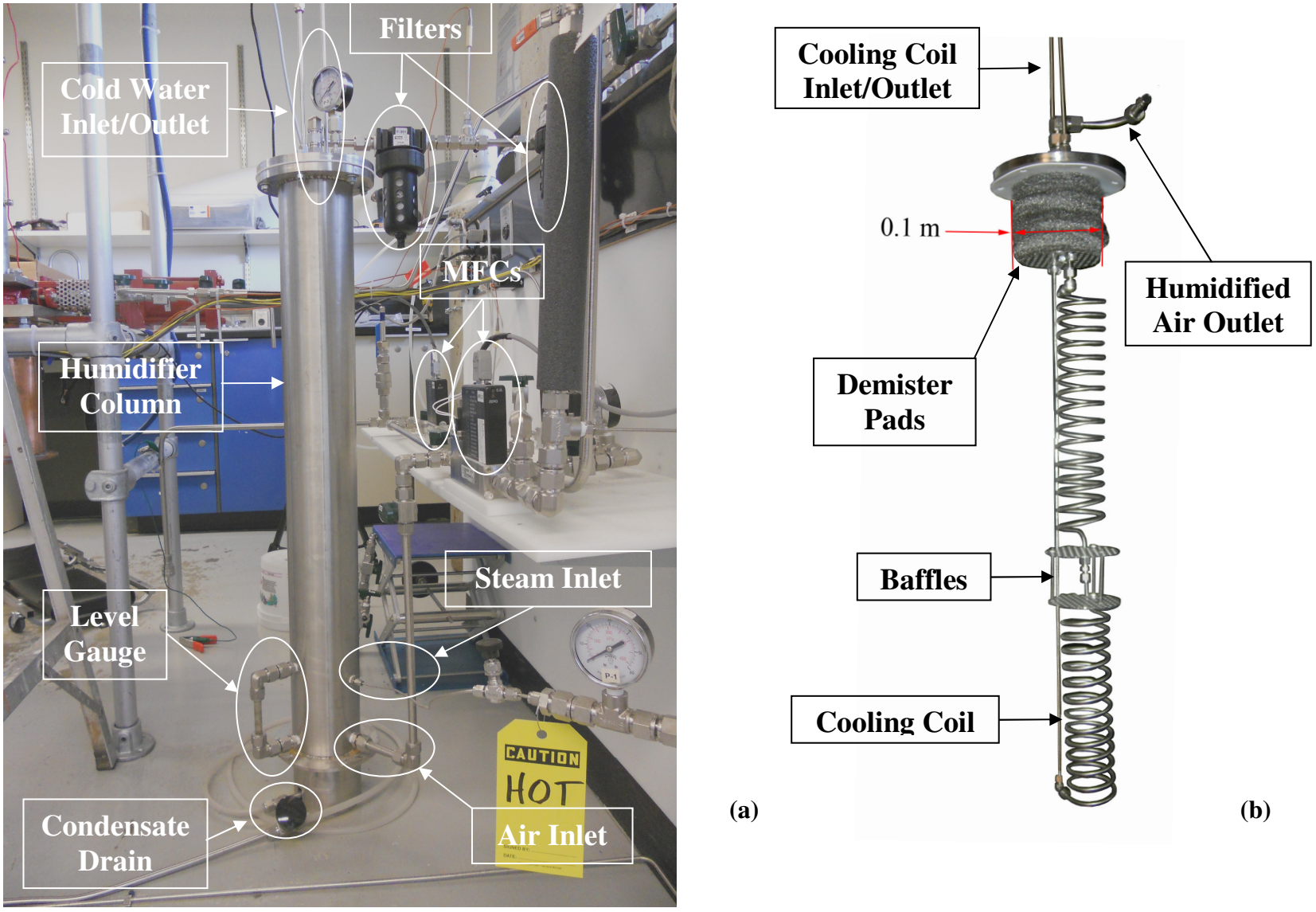

Figure 2-4: (a) Picture of the Humidification system. (b) Cooling Coil.

2.2. Fluidizing Gas

The fluidizing gas was compressed air supplied by the building. The temperature and relative humidity of this air were approximately 23 ºC and 3%, respectively. The air was supplied at 689.5 kPa (100 psi), but it was regulated to 413.7 kPa (60 psi) by a pressure regulator (Parker Hannifin Corp). The regulator also contained a filter (5 μm rating), removing any particulates from the air stream.

2.3. Fluidizing Particles

The fluidizing particles were low density polyethylene (PE) resins, produced using a metallocene based catalyst in industrial gas-phase fluidized bed reactors of ExxonMobil. The resin was obtained from Univation Technologies Inc. (Texas, USA), a joint operation between ExxonMobil Chemical Company and Dow Chemical Company and a leader in licensing gas-phase polyethylene technology services. Relevant particles properties are provided in Table 2-1.

Table 2-1: Fluidizing particles (i.e., Polyethylene resins) properties.

Parameter	Symbol	Value	Units
Density	ρ_p	920	kg/m^3
Bulk Density	ρ_B	502.36 ± 0.52	kg/m^3
Size range		20-1500	μm
Mean diameter	D_P	625 ± 160	μm
Geldart Classification		B	
Fixed bed voidage	ε_{fb}	0.42	
Minimum fluidization voidage	ε_{mf}	0.46	
Minimum fluidization velocity	U_{mf}	0.131	m/s
Sphericity	ϕ	0.724	
Work function	φ	5.23	eV
Permittivity	ε	2.35	F/m
Electrical conductivity	κ	$<1.1x10^{-15}$	S/m
Initial charge-to-mass ratio	$(q/m)_i$	-0.12 ± 0.1	μC/kg

Density

The density of the particles was provided by the supplier (Univation Technologies Inc., USA).

Bulk Density

The mean bulk density of the polyethylene resin was measured to be 502.36 ±0.52 kg/m^3 using a pycnometer. As the pycnometer was tapped to aid settling, this was a tapped bulk density as opposed to a free settling bulk density.

Particle Size Distribution (PSD)

The resins size range and mean diameter were evaluated using a Malvern Mastersizer (Model: Series 2000) with a size range capability of 0.02 µm to 2000 µm using a laser diffraction technique with an accuracy of ±1%. Particles were passed through a laser beam and the light was scattered inversely proportional to the particle size. Detectors monitored the intensity of the scattered light at different angles to determine the particle size distribution (PSD). In this case, a mixture of water and ethanol (2:3) was used as the wet dispersant. A typical PSD for the initial particle size is provided in Appendix A; since an industrial resin was used each PSD was slightly different even though the same batch of particles was used.

Geldart Classification

With a mean particle diameter of approximately 625 µm, a density of 920 kg/m^3, and a fluidizing gas density (ρ_f) of approximately 1.2 kg/m^3 the Geldart classification can be determined using the chart previously presented (Figure 1-2). These values place the particles in Group B. Therefore, fluidization of particles should be easy due to vigorous bubbling promoting particle circulation. In this group small bubbles form near the distributor plate and coalesce while moving upward through the bed (Kunii and Levenspiel, 1991).

Fixed bed voidage

Fixed bed voidage was calculated based on the fixed bed height (L) to column diameter (D_C) ratio ($L/D_C = 4$), the density, and the mass of the particles according to the following equation:

$$\varepsilon_{fb} = 1 - \frac{\left(\frac{0.001 \frac{kg}{g} \cdot m_i}{\rho_P} \right)}{\left(\frac{1}{4} \pi \cdot L \cdot D_C{}^2 \right)} \qquad \textbf{Eq. 2-1}$$

where, m_i is the initial mass of the particles (approximately 1053.75g).

Minimum fluidization velocity (U_{mf})

The minimum fluidization velocity was determined both experimentally and theoretically. Experimentally, the differential pressure (ΔP) signal was plotted against superficial gas velocity, as recommended by Kunii and Levenspiel (1991). At superficial gas velocities lower than minimum fluidization, differential pressure increases with increasing gas velocity; at velocities greater than minimum fluidization, differential pressure drop remains almost constant. The intersection between the sloped line of increasing ΔP and the line through constant ΔP is considered to be at the U_{mf}. Determination of U_{mf} was performed with both increasing and decreasing gas velocities ranging from 0 to 0.546 m/s; the results of this experiment are presented in Appendix A.

The experimental U_{mf} was compared with two different calculations of the theoretical value. The first was calculated based on equation from Leva (1959) and reported by Yang (2003):

$$U_{mf} = \frac{(\mathrm{Re})_{mf} \cdot \mu}{D_P \cdot \rho_f} \qquad \textbf{Eq. 2-2}$$

where D_P is taken as the mean particle diameter from particles size analysis, and μ is the viscosity of the fluid. $(\mathrm{Re})_{mf}$ can found by **Eq. 2-3** (Yang, 2003) with constants defined by Grace (1982):

$$(\mathrm{Re})_{mf} = \sqrt{C_1^2 + C_2 Ar} - C_1 \qquad \textbf{Eq. 2-3}$$

where C_1 is equal to 27.2 and C_2 is 0.0408. Ar is the Archimedes number and is defined by Eq. 2-4:

$$Ar = \frac{D_P \cdot \rho_f (\rho_P - \rho_f) g}{\mu^2} \qquad \textbf{Eq. 2-4.}$$

The second method was from Kunii and Levenspiel (1991):

$$U_{mf} = \frac{{D_P}^2 \cdot (\rho_P - \rho_f) g}{150\mu} \cdot \frac{{\varepsilon_{mf}}^3 \phi^2}{1 - \varepsilon_{mf}} \qquad \textbf{Eq. 2-5}$$

where g is gravitational acceleration.

The results of these calculations are presented in Table 2-2. Both theoretical values of U_{mf} are similar to that obtained through experimentation.

Table 2-2: Comparison of U_{mf} values

Method	U_{mf} (m/s)
Experimental	0.131
Grace (1982)	0.136
Levenspiel and Kunii (1991)	0.130

Particle surface morphology and sphericity

Polyethylene particles are non-spherical, porous and have a rough surface. Figure 2-5 presents a typical image of polyethylene resins used in this study taken by Scanning Electron Microscopy (SEM) with a Tescan Vega-II XMU VPSEM at Carleton University. The sphericity was determined from SEM pictures using Photoshop software. This was accomplished by using the measurement tool in Photoshop and setting the scale based on the scale given on the SEM picture. The measurement tool was able to calculate the circularity of the particles based on the area and perimeter of the selected object (**Eq. 2-6**), where a value of 1.0 is a perfect circle.

$$Circularity = 4\pi\left(\frac{area}{perimeter^2}\right) \qquad \textbf{Eq. 2-6}$$

By taking measurements of numerous particles, an average of the circularity could be calculated. It could then be assumed that the average circularity was approximately equal to the sphericity of the particles.

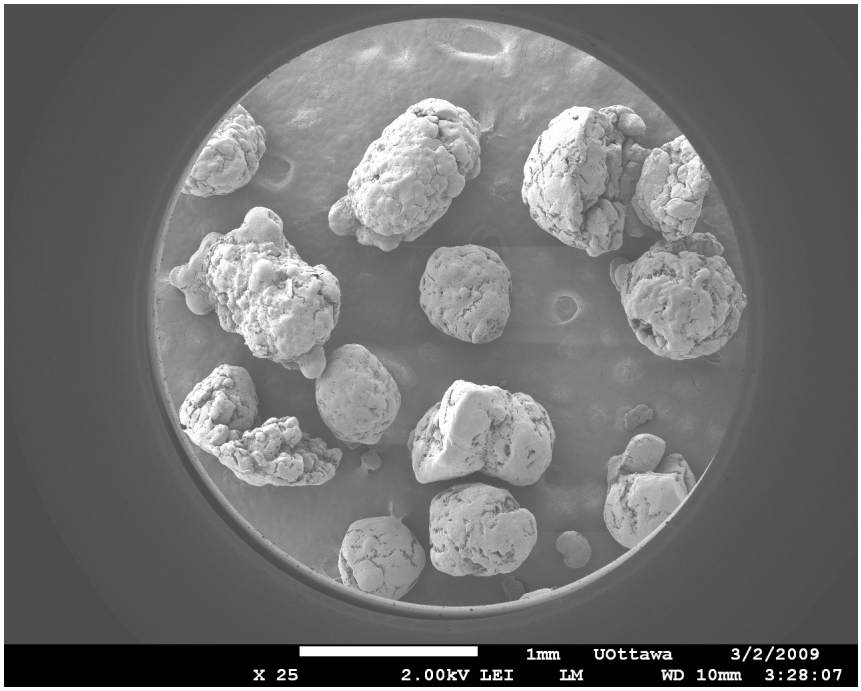

Figure 2-5: SEM image of polyethylene resin.

Work function

As discussed in Chapter 1, work function is an important physical property in determining expected particle electrification from contact. In the case of polyethylene, the value of work function is 5.23 eV (Tanoue and Masuda, 2006).

Permittivity

Permittivity is the response of a material to an electric field and quantifies how quickly an electrical signal can travel through the material. The permittivity of polyethylene was found in the Electrical Engineer's Reference book (Pryer and Gale, 2003) as 2.35 F/m. This evaluated at a temperature of 20ºC.

Electrical conductivity

Electrical conductivity is a measure of the ability of a material to conduct an electric current. The electrical conductivity of polyethylene is less than $1.1x10^{-15}$ S/m (Hindermann-Bischoff and Ehrburger-Dolle, 2001). A related concept is that of electrical resistivity which is equal to the inverse of conductivity.

Initial particles net charge-to-mass ratio (q/m)

The initial charge of the particles was measured using a bench-scale Faraday cup connected to the same electrometer used for fluidization system experiments. The mass of the particles was measured prior to charge measurement so that results could be normalized by calculating charge-to-mass ratio (q/m). As the particles used for experimentation were industrial resin, it was likely that there would be some variation in initial particle charge. The initial net q/m measurement was performed prior to each experiment to ensure that the results of all trials would be comparable.

Initial particles mass distribution

The mass distribution, the quantity of particles within a certain size range, of the industrial resin is an important aspect contributing to the electrification of the bed. In previous research, and in the current work, smaller particles were found to be predominately positively charged while the larger particles were found to be predominately negatively charged. Thus, if the industrial resin has more of the smaller particles, then a slightly less negatively charged or slightly more positively charged bed would be expected.

A set of 8 sieves were used to separate samples of 75 grams of the same industrial resin used for all fluidization trials. The results are presented in Figure 2-6 in terms of the percentage of initial mass (m%) found in each sieve; these results are the average m% collected over 5 repetitions. The mesh sizes were normalized using the mean particle diameter due to confidentially issues (>1.60, 1.14-1.60, 0.96-1.14, 0.80-0.96, 0.68-0.80, 0.48-0.68, 0.34-0.48, <0.34). In addition the mean of the 10 ($D_{P\ 0.1}$), 50 ($D_{P\ 0.5}$), 90 ($D_{P\ 0.9}$) percentile of particle size distributions for each sieve were analyzed (Appendix A). The largest quantity of particles, over 25%, were found in the 1.14-1.60 sieve. The smallest quantity of particles,

<5%, was found in the <0.34 sieve with a mean particle size of approximately 0.32 μm. The majority of mean particle sizes were slightly larger than the mesh size of the sieve in which they were found. This is likely due to the non-spherical shape of these particles as they could turn on their side and slip through the mesh into the next sieve.

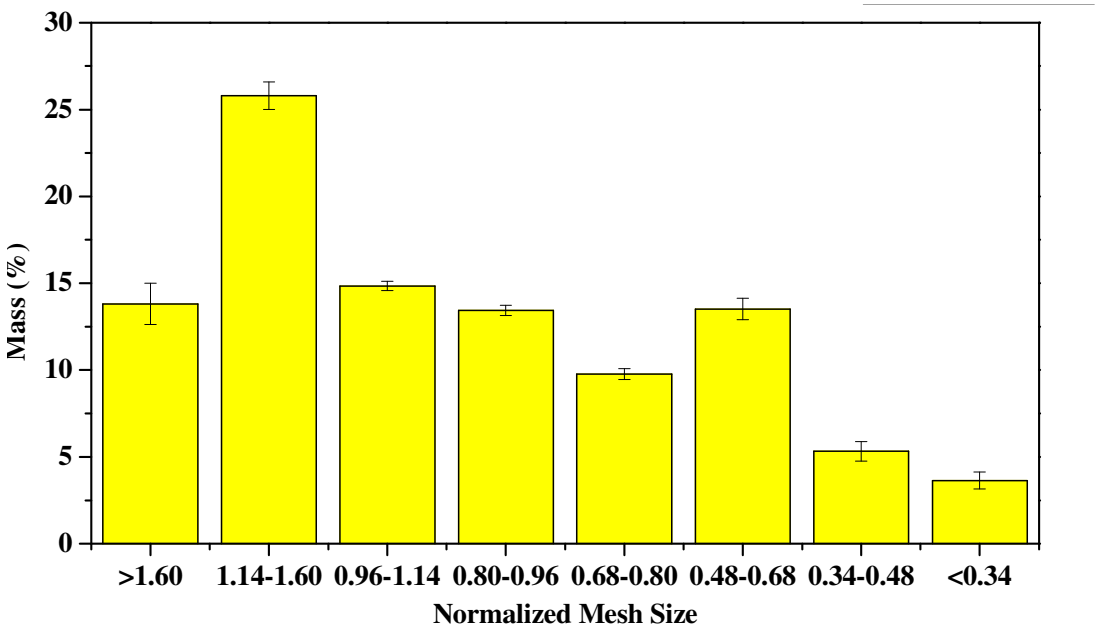

Figure 2-6: Normalized distribution within initial particle sample by m%.

Initial particles charge-to-mass distribution

The net charge-to-mass ratio of the initial particles was measured as described above. However, the resin could consist of both positively and negatively charged particles. Therefore, knowing the charge-to-mass distribution within the initial industrial resin was important in understanding how the particles charge changes during fluidization. This measurement was conduced by a device designed by my research group as seen in Figure 2-7. The device consisted of four Faraday cups located below two copper plates positioned at an angle. A high voltage power supply (Ultravolt HV Rack Model 1-250-00265) was used to charge one of the plates to a positive charge of approximately 39 kV, while the other plate was grounded to act as a negatively charged plate. Each of the four Faraday cups was attached to a digital electrometer (Keithley 6514). Small copper strips were placed on top of the Faraday cups to prevent the measurement from being affected by the electric field of the positively charged copper plate and the particles as they fell down into the cups. The entire

system was encased in an isolative box for safety purposes (i.e., high voltage field). The box was composed of polyethylene walls at the back and bottom, and Plexiglas at the front and top. The top side of the box had an opening approximately 7.6 cm in diameter to allow particles to be poured into the box and between the copper plates. The front panel was removable so that the boxes could be removed for particles mass measurement and size distribution analysis.

In these trials small samples of the initial particles (approximately 20 g) were tested. In all trials, some particles were found strongly attracted and thus adhered to the positive plate while the rest of the particles fell into the four Faraday cups allowing for their charge measurement. The particles that attached to the positive plate must have been highly negatively charged, however their actual charge could not be measured. The mass of the particles collected in the cups was measured to allow for q/m calculation (Figure 2-8). Tests were repeated three times to confirm the reproducibility of results.

The net charge-to-mass ratio (shown on Figure 2-8 as Net) was calculated based on the measured net charge (q) divided by the total mass collected. This resulted in a different net q/m than if the q/m of each Faraday cup were added together.

A particle size distribution analysis on particles collected in each Faraday cup and those found on the positive plate was completed. The mean $D_{P\ 0.1}$ (diameter of particles in the 10^{th} percentile), $D_{P\ 0.5}$ (mean particle diameter), and $D_{P\ 0.9}$ (diameter of particles in the 90^{th} percentile) are presented in Figure 2-8b (average PSDs are presented in Appendix A). The Net values this graph are those for the full sample of polyethylene resin prior to separation. The PSD was conducted to determine if there was a trend with particle size and the charge on the particles. Very little difference in particle sizes between the four Faraday cups was found. This indicated that the particles in the range of approximately 0.48-1.92 had a range of magnitude and polarity of charge. However, the particles that adhered to the positive plate, which must have been negatively charged, were smaller than those particles that were collected in the Faraday cups. This indicated that finer particles typically were initially negatively charged.

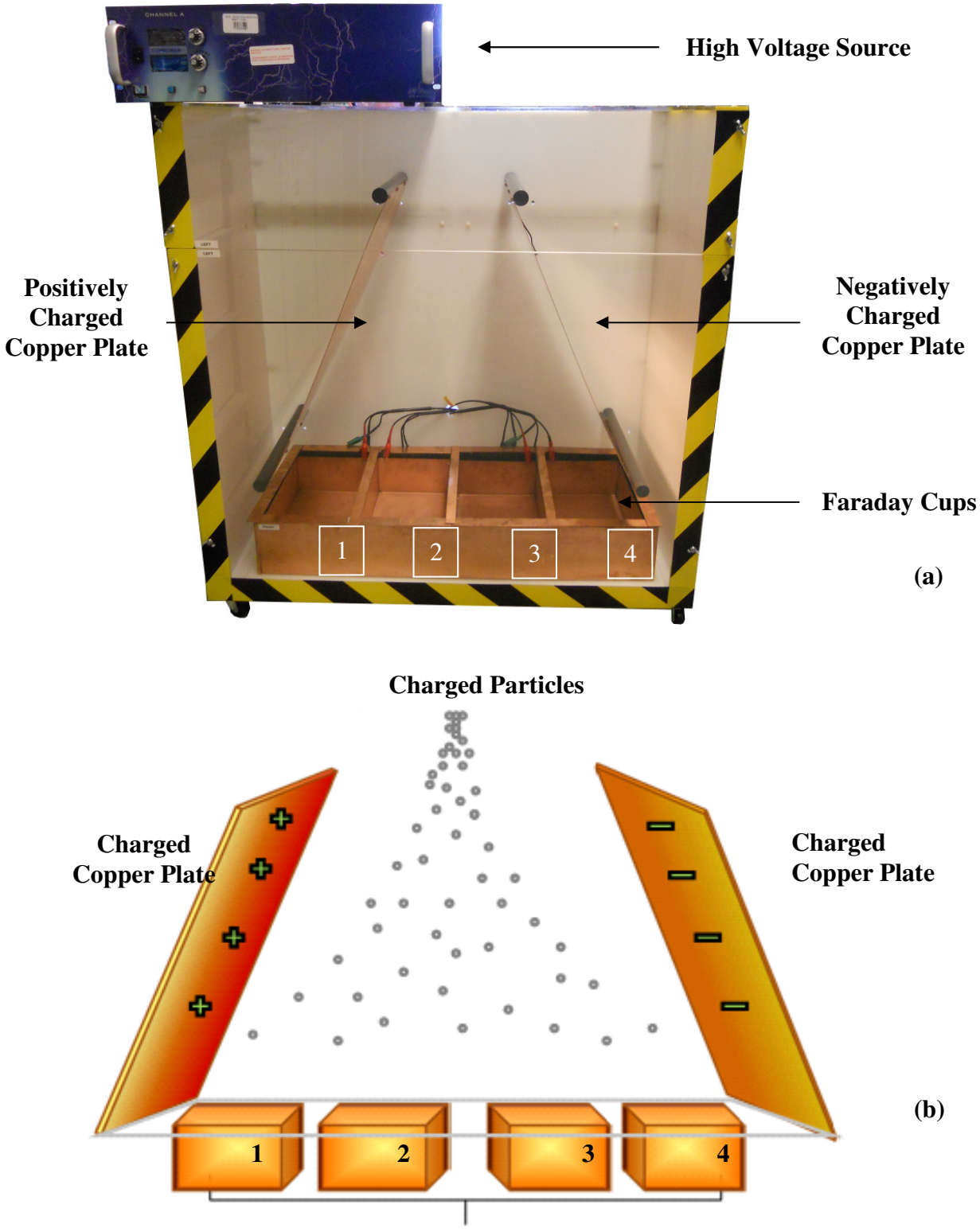

Figure 2-7: Measurement of charge distribution: (a) picture, and (b) schematic.

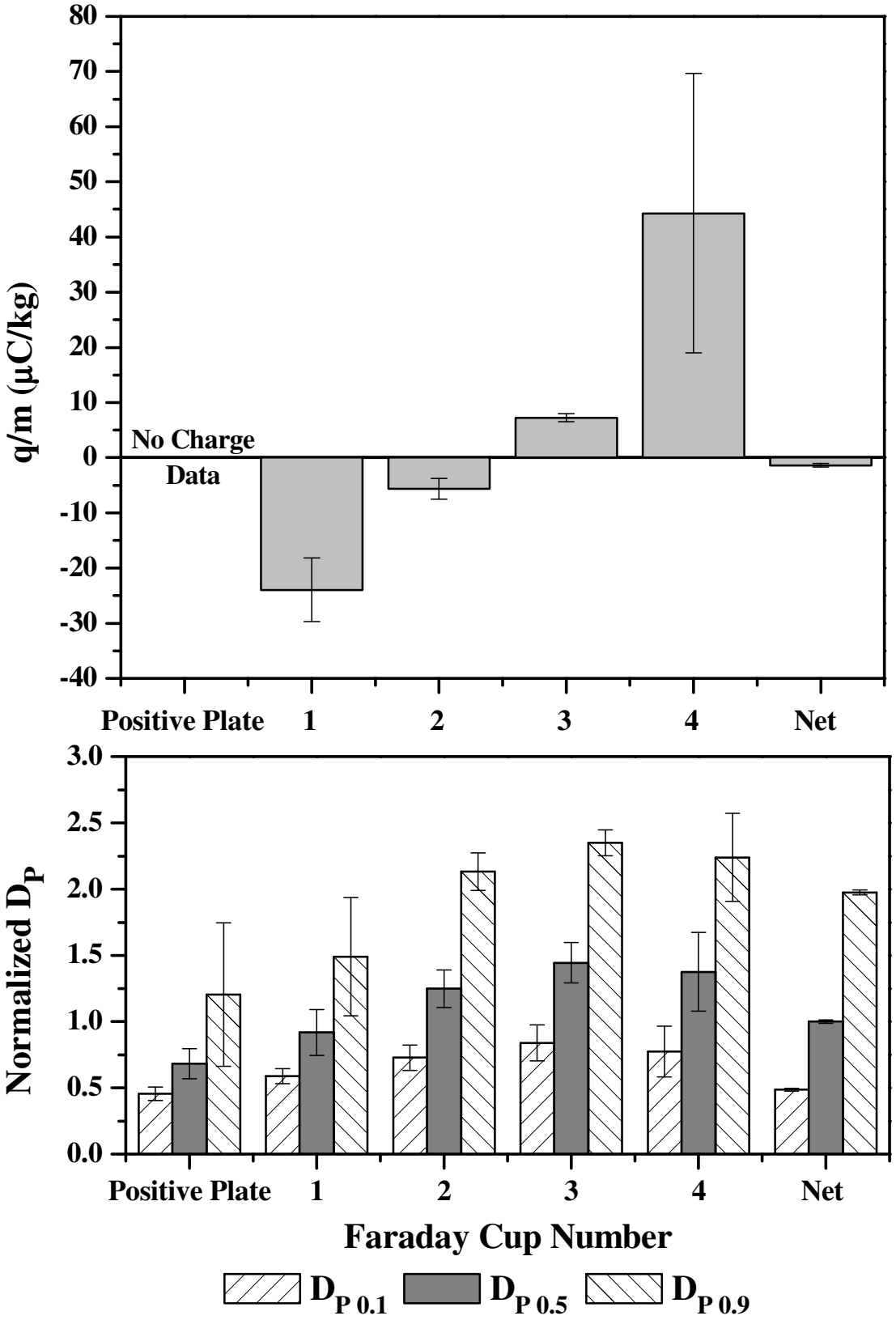

Figure 2-8: Charge separation experiments (a) charge-to-mass distribution of initial particle sample, and (b) $D_{P\ 0.1}$, $D_{P\ 0.5}$, $D_{P\ 0.9}$ of particles in each plate.

2.4. Experimental Method

The fluidization column was separated into four different sections where the particles mass, size distribution and charge were measured and recorded for each experimental run. As shown in Figure 2-9a, the four sections were:

- The initial particles used before fluidization **(Initial)**,
- The fines entrained from the column during fluidization period that were caught in the top Faraday cup **(Fines)**,
- The bulk particles that were dropped into the bottom Faraday cup upon the completion of the fluidization period **(Dropped)**, and
- The particles that were adhered to the column wall **(Wall)**.

Three additional sampling locations were evaluated only for PSD analysis (Figure 2-9b). For a few trials with longer fluidization times some particles, between the collection of dropped and wall samples, dislodged from the wall and fell to the ground (**Intermediate Wall**). Intermediate wall samples were only collected at extended fluidization times for a limited number of trials. In some trials, following the collection of the wall particles, some particles, which were highly electrostatically charged, remained adhered to the column wall. These charges caused the particles to be attracted to the column wall and remain adhered even after fluidization was stopped and the distributor plate was removed. The PSDs of these particles were measured on samples taken from the bottom of the column (**Bottom Column**), which was present at all velocities, and the top of the column (**Top Column**), only for higher gas velocities. Since these particles could only be removed by scrapping the column, their charge and mass were not measured.

Throughout this work, mass is reported as mass percent (m%). This is the percentage of the initial mass found in each region of the bed. The mass of the three regions (i.e. Dropped, Wall, and Fines) were added up and the difference between that value and initial mass was considered as irretrievable due to tight adherence to the column wall or loss during sampling.

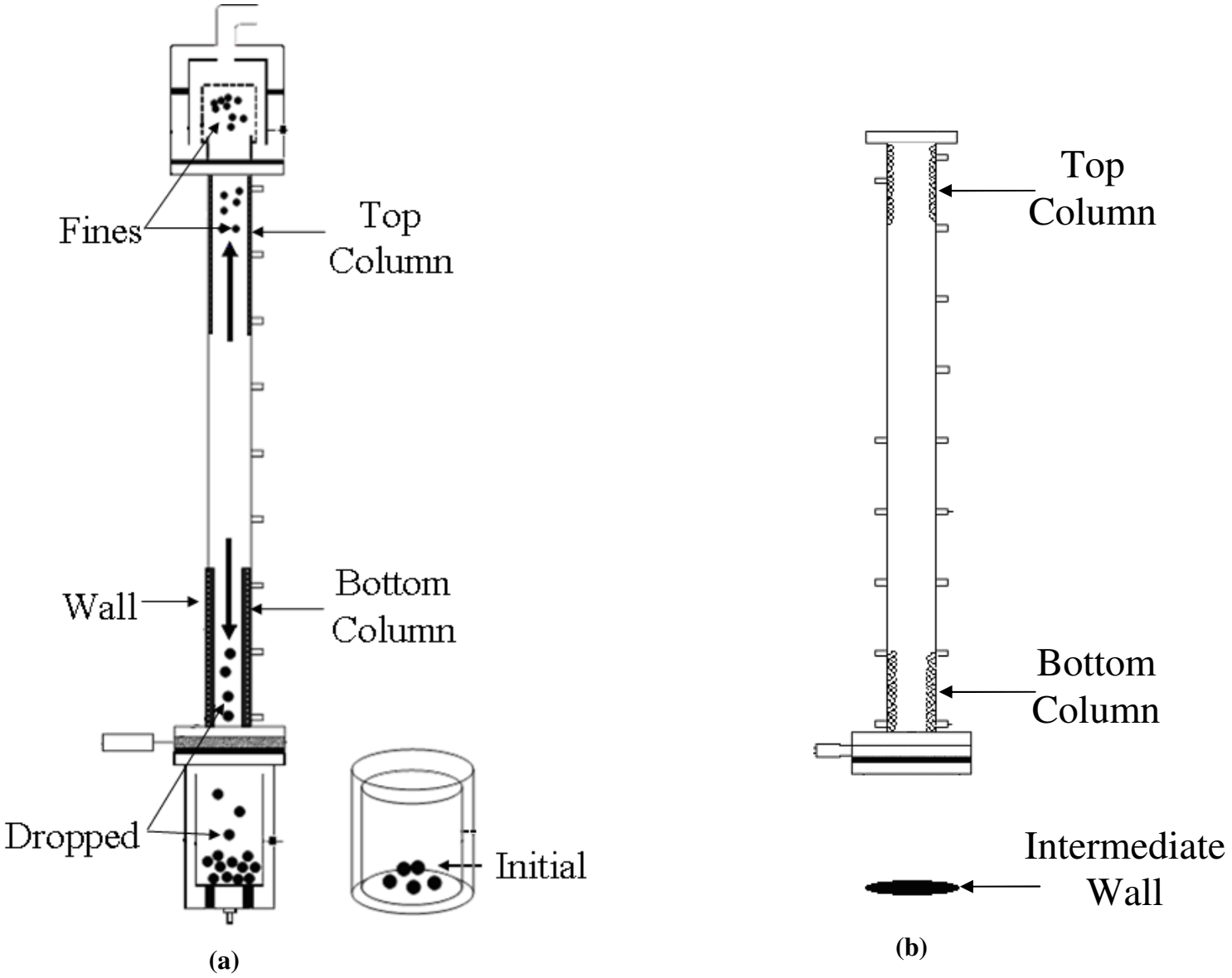

Figure 2-9: Measurement points: (a) Charge, mass, & PSD, (b) Additional PSD points.

As different masses were collected in each region for each experiment, charge was normalized for comparison. This was accomplished by dividing particles charge by the collected mass in each region giving a charge-to-mass ratio.

Due to confidentiality reasons, all PSDs were normalized. This was done by dividing all PSD measurements by the initial mean particle diameter ($D_{P\,0.5}$) of each trial. This resulted in a scale ranging from just above 0 to approximately 3.0. Anything greater than 1.0 was larger than the mean particle size.

Prior to each trial, the inside of the fluidization column was thoroughly cleaned and the knife gate valve was closed. Fresh batches of particles were utilized for each experimental run. In each experiment, a mass of 1053.75g of particles was measured as this was the quantity necessary to maintain an $L/D_C = 4$. The initial charge of the particles was measured with a bench-scale Faraday cup prior to filling the column. After ensuring that the distributor plate was closed, particles were poured into the column from the top. Previous tests had shown that pouring did not generate any significant amount of charge. The filter bag was then mounted on the top of the column with a Teflon connector, and the Faraday cup was attached to the top of the column via Teflon bolts. The top Faraday cup was connected to the electrometer to measure the cumulative charge of elutriated fines during fluidization. The filter bag contained four layers of dustluck filters which were replaced for each experiment.

The fluidization column was grounded for a short period of time to eliminate any stray charges. During fluidization the top and bottom cups were grounded and the column was electrically isolated, as was the distributor plate. This was to prevent any electrical discharge so that the full capacity of the charge generation within the system could be evaluated.

At this point, the digital electrometer connected to the top Faraday cup was made to record charge for 60 seconds, before the fluidizing gas was introduced. This would allow for an electrical background check of the instrument. Fluidization gas was then introduced into the column, slowly increasing in flow (at approximately 2 SLPM per second) until the desired flow rate was obtained. This was achieved by the mass flow controller (MFC 1) via the Lab View software. Fluidization continued for the desired fluidization time. Upon the completion

of this period, the gas flow rate was slowly decreased (at approximately 2 SLPM per second).

At this point, the top Faraday cup was removed to access the elutriated fines trapped within the filter bag. The filter bag was removed to determine the mass of entrained fines. The bottom Faraday cup was then connected to the electrometer and a baseline reading was taken for 60 seconds. The knife gate valve was then opened so that the bulk particles would be dropped into the bottom Faraday cup for their charge to be measured. The bottom Faraday cup was removed to measure the mass of the particles collected. At this point the inner column wall was inspected for any wall fouling. Images were taken from the bottom of the open column of the particles adhered to the inner column wall that comprised the wall region. Then, the bottom Faraday cup was cleaned and placed back on the column. A background charge of the empty Faraday cup was recorded for 60 seconds. The top of the column was then tapped with a mallet so that the particles attached to the column wall would dislodge from the wall and fall into the cup for their charge to be measured. This was continued until no change in charge was measured, indicating that either no particles left on the column wall or the particles remaining on the wall were too tightly adhered to be easily removed for measurement without additional handling. The bottom Faraday cup was then removed to measure the mass of the wall particles.

Figure 2-10 presents typical charge data collected for initial, dropped wall, and fines particles during each experimental run.

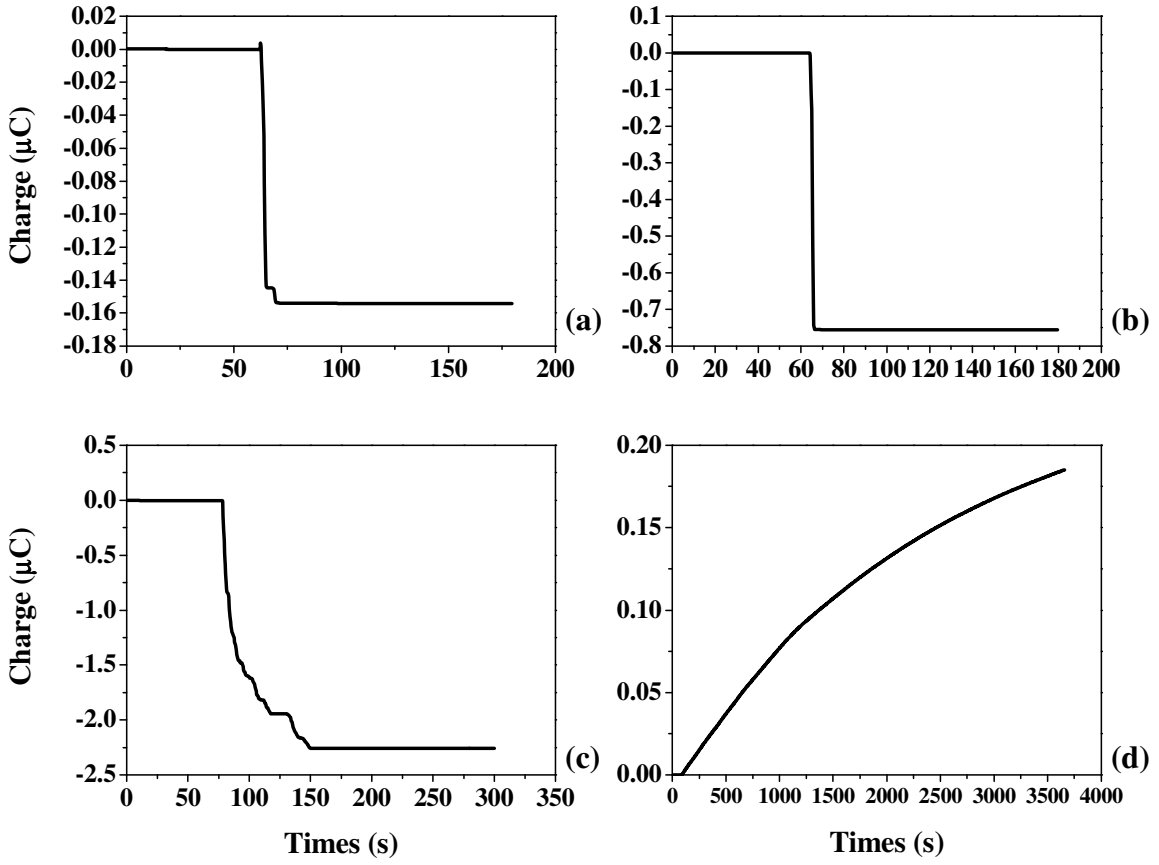

Figure 2-10: Typical data collection during an experimental run: (a) Initial, (b) Dropped, (c) Wall, and (d) Fines.

A sample of the particles was collected for PSD analysis from the fines, dropped and wall regions. Additionally, a sample was scraped off of those particles whose removal was not possible at both the bottom and the top of the column. During long fluidization times, between collections of the dropped and wall particles occasionally some loosely adhered particles would detach from the column wall. Some of these particles were collected for PSD analysis.

Following each fluidization experiment, the column was cleaned first with a wet cloth followed by a dry cloth. Then the inside of the column was vacuumed with special attention given around the ports and along the distributor plate.

Throughout all experimental runs, the room relative humidity and temperature were measured by a designated relative humidity transmitter mounted on the structure of the

apparatus, and data were recorded by a computer. For every run, all data logging (charge, gas and room relative humidity and temperature, pressure fluctuations, and gas flow rate), and control (gas flow rate) were performed by using Lab View program (Version 8.5, National Instruments Inc., USA). All data sampling occurred at approximately 8 Hz. Before and after each charge measurement the value on the electrometer, without any changes occurring, was recorded for a minimum of 1 minute and up to 5 minutes. This was to ensure that only a minimum amount of measurement drift was taking place.

For humidity trials, the inlet air stream was partially directed through the humidifier to produce 100% saturated stream prior to mixing with the low humidity stream. The flow rates required for both streams were calculated based on desired flow rate and relative humidity of the humidified stream to enter the fluidization column (Appendix A). The humidified stream was first vented to the room to allow reaching steady state prior to fluidization.

Chapter 3. Effect of Fluidization Time on Bed Electrification in Bubbling and Slugging Flow Regimes

Fluidization time is an important parameter to understand in investigation of electrostatic charge generation within gas-solid fluidized beds. Extended particles residence time inside the bed increases particle-particle and particle-wall contacting which may increase the amount of charge that may develop within the bed, in addition to a maximum or "saturation" charge that may occur. Therefore, by studying this parameter the presence of charge saturation, if/when it occurs, and whether it varies between different regions of the bed can be evaluated. Additionally, the time that it takes for the particle layer formation on the column wall due to adhesion of particles, can be identified.

Previous research has identified varying times to reach charge saturation from 2-5 and up to 100 minutes (Ali et al., 1999; Rojo et al., 1986). The research reported in literature has varied in particles size, column wall material, and measurement techniques. None have investigated the effect of time on reactor wall fouling and the charge distribution throughout the bed. Therefore, a comprehensive study of fluidization time is required to provide a complete picture of how the duration of fluidization affects charge generation.

The effect of fluidization time on charges generated on industrial polyethylene resin is presented within this chapter. Six different fluidization times were assessed (15, 30, 60, 120, 180, and 360 min) at four different fluidizing gas velocities at factors of U_{mf}, representing two fluidization regimes of bubbling (1.5 and 1.75 U_{mf}) and slugging (3.5 and 4 U_{mf}). The shortest fluidization time was chosen as 15 minutes since that was the minimum time required in each run to allow the desired gas flow rate to be introduced to the column and the system to reach steady state. 30 minute was chosen next to compare results with those few found in literature that studies times ranging 20 to 40 min (Ciborowski and Wlodarski, 1962; Kisel'nikov et al., 1967). 60 minute was also identified as a possible period for charge saturation to occur (Revel et al., 2003; Wolny and Opalinski, 1983). Three additional times

of 120, 180, and 360 minutes were chosen to determine whether the charge distribution within the bed and the particles wall layer changes with longer fluidization times.

The four gas velocities tested allowed the determination of the effect of fluidization time in the two flow regimes of bubbling and slugging. No gas velocities were chosen between 2 and 3 U_{mf} because these velocities were determined to be in the transition zone between the regimes, resulting in a mixture of different bed hydrodynamics that would make the determination of the dominating charging mechanisms challenging.

For each experimental run, the particles charge, mass and size distribution was measured, along with the particle layer formed on the column wall through images taken from the bottom of the column. The particles mass percent and charge-to-mass ratio were then calculated using the mass and charge of the initial particles and those collected in each region of the bed.

Results presented in this chapter have already been published in the Journal of Electrostatics: *Giffin, A., Mehrani, P. (2010), Comparison of Influence of Fluidization Time on Electrostatic Charge Buildup in Bubbling vs. Slugging Flow Regimes in Gas-Solid Fluidized Beds, Journal of Electrostatics (68, 492-502)* and in the proceedings of Fluidization XIII: *Giffin, A., Sowinski, A., Mehrani, P., Investigation of the Effect of Fluidization Time on Electrostatic Charge Generation in Gas-Solid Fluidized Beds, Fluidization XIII: New Paradigm in Fluidization Engineering (2010, South Korea).*

3.1. Bubbling Flow Regime

Two different gas velocities were tested in the bubbling flow regime: 1.5 U_{mf} and 1.75 U_{mf}. In this section results of the particles mass collected, charge-to-mass ratio, size distribution, and particle layer formation on the column wall, are first presented for individual velocities, and then compared.

3.1.1. 1.5 U_{mf} Gas Velocity Results and Discussion

The results obtained for the fluidization gas velocity of 1.5 U_{mf} and the associated discussion are presented in this section.

3.1.1.1. Mass Collected (m%)

Figure 3-1 presents the average particles m% collected in different regions of the fluidized bed. In the dropped region, the m% collected decreased as fluidization time increased and finally levelled out with extended fluidization times. This indicates that the particles from the bulk of the bed were either migrating to the column wall or being elutriated from the column. If the particles migrated to the wall, the cause was probably electrostatic effects; however, if they were entrained from the bed, it was probably due to their small particle sizes.

In the wall region, m% increased as the fluidization time lengthened (Figure 3-1b) indicating that the number of particles adhering to the wall also increased. Thus, as fluidization progressed, a particle layer built on the column wall and grew bigger over time. In each experiment, particles were collected from the three regions of the bed; however, for the wall region, some particles were not collected due to strong electrostatic forces keeping them attached to the wall. This shows that the particles closer to the wall had more charge and thus were more tightly attached to the wall than those in the outer layer.

The m% of fines for all fluidization times was comparable indicating that a minimal amount of fines were leaving the column after 15 minutes. Most of the particles with a terminal velocity less than that of the superficial gas velocity were expelled from the bed within 15 minutes following the onset of fluidization.

Since by the increase in fluidization time, the m% of fines remained constant while that of the dropped and wall particles continued to decrease and increase, respectively, it is concluded that the majority of particles leaving the dropped region must have been migrating to the wall.

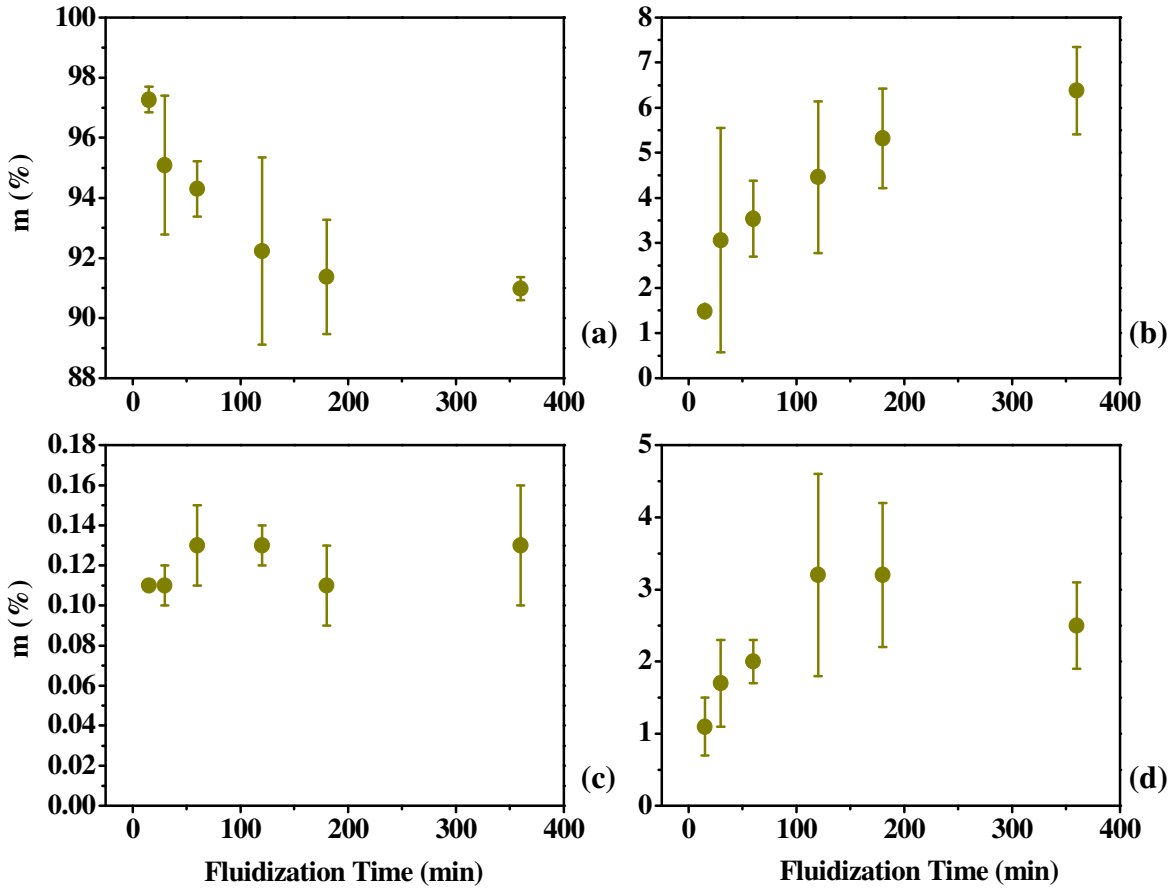

Figure 3-1: Mean m% at 1.5 U_{mf} for different fluidization times: (a) Dropped, (b) Wall, (c) Fines, and (d) Irretrievable.

3.1.1.2. Charge-to-Mass Ratio (q/m)

Figure 3-2 presents q/m results of the fluidizing particles in all measurement regions. Overall, small (entrained fines) and large (dropped and wall) particles were predominately positively and negatively charged, respectively. This supports the bipolar particle charging theory previously reported in literature (Ali et al., 1998; Cartwright et al. 1985; Inculet et al., 2006; Park et al., 2002a; Singh and Hearn, 1985; Zhao, 2002). Initial particles had the smallest magnitude net q/m (approximately -0.1 ± 0.02 μC/kg), followed by the dropped particles, (-0.4 to -1.0 μC/kg) and the wall particles, that were almost two orders of magnitude larger (-40 to -90 μC/kg). The fine particles had the highest magnitude, but were positively charged (+40 to +320 μC/kg). The bulk was likely comprised of both positively

and negatively charged particles, combining together to give a small net q/m, thus explaining the low magnitude of q/m of the dropped particles. Also, highly charged particles likely migrated towards the column wall due to electrostatic forces attracting them to the wall or repelling them from the centre of the bulk. Once they reached the column wall, they likely adhered, effectively entering the wall section and removing that high charge out of the dropped region.

There was a slight increase in the magnitude of the net q/m (i.e., becoming more negative) of dropped particles up to 60 min fluidization times (Figure 3-2b), while a plateau seemed to be reached for times of 60 minutes and greater. This showed that with a fluidization time less than 60 minutes, the bulk particles did not have time to generate enough charge to reach saturation. On the other hand, the mass of dropped particles collected continued to decrease as fluidization time increased. This indicated that regardless of collected mass, a similar q/m was obtained with extended fluidization times suggesting that this was the maximum net q/m that could be generated.

The wall particles experienced a decrease in q/m magnitude, becoming less negative up to 60 min, but there seemed to be a q/m plateau at greater fluidization times (Figure 3-2c). The wall particles had a large negative net q/m. For a particle layer to build up on the column wall, a positive charge must have been generated to provide an opposite charge to attract the particles. The column wall was made of stainless steel, which has a tendency to donate electrons, when coming into contact with insulating materials, thus gaining a positive charge. The validity of this exchange is based on the relative triboelectric series (Diaz and Felix-Navarro, 2004) where a qualitative ranking is used to place various materials based on relative polarity of the charge acquired, and work function values (Cross, 1987; Tanoue and Masuda, 2006). As stainless steel is placed higher than polyethylene on the triboelectric series, when it comes in contact with polyethylene, it will become positively charged and the polyethylene will become negatively charged. In comparison, work function of the materials in contact can be utilized, which are based on quantitative values. Polyethylene has a larger work function (5.23 eV) than that of stainless steel (4.25 eV). These two methods both indicate that the stainless steel column is likely to be positively charged following interaction with polyethylene particles. Therefore, it is anticipated that the comparatively

larger, negatively charged polyethylene particles would be initially attracted to the column wall, creating a negatively charged layer. After the formation of the base negative layers, positively charged particles may likely to be attracted to this layer, which then would draw more negatively charged particles to the wall, creating a bi-polar layer and decreasing the net q/m. As the fluidization period lengthened to 60 min, the net q/m decreased in magnitude; therefore, as the mass of the wall particles collected increased with time, the positively charged particles adhering to the wall experienced either an increase in magnitude while the negatively charged particles decreased in magnitude, or there was an increase in the amount of positively charged particles. The increase in magnitude of positively charged particles is collaborated by the increase in fines net q/m with fluidization time. As the mass of fines remained relatively constant, the charge on these particles must have been increasing which is likely also true for the fine particles remaining in the bed and eventually adhering to the wall.

The q/m of the fines elutriated from the column relatively increased with fluidization time until 180 min (Figure 3-2c). The fines q/m at 360 min was similar to those at 180 min suggesting that a maximum net q/m had been reached at this point. Even though the q/m of these particles slightly increased with fluidization time, the mass of particles remained relatively constant. This indicated that the few particles leaving after an extended residence time inside the bed were more charged than particles initially leaving. This was expected as the particles had higher residence time inside the bed, thus accumulating more charge. As previously discussed in Chapter 2, initially the smaller particles tended to be negatively charged. Since the entrained fines were found to be positively charged, then charge generation must have taken place during fluidization due to the particles-wall and large and fines particles contacts.

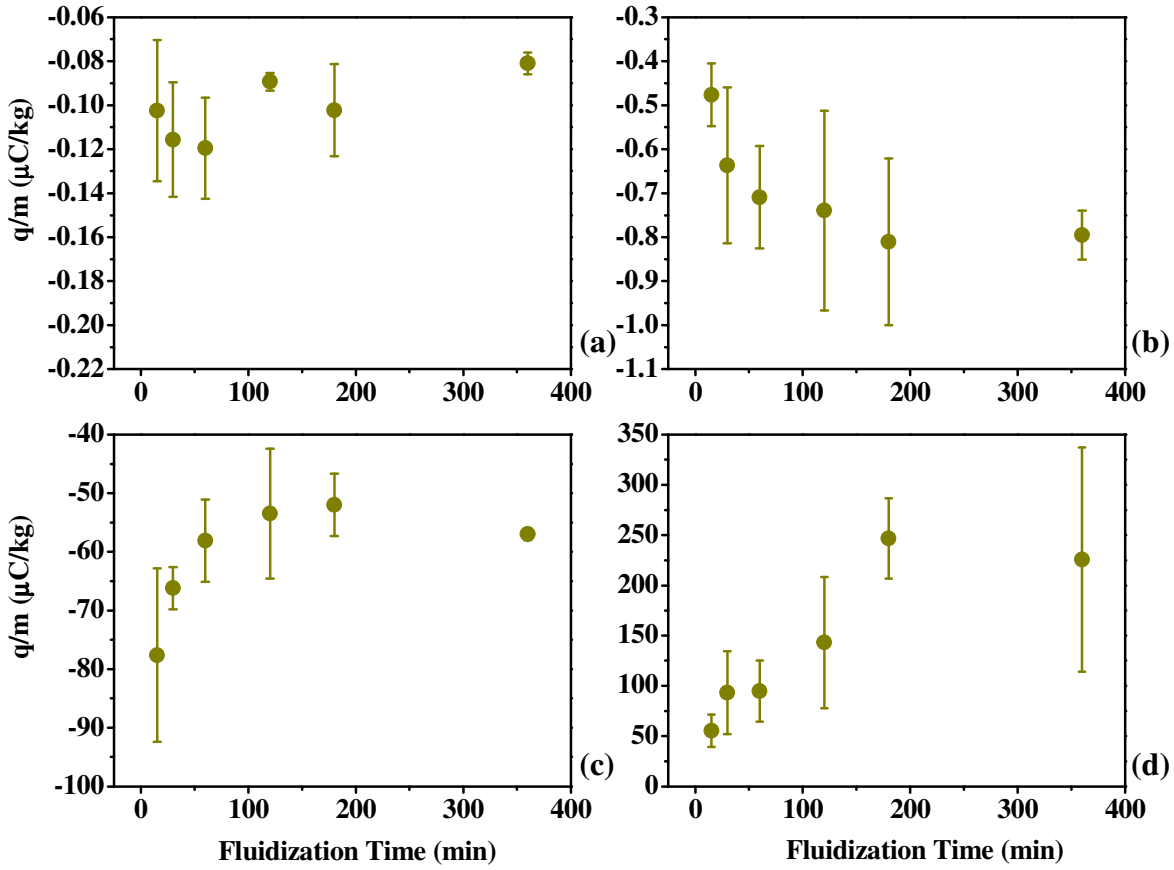

Figure 3-2: Mean net q/m at 1.5 U_{mf} for different fluidization times: (a) Initial, (b) Dropped, (c) Wall, and (d) Fines.

3.1.1.3. Wall Particle Layer

After the dropped particles were removed from the column a picture was taken of the particle layer covering the column wall (Figure 3-3). This image was used to evaluate particle layer formation on the column wall. In these images, regardless of fluidization time, there are two gaps where no particles have adhered to the wall: approximately 1/3 of the way up the column (most easily seen in Figure 3-3 e and f), and near the distributor plate. The first gap corresponds to the static bed height, which was likely created due to bed oscillations at this height. The second gap was likely due to minimal motion of particles in the radial direction just above the distributor plate at this gas velocity. As a result, few particle-wall interactions occurred in this region leading to minimal particle wall fouling. However, at 360 min, less of a gap in this area was observed; after such a long fluidization

time sufficient particle-wall contacts have likely occurred for particles to begin to adhere to the wall.

As fluidization time increased, the magnitude of the particle wall fouling seemed to increase. The particle layer coverage grew from the fixed bed height toward the bottom of the column. These results support those obtained from the collected m% in this region.

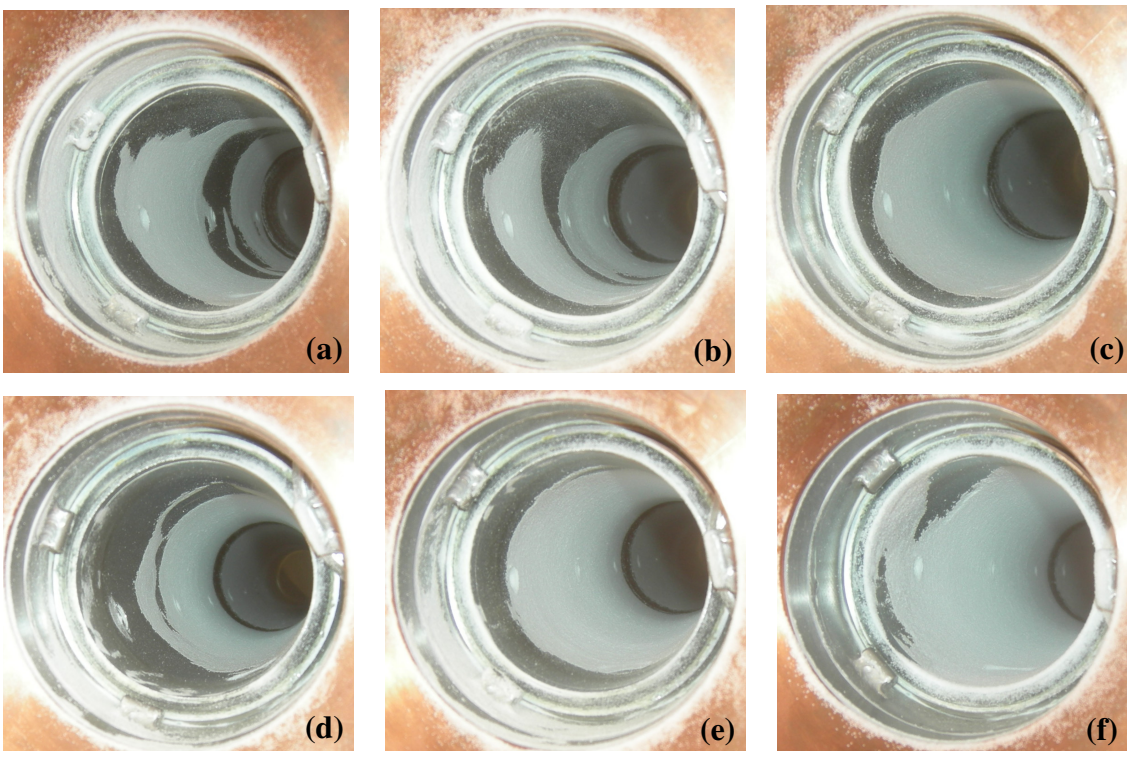

Figure 3-3: Images of particle layer on the column wall at 1.5 U_{mf} for different fluidization times: (a) 15 min, (b) 30 min, (c) 60 min, (d) 120 min, (e) 180 min, and (f) 360 min.

3.1.1.4. Particle Size Distribution (PSD)

Results demonstrated that particles collected within a single region were similar regardless of fluidization time (Figure 3-4); each region had a different PSD. Larger versions of the PSDs for each region and values for $D_{P\,0.1}$, $D_{P\,0.5}$, and $D_{P\,0.9}$ can be found in Appendix B.

The sizes of particles collected in the dropped section were comparable to the initial particles. This was expected as the dropped particles comprise the majority of the particles in the bed. The PSD in the wall region was comparable for all fluidization times indicating that the same size particles were adhering to the wall. Therefore, this particle range must be between those particles small enough to be elutriated from the bed by the fluidizing gas and those large enough that the gravitational force exceeds that of the electrostatic force binding them to the wall.

The fine particle PSDs were similar for all experiments. However, there could have been discrepancies in the amount of fines originally present in the initial particles in each experiment. Since the fines compose only a small portion of the overall size distribution of the initial particles (Figure 2-6), a slight difference in their sizes would not be enough to affect the initial PSD. However, with such a small amount of fines collected, any variation in their concentration in the initial sample could have an effect on their final mass collected. There were some larger particles present in the fines PSD; these particles were likely polymer fibres inherently present in the industrial resins, and were lightweight, thus easily elutriated from the bed.

Figure 3-4 also shows the PSD results of the particles in the extra sampling locations, intermediate wall and bottom column. The intermediate wall particles were slightly smaller than the dropped, and larger than those collected off the wall. These particles formed the outer layer of the wall particles. Thus, it was expected that they were loosely attached to the wall following the collection of the dropped particles, but were too large to remain adhered to the wall for an extended period of time. The bottom column particles varied in size for all trials but there was no obvious trend with fluidization time. The PSDs for this region consisted of particles smaller than those found in the wall region. This indicated that closer to the column wall, the size of particles was smaller.

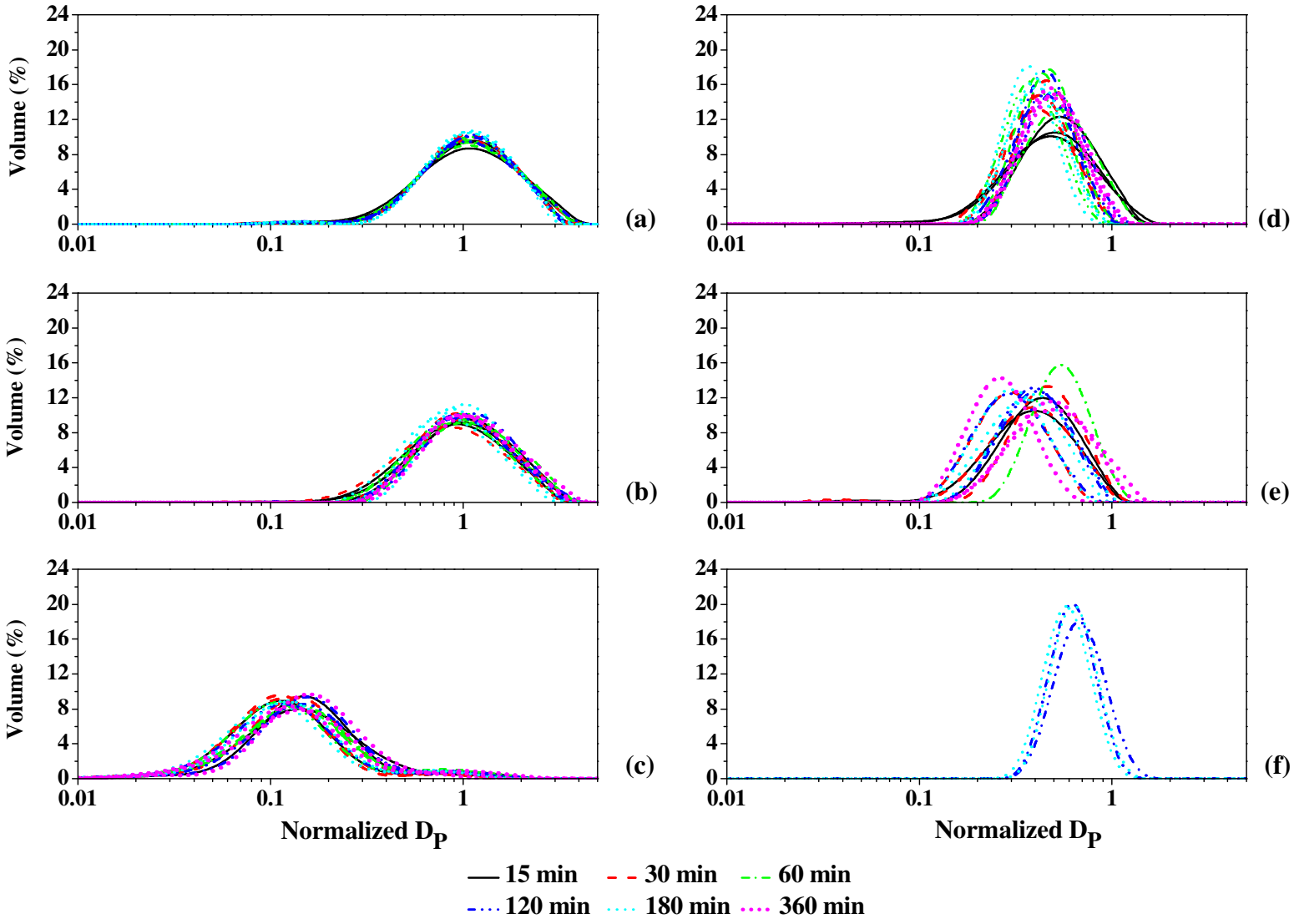

Figure 3-4: Normalized PSDs at 1.5 U_{mf} for different regions of the bed: (a) Initial, (b) Dropped, (c) Fines, (d) Wall, (e) Bottom Column, and (f) Intermediate Wall.

To compare the size range of particles collected at different sections of the bed, PSDs from all samples were plotted together for each fluidization time. All trials showed similar results. Figure 3-5 presents typical results from one trial at each of the different fluidization times. Overall, the fines were the smallest, followed by the column bottom, wall, intermediate wall and dropped particles. It can be seen that there was some size overlap between particles of all regions. This supports the previously suggested wall layer effect where particles with positive and negative charges, finer and larger particles respectively, form a layer on the column wall. The fines/wall overlap indicated that some smaller particles were adhering to the wall instead of being expelled from the bed. As these particles were most likely positively charged, based on the polarity of the collected fines, they provided the positive aspect of the layering. While larger particles which were more likely negatively charged, provided the opposite polarity layer. There was also a large overlap in the wall/dropped PSDs indicating that both regions shared similar size of particles. Two additional PSDs were considered: the particles remaining on the bottom of the column after the wall sample was collected and the particles that dropped off the wall between the collection of wall particles, only collected at longer fluidization times. The particles that fell on the ground were larger than the wall particles, while those that remained on the column were smaller; this suggested that the comparatively smaller particles of predominately negative charge adhered to the wall first followed by the larger particles building-up over time.

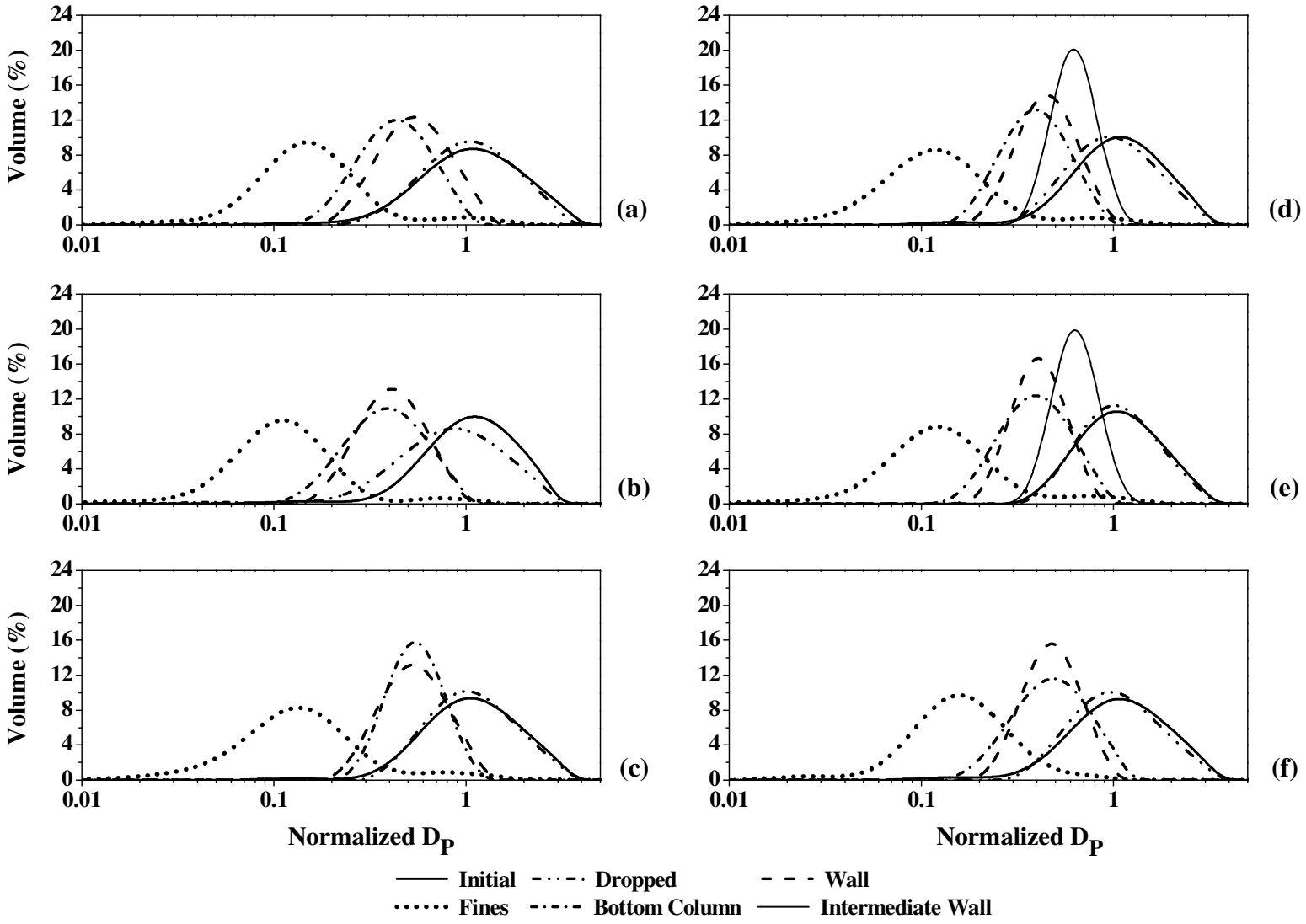

Figure 3-5: Example PSDs at 1.5 U_{mf} for all regions of the bed for different fluidization times: (a) 15 min, (b) 30 min, (c) 60 min, (d) 120 min, (e) 180 min, and (f) 360 min.

3.1.2. 1.75 U_{mf} Gas Velocity Results and Discussion

The results obtained for a fluidization gas velocity of 1.75 U_{mf} and the discussion of those results are presented in this section.

3.1.2.1. Mass Collected (m%)

Figure 3-6 shows the results of the m% found for different regions of the bed at different fluidization times. Overall, the m% of dropped particles decreased with fluidization time while that of the wall and the fines increased. This indicated that as fluidization time lengthened, particles either migrated from the bulk of the bed to the wall, or were elutriated from the bed. Since the m% of the wall increased over time, particles must have continued to adhere to the column wall due to electrostatic forces. The m% of fines collected increased slightly between 60 and 120 minutes after which a plateau seemed to be reached. As fluidization time increased, the smaller particles that remained in the bulk would have had the time to be elutriated. However, at longer fluidization lengths, either no more fines were left in the bulk or the fines had migrated to the wall layer due to electrostatic force.

The amount of particles that were not retrieved during the collection of the dropped, wall, and fine particles (Irretrievable) seemed to experience a slight increase up to 30 min and then a plateau was reached (Figure 3-6d). With longer fluidization times the particles close to the wall were likely to have more charge which prevented their easy detachment from the wall, resulting in a higher m% of particles that were not retrieved.

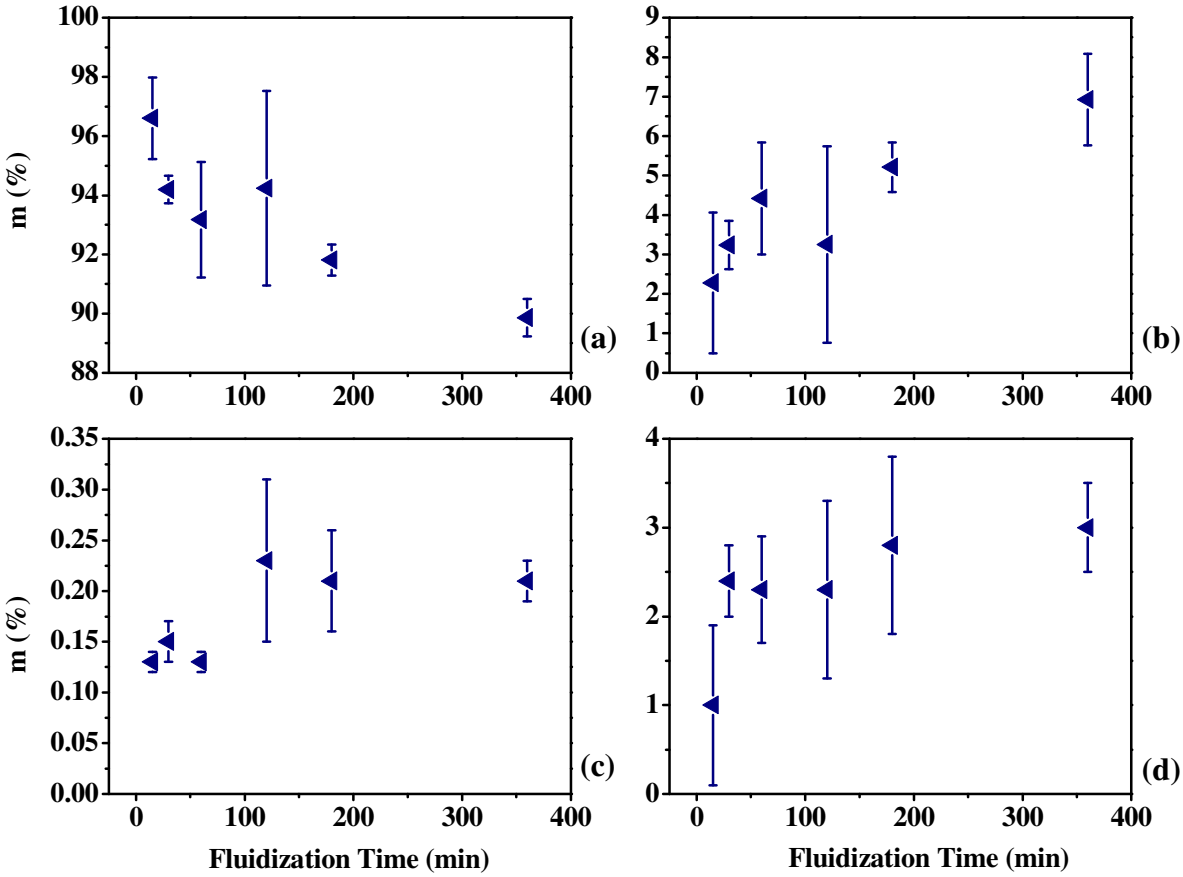

Figure 3-6: Mean m% of particles collected at 1.75 U_{mf} for different fluidization times: (a) Dropped, (b) Wall, (c) Fines, and (d) Irretrievable.

3.1.2.2. Charge-to-Mass Ratio (q/m)

The overall results of the average net q/m for all experimental runs are presented in Figure 3-7. The initial q/m of all particles was similar for all trials (Figure 3-7a). 120 minutes had the largest variation in the initial net q/m; however, in comparison to the values obtained for the other measurements the difference was minor, as all regions had values for q/m at least one magnitude larger than the initial values.

The magnitude of net q/m for each region of the bed differed from the other regions. The initial particles had the lowest q/m, ranging from -0.08 to -0.15 µC/kg, followed by the dropped particles, ranging approximately -0.35 to -0.95 µC/kg. The wall particles had q/m magnitudes approximately two times larger than that of the initial particles, ranging

approximately -35 to -80 μC/kg. In comparison to the negative net q/m of the other three regions, the fine particles had a positive net q/m, ranging from 25 to 275 μC/kg. These results of positively and negatively charged polyethylene particles supports the theory of bi-polar charging as the large and small particles gained opposite polarity.

The magnitude of the net q/m for the dropped and wall particles seemed to be similar for all fluidization times, due to the large amount of variation in results for all trials (Figure 3-7). This is an indication that a saturation of net q/m was achieved within the first 15 minutes of fluidization for both regions. Since the dropped region m% collected decreased with fluidization time, the net charge must have become less negative to maintain a constant q/m ratio. Thus, either the particles leaving the dropped region of the bed had a high magnitude of negative charge or some of the particles remaining became more positively charged as fluidization progressed. Since the magnitude of q/m of the dropped particles was low compared to other regions of the bed, two explanations are possible: this region was composed of both positively and negatively charged particles or the majority of bulk particles did not gain much charge. At this gas velocity, the bed was in the bubbling flow regime where a large amount of mixing and particle-particle contacts took place, likely generating charge. Thus, it is probable that the second hypothesis is valid, creating a low magnitude net q/m.

In the wall region, since the m% collected increased with fluidization time, the net charge must have become more negative to keep the q/m ratio constant. This indicates that over time more of the bulk particles became charged and migrated toward the column wall due to the electrostatic forces. As previously discussed, the column wall would become positively charged following particle-wall contacts, due to the work function differences between the two materials. Therefore, the inner particle layer (i.e., those particles closest to the stainless steel column wall) must have had a strong negative net charge. In order for additional particles to adhere to the wall, positive charge would be required for an alternating charge sequence that would allow particles to adhere to one another. Therefore, two alternative events could be occurring. The particles moving from the bulk of the bed to the wall region were likely predominately composed of particles with small positive and large negative charges, where the large particles were more negatively charged as the distance from the

wall increased. Alternatively, the column wall could provide the majority of positive charge required to attract negatively charged particles throughout the building of the particle layer, supplemented by a small number of finer, positively charged particles. Finally, the net negative charge of the bulk particles would create repulsion between negatively charged particles and thus forcing them towards the column wall.

The net q/m of the fine particles increased in magnitude with fluidization time. Since the m% collected increased slightly with time, the charge would have had to increase at a greater rate than m%, to keep their ratio rising. With extended fluidization periods the particles were likely more charged due to an increased residence time within the reactor that allowed for more interactions to take place; thus generating more charge.

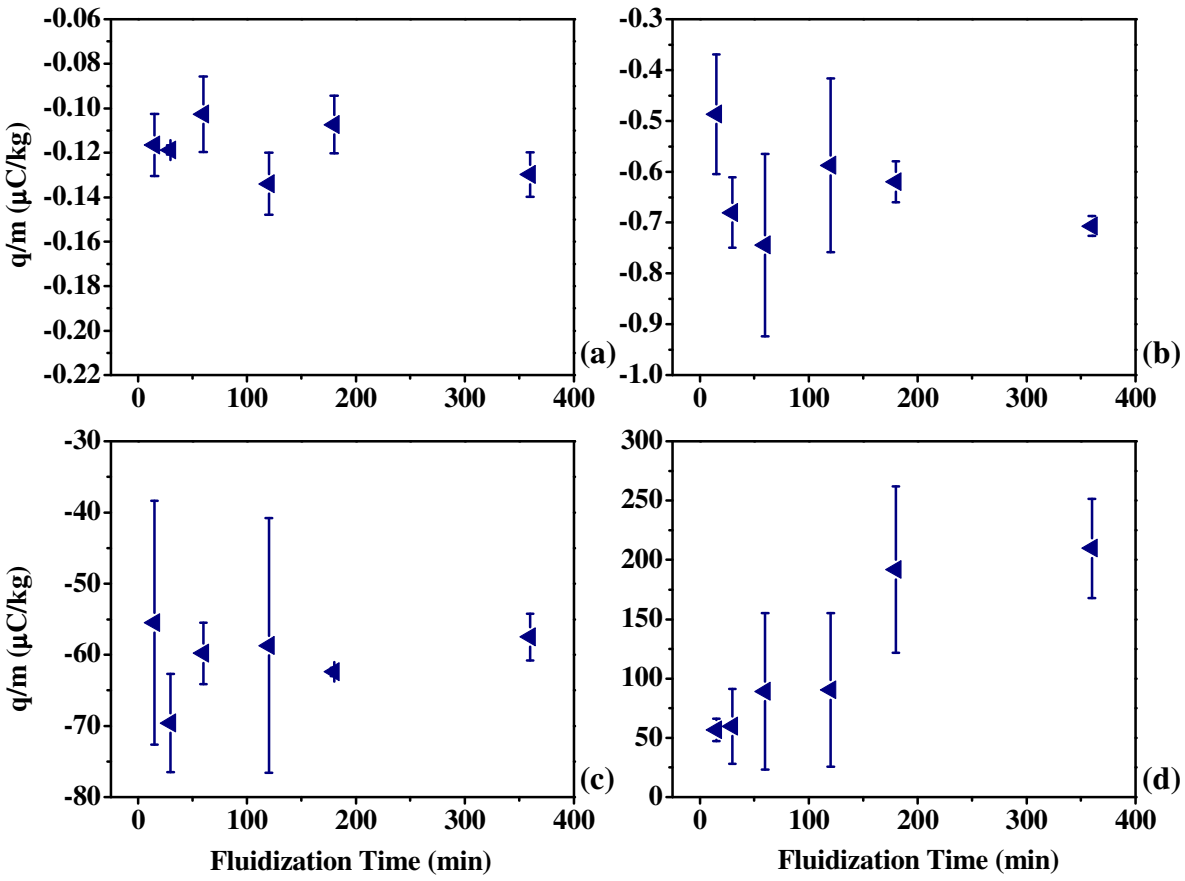

Figure 3-7: Mean net q/m at 1.75 U_{mf} for different fluidization times: (a) Initial, (b) Dropped, (c) Wall, and (d) Fines.

3.1.2.3. Wall Particle Layer

The examples of the wall particle layers at different fluidization times for 1.75 U_{mf} are presented in Figure 3-8. A similar gap to that observed in 1.5 U_{mf}, was found in wall layer approximately 1/3 of the way up the column. This gap is located at the height of the static bed and is likely due to bed oscillations. At this gas velocity there was no clearly defined gap at the bottom of the column above the distributor plate.

As fluidization time increased, the m% of particles collected from the wall increased. However, from observation it was difficult to see a clear progression of increased wall layer coverage with fluidization time since the length of the layer was similar for all times with the exception of 15 min, which as can be seen had less of a layer. Therefore, it was likely that the increase in m% collected was due to an increase in the layer thickness; however, a measurement of wall thickness was not made.

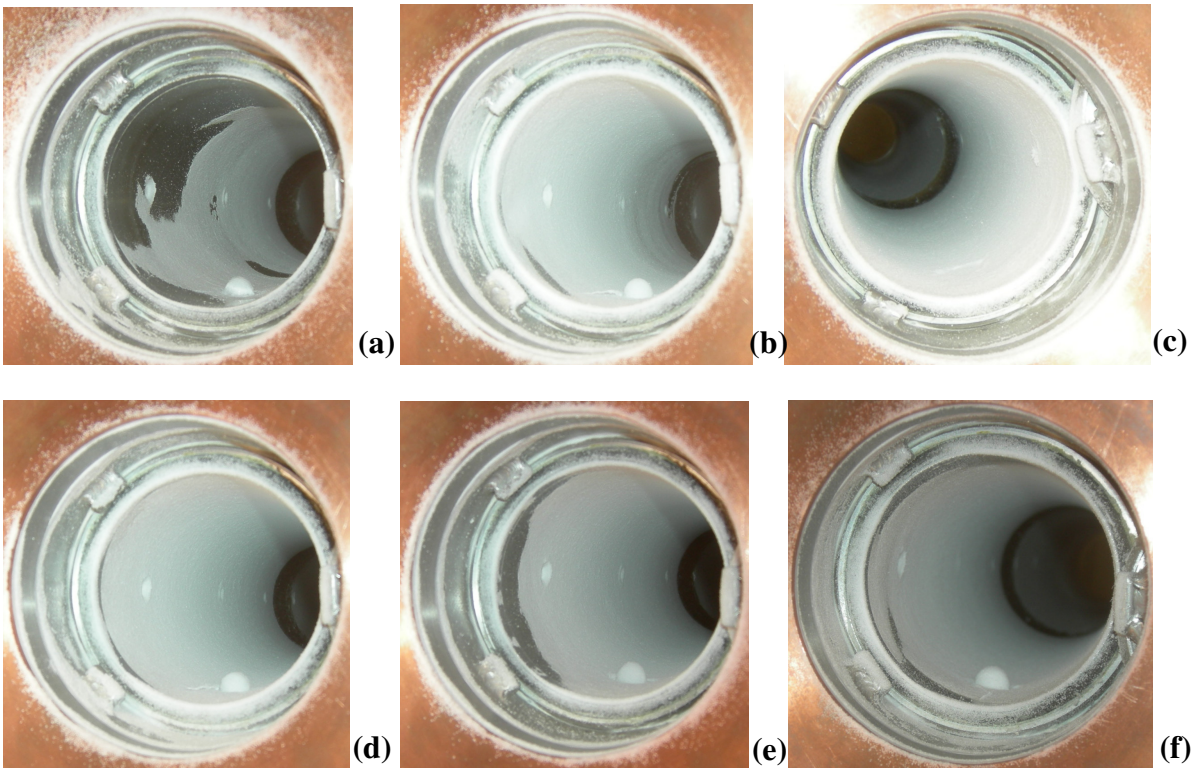

Figure 3-8: Images of particle layer on the column wall at 1.75 U_{mf} for different fluidization times: (a) 15 min, (b) 30 min, (c) 60 min, (d) 120 min, (e) 180 min, and (f) 360 min.

3.1.2.4. Particle Size Distribution (PSD)

The normalized mean particle sizes for all trials are presented in Figure 3-9. Individual versions of these graphs and values for $D_{P\ 0.1}$, $D_{P\ 0.5}$, and $D_{P\ 0.9}$ can be found in Appendix B. It can be seen that for all trials, the dropped, wall and fine particles maintained a similar size with respect to the fluidization time, with some variation present in the dropped and wall regions. The dropped mean particle size was similar to that of the initial particles. This similarity was expected as the dropped region was composed of the majority of particles initially put into the fluidization column. For the wall and fine particles, there was no apparent trend with fluidization time. This indicates that only particles of a certain size could adhere to the wall or be elutriated from the bed at this gas velocity, regardless of fluidization time.

The fine particles PSD was similar for all trials regardless of fluidization time (Figure 3-9d). Therefore, this was the size of particles able to be elutriated from the bed at this gas velocity. As previously mentioned, the presence of some larger particles in the fines PSD, was likely due to polymer fibres present in the industrial resin.

The particles collected from the column bottom were either slightly small or very similar to those in the wall region. These two regions have the most variance in particles size. This is likely due to two reasons. The first is that as the particle layer builds on the column wall there is variance between trials in how the particles adhere to the wall; even though similar sized particles are found throughout the layer where those particles that are within the layer may vary slightly. This means that although the bottom column PSD sample was removed from the same location, the particles that were present were unlikely to be exactly the same from trial to trial. The second reason is the method of sampling. The wall region was collected due to vibration overcoming the electrostatic force binding particles to the wall and then all of these particles fell into the same cup. As a result, the exact location of the PSD sampling on the wall may not be continuous causing slight differences in results. However, based on the mean values of $D_{P\ 0.1,}$ $D_{P\ 0.5}$, and $D_{P\ 0.9}$ (Appendix B) the results show that particles of specific size consistently compose the column wall.

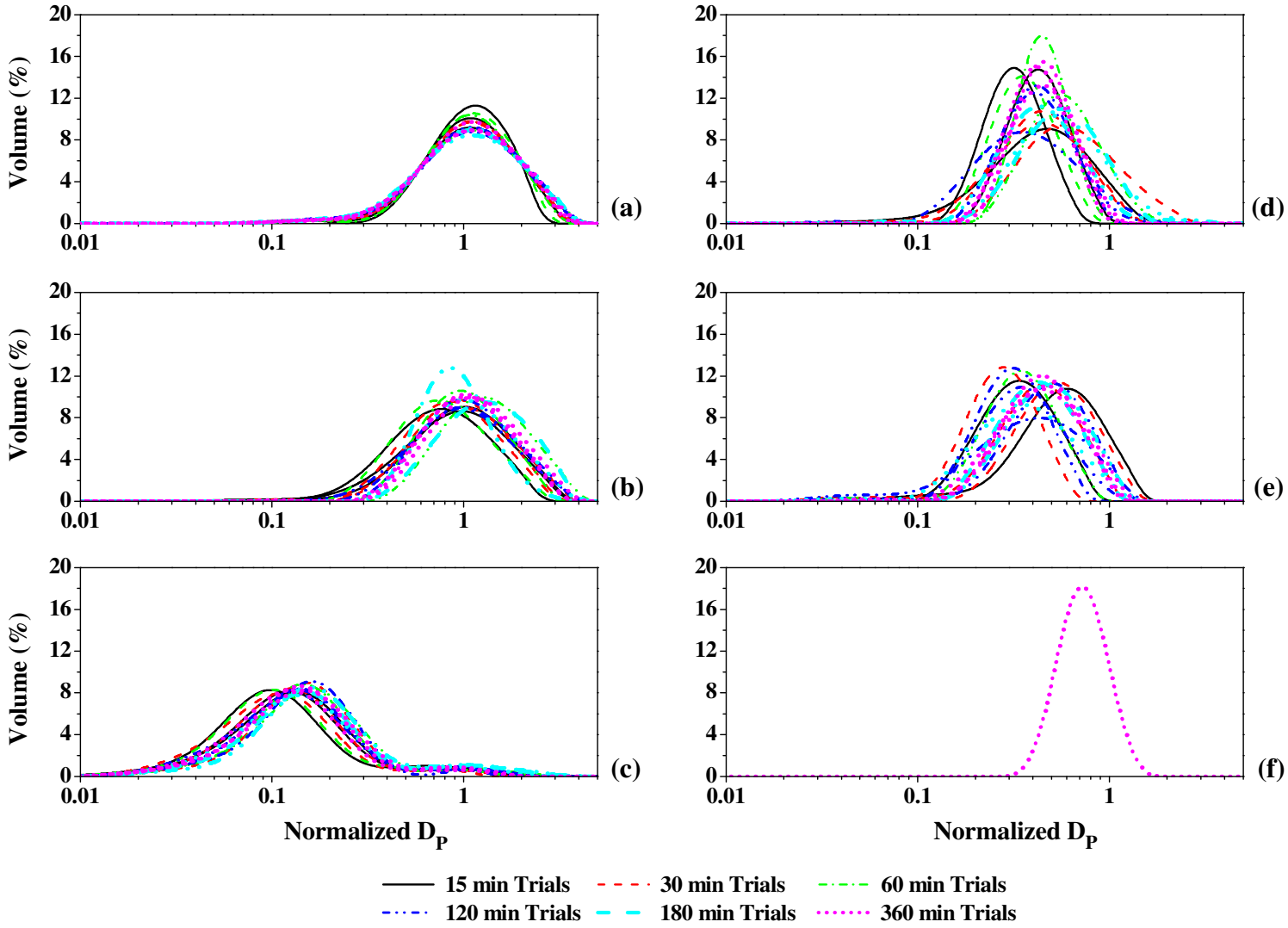

Figure 3-9: Normalized PSDs at 1.75 U_{mf} for different regions of the bed: (a) Initial, (b) Dropped, (c) Fines, (d)Wall, (e) Bottom Column, and (f) Intermediate Wall.

The PSDs of all different regions of the bed for each different fluidization time are depicted in Figure 3-10. For all fluidization times, the initial particles were slightly larger than the dropped particles, the intermediate wall particles were next in size, followed by the wall and the bottom column particles, which were either similarly sized or the latter was slightly smaller. The fines were the smallest particles of all the regions. There was some overlap between several regions within the fluidized bed. This indicated that where the particles were initially located in the bed prior to fluidization partially influenced which region of the bed these particles finally end up. If the particles were near the wall, they were more likely to adhere to the wall, whereas if they were near the top of the bed then they were more likely to be elutriated from the bed. If they were in the centre of the bulk, they were likely to stay in the bulk.

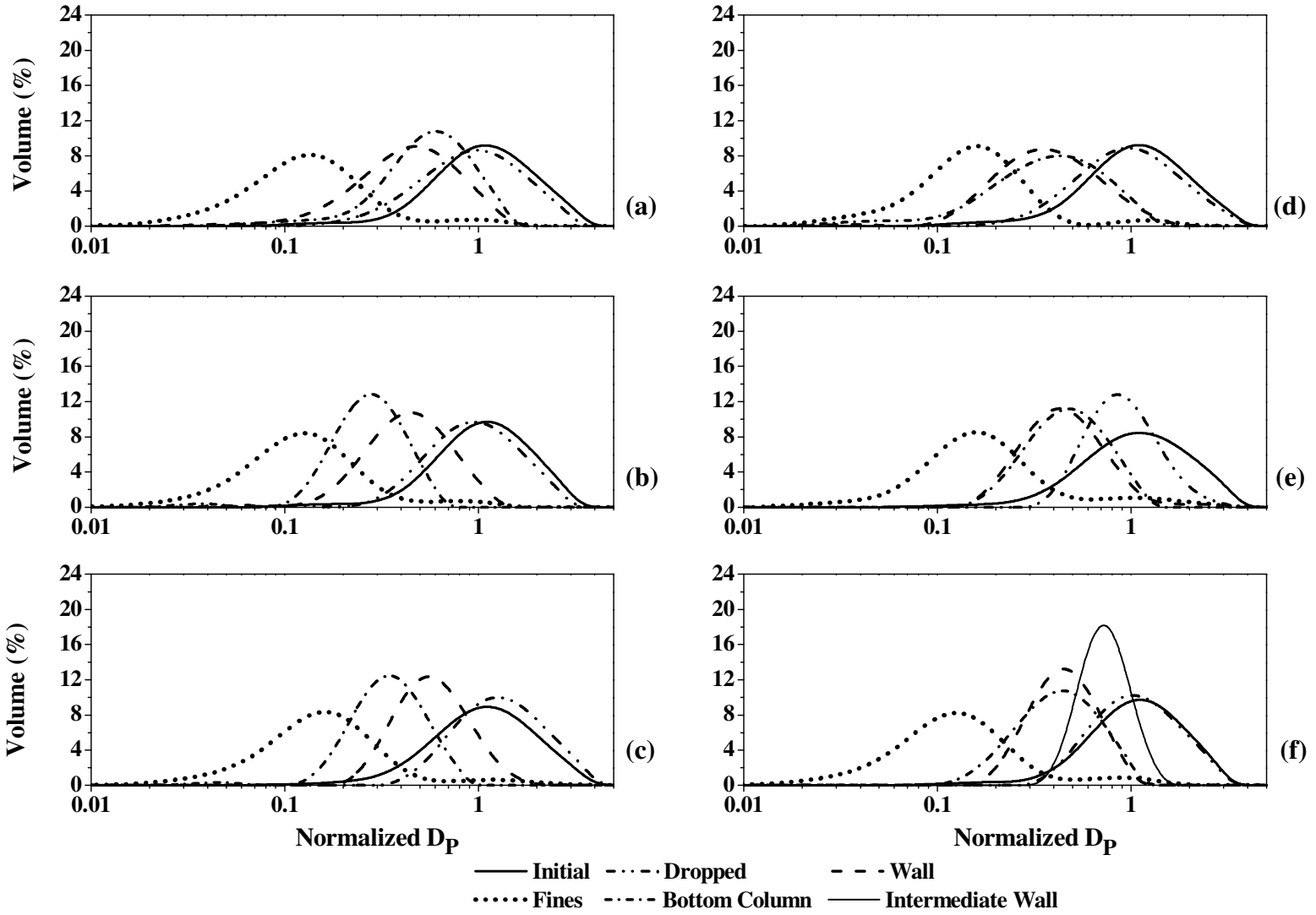

Figure 3-10: Example PSDs at 1.75 U_{mf} for all regions of the bed for different fluidization times: (a) 15 min, (b) 30 min, (c) 60 min, (d) 120 min, (e) 180 min, and (f) 360 min.

3.1.3. Bubbling Flow Regime Comparison

This section compares the results obtained for the two gas velocities of 1.5 and 1.75 U_{mf} examined in the bubbling flow regime.

3.1.3.1. Mass Collected (m%)

The m% of dropped particles collected at the two different velocities followed similar trends; as fluidization time increased the m% collected decreased (Figure 3-11a). This indicated that with both gas velocities the particles either migrated away from the bulk to the wall region or were elutriated as fines. The magnitudes of the m% of dropped particles for each gas velocity were similar for all fluidization times. Thus, within the bubbling flow regime, similar amounts of particles were leaving the bulk as fluidization time increased regardless of fluidizing gas velocity. Therefore, for the velocities tested in this study, the amount of particles in the dropped region within the bubbling flow regime is more dependent on fluidization time than on gas velocity.

In the wall region, the m% collected depicted similar trends for both velocities (Figure 3-11b). The values of m% obtained were relatively similar for each fluidization time with both gas velocities with the average values of the 1.75 U_{mf} being abit larger. Overall, it can be concluded that similar amounts of particles were adhering to the column wall. This is expected as the particles have more opportunity to adhere to the column wall with extended fluidization times. Therefore, for the velocities examined in this study, the quantity of particles found in the wall region in the bubbling flow regime is dependent on fluidization time, but not on gas velocity.

For 1.5 U_{mf}, the m% of fines collected was similar for all fluidization times, whereas for 1.75 U_{mf}, the m% of fines increased slightly between 60 minutes and 120 minutes (Figure 3-11c). The magnitude of m% collected at each fluidization time was the same or higher for gas velocities of 1.75 U_{mf}. This was expected as with a higher gas velocities particles of larger size are able to be elutriated from the bed, as well as more particles are entrained; this was most evident after 60 min. This increase could be the time necessary to enable finer

particles at the bottom of the bed to make their way to the top of bed to be elutriated; after which a plateau was reached. However, as demonstrated by the magnitude of the m% collected at 1.5 U_{mf} at short fluidization times versus the longer fluidization times, the majority of particles were elutriated from the bed within the first 15 minutes of fluidization.

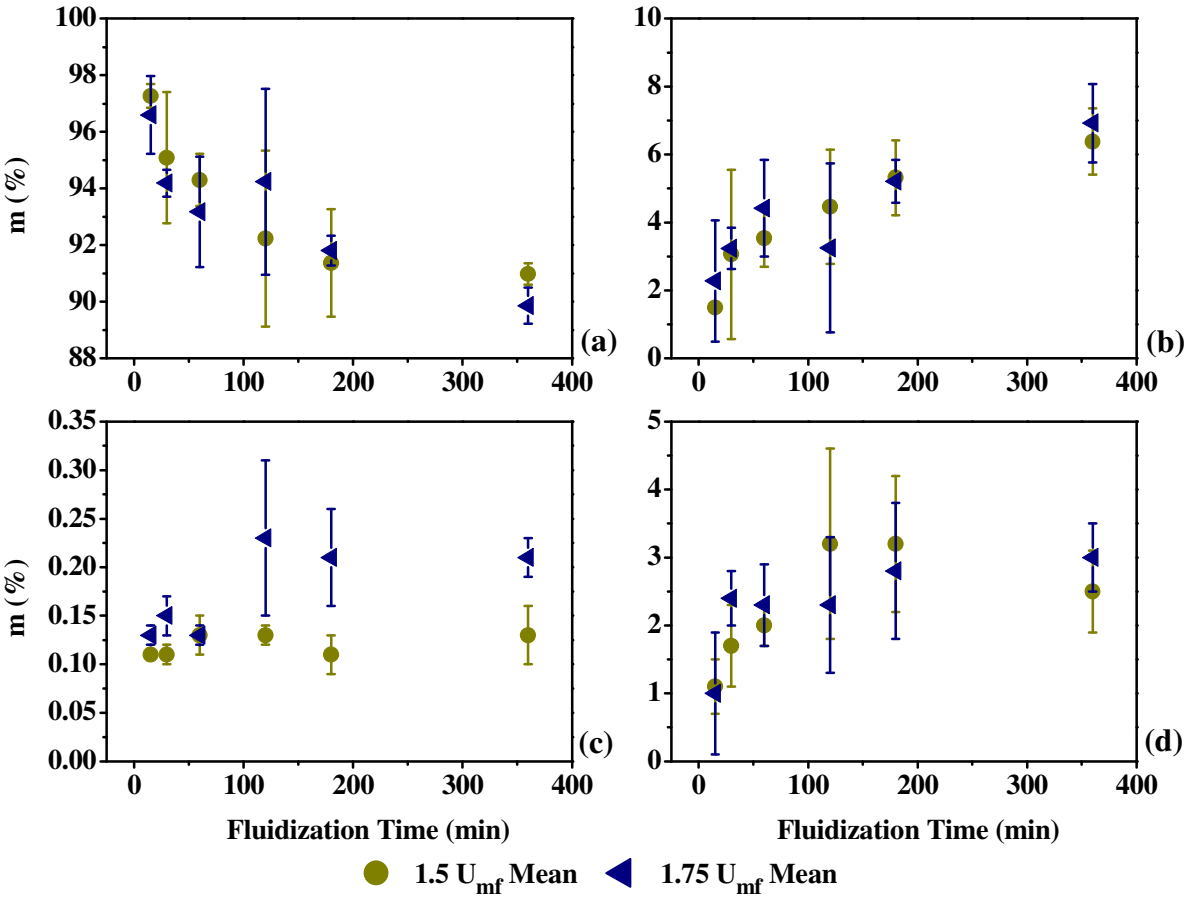

Figure 3-11: Comparison of m% for two velocities in bubbling flow regime: (a) Dropped, (b) Wall, (c) Fines, and (d) Irretrievable.

For each gas velocity, there was a slight increase in the amount of particles unable to be collected during the shorter fluidization times and then reached a plateau at later fluidization times. As the particle layer built on the wall with fluidization time, it was more difficult to remove particles from the wall, as this was where the majority of particles lost during sampling remained.

3.1.3.2. Charge-to-Mass Ratio (q/m)

The initial particle net q/m was comparable for all fluidization times with the exception of the 120 and 360 minute trials (Figure 3-12a). However, the values for both of these fluidization times fell into the variation of other fluidization times which resulted in the assumption that the initial charge was similar enough to be compared.

The trends for net q/m for the dropped region differed for 1.5 U_{mf} and 1.75 U_{mf} gas velocities (Figure 3-12b). For 1.5 U_{mf}, the mean net q/m seemed to increase in magnitude as the fluidization time increased with a plateau reached after 60 minutes, whereas at 1.75 U_{mf}, the q/m was comparable for all trials. Therefore, the maximum net q/m values cannot be obtained in short fluidization times for a gas velocity of 1.5 U_{mf}, however at 1.75 U_{mf} the bed was able to reach q/m saturation within 15 minutes. The mean values for charge obtained for each fluidization time are comparable regardless of gas velocity due to the variation within each sample point.

The net q/m for the wall region at 1.5 U_{mf} follows a trend of decrease in magnitude with fluidization time until after 60 minutes where the q/m reached a plateau; the net q/m for 1.75 U_{mf} showed comparable values for all fluidization times (Figure 3-12c). This suggested that with a gas velocity of 1.75 U_{mf}, maximum net q/m on the wall was reached shortly after fluidization began. However, with lower gas velocity a net q/m saturation requires a longer fluidization time. This concludes that within the bubbling flow regime the higher the gas velocity, the higher the number of particle-particle and particle-wall contacts resulting in more charge generation. The magnitude of q/m at each fluidization time is comparable; therefore the net q/m is not dependent on gas velocity.

The net q/m for the fine particles increased with fluidization time for both gas velocities (Figure 3-12d). This was expected, as with both velocities, the increased fluidization time allowed slightly more particles to leave the bed and those particles had more time inside the bed to gain additional charge. The magnitude of the net q/m is comparable for both gas velocities. As the m% of fines collected is higher for 1.75 U_{mf}, the net charge generated must have increased as well.

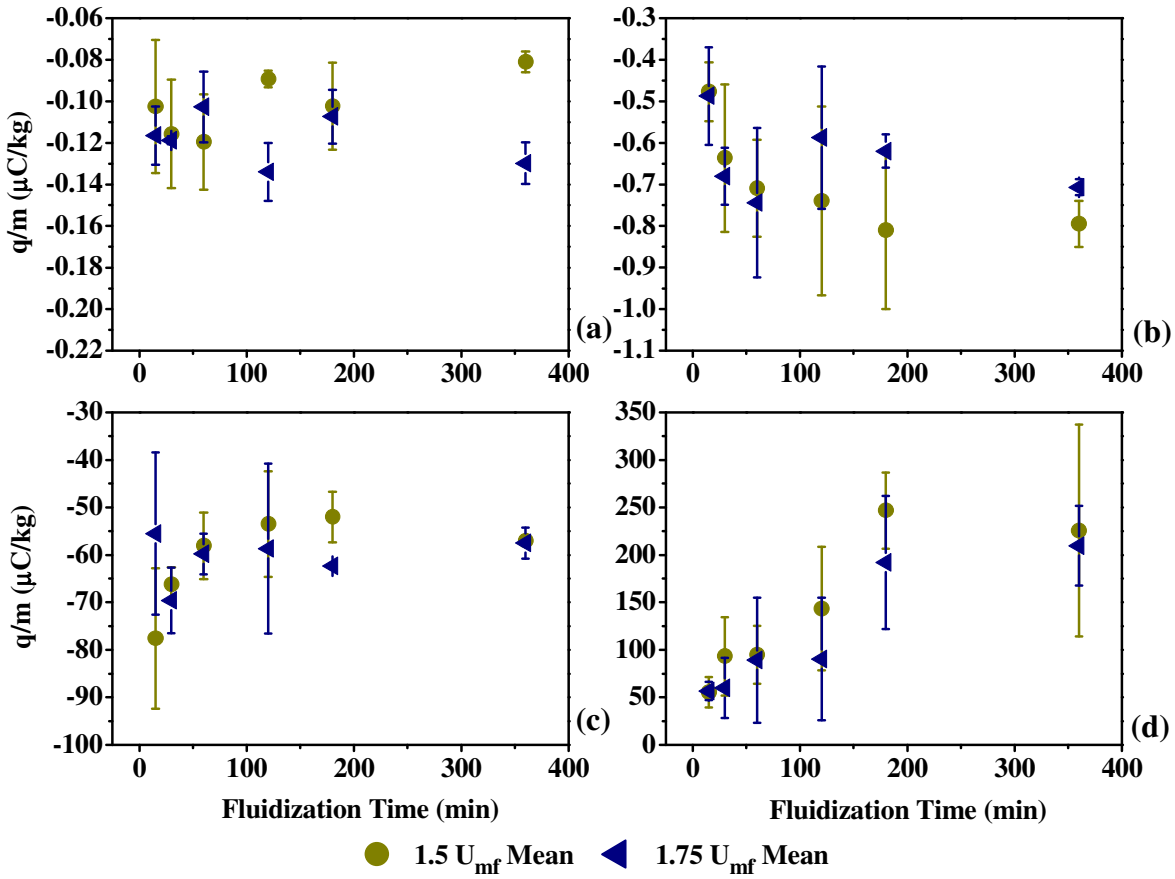

Figure 3-12: Comparison of mean net q/m for two velocities in bubbling flow regime: (a) Initial, (b) Dropped, (c) Wall, and (d) Fines.

3.1.3.3. Particle Size Distribution (PSD)

Figure 3-13 compares the normalized PSD ($D_{P\ 0.1}$, $D_{P\ 0.5}$, $D_{P\ 0.9}$) for the dropped, wall and fines regions. The PSDs for each region are comparable for both gas velocities. This indicated that similar sized particles were found in each region regardless of gas velocity. However, it is important to note that the $D_{P\ 0.9}$, at 1.75 U_{mf} of both the wall and the fine regions had slightly higher values. Thus there were some large particles present in these areas due to the higher gas velocity. With respect to the wall region, this was likely a result of more vigorous mixing, due to the higher gas velocity, leading to more interactions, and therefore more charge generation on individual particles. This increased charge would allow the electrostatic force on these larger particles to counter the gravitational force preventing them from adhering to the wall. However, since the particles were larger, the increased

charge did not impact the net q/m as the ratio remained the same. The slightly larger fine particles were due to the ability of the higher gas velocity to elutriate larger particles.

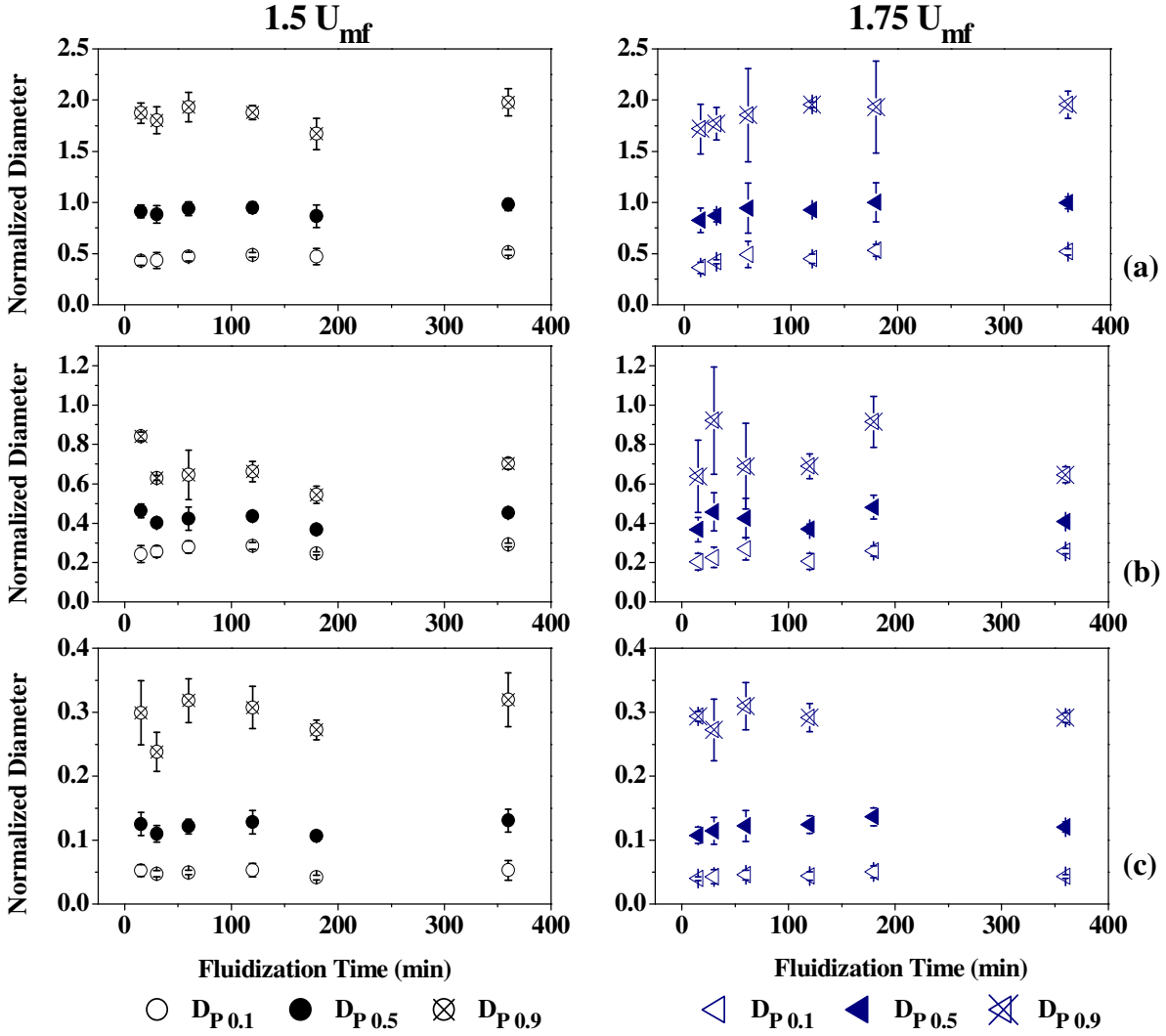

Figure 3-13: Comparison of normalized PSDs for two velocities in bubbling flow regime: (a) Dropped, (b) Wall, and (c) Fines.

3.1.4. Bubbling Flow Regime Summary

Net q/m saturation was reached by 60 min for both the dropped and the wall regions at 1.5 U_{mf}. This was comparable to previous studies that also found that charge saturation was reached at 60 min (Fujino et al., 1985; Revel et al., 2003; Wolny and Opalinski, 1983). These three studies all used acrylic columns with a variety of particles. At 1.75 U_{mf}, charge

saturation was reached before 15 min of fluidization time had elapsed; this also corresponds to some of the previous studies reported in literature (Ali et al., 1999; Guardiola et al., 1992; Murtomaa et al., 2003; Wolny and Kazmierczak, 1989). These studies used a variety of columns (i.e., steel, acrylic, and glass) and a range of sizes from 98 μm to 1130 μm for different particles. Overall, results of the net q/m showed that more charges were generated at the higher gas velocity which correlates well with the fact that higher gas velocity results in more contacts between particles themselves and those with the column wall.

Both gas velocities tested in the bubbling flow regime resulted in reactor wall fouling. However, the particle layers were slightly different between the two velocities. At the lower gas velocity, the height of the particle layer increased as fluidization time increased. This growth correlated with more m% collected with additional fluidization time. In contrast, at the higher gas velocity, the wall particle layer covered most of the column wall at shorter fluidization times of 30 min after which the increase in m% was likely due to an increase in thickness of the wall layer. At both velocities, a gap in the layer was found 1/3 up the column from the distributor plate where bed surface oscillations were occurring.

3.2. Slugging Flow Regime

Two gas velocities were examined in this flow regime, 3.5 and 4.0 U_{mf}. In this section, results obtained for each velocity are first discussed separately and then compared..

3.2.1. 3.5 U_{mf} Gas Velocity Results and Discussion

The results obtained for the fluidization gas velocity of 3.5 U_{mf} and the associated discussion are presented in this section.

3.2.1.1. Mass Collected (m%)

The mass of particles collected from the dropped and the wall regions were similar regardless of fluidization time indicating that the amount of particles that migrated from the

dropped region to the wall did not increase as fluidization time increased (Figure 3-14). Therefore, either the particles remained in the region of the bed where they were initially found, or the same amount of particles migrated from the bulk to the wall as from the wall to the bulk, maintaining an equal flux. The fines m% increased with fluidization time with a plateau reached after 180 minutes. Therefore, the majority of fine particles were elutriated or had adhered to the column wall within 180 minutes of the onset of fluidization.

The amount of particles that were not retrieved during the collection processes of different regions was comparable for all fluidization times (Figure 3-14d). These particles were mostly those that adhered to the column wall, both at the top and bottom of the column, although some may also have been lost during the sampling process.

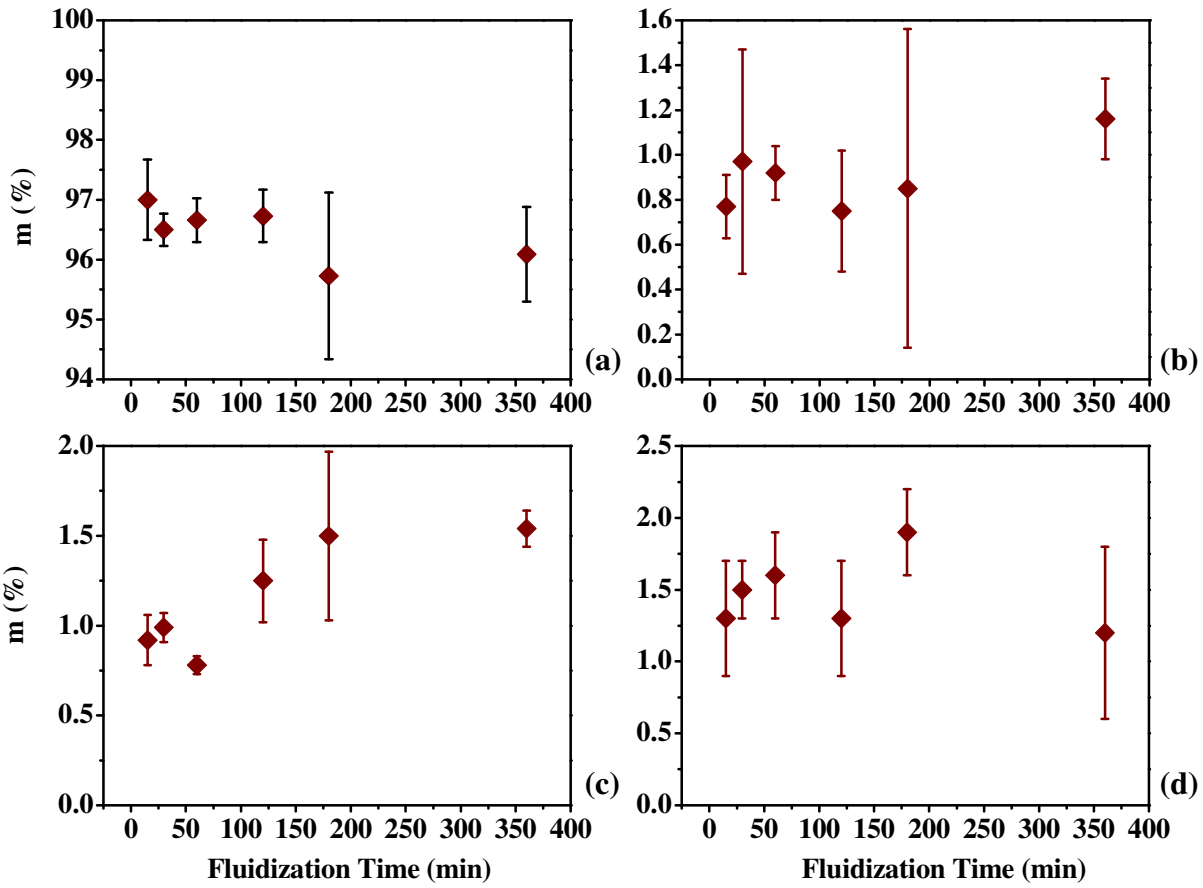

Figure 3-14: Mean m% at 3.5 U_{mf} for different fluidization times: (a) Dropped, (b) Wall, (c) Fines, and (d) Irretrievable.

3.2.1.2. Charge-to-Mass Ratio (q/m)

While the initial net q/m had some variation, all the mean values were in the same range, and similar enough to assume that the starting net q/m was equivalent for all trials (Figure 3-15a).

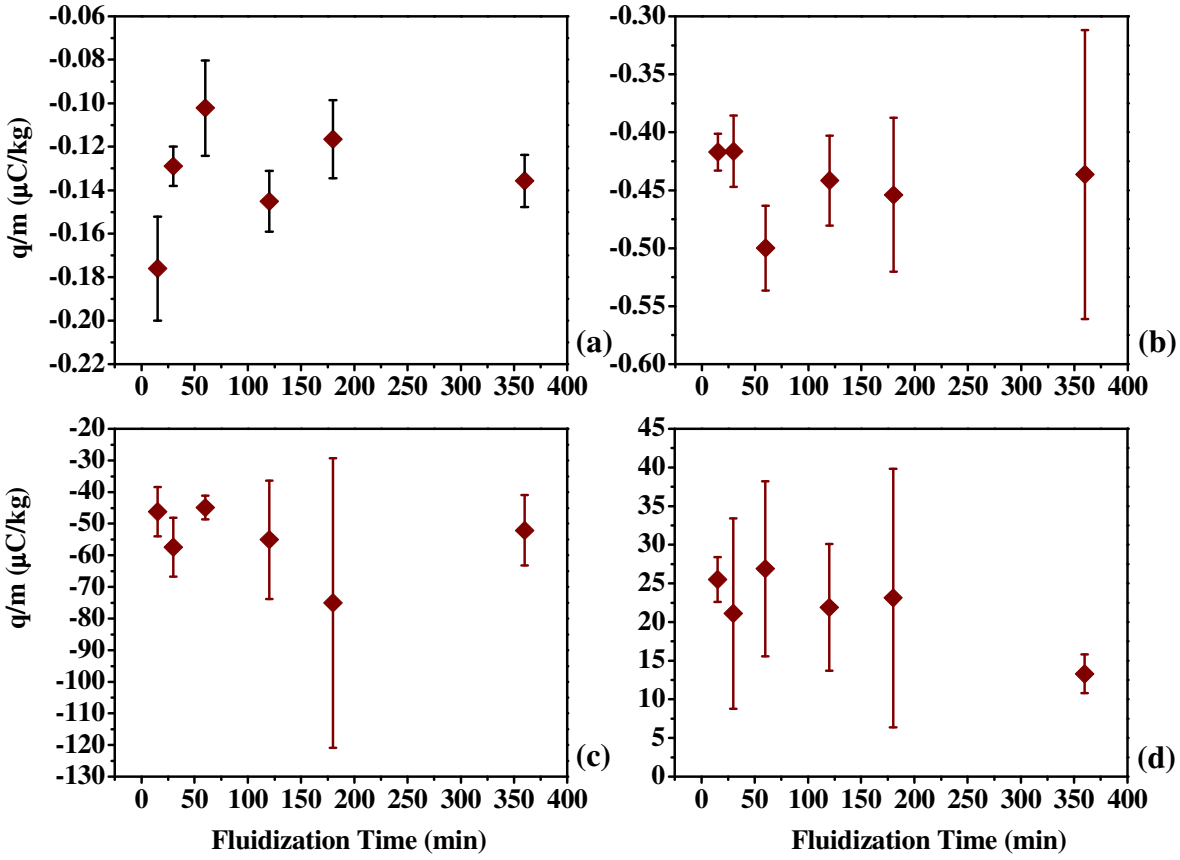

Figure 3-15: Mean net q/m at 3.5 U_{mf} for different fluidization times: (a) Initial, (b) Dropped, (c) Wall, and (d) Fines.

The difference in magnitude of the net q/m for each region of the bed is important to note. The initial particles had a small q/m, ranging approximately from -0.08 to -0.20 µC/kg. Thus, since all other regions had a much larger net q/m, the particles obviously gained charge during fluidization. The dropped particles had the next smallest magnitude, ranging approximately from -0.42 to -0.50 µC/kg, likely due to the combination of large negatively charged and small positively charged particles. The wall particles had the largest negative magnitude, ranging approximately from -44.9 to -75.1 µC/kg; thus, the wall region was mainly composed of negatively charged particles. As mentioned in previous sections, the

work functions of stainless steel and polyethylene predicted that the stainless steel column would become positively charged when contact was made with polyethylene, which would become negatively charged; thus, explaining the high negative charge in the wall region. The fine particles had a slightly smaller magnitude than the wall particles, ranging approximately from 16.2 to 32.7 μC/kg, but were positively charged. These results support the bipolar charging theory as mentioned previously since they indicated that in the system under study, larger polyethylene particles become negatively charged while smaller particles become positively charged. In addition, since the initial charge of these smaller particles was negative (Figure 2-8), these particles are not only gaining charge but also changing polarity.

As seen in Figure 3-15 in the dropped and wall regions, the net q/m measurements had constant values for all fluidization times which indicated that q/m saturation was reached shortly after the onset of fluidization. This could have been due to the bed hydrodynamics of the slugging flow regime. In this regime, relatively less mixing takes place in the bulk due to slug formation, which minimizes the radial movement of the particles. As such, the amount of particle-particle interactions in the bulk probably did not increase significantly with increased fluidization length. Along the wall, particle-wall contacts below the fixed bed height would only be present for a short period of time before a particle layer built upon the reactor wall. After that time, the majority of interactions would be between particles on the outer layer of the bulk and particles adhered to the column wall. Thus, the total amount of charge generated in this area would have been minimal compared to the charge generated by the contact between particles and the stainless steel column wall at the start of fluidization, resulting in little impact on the net q/m. However, some frictional charging likely took place as particle-wall contacts could have occurred by the slugs movements up and down the column wall. However, in this area particles would be unable to adhere to the wall due to the movement of the next slug brushing them off the wall. Therefore, these particles would have fallen back into the bulk and were expected to have little effect on the net q/m in that region as the percentage of particles charging in this manner would be minimal compared to the overall number of particles.

The net q/m for the fine particles was comparable for all fluidization times. Therefore, as the m% of these particles increased with fluidization time, they must have gained more

charge to maintain a constant net q/m. A longer residence time within the column would have allowed for more particle interactions with other particles and the column wall, thus generating more charge.

3.2.1.3. Wall Particle Layer

The magnitude of the column wall fouling for different fluidization times was qualitatively examined from pictures taken from inner column wall as shown in Figure 3-16. As seen, there are some particle accumulations at the bottom of the column, followed by a gap. This gap likely corresponds to where slugs are fully formed; thus having the frictional force to brush particles off of the column wall. Particles accumulation is further seen above this gap where the bursting of slugs and the elutriation of particles allows for a particle layer to build. Most of the fluidization times resulted in similar layers on the bottom of the column. This correlates with the similar m% collected for all fluidization times.

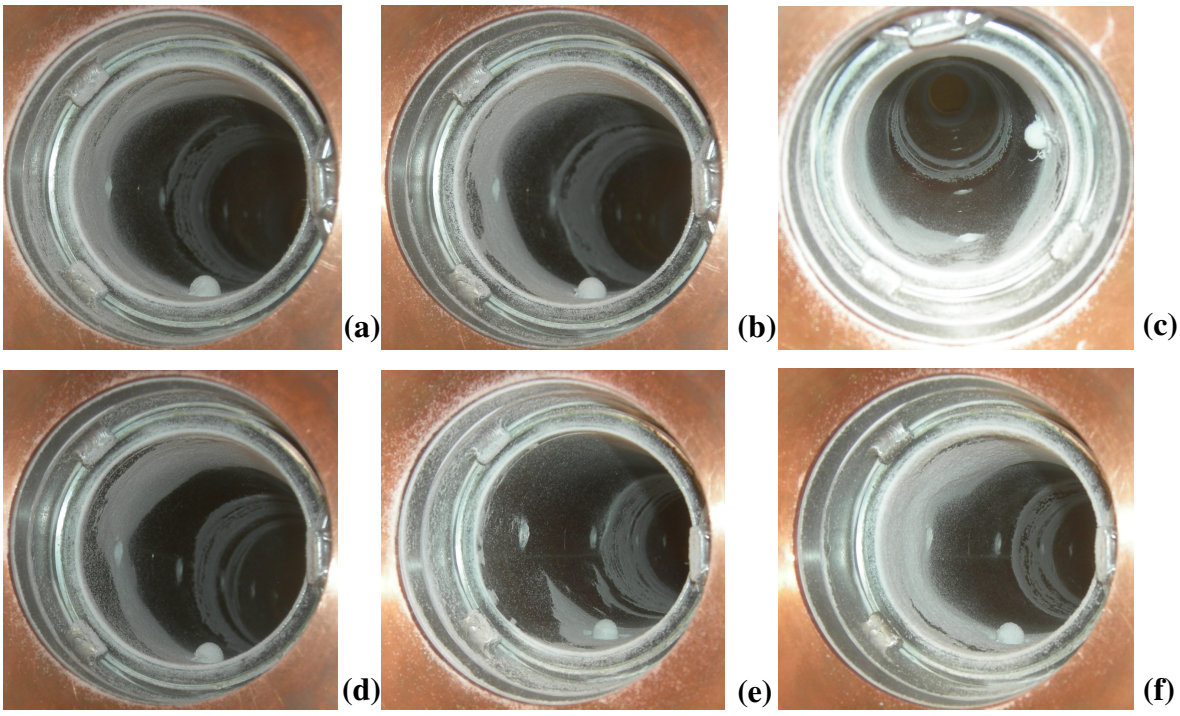

Figure 3-16: Images of particle layer on the column wall at 3.5 U_{mf} for different fluidization times: (a) 15 min, (b) 30 min, (c) 60 min, (d) 120 min, (e) 180 min, and (f) 360 min.

3.2.1.4. Particle Size Distribution (PSD)

The size range of particles in each region of the bed was found to be not dependent on fluidization time since they were all comparable (Figure 3-17). Individual versions of these graphs and values for $D_{P\ 0.1}$, $D_{P\ 0.5}$, and $D_{P\ 0.9}$ can be found in Appendix B. Some of the regions of the bed had a trial that varied from the overall trend; this was likely due to small variation in the initial resins used for experiments.

The largest particles in the bed were in the dropped region, which were similar in size to the initial mean particle diameter. The next largest particles were the wall and those collected from the bottom of the column. These two samples were close in terms of mean particle diameter, indicating that particles on the wall were of comparable size. Thus, this was the size of particles that could gain enough electrostatic charge to be able to adhere to the column wall and withstand the motion of the slugs against the particle layer. As the slugs moved up the column, loosely adhered particles could fall off due to the friction created between the particles in the bulk rubbing against the particles on the wall. Thus, only particles tightly adhered to the wall would remain as part of the wall particle layer. The smallest particles in the bed were the fines and those collected from the top of the column wall, which had comparable size.

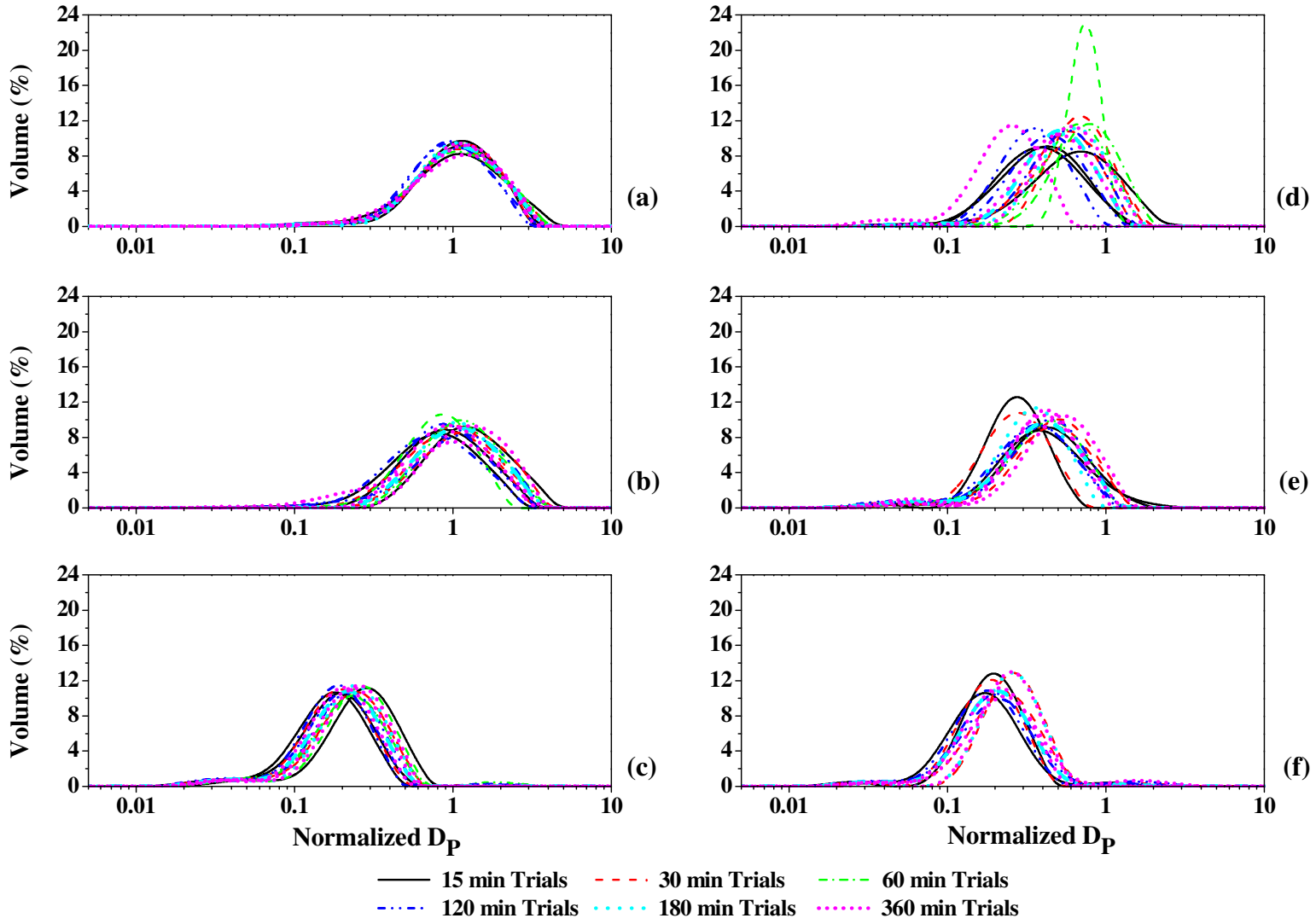

Figure 3-17: Normalized PSDs at 3.5 U_{mf} for different regions of the bed: (a) Initial, (b) Dropped, (c) Fines, (d) Wall, (e) Bottom Column, and (f) Top Column.

In Figure 3-18 the PSDs for all particle regions are compared for different fluidization times. It is obvious from these results that the main regions (i.e. initial, dropped, wall, and fines) all have different PSDs; however, each region is similar regardless of fluidization time. It is also clear that the bottom of the column and the wall, as well as the top of the column and the fines, had comparable PSDs. The overlap within regions suggested that particles of a certain size range can be found in any region of the bed; therefore, the final location of these particles is likely more due to initial particle location, bed hydrodynamics, or electrostatic forces. If a particle was initially at the top of the bed, and of a size where it could be elutriated from the bed by the gas velocity, then it was likely entrained. However, if a particle was at the bottom of the bulk and hydrodynamics forced it to move close to the column wall where it was attracted to the particles adhered to the wall, then it was more likely it would join the particle layer. Finally, if the particle was in the middle of the bed then it may have remained in the dropped region or migrated to the sides of the column and adhered to the wall due to repulsive or attractive electrostatic forces.

Both the wall and the bottom column particles had the most variation of all the PSD samples collected. This was due to the variability of the sampling location. Since the wall particles were dislodged from the column due to the application of slight vibration to the wall, and the bottom column was collected from those particles remaining on the wall, the sample for PSD analysis was susceptible to inconsistencies in sampling. Although much effort was put into maintaining a reproducible sampling technique, some variation was expected. If more or less particles were removed from the wall during wall particle or bottom column collection, the size range of particles would vary. Additionally, the high static charges present on the particles, especially in the wall and bottom column regions, caused difficulty in taking PSD samples due to the attraction and repulsion of particles, either during initial collection or during transfer to the Malvern Instrument for PSD analysis, which might skew the PSD results. Slight variation in the samples was expected; however, the main focus of these results was to determine if particles of the same size were consistently found in each region and to determine how the size range of each region compared to one another.

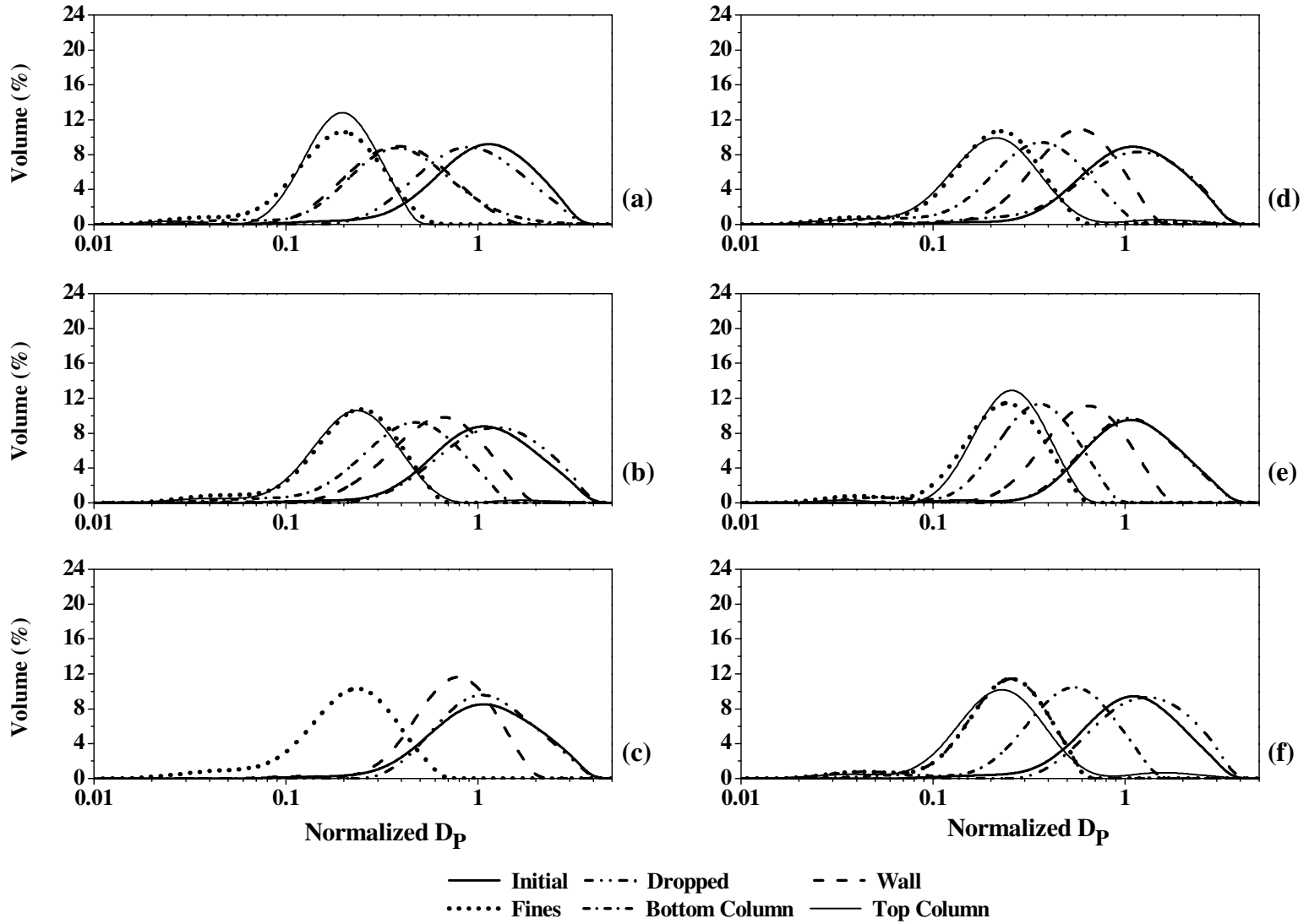

Figure 3-18: Example PSDs at 3.5 U_{mf} for all regions of the bed for different fluidization times: (a) 15 min, (b) 30 min, (c) 60 min, (d) 120 min, (e) 180 min, and (f) 360 min.

3.2.2. 4 U_{mf} Gas Velocity Results and Discussion

The results obtained for a fluidization gas velocity of 4 U_{mf} and the associated discussion are presented in this section.

3.2.2.1. Mass Collected (m%)

Neither the mass collected from the dropped region, nor from the wall at this gas velocity demonstrated a trend with fluidization time (Figure 3-19). However, it was clear that the mass of the wall and the dropped particles were related. For example, a larger mass collected in the dropped region for the 60 minute trials resulted in a smaller mass collected in the wall region. In contrast, for the 360 minute trials, the lower mass collected in the dropped region resulted in a higher mass collected in the wall region. This is an indication that some of the particles leaving the dropped region, if not the majority, were migrating to the wall region and vice versa. This migration seemed to reach an equilibrium flux shortly after the onset of fluidization and it was maintained even as the duration of fluidization lengthened.

The mass of the fines being elutriated from the bed was directly dependent on the fluidization time. The amount of collected mass seemed to level off with fluidization times of 120 minutes or greater indicating that after extended fluidization periods there were no longer many fines available to be elutriated from the bed. Thus, the fines originally present in the bed must have either entrained or have attached to the column wall.

The mass of particles that were not retrieved during sample collection was not influenced by fluidization time (Figure 3-19d). Most of the particles that were not collected were still adhered to the column wall following wall region collection. Additionally, a small amount of particles were lost while removing the filter bag or collecting the wall and dropped samples.

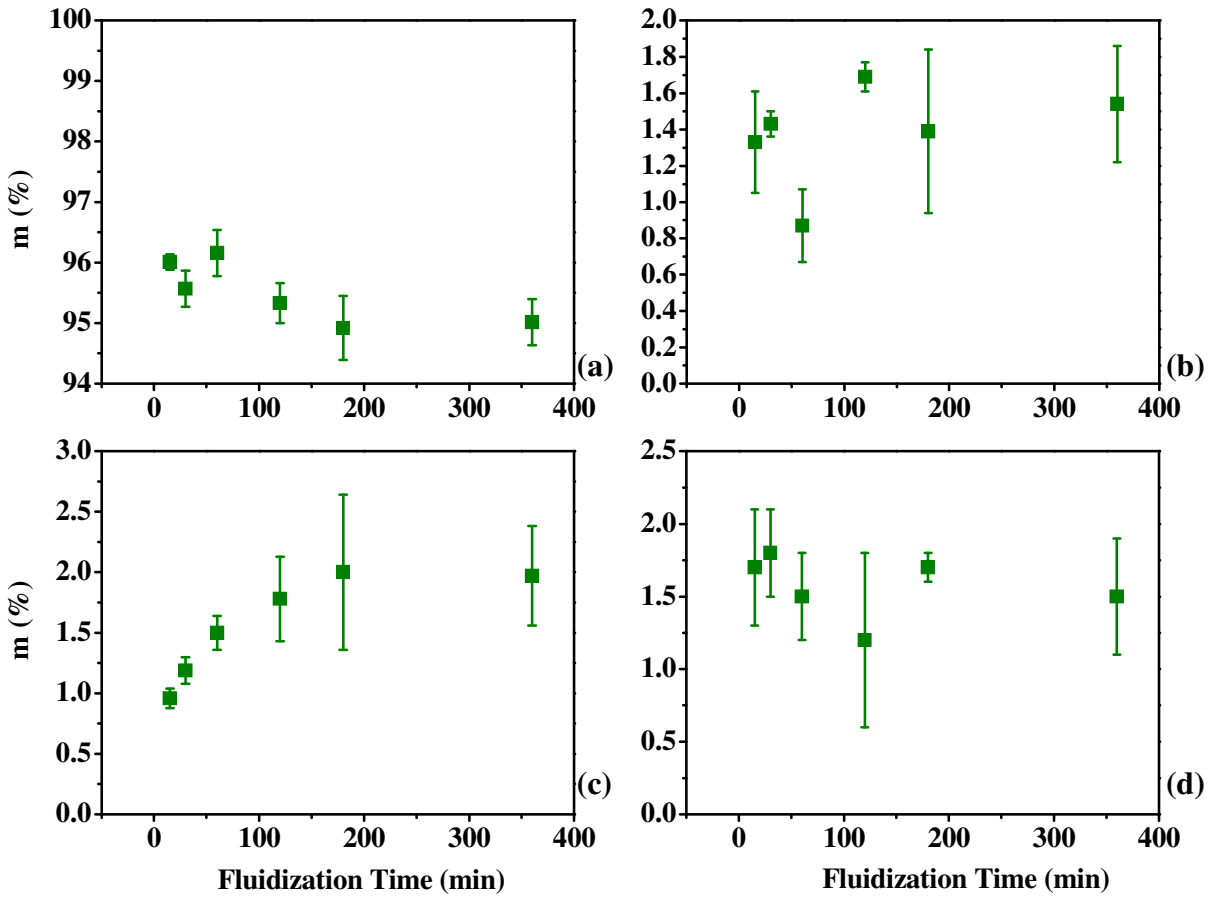

Figure 3-19: Mean m% at 4 U_{mf} for different fluidization times: (a) Dropped, (b) Wall, (c) Fines), and (d) Irretrievable.

3.2.2.2. Charge-to-Mass Ratio (q/m)

As can be seen in Figure 3-20, the net q/m for the initial particles was comparable for all fluidization trials. Thus, all trials could be compared.

The magnitude and/or sign of the net q/m differed for each region of the bed. Prior to the experiment, the particles net q/m had a range of approximately -0.075 to -0.102 μC/kg while those of the dropped and wall particles were measured at approximately -0.50 to -0.61 μC/kg and -44.3 to -65.8 μC/kg, respectively. The fine particles had a range of approximately +16.2 to 32.7 μC/kg. Smaller particles tended to be predominately positively charged while the larger particles tended to be predominately negatively charged. This correlated with the

smaller magnitude of q/m in the bulk of the bed, as this region was comprised of both large and small particles resulting in a small net q/m. This experimental result supports the bipolar charging theory since the polyethylene particles became either positively or negatively charged depending on their size.

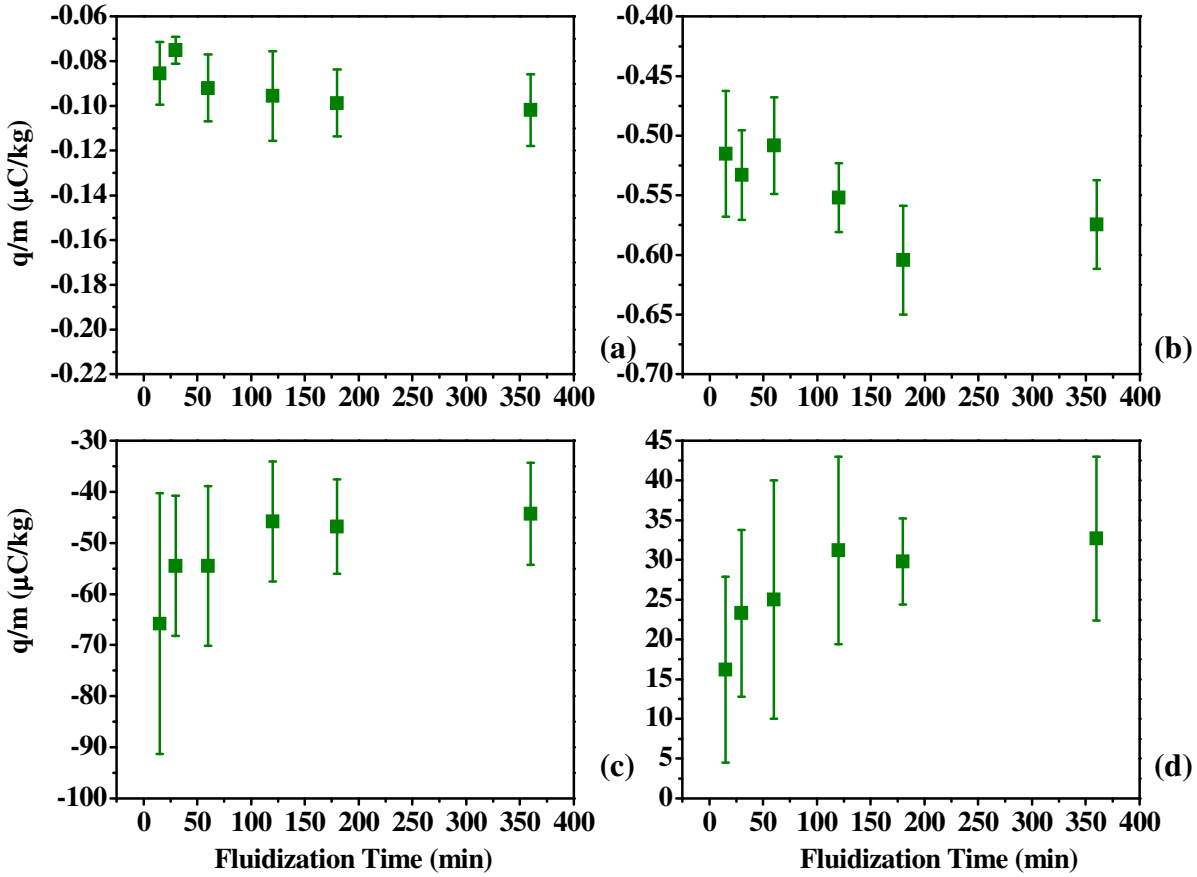

Figure 3-20: Mean net q/m at 4 U_{mf} for different fluidization times: (a) Initial, (b) Dropped, (c) Wall, and (d) Fines.

The net q/m of the dropped particles seemed to experience a slight increase in magnitude at approximately 60 minutes (Figure 3-20). Trials of fluidization times 60 minutes or less all had a mean net q/m magnitude less than -0.55 µC/kg while the trials greater than 60 minutes were of greater magnitude. Thus, in shorter fluidization times slightly less net q/m was generated in the bulk than in longer fluidization times. However, the variance in these samples is important to note as the standard deviations of all fluidization times overlapped.

The mean net q/m for the wall particles seemed to decrease slightly in magnitude up to 60 minutes with a plateau reached with greater fluidization periods. The wall particles had a large negative q/m, as expected due to the assumption that the reactor wall was positively charged, which resulted in a wall layer of alternating positively and negatively charged particles. This theory also supports the slight decrease in q/m magnitude for the wall particles for 15 to 60 minutes. Initially, large quantities of negatively charged particles were attracted to the column wall. Over time, positive particles were attracted to these negatively charged particles. After 60 minutes, particles of both positive and negative charges alternated in attraction to the wall in similar amounts, resulting in charge equilibrium.

The fine particles followed a similar trend to the wall particles where the average net q/m for each fluidization time increased in magnitude until a plateau was reached around 60 minutes. Both the net q/m and the mass of the fines reached a plateau after extended fluidization times, thus the majority of fine particles must had been elutriated from the bed by 60 minutes. As fluidization time increased, the particles leaving the bed had more time to interact with other particles and the column wall and thus having a larger magnitude of charge. Finally, only a few particles were left that were small enough to be entrained leading to a plateau in q/m.

3.2.2.3. Wall Particle Layer

With all fluidization times tested, reactor wall fouling was observed as shown in Figure 3-21. For each fluidization time there was a gap where no wall fouling was taken place. This was likely at the point where slugs were fully formed. After this height, the frictional force created by the slugs prevented a stable particle layer to form on the wall. Similar wall particle layers were developed at the bottom of the column with a height reaching above static bed height, regardless of fluidization time, correlating with the similar amount of collected m% found in this region.

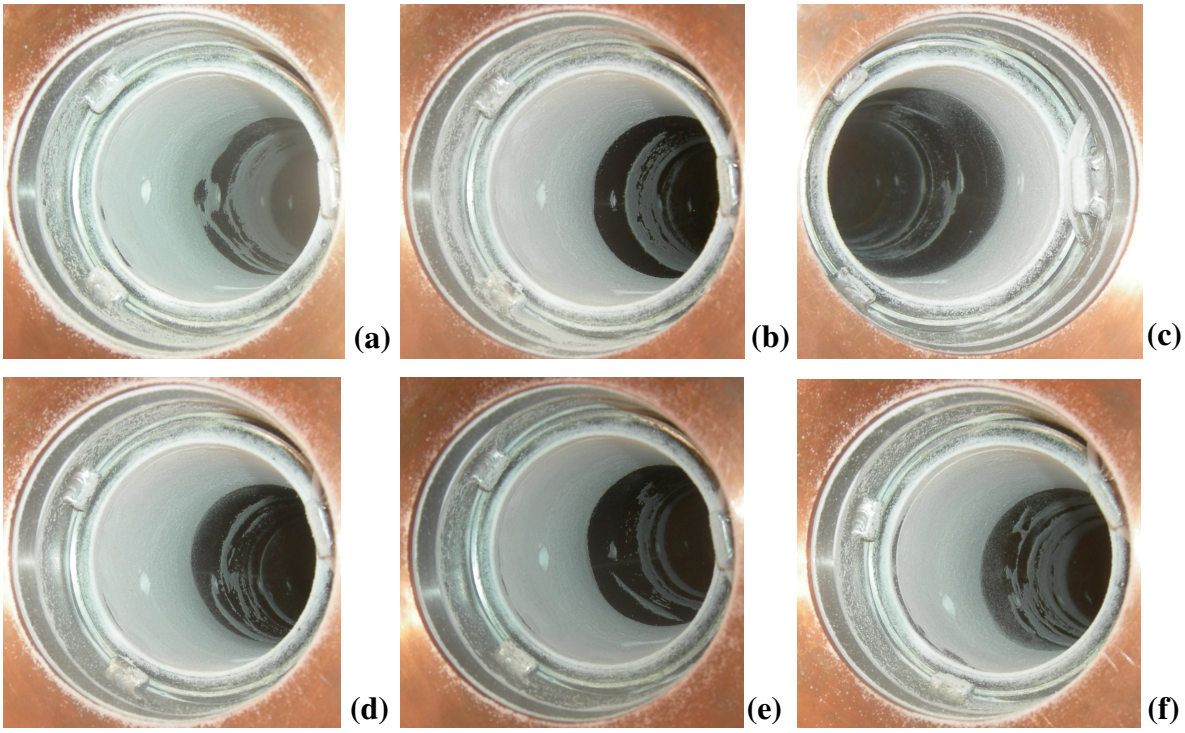

Figure 3-21: Images of particle layer on the column wall at 4 U_{mf} for different fluidization times: (a) 15 min, (b) 30 min, (c) 60 min, (d) 120 min, (e) 180 min, and (f) 360 min.

3.2.2.4. Particle Size Distribution (PSD)

As seen in Figure 3-22, the initial and dropped particles were similar in size and were comprised of the largest sized particles. The wall particles were slightly smaller than dropped, but were larger than the fines, which as anticipated were the smallest group of particles collected. The particles collected from the bottom of the column wall were slightly smaller than those collected from the wall particles. This demonstrated that smaller particles attached to the wall compared to those in the outer region of the particle layer. The particles attached to the top of the column were of similar size to those particles elutriated from the bed. Individual versions of these graphs and values for $D_{P\,0.1}$, $D_{P\,0.5}$, and $D_{P\,0.9}$ can be found in Appendix B.

The wall particles had a narrow size distribution. This suggested that there was a maximum particle size that could adhere to the column wall. Since the particles adhered to the wall

increased in size, two forces acted in competition: electrostatic and gravitational. Once the gravitational force exceeded the electrostatic force, the particles were too large to remain on the wall and fell back into the bulk. This has been discussed in previous works (Sowinski et al., 2009 and 2010). In the slugging flow regime, bed hydrodynamics also contributes to the maximum particle size. The slugs cause particles to rub together more violently, making loosely adhered particles to fall off the wall. As the particle layer grows in thickness, the particles slightly increase in size; with the motion of the slugs brushing off the outer most particles of the layer, the particle size would be restricted.

The particle size distributions for all trials were compared (Figure 3-22) depicting that particles collected within a single region were similar regardless of fluidization time; however, most regions had different PSDs.

It seems as though wall particles found from 180 and 360 min trials had a slightly narrower PSD than the rest of the fluidization times resulting in a lower maximum particle size. 120 min had some PSDs similar to the longer times and some similar to the shorter times. This could be due to bed hydrodynamics and charge generation. As previously mentioned, both the wall and the dropped regions reached a charge saturation at approximately 60 min. As fluidization continued the particles on the outside of the wall layer were unlikely to become more charged, however the motion of the slugs continued. With continuous rubbing, the electrostatic force may have been overcome by the contact of particles being forced upwards in the slug, resulting in the slightly larger particles becoming brushed off the wall.

As seen, there was some overlap in particle sizes between various regions of the bed. Particles of comparatively moderate size could be found in any portion of the bed and the final location of these particles was probably determined by the combination of initial particle location, bed hydrodynamics, and electrostatic forces, as previously discussed.

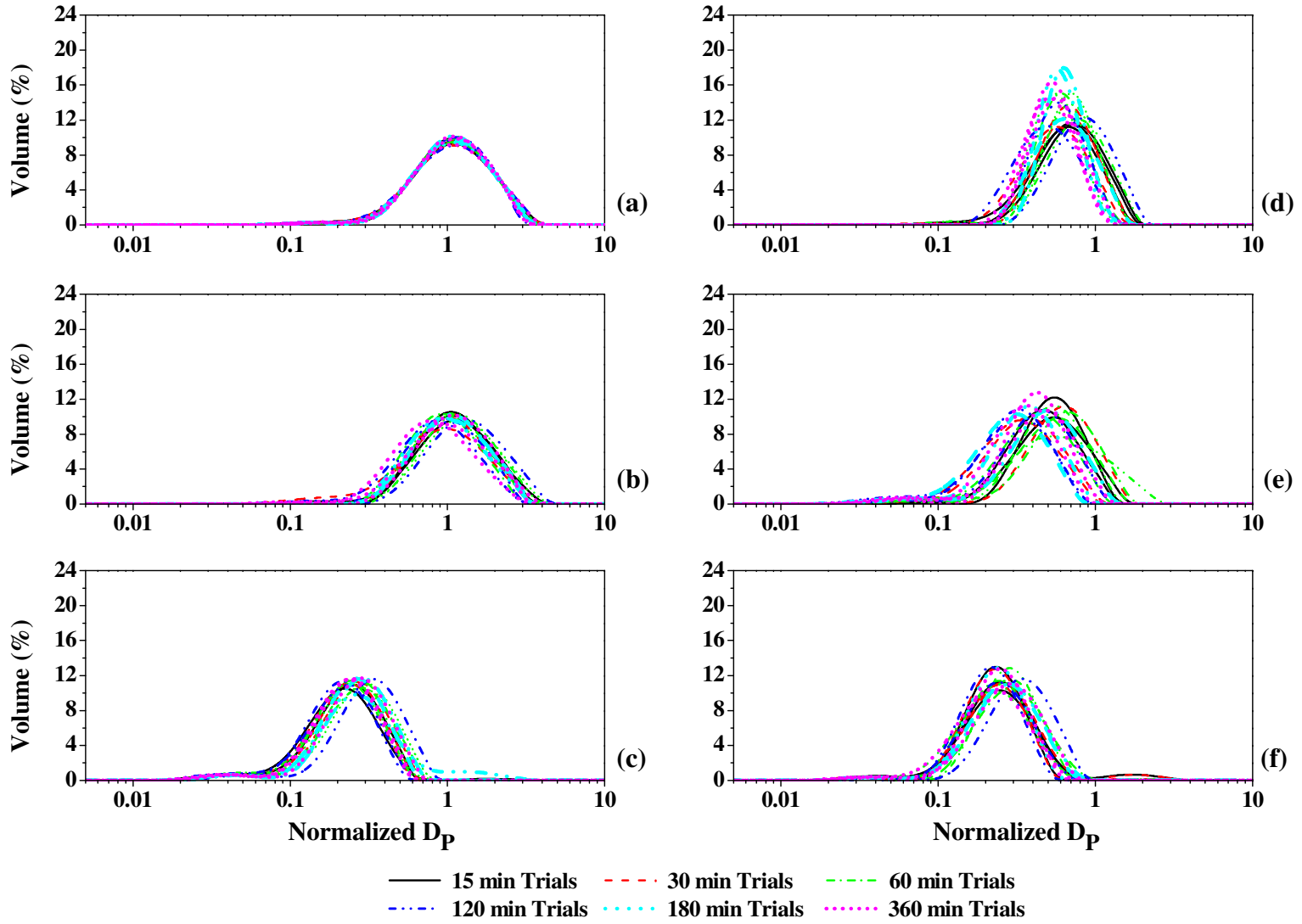

Figure 3-22: Normalized PSDs at 4 U_{mf} for different fluidization times: (a) Initial, (b) Dropped, (c) Fines, (d) Wall, (e) Column Bottom, and (f) Column Top.

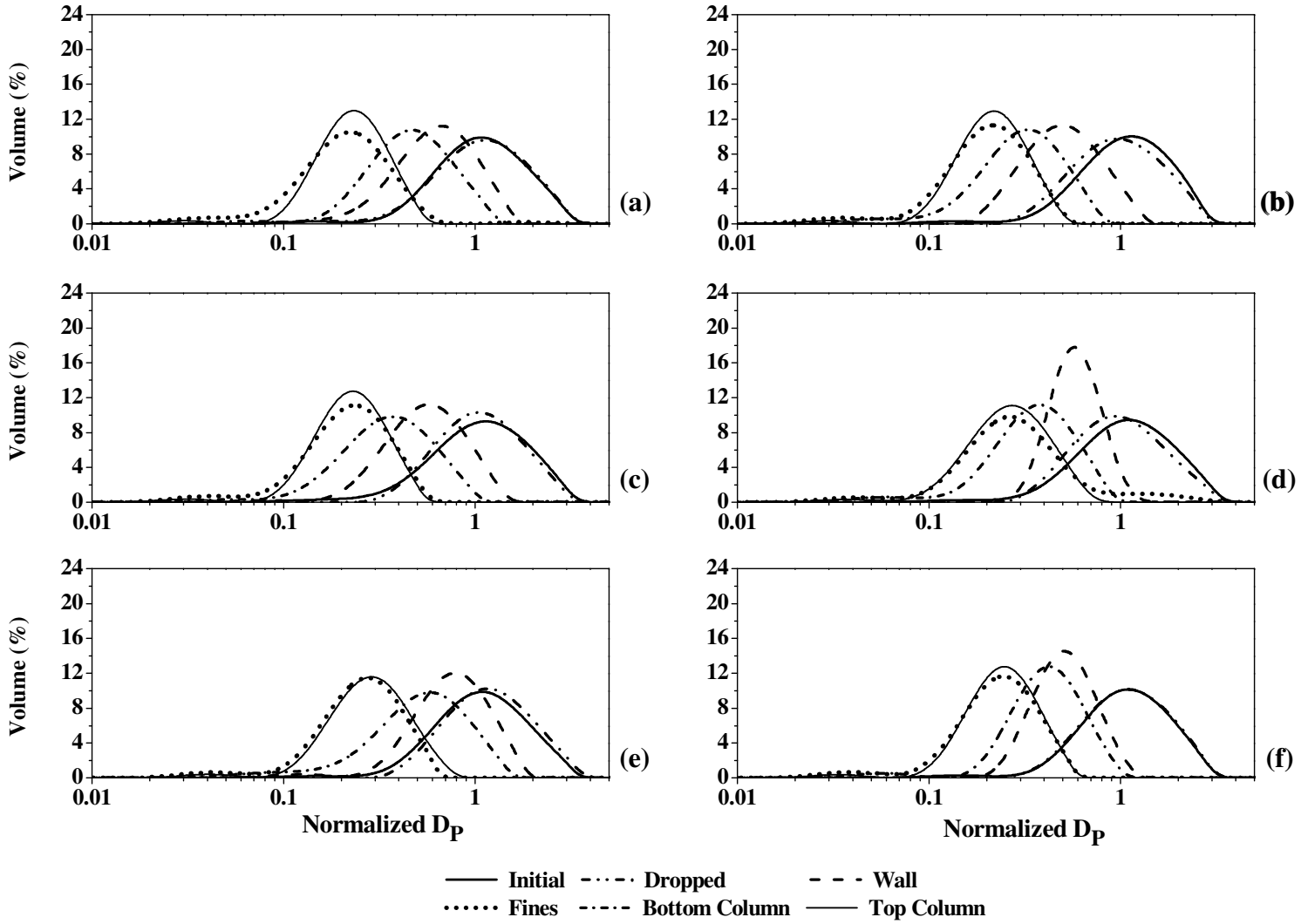

Figure 3-23: Example PSDs at 4 U_{mf} for all regions of the bed for different fluidization times: (a) 15 min, (b) 30 min, (c) 60 min, (d) 120 min, (e) 180 min, and (f) 360 min.

3.2.3. Slugging Flow Regime Comparison

Two gas velocities, 3.5 U_{mf} and 4 U_{mf}, were compared for all fluidization times to determine if any trends within the slugging flow regime could be identified.

3.2.3.1. Mass Collected (m%)

As seen in Figure 3-24, neither 3.5 U_{mf}, nor 4 U_{mf} demonstrated a trend of m% collected from the dropped and wall regions of the bed with fluidization time. This concludes that in the slugging flow regime few particles migrated from the dropped region to other parts of the bed after 15 min of fluidization. The magnitude of the m% collected was larger for 3.5 U_{mf} than for 4 U_{mf} in the dropped region, while it was less in the wall region. This indicates that more particles adhered to the wall at the higher gas velocity, likely due to the increase in particle interactions in the bed, generating more electrostatic charge. As the gas velocity increased, the quantity of particle-particle and particle-wall contacts increased as well, resulting in more charges being generated on the particles. This increase in charge generation could have resulted in more reactor wall fouling due to an increase in electrostatic attraction.

The m% collected of fine particles increased with fluidization time for both 3.5 U_{mf} and 4 U_{mf}; however, both velocities seemed to reach a plateau between 180 and 360 minutes. Thus, the amount of fine particles elutriated from the bed increased with fluidization time. However, the majority of fine particles had left the bed by 180 minutes. The magnitude of fine particles collected was similar for both gas velocities for the shorter fluidization times (i.e., 15 and 30 min), while for longer trials more m% was collected with a gas velocity of 4 U_{mf}. At shorter fluidization times, the majority of particles leaving the bed were those located near the bed surface, thus easily elutriated. However, as fluidization time increased, in order for additional particles to leave the bed, the fine particles had to migrate from the middle or bottom of the bulk, which was easier with the higher velocity. Additionally, the higher velocity was able to elutriate larger particles, thus increasing the m% collected.

There was no apparent trend with fluidization time for irretrievable particles for either gas velocity. Therefore, the amount of particles lost from sampling was not dependent on gas velocity.

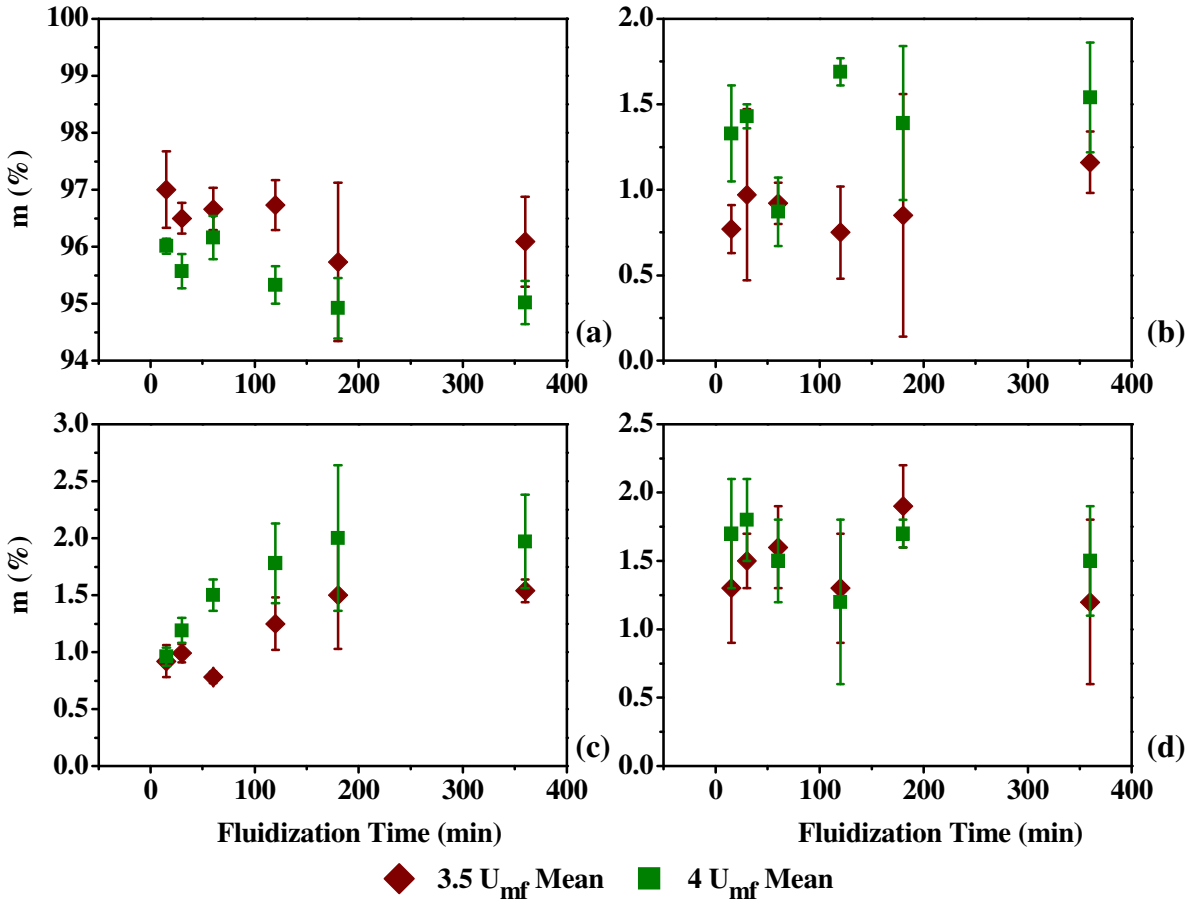

Figure 3-24: Comparison of m% for two velocities in slugging flow regime: (a) Dropped, (b) Wall, (c) Fines, and (d) Irretrievable.

3.2.3.2. Charge-to-Mass Ratio (q/m)

The q/m ratio for the initial particles was slightly different for each gas velocity (Figure 3-25a). However, the difference between these values was minimal. The magnitude of the net q/m of the initial particles was less than the other regions of the bed. Therefore, it was assumed that the differences in magnitude were minor enough that the two velocities could be compared.

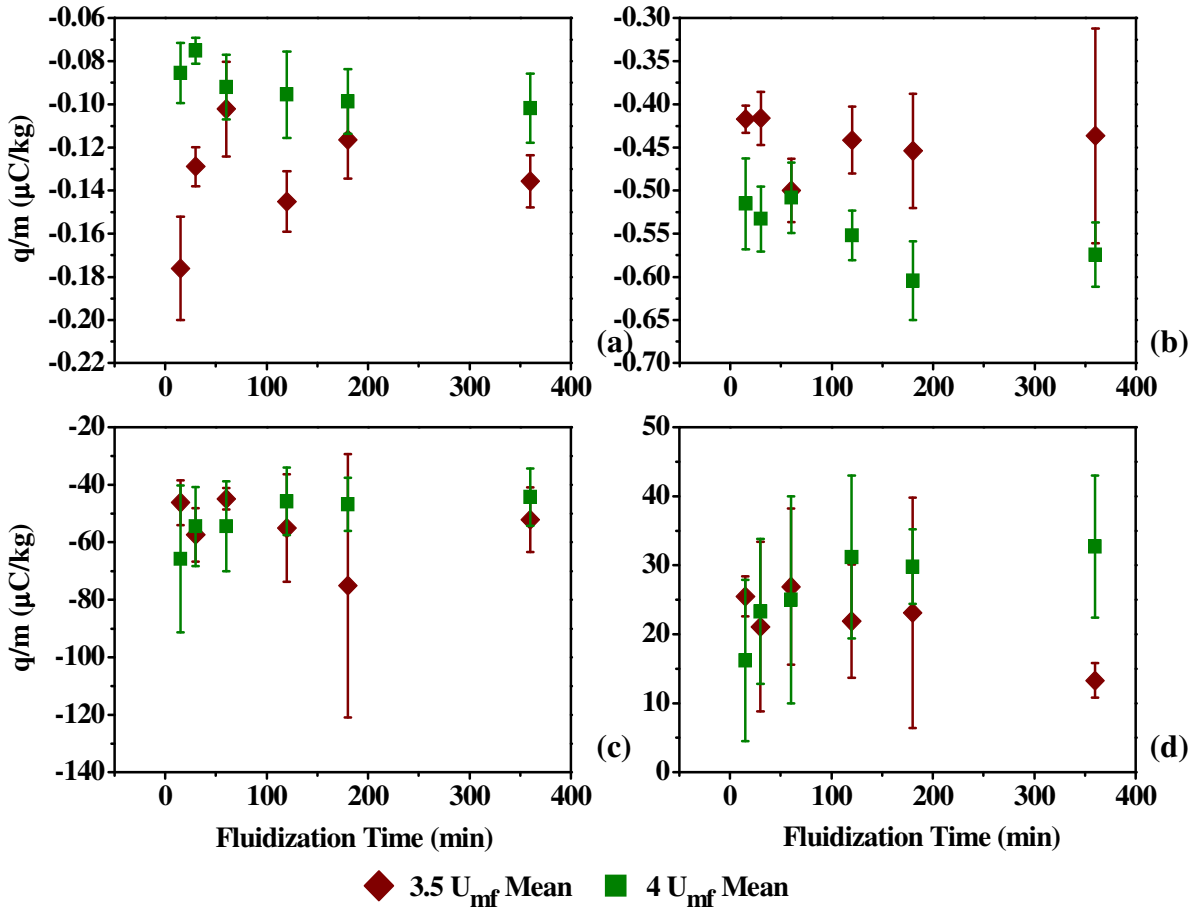

Figure 3-25: Comparison of net q/m for two velocities in slugging flow regime: (a) Initial, (b) Dropped, (c) Wall, and (d) Fines.

The net q/m for the dropped particles showed a similar trend regardless of gas velocity; neither velocity demonstrated a change with fluidization time (Figure 3-25b). Thus in the slugging flow regime, the majority of charge in the bulk was generated within the first 15 minutes of fluidization. The magnitude of the 3.5 U_{mf} trial was less negative than that of the 4 U_{mf} which indicated that the gas velocity impacted the amount of charge generated in the dropped region. Two explanations probably contributed to the more negative net q/m for the higher gas velocity. First, since additional smaller, positively charged particles were able to leave the bed quicker at the higher gas velocity, it is reasonable to assume that this would result in a more negative net q/m on the particles left behind in the bulk (i.e., dropped region). Secondly, as the particles were undergoing more vigorous movement at the higher gas velocity, more charge would have been generated resulting in more particles adhering to the wall.

The net q/m magnitude of fine particles of both gas velocities was similar regardless of fluidization velocity However, to obtain similar magnitudes, the higher gas velocity must have had more charge generated on the particles since a higher m% was collected for these trials. This larger quantity of charge generation was expected as with a higher velocity more particle-particle and particle-wall interactions would take place, which would increase the amount of charge generation within the bed.

3.2.3.3. Particle Size Distribution (PSD)

The PSD of the particles ($D_{P\ 0.1}$, $D_{P\ 0.5}$ and $D_{P\ 0.9}$) were compared for both gas velocities for all fluidization times. The dropped region had comparable particle sizes for both gas velocities. Thus, similar sized particles were remaining in the bulk in the slugging flow regime. The 4 U_{mf} had a slightly larger particle size range, than 3.5 U_{mf}, in the wall region of the bed. This was likely due to increased charge generation on the particles which allowed for larger particles to adhere to the column wall. The fines region of 3.5 U_{mf} seemed to have slightly smaller particles than that of the 4 U_{mf}. This was due to larger particles being elutriated from the bed with the higher gas velocity, shifting the PSD to a slightly larger particle diameter.

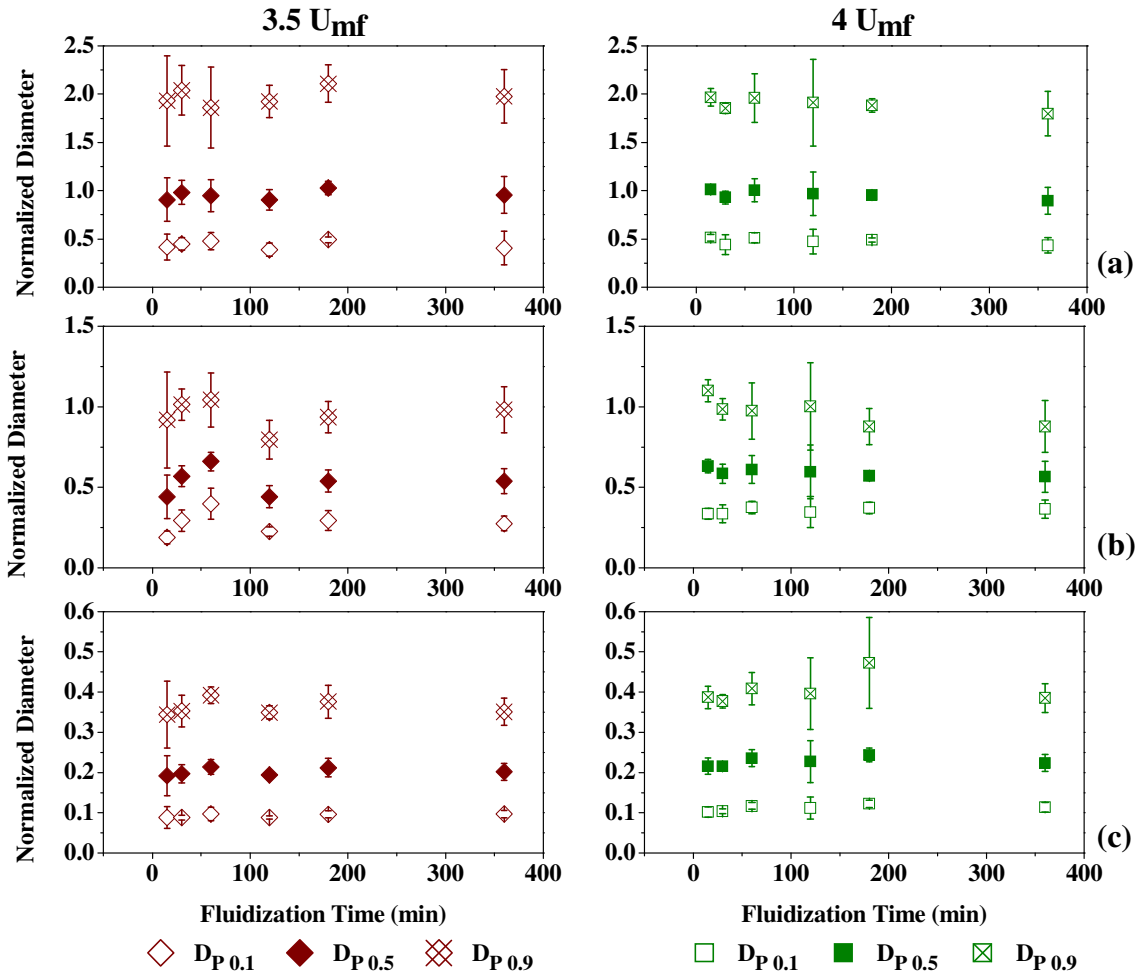

Figure 3-26: Comparison of Normalized PSDs for two gas velocities in slugging flow regime: (a) Dropped, (b) Wall, and (c) Fines.

3.2.4. Slugging Flow Regime Summary

Charge saturation was achieved in all regions of the bed by 60 min for both gas velocities. This indicated that there is a maximum net q/m that can be reached within the bed.

Particle wall fouling was observed in this flow regime with a higher magnitude found at the higher gas velocity. The particle layer reached a height approximately equal to that of the static bed height. The amount of wall fouling did not seem to be dependent on fluidization time.

3.3. Comparison of Results of the Two Flow Regimes

The net q/m of the initial particles had some variation, however, the mean values were in the same range, and were similar enough to assume the starting q/m was equivalent for all trials. The mean particle diameter for these particles was similar for all runs. Any slight variation was due to the use of resin directly received from industrial reactors. The similarities between trials allowed for comparison of all experiments.

The trends observed in each of the areas investigated were different for the bubbling and slugging flow regimes. Without doubt, the bed hydrodynamics associated to each fluidization regime affected the electrostatics observed in each region of the bed.

3.3.1. Mass Collected (m%)

As seen previously and in Table 3-1 below, in the bubbling fluidization flow regime there was a decrease of approximately 6% in dropped particles mass collected as fluidization time increased whereas during the gas velocities tested in the slugging flow regime there was very little change, approximately 1%. Overall the magnitude of m% collected for the dropped particles during the slugging flow velocities was more than that in the bubbling flow velocities. The mass collected for the wall increased as the fluidization time increased in the bubbling velocities while for slugging velocities little change was observed. This could be attributed to the bed hydrodynamics in each flow regime. In the bubbling regime, particle mixing was more vigorous resulting in more particles charging which then promoted migration of particles to the wall region. This also resulted in formation of longer particle layers on the column wall and more mass collected as fluidization time increased. Conversely, during the slugging flow regime less mixing took place, as most of the motion occurred vertically as slugs moved up and down the column. This resulted in decreased particle-particle contacts within the bulk and less charge generation due to triboelectification. In addition, not all particles may have had the opportunity to move from one location of the bed to another, due to reduced radial movement, thus reducing the particles opportunity to adhere to the column wall. Also, the motion of the slugs against the

column wall acted against particle adhesion as the slug detached particles loosely attached to the particle layer or the wall. The main particle layer was built up during the first 15 minutes of the slugging flow velocities; whereas during bubbling regime the particle layer continued to build as fluidization time increased.

Table 3-1: Comparison of m% for all regions for different fluidization times and gas velocities.

	Initial				Dropped			
Fluidization Time	1.5 U_{mf}	1.75 U_{mf}	3.5 U_{mf}	4 U_{mf}	1.5 U_{mf}	1.75 U_{mf}	3.5 U_{mf}	4 U_{mf}
	m	m	m	m	m	m	m	m
min	%	%	%	%	%	%	%	%
15	100.0 ± 0.0	100.0 ± 0.0	100.0 ± 0.0	100.0 ± 0.0	97.3 ± 0.4	96.6 ± 1.4	97.0 ± 0.7	96.0 ± 0.1
30	100.0 ± 0.0	100.0 ± 0.0	100.0 ± 0.0	100.0 ± 0.0	95.1 ± 2.3	94.2 ± 0.5	96.5 ± 0.3	95.6 ± 0.3
60	100.0 ± 0.0	100.0 ± 0.0	100.0 ± 0.0	100.0 ± 0.0	94.3 ± 0.9	93.2 ± 1.9	96.7 ± 0.4	96.2 ± 0.4
120	100.0 ± 0.0	100.0 ± 0.0	100.0 ± 0.0	100.0 ± 0.0	92.2 ± 3.1	94.2 ± 3.3	96.7 ± 0.4	95.3 ± 0.3
180	100.0 ± 0.0	100.0 ± 0.0	100.0 ± 0.0	100.0 ± 0.0	91.4 ± 1.9	91.8 ± 0.5	95.7 ± 1.4	94.9 ± 0.5
360	100.0 ± 0.0	100.0 ± 0.0	100.0 ± 0.0	100.0 ± 0.0	91.0 ± 0.4	89.9 ± 0.6	96.1 ± 0.8	95.0 ± 0.4
	Wall				**Fines**			
Fluidization Time	1.5 U_{mf}	1.75 U_{mf}	3.5 U_{mf}	4 U_{mf}	1.5 U_{mf}	1.75 U_{mf}	3.5 U_{mf}	4 U_{mf}
	m	m	m	m	m	m	m	m
min	%	%	%	%	%	%	%	%
15	1.5 ± 0.0	2.3 ± 1.8	0.8 ± 0.1	1.3 ± 0.3	0.11 ± 0.00	0.13 ± 0.01	0.92 ± 0.14	0.96 ± 0.08
30	3.1 ± 2.5	3.2 ± 0.6	1.0 ± 0.5	1.4 ± 0.1	0.11 ± 0.01	0.15 ± 0.02	0.99 ± 0.08	1.19 ± 0.11
60	3.5 ± 0.8	4.4 ± 1.4	0.9 ± 0.1	0.9 ± 0.2	0.13 ± 0.02	0.13 ± 0.01	0.78 ± 0.05	1.50 ± 0.14
120	4.5 ± 1.7	3.3 ± 2.5	0.8 ± 0.3	1.7 ± 0.1	0.13 ± 0.01	0.23 ± 0.08	1.25 ± 0.23	1.78 ± 0.35
180	5.3 ± 1.1	5.2 ± 0.6	0.8 ± 0.7	1.4 ± 0.4	0.11 ± 0.02	0.21 ± 0.05	1.50 ± 0.47	2.00 ± 0.64
360	6.4 ± 1.0	6.9 ± 1.2	1.2 ± 0.2	1.5 ± 0.3	0.13 ± 0.03	0.21 ± 0.02	1.54 ± 0.10	1.97 ± 0.41

In the slugging flow, as expected the majority of fine particles were elutriated within shorter fluidization times and the mass collected was much higher compared to that during the bubbling flow velocities. The fines m% for slugging velocities increased between 15 minutes and 60 minutes and then levelled out for extended fluidizations. Whereas, with the bubbling velocities it was relatively constant as fluidization time increased.

To further investigate the effect of fluidization time on the particle wall fouling, pictures were taken from this layer for all trials, before the wall particles charges were measured. The particle wall layer height (h) was determined from the images and results are summarized in Table 3-2. Results indicated that the hydrodynamics of the fluidized bed affected the particle layer formation. The trends of long layers that continued to lengthen for the bubbling flow

velocities and short layers that remained at a constant height for the slugging flow is clearly depicted from the results. Visible observations suggested that the layer for the slugging flow velocities was thicker than that for the bubbling flow velocities. In each flow regime, a gap was observed in the particle layer. In the bubbling flow regime, this gap was approximately at the static bed height and was probably created due to bed oscillations at that location. For the slugging flow regime, the gap was much lower, probably at the height of slug formation where their upward movement, helped dislodge the particles off of the wall. The hydrodynamics of the fluidized bed also affected how the particle layer formed on the column wall. During the bubbling flow regime, the particle layer was long and thin; whereas, during the slugging flow regime the particle layer was shorter and thicker. Therefore, the manner in which the particle layer developed on the column wall was dependent on the flow regime of the bed.

Table 3-2: Particle wall layer height with respect to fluidization time and gas velocity.

Fluidization Time	1.5 U_{mf}	1.75 U_{mf}	3.5 Uu_{mf}	4 U_{mf}
min	h m	h m	h m	h m
15	0.31 ± 0.04	0.30 ± 0.08	0.07 ± 0.03	0.16 ± 0.02
30	0.34 ± 0.03	0.35 ± 0.02	0.12 ± 0.00	0.19 ± 0.05
60	0.33 ± 0.03	0.38 ± 0.01	0.13 ± 0.04	0.13 ± 0.03
120	0.37 ± 0.03	0.29 ± 0.18	0.09 ± 0.03	0.18 ± 0.01
180	0.37 ± 0.02	0.36 ± 0.02	0.18 ± 0.17	0.16 ± 0.02
360	0.41 ± 0.01	0.43 ± 0.03	0.11 ± 0.05	0.13 ± 0.03

3.3.2. Charge-to-Mass Ratio (q/m)

Table 3-3 summarizes all results obtained for net q/m for different fluidization times and gas velocities. The average q/m of the dropped particles, for all gas velocities tested, was relatively similar for the shorter fluidization times suggesting that during these periods charge generation was less dependent on bed hydrodynamics. Therefore, any form of interaction initially resulted in similar charge build-up. The net q/m for velocities of 1.75, 3.5 and 4 U_{mf} did not change with increased residence time; however, 1.5 U_{mf} experienced a

slight increase in magnitude until 60 minutes, after which a plateau seemed to be reached. Therefore, a longer time was required for charge saturation with the lower velocity.

Table 3-3: Comparison of net q/m for all regions of the bed for different fluidization times and gas velocities.

Fluidization Time	Initial				Dropped			
	1.5 U_{mf} q/m	1.75 U_{mf} q/m	3.5 U_{mf} q/m	4 U_{mf} q/m	1.5 U_{mf} q/m	1.75 U_{mf} q/m	3.5 U_{mf} q/m	4 U_{mf} q/m
min	µC/kg	µC/kg	µC/kg	µC/kg	µC/kg	µC/kg	µC/kg	µC/kg
15	-0.103 ± 0.032	-0.116 ± 0.014	-0.176 ± 0.024	-0.085 ± 0.014	-0.477 ± 0.071	-0.487 ± 0.118	-0.417 ± 0.016	-0.515 ± 0.053
30	-0.116 ± 0.026	-0.119 ± 0.002	-0.129 ± 0.009	-0.075 ± 0.006	-0.637 ± 0.178	-0.680 ± 0.069	-0.416 ± 0.031	-0.533 ± 0.038
60	-0.120 ± 0.023	-0.103 ± 0.017	-0.102 ± 0.022	-0.092 ± 0.015	-0.709 ± 0.116	-0.744 ± 0.180	-0.500 ± 0.037	-0.508 ± 0.041
120	-0.089 ± 0.004	-0.134 ± 0.014	-0.145 ± 0.014	-0.096 ± 0.020	-0.740 ± 0.227	-0.587 ± 0.171	-0.442 ± 0.039	-0.552 ± 0.029
180	-0.102 ± 0.021	-0.107 ± 0.013	-0.117 ± 0.018	-0.099 ± 0.015	-0.810 ± 0.190	-0.620 ± 0.040	-0.454 ± 0.066	-0.605 ± 0.046
360	-0.081 ± 0.005	-0.130 ± 0.010	-0.136 ± 0.012	-0.102 ± 0.016	-0.795 ± 0.056	-0.706 ± 0.020	-0.436 ± 0.125	-0.574 ± 0.037

Fluidization Time	Wall				Fines			
	1.5 U_{mf} q/m	1.75 U_{mf} q/m	3.5 U_{mf} q/m	4 U_{mf} q/m	1.5 U_{mf} q/m	1.75 U_{mf} q/m	3.5 U_{mf} q/m	4 U_{mf} q/m
min	µC/kg	µC/kg	µC/kg	µC/kg	µC/kg	µC/kg	µC/kg	µC/kg
15	-77.6 ± 14.8	-55.5 ± 17.1	-46.2 ± 7.8	-65.8 ± 25.5	55.5 ± 16.0	56.6 ± 9.5	25.5 ± 2.9	16.2 ± 11.7
30	-66.2 ± 3.6	-69.6 ± 6.9	-57.4 ± 9.3	-54.5 ± 13.7	93.3 ± 41.2	59.7 ± 31.6	21.1 ± 12.3	23.3 ± 10.5
60	-58.1 ± 7.0	-59.8 ± 4.3	-44.9 ± 3.8	-54.5 ± 15.6	94.9 ± 30.4	89.3 ± 65.9	26.9 ± 11.3	25.0 ± 15.0
120	-53.5 ± 11.1	-58.7 ± 17.9	-55.1 ± 18.7	-45.8 ± 11.7	143.3 ± 65.2	90.4 ± 64.6	21.9 ± 8.2	31.2 ± 11.8
180	-52.0 ± 5.3	-62.4 ± 0.6	-75.1 ± 45.8	-46.8 ± 9.2	246.7 ± 40.1	191.9 ± 70.1	23.1 ± 16.7	29.8 ± 5.4
360	-57.0 ± 1.0	-57.5 ± 3.3	-52.1 ± 11.2	-44.3 ± 10.0	225.6 ± 111.6	209.8 ± 41.9	13.3 ± 2.5	32.7 ± 10.3

The average net q/m for the wall region was comparable for all gas velocities. As previously discussed, more particles adhered to the wall during the bubbling regime; with increased mass, charge had to also increase to provide a similar magnitude of net q/m. This suggested that there was a greater ability to generate charge in the bubbling regime than in the slugging regime. Other research has postulated that the charge generated during bubbling is mainly due to triboelectrification having greater potential to generate charge while the main driving force during slugging is frictional charging (Sowinski et al., 2010). The trends of net q/m for the wall particles during both the 1.5 U_{mf} and 4 U_{mf} were similar with a decline in magnitude for the shorter fluidization times and finally reaching a plateau for the longer periods. Therefore, for both gas velocities the q/m remained constant for extended fluidization times suggesting that the wall particles reached the lowest net q/m that could be obtained and that value was influenced by the hydrodynamics of the bed and the amount of fines elutriated, due to the removal of positively charged particles. In comparison, both the 1.75 U_{mf} and the 3.5 U_{mf} demonstrated no apparent trend with fluidization time.

The fines q/m in the bubbling regime increased with fluidization time while it remained relatively constant for the slugging regime. This correlates with the mass collected as previously mentioned. It was expected that for longer fluidization times more charge would build-up on the particles. With increasing charge, but constant mass, the q/m increased for the bubbling regime; however, with both the mass collected and charge increased, the q/m for slugging remained at the same magnitude.

3.3.3. Particle Size Distribution (PSD)

The normalized $D_{P\ 0.5}$ for all fluidization times and gas velocities is presented in Table 3-4. The particles $D_{P\ 0.5}$ in the dropped region was comparable for all fluidization times for both the slugging and bubbling flow regimes. The $D_{P\ 0.5}$ of the wall particles was larger in the slugging regime than the bubbling, for all fluidization times. While more particles built up on the column wall in the bubbling flow regime, the layer was spread out over a much larger area allowing for a larger quantity of smaller particles to be part of the wall layer. On the other hand, the particle layer in the slugging flow regime was much shorter but thicker meaning that the layer built outwards with particles size increasing moving away from the wall. This also confirms previous findings by Sowinski et al. (2010). As for the entrained fines, it was expected that with a higher gas velocity larger particles would be expelled from the bed.

Table 3-4: Normalized $D_{P\ 0.5}$ for all regions for different fluidization times and gas velocities.

Fluidization Time min	Dropped 1.5 U_{mf} $D_{P\ 0.5}$	Dropped 1.75 U_{mf} $D_{P\ 0.5}$	Dropped 3.5 U_{mf} $D_{P\ 0.5}$	Dropped 4 U_{mf} $D_{P\ 0.5}$	Wall 1.5 U_{mf} $D_{P\ 0.5}$	Wall 1.75 U_{mf} $D_{P\ 0.5}$	Wall 3.5 U_{mf} $D_{P\ 0.5}$	Wall 4 U_{mf} $D_{P\ 0.5}$
15	0.91 ± 0.06	0.82 ± 0.12	0.91 ± 0.23	1.01 ± 0.02	0.46 ± 0.03	0.37 ± 0.06	0.44 ± 0.14	0.63 ± 0.04
30	0.88 ± 0.09	0.87 ± 0.06	0.98 ± 0.13	0.93 ± 0.07	0.40 ± 0.02	0.46 ± 0.10	0.57 ± 0.06	0.58 ± 0.06
60	0.94 ± 0.07	0.94 ± 0.24	0.95 ± 0.17	1.01 ± 0.12	0.42 ± 0.06	0.43 ± 0.10	0.66 ± 0.06	0.61 ± 0.09
120	0.95 ± 0.05	0.93 ± 0.03	0.91 ± 0.11	0.97 ± 0.23	0.44 ± 0.03	0.37 ± 0.02	0.44 ± 0.07	0.60 ± 0.17
180	0.87 ± 0.11	1.00 ± 0.19	1.03 ± 0.07	0.95 ± 0.04	0.37 ± 0.02	0.48 ± 0.06	0.54 ± 0.07	0.57 ± 0.03
360	0.98 ± 0.06	1.00 ± 0.06	0.96 ± 0.19	0.89 ± 0.14	0.45 ± 0.02	0.41 ± 0.02	0.54 ± 0.08	0.57 ± 0.10

Fluidization Time min	Fines 1.5 U_{mf} $D_{P\ 0.5}$	Fines 1.75 U_{mf} $D_{P\ 0.5}$	Fines 3.5 U_{mf} $D_{P\ 0.5}$	Fines 4 U_{mf} $D_{P\ 0.5}$	Bottom Column 1.5 U_{mf} $D_{P\ 0.5}$	Bottom Column 1.75 U_{mf} $D_{P\ 0.5}$	Bottom Column 3.5 U_{mf} $D_{P\ 0.5}$	Bottom Column 4 U_{mf} $D_{P\ 0.5}$
15	0.13 ± 0.02	0.11 ± 0.01	0.19 ± 0.05	0.22 ± 0.02	0.38 ± 0.03	0.40 ± 0.18	0.45 ± 0.13	0.47 ± 0.04
30	0.11 ± 0.01	0.11 ± 0.02	0.20 ± 0.02	0.22 ± 0.01	0.29 ± 0.05	0.38 ± 0.12	0.36 ± 0.10	0.40 ± 0.15
60	0.12 ± 0.01	0.12 ± 0.02	0.21 ± 0.02	0.24 ± 0.02	0.51 n/a	0.32 n/a	0.42 n/a	0.50 ± 0.07
120	0.13 ± 0.02	0.12 ± 0.01	0.19 ± 0.00	0.23 ± 0.05	0.34 ± 0.05	0.37 ± 0.07	0.38 ± 0.06	0.32 ± 0.07
180	0.11 ± 0.01	0.14 ± 0.01	0.21 ± 0.02	0.24 ± 0.02	0.32 ± 0.04	0.39 ± 0.06	0.34 ± 0.02	0.34 ± 0.09
360	0.13 ± 0.02	0.12 ± 0.01	0.20 ± 0.02	0.22 ± 0.02	0.38 ± 0.12	0.41 ± 0.01	0.40 ± 0.06	0.37 ± 0.05

Fluidization Time min	Top Column 1.5 U_{mf} $D_{P\ 0.5}$	Top Column 1.75 U_{mf} $D_{P\ 0.5}$	Top Column 3.5 U_{mf} $D_{P\ 0.5}$	Top Column 4 U_{mf} $D_{P\ 0.5}$	Intermediate Wall 1.5 U_{mf} $D_{P\ 0.5}$	Intermediate Wall 1.75 U_{mf} $D_{P\ 0.5}$	Intermediate Wall 3.5 U_{mf} $D_{P\ 0.5}$	Intermediate Wall 4 U_{mf} $D_{P\ 0.5}$
15	n/a n/a	n/a n/a	0.20 ± 0.05	0.22 ± 0.01	- -	- -	- -	- -
30	n/a n/a	n/a n/a	0.21 ± 0.03	0.22 ± 0.01	- -	- -	- -	- -
60	n/a n/a	n/a n/a	0.18 n/a	0.24 ± 0.03	- -	- -	- -	- -
120	n/a n/a	0.15 n/a	0.20 ± 0.01	0.24 ± 0.06	0.61 ± 0.04	- -	- -	- -
180	n/a n/a	n/a n/a	0.23 ± 0.04	0.24 ± 0.02	0.57 ± 0.03	- -	- -	- -
360	0.13 n/a	n/a n/a	0.21 ± 0.02	0.23 ± 0.03	- -	0.68 -	- -	- -

Figure 3-27 presents the results of typical runs where the normalized PSDs of particles from all regions of the system are compared. All other results at different fluidization times had showed similar trend and thus are not presented here. Overall, the results demonstrated that each region of the bed had a different size range. The initial particles were slightly larger than those in the dropped region, followed by the wall and the bottom of the column. The fines were the smallest particles of all the regions. There was some overlap between several areas within the fluidized bed. Both the wall and the bottom column samples contained smaller particles confirming that there were some smaller particles embedded in the wall particle layer. These finer particles were likely the positively charged particles necessary for building the wall layer by providing opposing polarity. As few of the relatively large particles adhered to the column wall, it seemed that a maximum particle size could adhere to

the wall and form the particle layer. In the four graphs presented, the bottom column and wall PSDs demonstrate trends consistent with the earlier presented theory. In the bubbling flow regime, the particle layer built along the column wall was longer but thinner than that formed in the slugging flow regime. As such, the outward building of the particle layer is reduced resulting in similarly sized particles on the wall and bottom column. In the slugging flow regime, the particle layer built was shorter and thicker. This is evident from the difference in the PSD ranges in the wall and the bottom column samples. For the lower velocity tested, the bottom column and wall regions have similar ranges; however, for the higher velocity, the bottom column has a smaller range than the wall region. As the gas velocity increased, the particle layer increased in the radial direction where, as presented in previous works (Sowinski et al., 2010), the particle size increases. This is evident from Figure 3-27d where the wall PSD has shifted towards the right (i.e., larger particles) compared to those at the lower gas velocity.

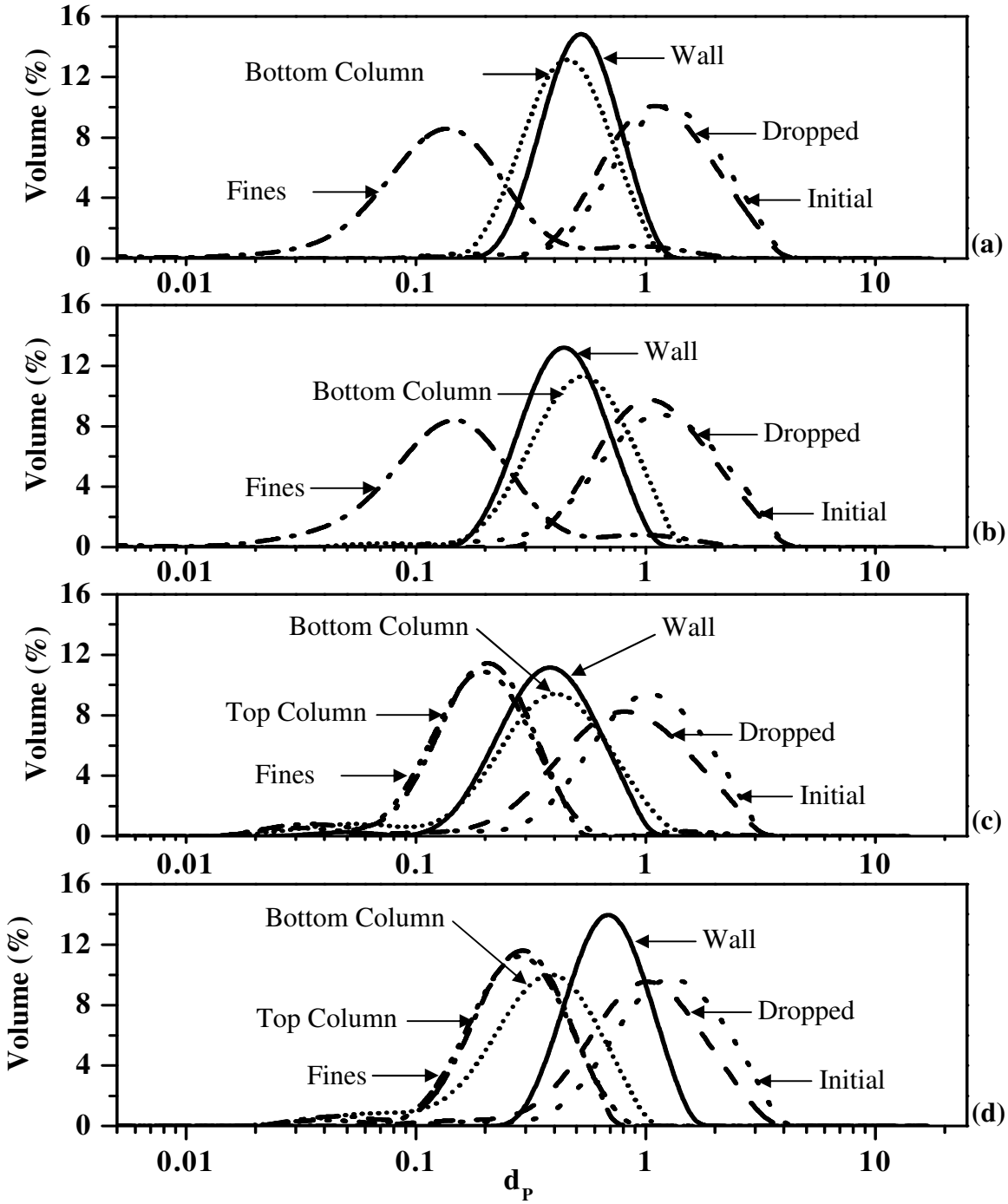

Figure 3-27: Normalized PSDs for all regions of the bed at a fluidization time of 120 minutes: (a) 1.5 U_{mf}, (b) 1.75 U_{mf}, (c) 3.5 U_{mf}, and (d) 4 U_{mf}.

3.4. Charge Saturation

Overall results showed that the fines were predominately positively charged, while the wall and dropped particles were predominantly negatively charged. This confirms the existence of bipolar charging in this system. In addition, in all cases the wall particles had a large negative net q/m. For a particle layer to build up on the column wall, a positive charge must have been generated to provide an opposite charge to attract the polyethylene particles. The column wall, which was not grounded, was made of stainless steel, which is likely to be positively charged following interaction with polyethylene particles. The validity of this exchange is based on the relative work function values, and the triboelectric series. Therefore, it was anticipated that the negatively charged polyethylene particles would be initially attracted to the column wall, creating a negatively charged layer. After the formation of the base negative layers, positively charged particles are likely to be attracted to this layer, which would then draw more negatively charged particles to the wall, creating a bi-polar layer. However, it is important to note that in this work due to the nature of the experimental setup the charge of the column wall itself was not measured, and thus a charge balance could not be conducted.

In addition to reasoning previously explained behind the charge saturation that was observed in some of the experimental runs, the possibility of the air breakdown to the maximum q/m was also explored. Air breakdown is when the strength of the electric field causes the air to ionize and neutralize the charge. The maximum q/m values were calculated based on the limit of the charge dissipation due to air ionisation as presented by Cross (1987) and Revel et al. (2003):

$$\left|\frac{Q}{m}\right|_{\max} = \frac{\pi \varepsilon_O E_d D_C L}{M} \qquad \textbf{Eq. 3-1}$$

where D_C is the column diameter, L is the bed height, M is the mass of the particles in the bed, E_d is the electrical breakdown field of air (300,000 V), and ε_0 is the permittivity of free space (8.854×10^{-12} C^2/N.m). The results of this calculation are presented in Table 3-5. For all fluidization times, the measured $(q/m)_{max}$ was higher for 1.5 and 1.75 U_{mf} and lower for 3 and 4 U_{mf} than that calculated. During bubbling flow regime, the order of magnitude of the

theoretical values was similar to that of the experimental net q/m. This indicates that air ionization could be taking place at these velocities and contributing to the prevention of additional charge generation, besides many contributing factors discussed before. With the velocities tested in the slugging flow regime, the theoretical results suggest that there was no charge dissipation due to air ionization occurring and charge saturation must be controlled by other means as explained in previous sections. As particle migration during slugging flow regime was likely in equilibrium shortly after the onset of fluidization, it was probable that the exchange of particles between the dropped and wall regions prevented an increase in charge.

Table 3-5: Average experimental q/m and theoretical $|q/m|_{max}$ with respect to fluidization time and gas velocity.

Fluidization Time	Experimental				Theoretical $\left\|\frac{Q}{m}\right\|_{max}$			
min	1.5 U_{mf} µC/kg	1.75 U_{mf} µC/kg	3.5 U_{mf} µC/kg	4 U_{mf} µC/kg	1.5 U_{mf} µC/kg	1.75 U_{mf} µC/kg	3.5 U_{mf} µC/kg	4 U_{mf} µC/kg
15	-1.64	-1.64	-0.78	-1.45	2.34	2.34	2.37	2.38
30	-2.65	-2.99	-1.00	-1.34	2.36	2.37	2.37	2.38
60	-2.77	-3.38	-0.92	-0.96	2.36	2.37	2.37	2.39
120	-3.04	-2.75	-0.83	-1.34	2.39	2.37	2.37	2.38
180	-3.59	-3.94	-0.94	-1.29	2.39	2.38	2.39	2.40
360	-4.48	-4.74	-1.04	-1.27	2.38	2.39	2.38	2.40

3.5. Conclusion

The column wall particle layer for velocities in the bubbling flow regime continued to grow as fluidization time lengthened. However, little change was observed for the velocities in slugging flow regime. The particle wall layer was also found to be more widespread and thinner in the bubbling in comparison to shorter and thicker layers in the slugging flow regime. The magnitude of the q/m was influenced by the region of the fluidized bed that the particles came from. The initial particles net q/m were in the range of -0.1µC/kg while in the

dropped region they were up around -0.5 μC/kg. The wall particles had much larger values of approximately -50 μC/kg, while the fines were in the range of 25-300 μC/kg. The net q/m for the bulk particles was not influenced by extending the fluidization time, especially for periods of 60 minutes or greater. It was postulated that there was more potential for charge generation within the bubbling flow regime, at the velocities tested, than the slugging flow regime.

Charge saturation was reached in both the bulk and on the particles adhered to the wall for all velocities by 60 minutes of fluidization. Fine particles in the slugging flow regime reached charge saturation shortly after the onset of fluidization while the bubbling flow regime required more residence time. The calculated maximum q/m was larger than the measured q/m in slugging flow regime and at all fluidization times; however in the bubbling regime it was lower. This indicated that in slugging air ionization was probably not taking place. On the other hand, in bubbling many factors, such as particle migration, type and frequency of contact, and potentially air ionization contributed to determining charge saturation. The sizes of particles present in each region of the bed were unaffected by fluidization time for all gas velocities as similar mean particle sizes were found for all fluidization lengths. The particle size distribution in all regions for all fluidization times followed the same trend: initial particles were the largest, followed by the dropped, wall and bottom column, and finally top column and fines.

Chapter 4. Effect of Column Wall Material on Bed Electrification

Column wall material plays an essential role in bed electrification due to charge generation partially occurring during fluidizing particle-wall contacts. The magnitude and polarity of the charge generated is dependent on the material properties of the surfaces in contact such as work function, electrical conductivity, and surface chemistry and roughness. In addition, different fluidization flow regimes, bubbling versus slugging, will affect the charging since hydrodynamics dictate the fluidizing particles velocity and angle, as well as the number of impacts.

The influence of the column wall material on charge generation has been rarely reported in literature. Only three studies could be found that had investigated column material with respect to electrostatic charging: Boland and Geldart (1971/1972), Ally and Klinzing (1985), and Matsusaka et al. (2006). Boland and Geldart (1971/1972) suggested that the differences observed between electrostatic charging in three columns that they had used (i.e. Perspex, glass, and "Protectafilm") was due to the surface conductivity, which leads to a faster rate of charge leakage in a column with the highest conductivity. They reported that Perspex had the lowest conductivity resulting in the least charge leakage and the stronger particle-wall attractions than the other two column materials. Measurement of conductivity was not reported.

Ally and Klinzing (1985) and Matsusaka et al. (2006) both investigated different materials in pneumatic transport systems. Ally and Klinzing (1985) used pressure drop to investigate the influence of electrostatics on different systems in a vertical tube with particles that were transported upwards with humidified air. If the monitored pressure drop exceeded a base condition, where no electrostatics were observed (i.e., fluidizing gas with RH equal to 75%), then the difference in pressure drop was assumed to be due to electrostatic effects; this technique was seen as a method to measure the overall energy consumption level. They used combinations of glass, copper, and Plexiglas particles for both the tube and the particles and

found that combinations of glass/copper, with either one of these materials being the particles and the other material making up the piping, had the largest pressure drop while the combination of copper/Plexiglas had the least pressure drop. Larger pressure drop was assumed to be indicative of greater electrostatic effects; the authors definition of electrostatic effects was not given. Differences observed were likely due to the materials ability to release electrons with copper having the greatest ability while glass had the least ability. A copper/copper system was not tested. Particles charge-to-mass ratios were also reported; however, the same moisture ranges were not used for all trials due to using moisture levels based on kg moisture/kg particles. However, pressure drop followed the same pattern as the q/m with the exception of the crushed glass particles in the copper tube. It was postulated that the irregular shape of the crushed glass prevented full drainage of charge from the particles.

Matsusaka et al. (2006) found that alumina particles contacting stainless steel, 306 and 316, resulted in a positive charge on the particles while its contact with aluminum, brass, and copper resulted in a negative charge. The magnitude of charge on the alumina particles in the stainless steel, copper and brass tubes resulted in similar values while aluminum charged the least.

These three studies did not investigate differences in charge distribution within the bed or evaluate the amount of wall fouling with different column materials. Therefore, more intensive investigation is necessary to adequately determine material differences with respect to charge generation in gas-solid fluidized beds.

In this work, two columns, one of stainless steel 316 and one of carbon steel, with the same height and diameter were evaluated at two velocities within two fluidization flow regimes. These two materials were chosen since commercial polymerization reactors are generally made of carbon steel while stainless steel is used for reactors at the pilot-scale level. Gas velocities of 1.5 U_{mf} and 4 U_{mf} were used to fluidize the polyethylene particles for a period of one hour, as this was found to be the minimum length for charge saturation to occur (Chapter 3). The particles mass, charge-to-mass ratio and size distribution in different

regions of the bed were compared at both gas velocities in the two different columns, along with the magnitude of wall fouling.

4.1. Results

The results of the experiments investigating column wall material are presented in this section with the discussion to follow in the next section.

4.1.1. Mass Collected (m%)

At 1.5 U_{mf} the amount of mass collected in the dropped region was approximately the same for both the carbon steel and the stainless steel columns (Figure 4-1a). At 4 U_{mf} the values for mean m% were slightly different, with more particles being collected from the stainless steel column. This indicated that there would be more migration of particles from the bulk of the bed to either the wall or the fines region in the carbon steel column. However, it is important to note that by including the standard deviations the range of the values overlapped.

In the wall region, the m% collected was similar for both columns for 1.5 U_{mf}, but slightly different for 4 U_{mf} (Figure 4-1b). Slightly more mass was collected from the carbon steel column which may correspond to the difference in m% in the dropped region; thus, it is likely that more particles were migrating from the bulk to the wall in this column at this gas velocity.

In the fines region similar amounts of particles were collected at 1.5 U_{mf}; but at 4 U_{mf} there were slightly more particles elutriated from the bed in the stainless steel column (Figure 4-1c). This may be related to the decreased amount of particles in the wall region, meaning that fewer fine particles were necessary for layering during wall fouling. However, the standard deviations on these measurements indicate that there may be little difference, if any, between the two columns.

During each experiment some particles were not retrieved since they had adhered to the column wall due to strong electrostatic forces. Without additional handling, which would have impacted their charge, these particles could not be collected. At 1.5 U_{mf}, the quantity of these particles was greater in the stainless steel than the carbon steel column (Figure 4-1d). However at 4 U_{mf}, similar amounts were found in both columns.

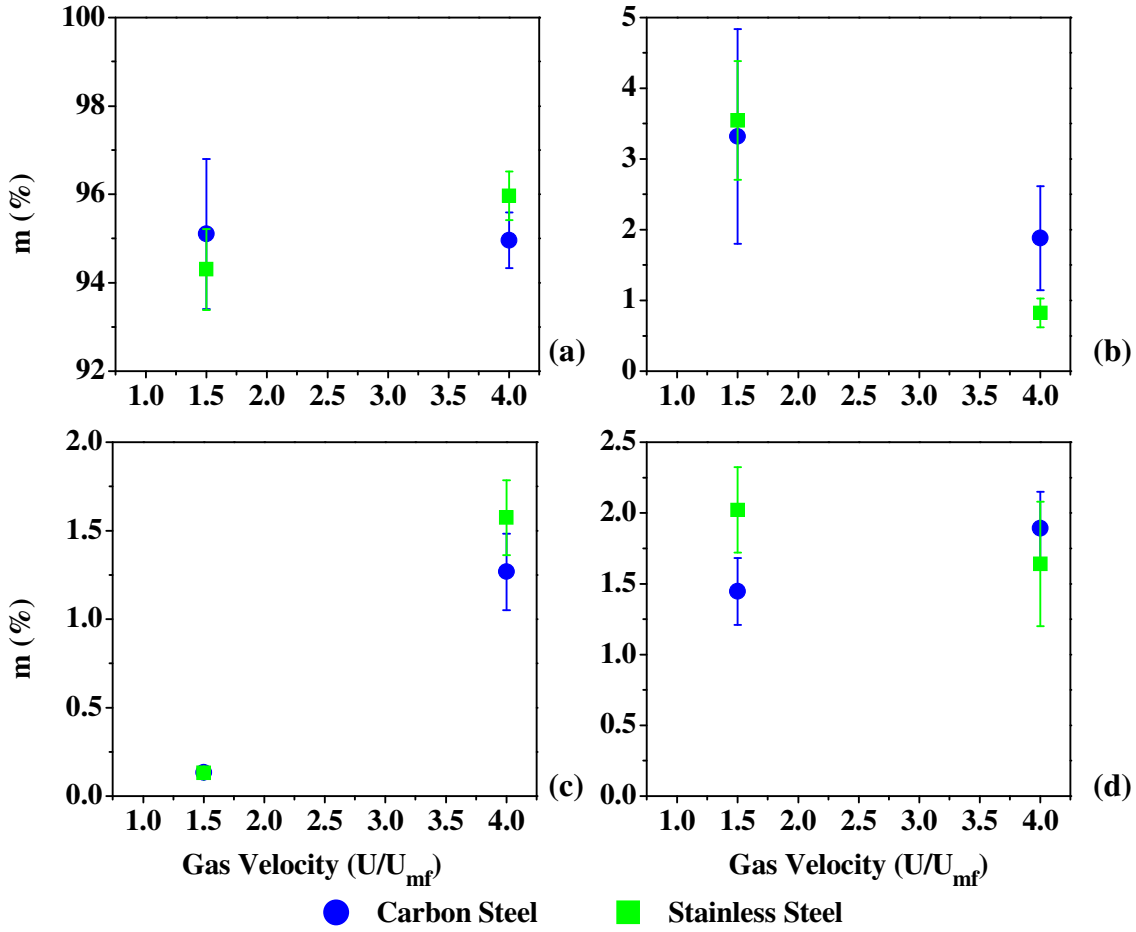

Figure 4-1: Mean m% collected for different column materials: (a) Dropped, (b) Wall, (c) Fines, and (d) Irretrievable.

4.1.2. Charge-to-Mass Ratio (q/m)

Initially, the net q/m was similar for both column materials at both fluidization gas velocities (Figure 4-2a) allowing for the comparison of all experiments. The charge polarities were the same for each region of the bed regardless of column wall material or fluidization gas

velocity, and the magnitude was also in the same range. For both the stainless steel and carbon steel columns, at 1.5 U_{mf} the largest magnitude net q/m was found in the fines region, followed by the wall; at 4 U_{mf} the largest magnitude was in the wall region followed by the fines. The dropped region had the next largest magnitude net q/m while the initial particles had the smallest magnitude. The initial particles had the lowest net q/m. As presented previously in Chapter 2, Figure 2-8, the smaller particles within the initial samples were highly negatively charged. Therefore, charge generation must have taken place in both columns since the fines entrained were found to be positively charged (Figure 4-2d),.

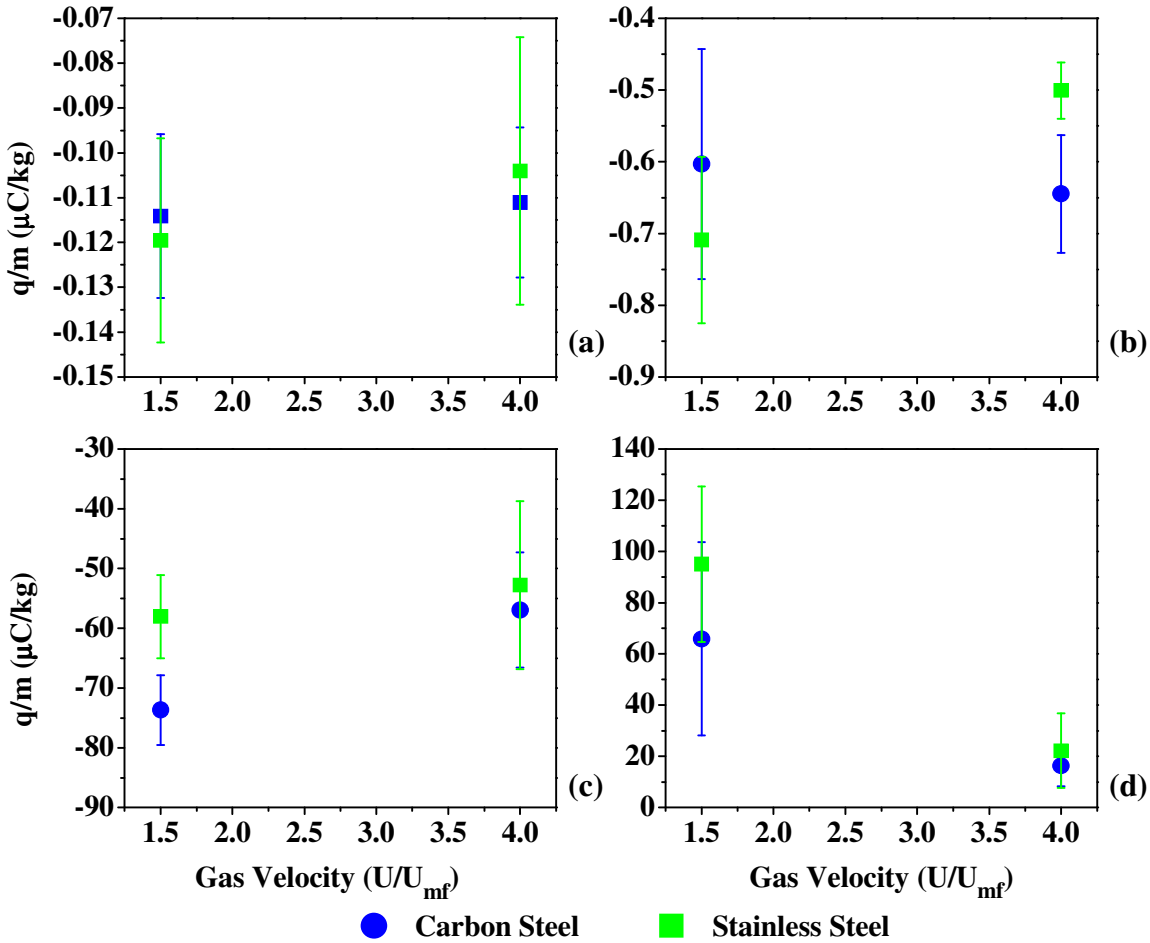

Figure 4-2: Mean net q/m for different column materials: (a) Initial, (b) Dropped, (c) Wall, and (d) Fines.

In the dropped region, the two columns produced similar net q/m at 1.5 U_{mf}. Since similar m% was also collected for both columns, the generated charge must have been almost equivalent regardless of column wall material. However, different magnitudes were

observed at 4 U_{mf} (Figure 4-2b). The particles from the carbon steel column were found to have a higher magnitude net q/m than those in the stainless steel column. As the m% from the stainless steel column was greater than the m% collected from the carbon steel column, the charge generated in the carbon steel column must have been greater than that generated in the stainless steel column or remained the same to result in a slightly higher net q/m.

In the wall region at 1.5 U_{mf}, the net q/m from the carbon steel column has a greater magnitude than that of the stainless steel column (Figure 4-2c). As the m% collected from both columns was similar, more charge must therefore have been generated on the particles in the carbon steel column to result in a higher net q/m. At 4 U_{mf} similar values of net q/m were obtained. As slightly more m% was collected from the carbon steel column, more charge must have been generated in this column to result in similar net q/m.

Overall, at 4 U_{mf}, both the dropped and wall particles carried a higher net negative charge in the carbon steel column compared to that of the stainless steel column. Two factors could have contributed to such a finding; higher charge generation inside the carbon steel column, or the presence of less positively charge particles (i.e. fines) inside the bed. The latter, is not valid in this case since less fines entrainment was observed in the carbon steel column (Figure 4-1c) resulting in more positively charged particles remaining inside the bed. Therefore, the first hypothesis of higher charge generation in the carbon steel column applies.

In the fines region at 1.5 U_{mf} slightly larger magnitude of net q/m was observed in the stainless steel column if only the mean values of q/m were considered (Figure 4-2d). As the m% was similar for both columns, then slightly more charge may have developed on the particles in the stainless steel column. At 4 U_{mf}, similar values of net q/m were measured; as similar m% was collected, no difference in charging was observed. This is due to the fact that at such high gas velocity, the majority of entrainment occurs in a very short period of time at the beginning of the run, and thus particles have smaller residence time inside the bed to affect their magnitude of charging.

4.1.3. Wall Particle Layer

Images of the layer of particles coating the column wall, taken after the collection of the dropped particles, are presented in Figure 4-3. Comparison of the pictures taken at 1.5 U_{mf} for the carbon steel column (Figure 4-3a) and the stainless steel column (Figure 4-3b) showed that the particle layer developed to approximately the same height, approximately that of the static bed height, with what seemed to be similar thickness from visual observation. This similar particle layer coverage correlates with the similar amount of m% collected in the wall region as seen previously (Figure 4-1b).

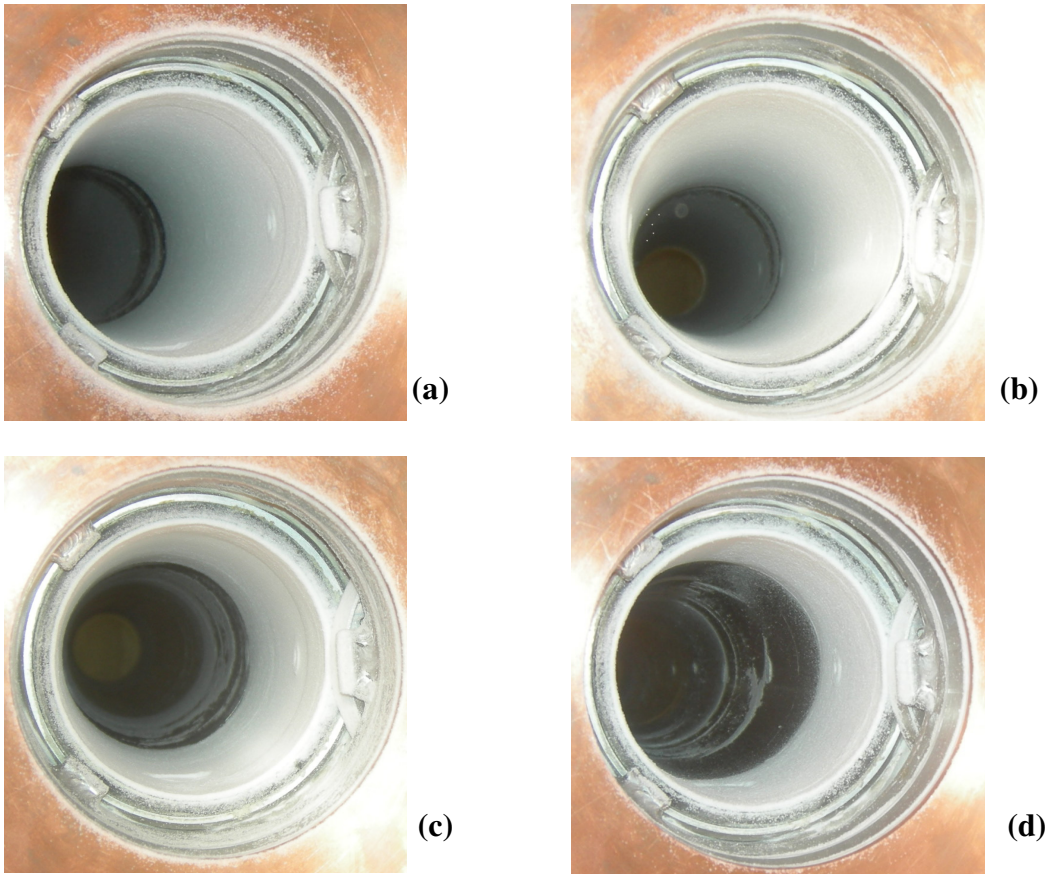

Figure 4-3: Images of particle wall layer: (a) Carbon Steel 1.5 U_{mf}, (b) Stainless Steel 1.5 U_{mf}, (c) Carbon Steel 4 U_{mf}, and (d) Carbon Steel 4 U_{mf}.

The images for 4 U_{mf} (Figure 4-3c and d) depict different particle coverage of the column wall for the different column materials. The carbon steel column had a particle wall layer that extended higher from the bottom of the column than the layer on the stainless steel

column. This difference corresponds to the difference in the amount of particles collected in the wall region of carbon steel column. This more extensive layer could be due to the higher charge generation found in this column, in addition to the greater presence of fines in the bed due to less entrainment flux observed in the carbon steel column. As indicated previously, more negative charges were found to be generated in this column which translates to higher charging of the column wall. This then will promote more negative particles adhering to the column wall explaining the larger coverage of the particles. Additionally, more positively charged particles (i.e., fines) present inside the bed promotes the wall layering effect postulated in the previous chapter. As more particles build on the wall, positive charges are necessary to allow for the attraction of additional negatively charged particles. As seen previously, at this velocity a layer of particles forms on the column wall shortly after the onset of fluidization; however elutriation of fines continues as fluidization progresses. Thus the negative layer forms on the column wall and then provides an attraction for positively charged particles. This reduces the amount of entrained fines and increases the layer of particles found on the column wall. It is difficult to quantify if there are any differences in thickness of particle layer between the two columns, but it is possible that the carbon steel column is not only longer but also thicker.

4.1.4. Particle Size Distribution (PSD)

Particle size distribution analysis was conducted for both the carbon steel and stainless steel columns. As previously mentioned the PSD data was normalized for each sample based on the mean particle size ($D_{P\ 0.5}$) from the initial sample for each experimental trial. This allowed for comparison of different trials with slightly different $D_{P\ 0.5}$ due to the large size range of the industrial resin.

4.1.4.1. 1.5 U_{mf} Gas Velocity

The results from one experimental trial, representing a typical PSD analysis for both carbon steel and stainless steel columns, are presented in Figure 4-4. PSDs are presented for the initial sample, the dropped particles, the wall, and the fines regions. For both columns, the particle size distributions were similar for each region. Therefore, the column wall material had little or no effect on particle size distribution.

For both the stainless steel and carbon steel columns, the initial particles constitute the largest particles in the bed, followed closely by the dropped particles. As the dropped region was composed of the majority of particles, it was expected that this region would have a similar PSD to the initial sample. The wall region had the midrange particles. The fine particles were the smallest particles within the bed and the size of these particles was dictated by the fluidization gas velocity.

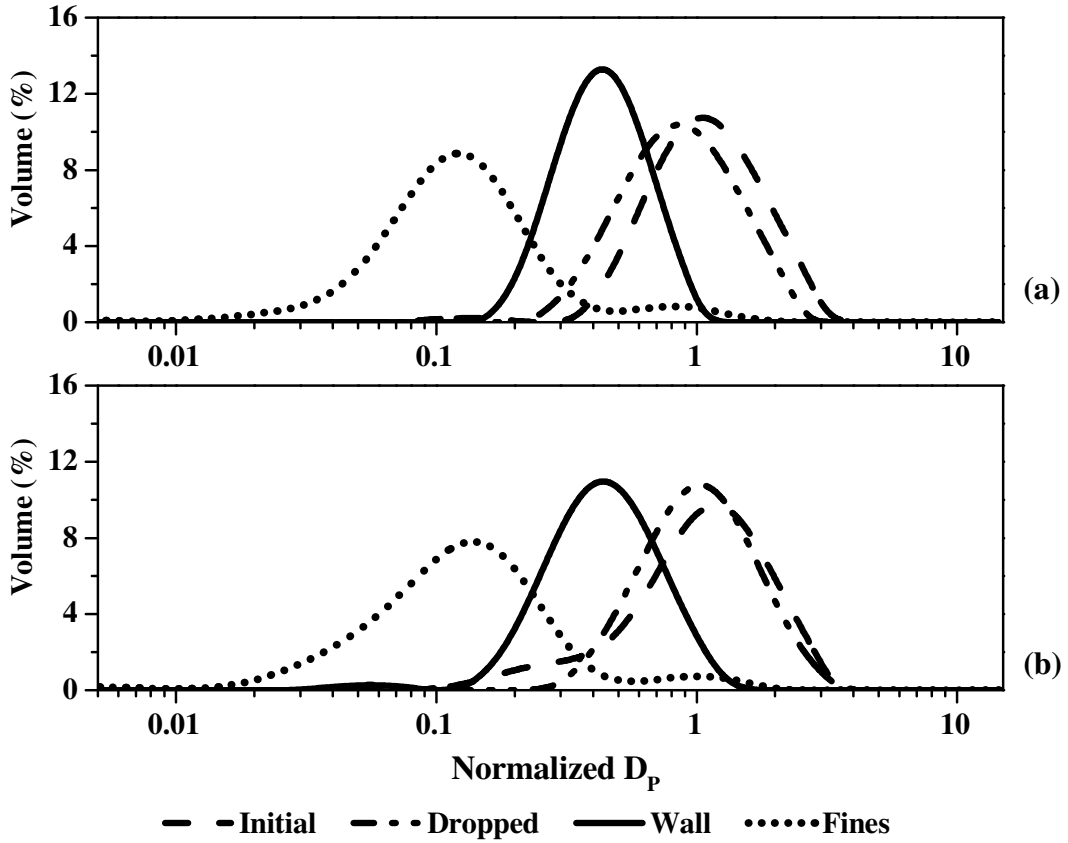

Figure 4-4: Example PSDs at 1.5 U_{mf} for all regions of the bed for different column materials: (a) Carbon steel column, (b) Stainless steel column.

4.1.4.2. 4 U_{mf} Gas Velocity

The particle size distributions for typical experiments at 4 U_{mf} in the carbon steel and stainless steel columns are presented in Figure 4-5. Initial, dropped, wall, and fines region PSDs are presented with an additional PSD from those particles collected from the bottom of the column from the particle layer still covering the column after wall collection.

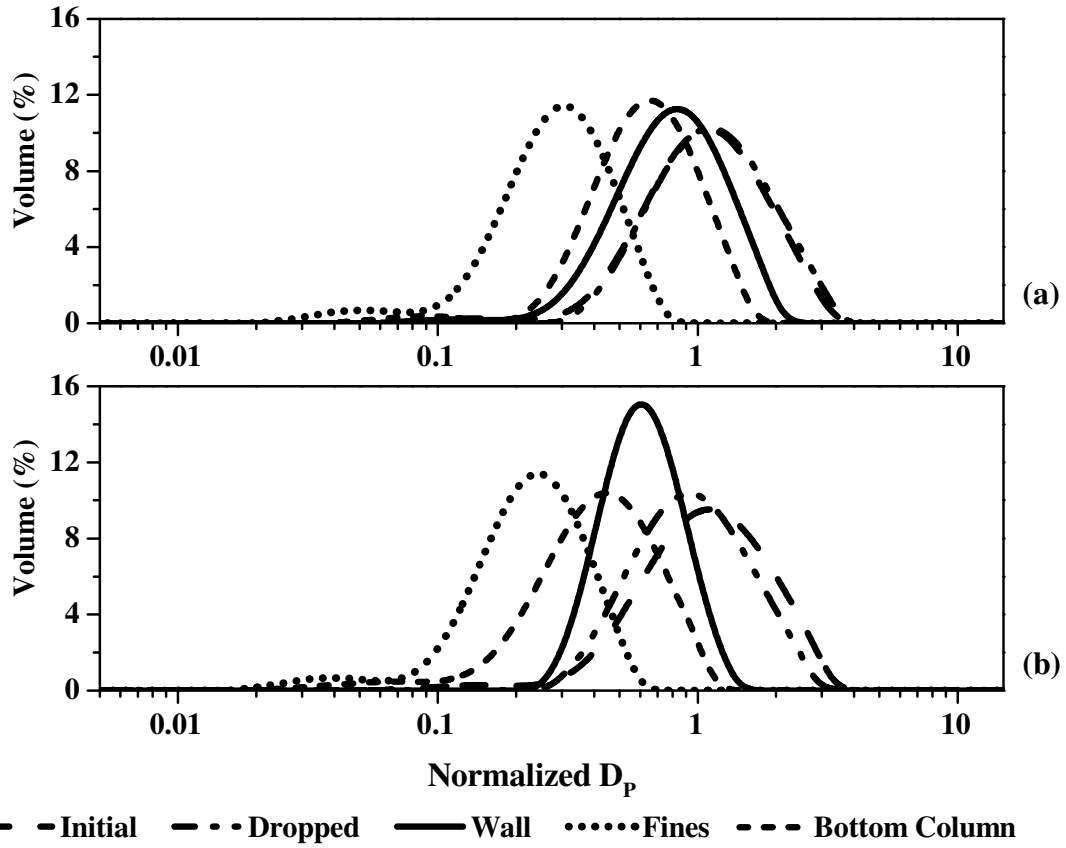

Figure 4-5: Example PSDs at 4 U_{mf} for all regions of the bed for different column materials: (a) Carbon steel column, (b) Stainless steel column.

The order of the regions with respect to particle sizes was similar for both column materials and to that, discussed previously, for 1.5 U_{mf}. The initial and dropped particles were the largest followed by the wall with the fines made up of the smallest particles. The inclusion of an additional PSD occurred between the wall and the fines regions. These particles were those most tightly adhered to the column wall, therefore it was likely that smaller sized particles adhered to the column wall first followed by particles increasing in size. As seen in the PSDs for the bottom column region, smaller particles adhered to the column first in the

stainless steel column compared to the slightly larger particles found in the carbon steel column.

The differences between the two columns could mainly be observed in the wall, fines, and bottom column regions. In the stainless steel column, the PSDs in the fines and wall regions were composed of a narrower range of particles. Also, the particles seemed to be smaller in size; although the lower bound of the PSDs were similar for both columns in those regions. In the bottom column region, the PSD seemed to be shifted to smaller sized particles for the stainless steel column.

In the wall region, as seen previously, the carbon steel column resulted in more wall fouling. Therefore, based on the wall layering effect, where particle sizes increase moving away from the column wall, more larger particles would be found in the wall region that has more extensive fouling (i.e., carbon steel). The larger particles found in the bottom column region of this column could be due to the particle-wall contacting resulting in more charge generation. More charge is generated in the carbon steel column, not only on the particles but also on the column itself. With a greater positive charge, the carbon steel column would have attraction for larger particles than the stainless steel column even in the initial stages of wall fouling resulting in relatively larger particles found in the bottom column. Additionally, this same positive charge could initially repel any positively charged particles until enough negatively charged particles were adhered to the column wall to switch the polarity of attraction, after which positive particles would be drawn to the particle layer.

4.2. Discussion

There are two main differences, besides material composition, between the two columns: surface electrical properties (i.e., work function and conductivity) and roughness. These properties may work together, or contribute individually to the differences in charge generations observed. Additional factor to consider is the hydrodynamics of the particles within the bed.

As mentioned in the previous chapter, polyethylene particle-wall contacting likely results in the column wall and the polyethylene resin being charged positively and negatively, respectively. This is due to the difference in work function of the materials in question. According to the Powder Technology Handbook (Masuda et al., 2006), the work function for polyethylene and carbon steel are approximately 5.23 eV and 4.5 eV, respectively. No values of work function were specifically found in literature for stainless steel. As presented in Table 4-1, surface conductivity of each of the column materials was slightly different, which would result in different work functions. However, it was anticipated that the difference would be small; thus, similar values were assumed. Based on the work functions, both column materials were likely to lose electrons on contact with polyethylene. Thus, it is unlikely that work function contributed much, if any, to the differences observed in electrification results obtained from the two columns.

Table 4-1: Materials surface conductivity.

Material	Conductivity (Siemens/m)	Resistivity (Ωm)	Reference
Carbon Steel	5.9×10^{6}	16.9×10^{-8}	TibTech Innovations (2010)
Stainless Steel	1.32×10^{6}	76×10^{-8}	TibTech Innovations (2010)
Copper	58.5×10^{6}	1.7×10^{-8}	TibTech Innovations (2010)
Polyethylene	$<1.1 \times 10^{-15}$	9.1×10^{12}	Hindermann-Bischoff and Ehrburger-Dolle (2001)

Increasing the surface conductivity can allow the charge to leak away, reducing overall charge within the fluidized bed (Forrest, 1953). Many studies and patents have used changes in surface conductivity as an explanation for the reduction of charge within fluidized beds (Bafrnec and Bena, 1972; Boland and Geldart, 1971/1972; Chirillio et al., 1986; Goode et al., 1987; Guardiola, 1996; Inculet et al., 2006; Katz and Sears, 1969; Park et al., 2002b; Yao, 2002). As a result of the differences in conductivity for the materials tested, the surface ability to conduct electrons and therefore transfer charge was slightly different, which may have impacted the charge generation capabilities during particle-wall interactions. However, when compared to conductivities of different materials such as copper (a highly conductive material) and more importantly, polyethylene, the conductivities of stainless steel and carbon steel can be considered fairly similar. Additionally, typically in previous studies the fluidization column was grounded to prevent large potentials from

building up as this would allow for charge leakage (Boland and Geldart, 1971/1972; Chirillio et al., 1986; Goode et al., 1987; Guardiola, 1996; Inculet et al., 2006). However in this system the column wall was electrically isolated which prevented any charge to escape. Thus the differences in surface conductivity likely did not lead to the differences observed in charge generation within the bed.

Another parameter to consider was surface roughness which greatly influences the generation of charge as seen by Shimizu et al. (1979) who concluded that surface scratching can increase charge by ten-fold. Surface roughness is related to the friction factor of a material, the more rough a surface, the higher the friction coefficient. With a higher friction coefficient more frictional energy would have been produced during the particle-wall contacts resulting in more charge being generated due to frictional charging.

The two columns used in these experiments were supplied by different manufacturers; thus, having different inner wall surface finish. The surface roughness of both columns was measured using a portable Mitutoyo surface roughness tester (Model: SJ-201 Mitutoyo, Japan). The range of the measurement was up to 360 μm with a resolution of 0.02 μm. Measurements were taken at 28 spots in approximately the same location on both columns. The average and standard deviation of the surface roughness for each column is presented in Table 4-2. In terms of roughness grade, carbon steel falls into the N9 category while Stainless steel is in the N5 category (Maryland Metrics, 2002). The N-scale runs from N1 (0.025 μm) to N12 (50 μm). Therefore, the stainless steel column was smoother than the carbon steel column. It is expected that the difference contributed to the variation in the bed electrification within the two columns.

Table 4-2: Surface roughness of column wall materials.

Column Material	Surface Roughness (μm)
Carbon Steel	6.57 ± 2.78
Stainless Steel	0.37 ± 0.15

With the higher surface roughness, the carbon steel column would be expected to result in more charge generation than the stainless steel column, especially in the wall region. This

was observed at 1.5 $U_{mf.}$ This indicated that although particle-particle charging is the predominant charging mechanism during the bubbling flow regime, due to vigorous mixing, particle-wall contacts influenced the development of charge in the wall region of the bed. Assuming that particle-particle contact frequencies were similar in both columns at this gas velocity, which they should be as the only difference between systems was the column material, then particle-wall contacts could result in the differences observed. The rougher carbon steel surface would be likely to generate more charge on those particles rubbing against the wall compared with similar particles rubbing against the stainless steel wall. These same particles would then become adhered to the column wall, creating the first layer of wall fouling. With more charge on these particles, the wall net q/m would be greater on the carbon steel column assuming that similar quantities of particles adhered to each column, which was observed. After this initial layer, particle-wall contacting would cease in this flow regime, resulting in similar net q/m observed in the dropped region. As similar amounts of particle-particle contacting would take place in both columns.

At 4 U_{mf} similar net q/m values were measured in the wall region for both column materials indicating more charge generation in the carbon steel column due to more m% collected. As previously mentioned, in the slugging flow regime the predominant charging mechanism is frictional charging due to the motion of the slugs against the column wall. Thus, particles closest to the wall would generate more charge in the carbon steel column compared to the stainless steel column due to the differences in surface roughness. In this flow regime, more particles adhered to the column wall in the carbon steel column than in the stainless steel column. As particle-wall interactions resulted in more charge developing in the carbon steel column, particles adhered to the column wall with a strong negative charge. This provided a strong driving force for the attraction of finer particles that were positively charged, which, following adhesion, would then provide attraction for additional negatively charged particles. This was correlated with the lower fines entrainment flux found in the carbon steel column. Due to the hydrodynamics of the slugs brushing particles off upper portions of the column wall, continuous particle-wall contacting occurred providing the carbon steel column with stronger electrostatic forces than the stainless steel column throughout fluidization. Additionally, with more electrostatic force, larger particles would be able to

remain adhered to the wall even with the brushing of slugs against the particle layer. This is supported by the larger size range of particles found in the carbon steel column compared to that in the stainless steel column.

At the higher gas velocity, a higher net q/m was observed in the dropped region for the carbon steel column compared to the stainless steel column. This was likely due to the manner at which particles form the layer on the column wall in the slugging flow regime. At 4 U_{mf} there is a portion of the column which does not become covered with particles due to the motion of the slugs preventing particle adhesion. This region remains uncovered throughout fluidization allowing for continuous particle-wall contacting, unlike in the bubbling regime where once a layer has built on the wall, there is little column material available for particle-wall contacting. The particles within the slug make contact with the wall, generating charge and then fall back into the bulk. With frictional charging being the dominant mechanism, the particles rubbing against the rougher carbon steel wall generate more charge than those rubbing against the smoother stainless steel wall. As previously mentioned, particle-wall contacting between carbon steel or stainless steel and polyethylene particles results in negatively charged particles. Thus, it is likely that even with similar frequency of contacts more net q/m would be produced in the carbon steel column.

4.3. Conclusion

Slightly different amounts of charge were generated in the two columns. Similar effects were observed at the different fluidization gas velocities: more charge was generated in the Carbon steel column at 1.5 and 4 U_{mf}. The differences in the surface roughness of the two materials was likely the contributing factor to the manner in which charge was generated within the bed. However, these impacts must also be influenced by the hydrodynamics of the bed as differences in charging were observed with gas velocity. During slugging flow, frictional charging is the more dominant mechanism resulting in more differences in charge generation between column materials in the slugging flow regime compared to that in the bubbling flow regime. Column wall fouling was observed in both columns with relatively similar magnitudes at the lower gas velocity, and higher magnitude in the carbon steel column at the elevated gas velocity.

Chapter 5. Effect of Fluidizing Gas Relative Humidity on Bed Electrification in Bubbling and Slugging Flow Regimes

The effect of fluidizing gas relative humidity (RH) on charge generation and/or dissipation of industrial polyethylene resins is presented in this chapter. Previous research has been performed in this area where relative humidity used as a charge reduction technique in gas-solid fluidized beds (see Table 1-5). Some studies have found that high relative humidities (>60%) were the most effective at reducing potential within the bed (Bafrnec and Bena, 1972; Boland and Geldart, 1971/1972; Guardiola et al., 1996; Wolny and Kazmierczak, 1989). However, excessive humidification (>75%) resulted in an instable bed that was difficult to fluidize due to high capillary forces (Guardiola et al., 1996; Park et al., 2002b). The resounding theory for these results is the formation of a water film, either on the particles (Chen et al., 2003) or on the column wall (Ciborowski and Wlodarski). This water film reduces the surface conductivity promoting the reduction of potential within the bed (Bafrnec and Bena, 1972; Boland and Geldart, 1971/1972). Porous structure, compared to spherical, has also been presented as an explanation for decreased potential due to relative humidity (Park et al., 2002b). Some studies note that affinity for water may effect how a system reacts to humidified fluidizing gas (Fujino et al. 1985; Guardiola et al., 1996)

These previous studies mainly focused on the bubbling flow regime without considering the investigation of the effects due different bed hydrodynamics in other flow regimes. Few studies investigated the effects of relative humidity in a metallic column (Bafrnec and Bena, 1972; Baron et al., 1987; Fujino et al., 1985; Mehrani et al., 2007) such as those used in industry. None of those four studies looked at distribution of charge within different regions of the bed but instead focused on either the effect on fines (Baron et al., 1987; Mehrani et al., 2007) or on the local charge within the bulk of the bed (Bafrnec and Bena, 1972; Fujino et al., 1985). The measurement system used in this thesis, with its novel charge measurement technique, provides an in-depth method of studying wall fouling, which is a significant problem in industry and the distribution of charge throughout the fluidized bed.

In this work, desired relative humidities were obtained by mixing different proportions of 100% saturated air with almost dry air (~3% RH). Relative humidity values were selected for a range of 0 to 100% RH with 20% increments. Five relative humidities (0%, 20%, 40%, 60%, and 80%) were evaluated for four different fluidization gas velocities at factors of U_{mf} (1.5, 1.75, 3.5 and 4 U_{mf}). A RH value of 100% was not tested since large values of relative humidity are likely to produce unstable beds with poor fluidization due to high capillary forces leading to large amounts of particles cohesion. For all experimental runs, the particles charge, mass and size distribution throughout the bed was evaluated, as well as the particle build-up on the column wall.

5.1. Bubbling Flow Regime

In the bubbling flow regime, two gas velocities were tested: 1.5 and 1.75 U_{mf}. These velocities were examined at five different relative humidities: 0, 20, 40, 60, and 80% for a fluidization time period of 1 hour. Results are presented for particles mass collected (m%), charge-to-mass ratio (q/m), particle wall layer, and particle size distribution (PSD).

5.1.1. 1.5 U_{mf} Gas Velocity Results and Discussion

The results obtained for the fluidization gas velocity of 1.5 U_{mf} are presented in this section along with the associated discussions.

5.1.1.1. Mass Collected (m%)

As can be seen in Figure 5-1a, in the dropped region of the bed there was a decline in particles m% collected at the mid range relative humidities (i.e. 20-40%), followed by an increase with increasing the relative humidity. This was mirrored in the wall region with an increase in m% with the increase of the relative humidity followed by a decline (Figure 5-1b). These findings indicate that there was an increase in the particle migrations from the

bulk of the bed to the wall region at mid range relative humidities, resulting in higher column wall fouling. On the other hand, at higher relative humidities, there were fewer particles along the wall, but more particles within the bulk.

As seen in Figure 5-1c relative humidity had no effect on the amount of fines collected as the mass of the elutriated fines remained constant, regardless of the gas relative humidity. This is an indication that it is unlikely that any particle agglomerations within the bed caused by electrostatic force were broken apart by the presence of moisture in the system. This contrasts to the result of Baron et al. (1987) who found that silica sand in a carbon steel column had an increased in entrainment flux between 7 to 30% RH. This could be due to silica sand being hydrophilic (Siddique, 2007) whereas polyethylene is hydrophobic. Without a strong affinity for water, at this moisture content the polyethylene particle agglomerates may not be able to break up due to dissipation of the electrostatic forces holding them together.

Fewer particles were lost during sampling at the higher relative humidities (Figure 5-1d); this was likely due to the decreased number of particles adhered to the column wall.

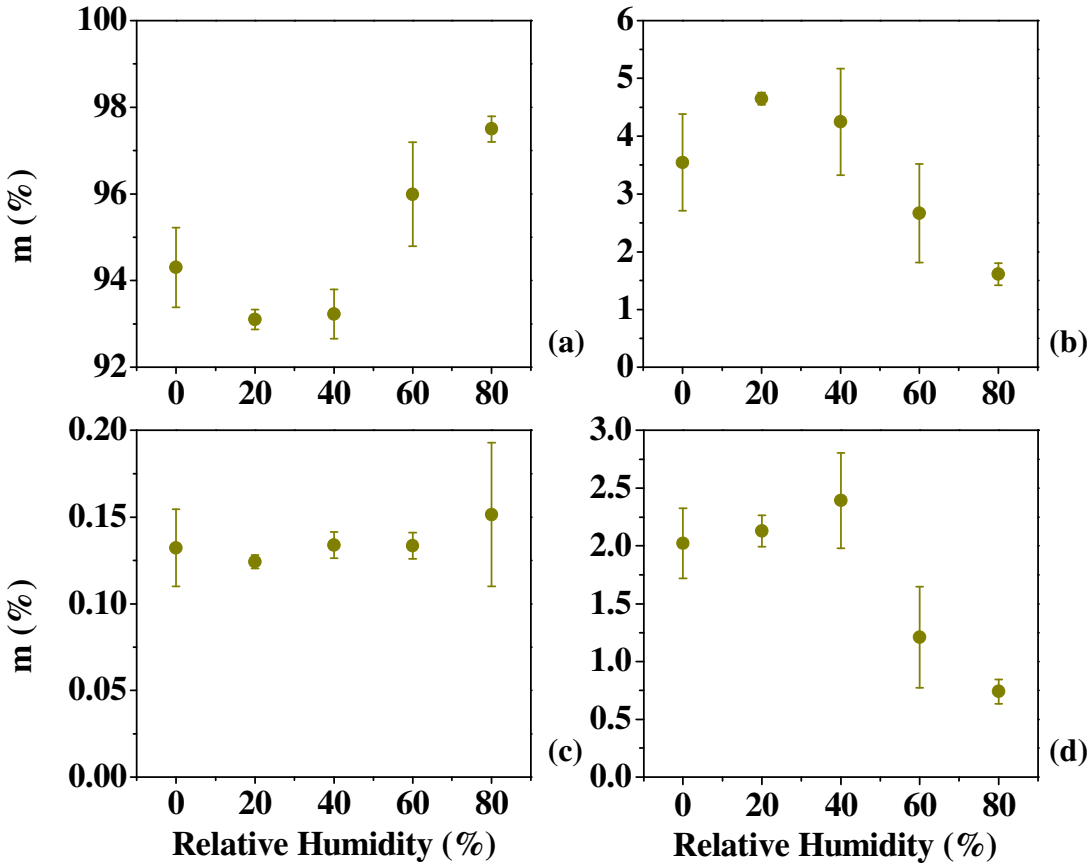

Figure 5-1: Mean m% at 1.5 U_{mf} for different relative humidities: (a) Dropped, (b) Wall, (c) Fines, and (d) Irretrievable.

5.1.1.2. Charge-to-Mass Ratio (q/m)

Figure 5-2 presents the results of the particles mean net q/m found in different regions of the bed at different gas relative humidities. The magnitude and/or polarity of the net q/m differs in each region of the bed. The fine particles have the largest net q/m, at approximately 23 to 146 μC/kg, followed by the wall particles, at approximately 50 to -72 μC/kg, and the dropped particles at -0.19 to -0.82 μC/kg. Both the dropped and the wall particles mean q/m were greater than that of the initial particles (approximate net q/m of -0.1 μC/kg), demonstrating that charge was being generated within the bed due to fluidization. The net charge polarity of the initial particles, as well as within the dropped and wall regions were negative while it was positive for the fines. Thus, the charge polarities were not impacted by a change in gas relative humidity, and bipolar charging was still observed for all conditions.

However, the initial particles charge distribution (Figure 2-8) showed that finer particles were likely negatively charged. Following fluidization, results show that these same particles were more likely to be positively charged. Therefore, charge of the opposite polarity developed on these particles during fluidization also indicating that charge generation was taking place within the bed.

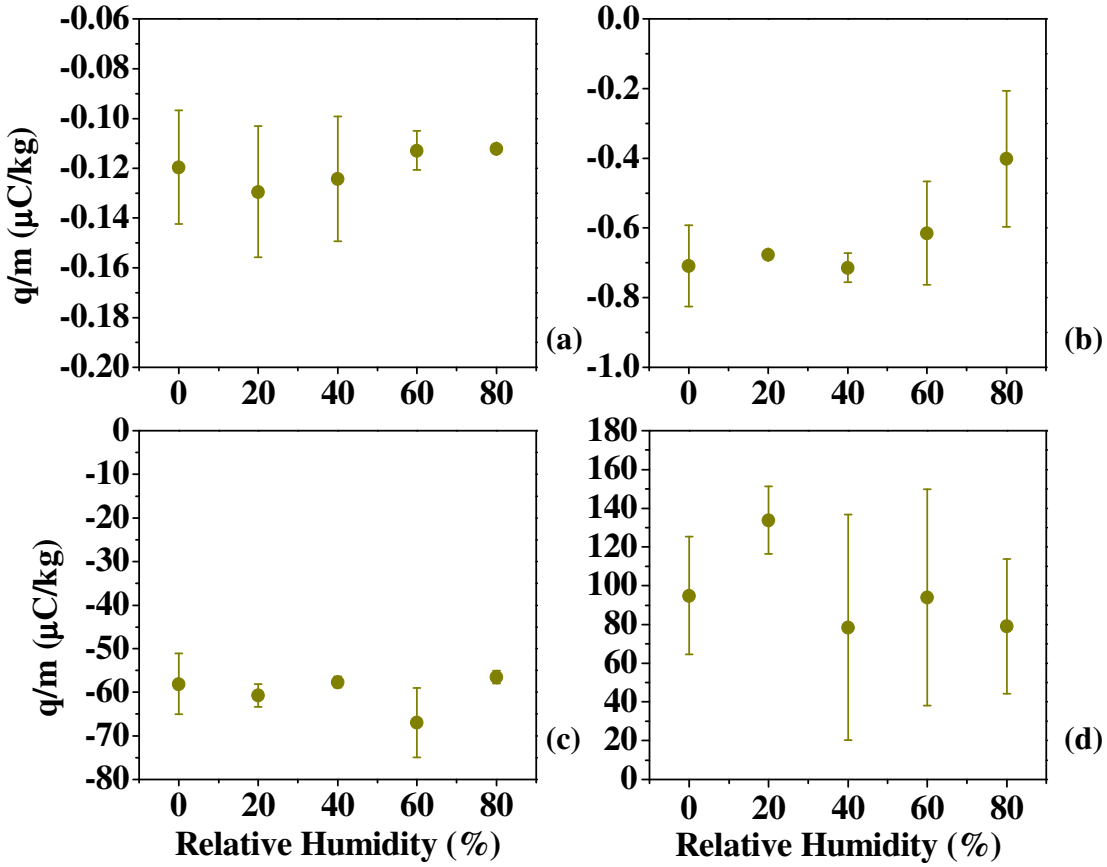

Figure 5-2: Mean net q/m at 1.5 U_{mf} for different relative humidities: (a) Initial, (b) Dropped, (c) Wall, and (d) Fines.

The mean net q/m for the initial particles was similar for all trials allowing for comparison at all relative humidities (Figure 5-2a). In the dropped region, the magnitude of the net q/m remained constant for relative humidites up to 40% and then decreased for 60 and 80% RH. Since the particles m% decreased somewhat in the bulk during the midrange humidities, the particles charge at these conditions must have also decreased in comparison to the 0% RH trials, to maintain a constant ratio. However, since the m% collected was increased at higher relative humidities, the charge must have remained constant or only increased slightly for

the net q/m to decrease. Thus, the change in relative humidity affected the charge on the dropped particles up to 40% RH with no impact on net q/m. However, for the higher relative humidities, the effect was likely due to the changes observed in m% rather than charge. The decrease in dropped net q/m is concerned with the incorporation of water onto a surface that may introduce ions into the system (Németh et al. 2003) which could increase surface charge dissipation. This charge dissipation could be due to a decrease in surface resistance which becomes apparent in polyethylene only after relative humidities of 60% or greater (Field, 1946). The increase in the surface conductivity then leads to the decrease in dropped particles net q/m at these relative humidities where even though particles charging occurs, but the dissipation rate may increase with added moisture.

The net q/m in the wall and fines regions remained fairly constant for all relative humidities. A slight increase in m% in the wall region occurred from 0% to 40% so to maintain a constant net q/m an increase in charge must have also occurred. However, a decrease in m% was observed at relative humidities of 60 % and 80% and thus the particles charge must have decreased during this period. This increase in electrification up to a certain humidity followed by a decrease has been observed in previous work by Ciborowski and Wlordarski (1962). They postulated that a water film was formed on the column wall which lowered its surface resistivity. Although the columns used in their work and present study are different, it may be that the difference in material just affects at what relative humidity the water film is formed on the column. In this work, results indicated that when particles had more charge, then more of them migrated to the wall, and the vice versa. Therefore, the amount of q/m is equivalent regardless of relative humidity even though the amount of charge is changing. In addition, this finding states that gas relative humidities beyond 40% reduce the particles charge, resulting in less particle wall fouling. In the fines region m% remained constant which indicates that the charge also remained constant. Therefore, the fine particles net q/m is likely not affected by relative humidity.

5.1.1.3. Wall Particle Layer

After collecting the bulk particles, pictures were taken from the inner column wall to examine the effect of RH on reactor wall fouling (Figure 5-3). These pictures correlate with results of the particles m% where a maximum was obtained at midrange humidities. At 20% and 40% RH, particles coated the column wall slightly more than when dry air was used, while 60% relative humidity resulted in slightly less particle wall adhesion. The 80% relative humidity trials resulted in the least particle coverage of the column wall. It was clear from these results that at 1.5 U_{mf} the effect of the fluidizing gas relative humidity was more prevalent at higher RH values as particles had a decreased ability to adhere to the column wall.

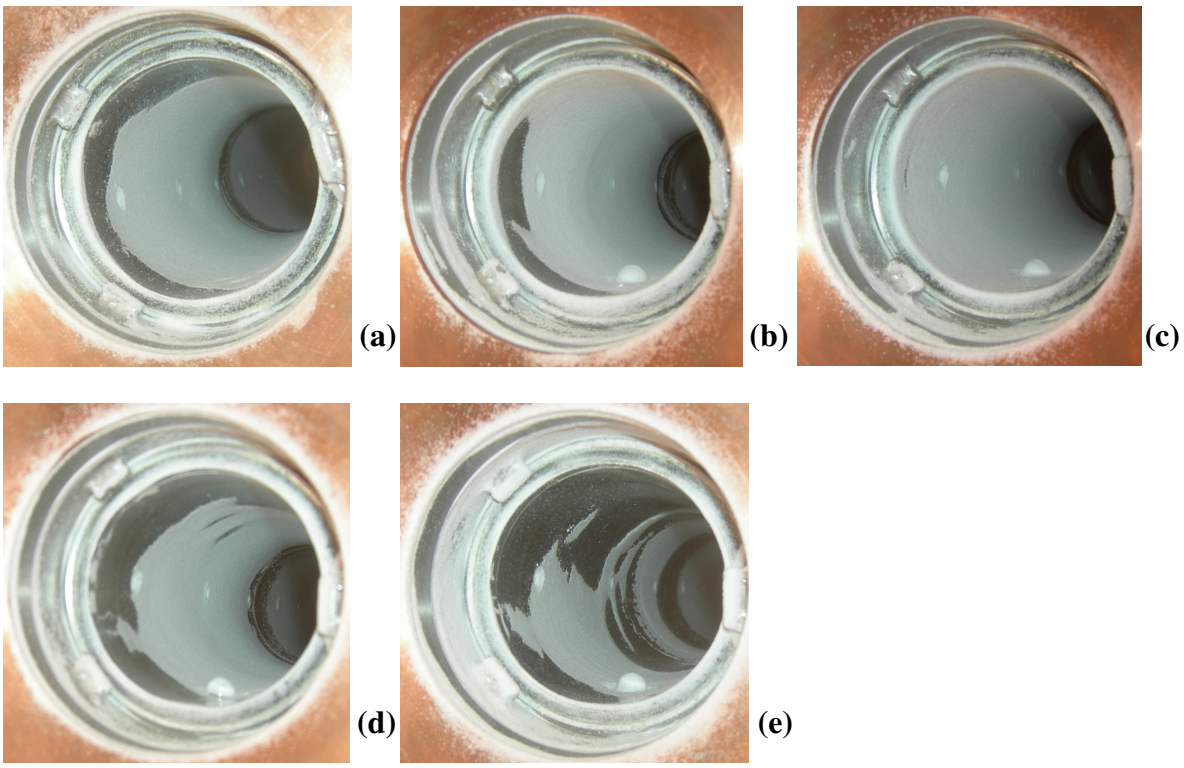

Figure 5-3: Images of particle layer on the column wall at 1.5 U_{mf} for different relative humidities: (a) 0%, (b) 20%, (c) 40%, (d) 60%, and (e) 80%.

Previous researchers have suggested that with the use of humid air a moisture film may develop on the fluidizing particles and/or the column wall (Harper, 1967; Németh et al., 2003). However, this phenomenon differs for different types of materials depending on their hydrophobicity. Polyethylene is not as susceptible to water as hydrophilic materials such as

glass (Forrest, 1935). On the other hand the column wall was composed of stainless steel which is hydrophilic but much less so than glass (Güleç et al., 2006), which may mean that higher humidities are required for this material so that a moisture film to form on its surface. This could explain as why in this work little or/no effect on particle layer development on the column wall was observed until 60 and 80% RH (Figure 5-3). At high relative humidities a film of water may have formed on the column wall increasing the system electrical conductivity and also reducing the contact between polyethylene particles and the stainless steel column wall, and thus slowing down the particle charge generation and adhesion to the wall.

5.1.1.4. Particle Size Distribution (PSD)

The particle size distributions in all regions of the bed for different relative humidities are presented in Figure 5-4 (see Appendix D for enlarged graphs and values for $D_{P\,0.1}$, $D_{P\,0.5}$, and $D_{P\,0.9}$). The initial particles had similar PSDs for all trials indicating that although an industrial resin with varying particle size was used all samples had approximately the same distribution allowing for comparison of results (Figure 5-4a). Different particle size ranges were found within the bed depending on the region (i.e., bulk, wall, bottom column, entrained fines, and top column); thus similarly sized particles were always migrating to specific areas of the bed. The initial and dropped particles were the largest with similar size ranges due to the dropped region comprising the majority of the bed particles. The wall region and those particles adhered to the bottom of the column had the next largest particle sizes. The wall region was composed of slightly larger particles than those closest and most tightly adhered to the column wall. Thus the smaller particles tend to adhere to the column wall first followed by slightly larger particles. Fines were the smallest particles and their size was dictated by the velocity of the fluidizing gas since the only particles that could be elutriated were those that had particles sizes resulting in a terminal velocity less than the gas superficial velocity.

It is important to note that both the wall and bottom column regions had the largest variations among their PSDs. This is likely due to a combination of how the particle layer

builds on the column wall and the sample collection process for the PSD analysis. It is unlikely that the particle layer builds uniformly on the column as fluidization progresses. This was clearly seen during fluidization time trials as certain areas of the wall were coated before other areas. It is also unlikely that the particles making up the wall layer would be of the same size in the same place with subsequent fluidization trials. Therefore, even though bottom column samples for PSD analysis were collected from the same location, when possible, it is expected that additional variation would be present. Also, while the wall sample is composed of particles that had adhered to the column wall, all collection goes into the same container resulting in particles from different areas of the wall (i.e. top, bottom, or middle) being mixed and leading to slight variations in PSDs. Additionally, as wall collection depends on overcoming the electrostatic forces holding the particles adhered to the column wall through vibration, the thickness of the particle layer following collection may differ from trial to trial affecting the PSD of both the wall and bottom column regions. This change in thickness could be due to the variation in local charges along the wall leading to stronger or weaker particle attraction, even though similar net wall charges-to-mass ratios were observed.

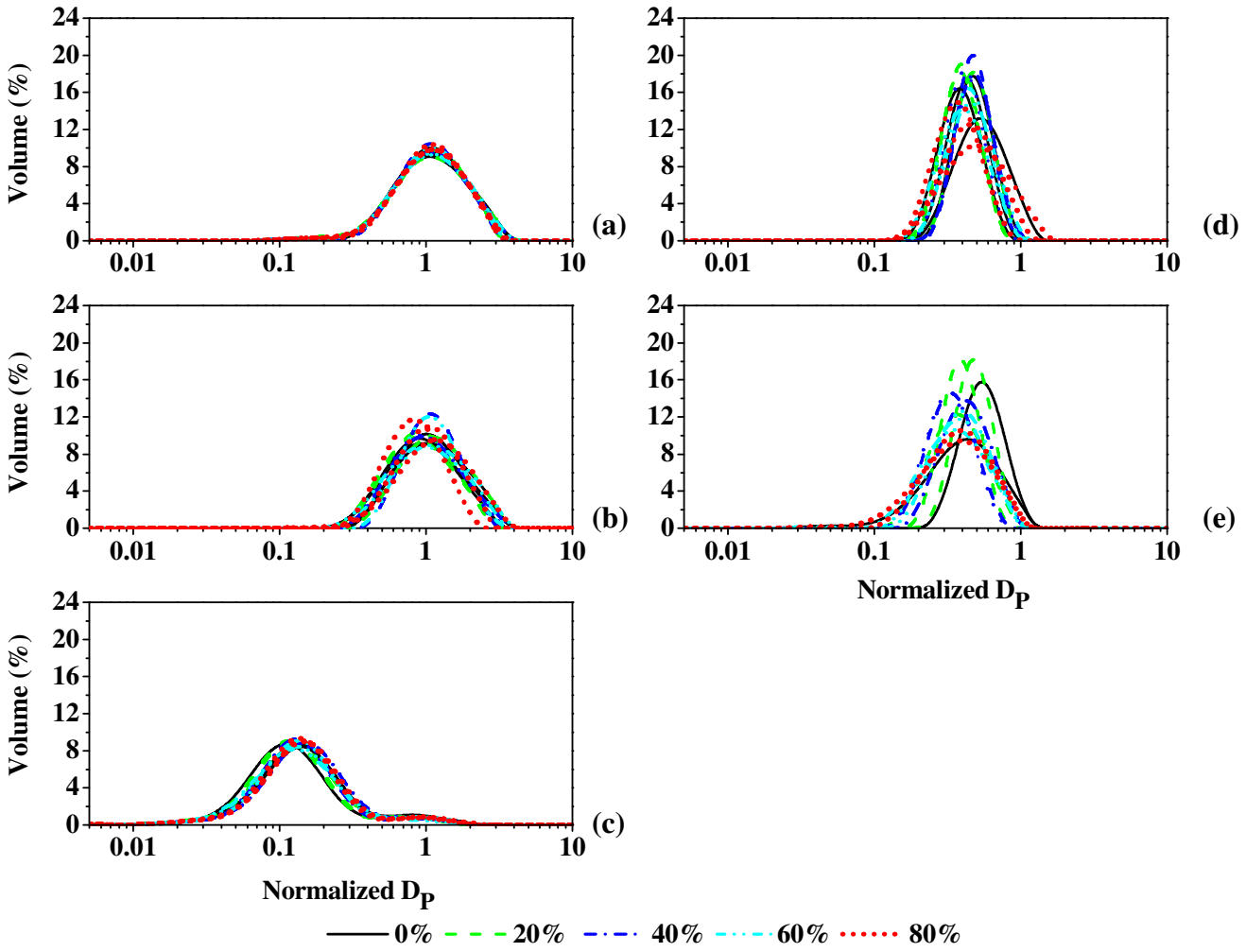

Figure 5-4: Normalized PSDs at 1.5 U_{mf} for different regions of the bed: (a) Initial, (b) Dropped, (c)Fines, (d) Wall, and (e) Bottom Column.

5.1.2. 1.75 U_{mf} Gas Velocity Results and Discussion

This section describes and discusses the results obtained for 1.75 U_{mf} gas velocity.

5.1.2.1. Mass Collected (m%)

Figure 5-5 presents the amount of particles collected in each region of the bed in terms of m%. Within the dropped region, there seemed to be a slight increase in m% from 0 to 40% relative humidity followed by slight decrease at 60%. The magnitude increased again at 80% relative humidity. This was mirrored in the m% of the wall with a decrease observed from 0 to 40% followed by an increase at 60%, and a decline at 80% relative humidity. Mirroring between the dropped and wall regions indicates that particles leaving the bulk were likely migrating to the wall region and vice versa. In the fines region, there was a slight increase in the amount of particles elutriated as the relative humidity increased with the exception of 60%. The exception could be related to the increase in m% in the wall region at 60% as finer particles may have become adhered to the column wall, to provide positive charges required for wall layer, instead of being elutriated.

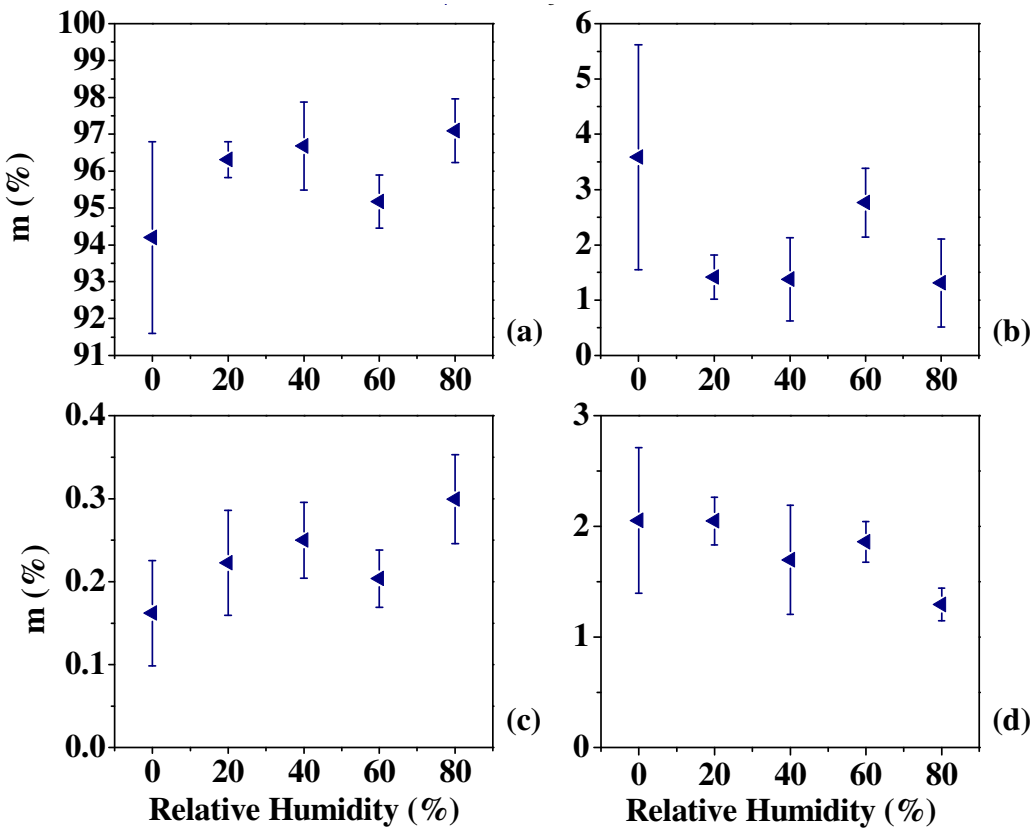

Figure 5-5: Mean m% at 1.75 U_{mf} for different relative humidities: (a) Dropped, (b) Wall, (c) Fines, and (d) Irretrievable.

5.1.2.2. Charge-to-Mass Ratio (q/m)

The mean net q/m results obtained for different gas relative humidities are shown in Figure 5-6. The initial net q/m differed slightly for all trials; however, the difference was minimal and the magnitude was much less than any net q/m obtained following fluidization. The dropped particles were closest to this value with a range of net q/m of approximately -0.3 to -0.9 μC/kg, followed by wall particles (-30 to -100 μC/kg), and the fine particles which had the largest magnitudes (30 to 140 μC/kg). The charge polarity of each region did not change with increasing gas relative humidity; that is, the fines remained predominately positively charged and the dropped and wall regions remained negatively charged.

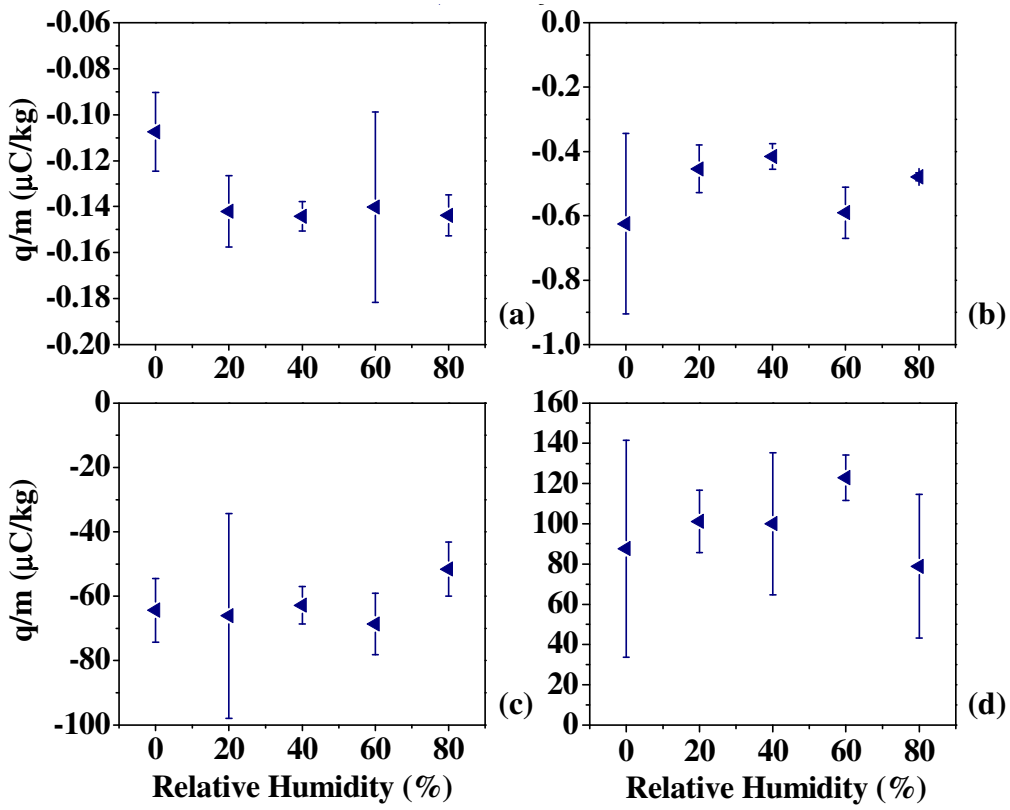

Figure 5-6: Mean net q/m at 1.75 U_{mf} for different relative humidities: (a) Initial, (b) Dropped, (c) Wall, and (d) Fines.

The dropped particles experienced a slight decrease in magnitude of net q/m from 0 to 20% RH after which the q/m remained unchanged, except with an increase at 60% RH. Since in this region the m% increased from 0 to 20% and then remained constant, with the exception of 60%, then the net q/m decrease indicates that the charge on the particles decreased slightly with an additional mass or remained the same. A net charge decrease could either be due to an increase in the amount of positively charged particles, or more likely a decrease in negatively charged particles. There was no obvious trend in the net q/m for the wall region with the exception of a slight decrease at 80% RH. However, the m% collected from the wall decreased with the addition of relative humidity from 0 to 20% and then remained steady. Thus, the charge must have also decreased at these relative humidities to maintain a constant net q/m. At 80% RH the charge must have decreased even more to produce a decline in q/m with almost equivalent values of m% to the midrange humidities. As for the fines, the net q/m did not change with increased relative humidity. However, since the mass

of collected fines slightly increased with relative humidity, their charge must have also elevated to keep the q/m ratio constant.

5.1.2.3. Wall Particle Layer

Images of the particle layer found on the column wall are presented in Figure 5-7. While the particle layer at 0% relative humidity looks extensive, there was a lot of variance in the particle layer between trials, as also seen in the m% collected in this region (Figure 5-5). Similar amounts of wall fouling were observed for the fluidizing gas at 20, 40, and 80% RH, with slightly more particles at 60%. It is interesting to note the shift in particle layer location from building up in the middle of the column for runs at 0% to 60% RH, to the bottom of the column at 80% RH.

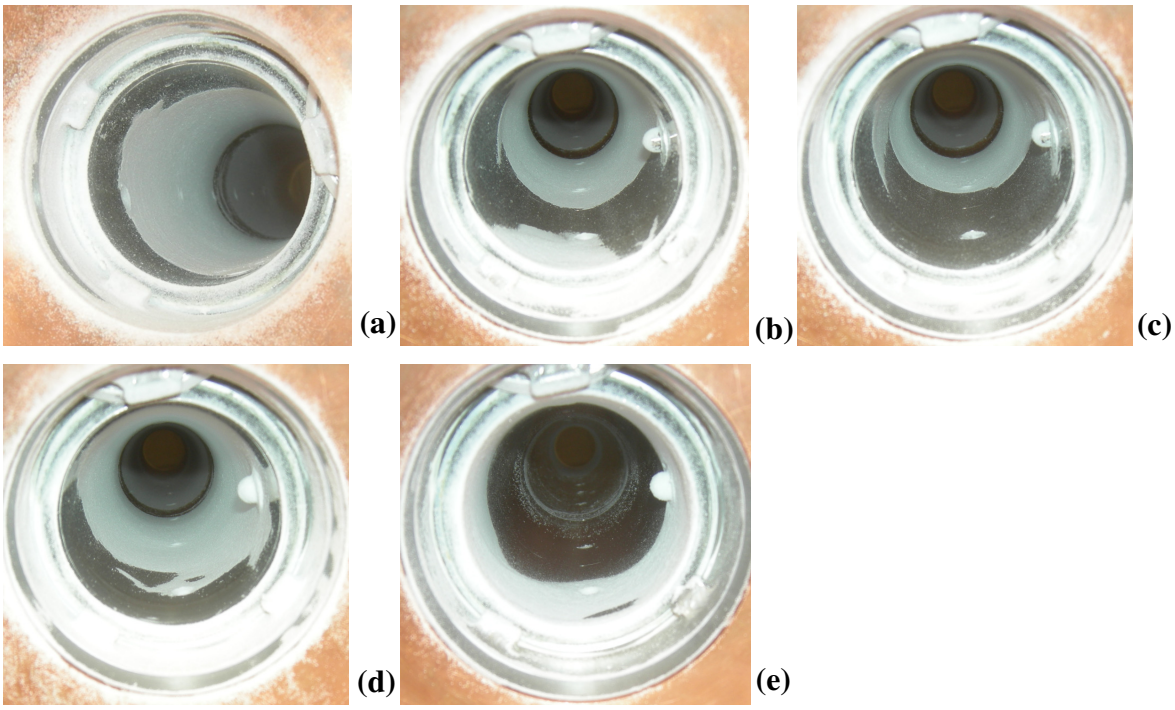

Figure 5-7: Images of particle layer on the inner column wall at 1.75 U_{mf} for different relative humidities: (a) 0%, (b) 20%, (c) 40%, (d) 60%, and (e) 80%.

A change in the location of the particle layer coating on the column wall took place at 80% RH at 1.75 U_{mf}. This could be due to the high moisture content passing through the bed at this relative humidity. According to Wolny and Kazmierczak (1989), at relative humidities

greater than 75% RH capillary forces within the bed can cause unstable fluidization. With unstable fluidization the patterns of flow within the bed could change slightly, but not enough to defluidize the bed or cause sluggish behaviour signified by changes in pressure drop. This could lead to charged particles being more likely to interact with the column wall at the bottom of the column as opposed to the middle of the column.

5.1.2.4. Particle Size Distribution (PSD)

Figure 5-8 shows the results of the normalized PSDs obtained at different gas relative humidities. Enlarged figures and values for $D_{P\ 0.1}$, $D_{P\ 0.5}$, and $D_{P\ 0.9}$ are presented in Appendix D. The initial particles had similar PSDs for all experiments; therefore, even though the industrial resin had a wide distribution the trials can be compared. None of the regions within the bed showed any trend with the change in relative humidity. The regions with the largest particles were the initial and the dropped regions, which comprised of the majority of the particles within the bed. The next largest particles were in the wall and bottom column regions. The wall and bottom column had similar particle sizes although slightly smaller particles were present closer to the wall, in the bottom column region. This indicated that the relatively smaller particles adhered to the column wall first, followed by slightly larger particles as the layer grew outward from the wall (refer to Table 5-3 for mean D_P values). These two regions also had the most variation in PSDs. This was because the particles adhered to the column wall likely alternated in polarity. As seen previously, the smaller particles were predominantly positive and larger particles were predominantly negative. Thus, with alternating particles of different sizes, it was expected to obtain a range of PSDs. However, it is important to note that the variation was still within a small range and showed no trend with relative humidity. The smallest particles were found in the fines region; their particle size was dependent on the velocity of the fluidization gas.

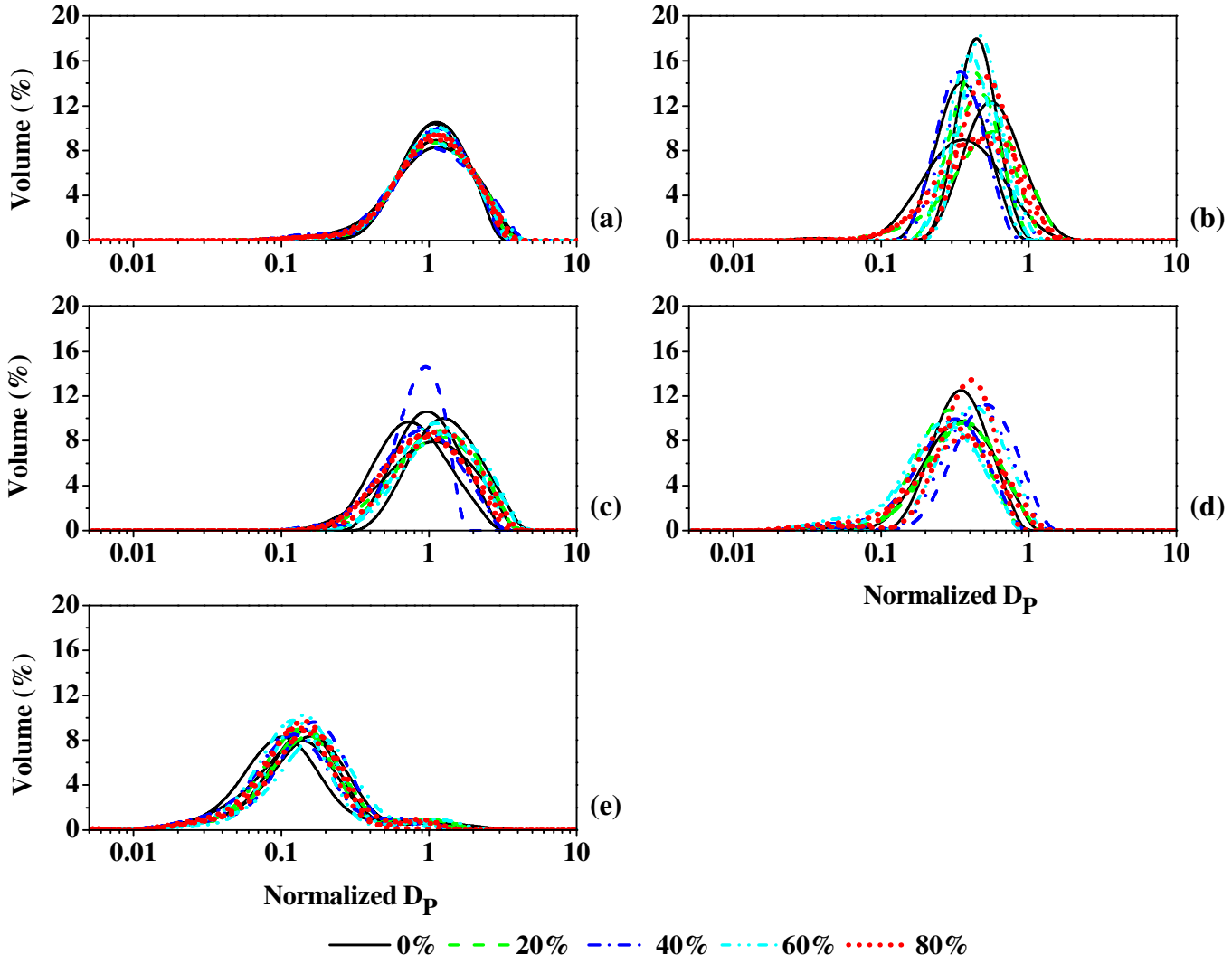

Figure 5-8: Normalized PSDs at 1.75 U_{mf} for different regions of the bed: (a) Initial, (b) Dropped, (c) Wall, (d) Fines, and (e) Bottom Column.

5.1.3. Bubbling Flow Regime Comparison

This section compares results obtained at both 1.5 and 1.75 U_{mf} gas velocities.

5.1.3.1. Mass Collected (m%)

The particles mass collected in the dropped and wall regions were similar for both velocities tested for the higher relative humidities of 60% and 80%, as well as the 0% RH (Figure 5-9a, Figure 5-9b). At the midrange humidities of 20 and 40%, at the higher gas velocity of 1.75 U_{mf}, fewer particles were collected in the dropped region while more particles were collected in wall region. This indicated that the effect of relative humidity may have occurred at lower RH values in the higher gas velocity compared to when the effect of relative humidity took effect in the lower gas velocity. This could be due to the mass flow rate of water vapour into the bed as at higher velocity more water vapour would be introduced over the same fluidization time.

In the fines region, more particles were collected at 1.75 U_{mf} (Figure 5-9c). This is due to the increased gas velocity allowing larger particles to be elutriated from the bed. Additionally, a trend of slightly increased m% of fines with increased relative humidity was observed at 1.75 U_{mf} while no obvious trend was seen at 1.5 U_{mf}. This indicates that a higher gas velocity in the bubbling flow regime could result in some agglomerates within the bulk due to electrostatic charging, which being broken up by increasing relative humidity. This result corresponds to that found by Baron et al. (1987) who found that the entrainment flux increased with increasing relative humidity. The difference between gas velocities could, again, be due to the increase in mass flow rate of water.

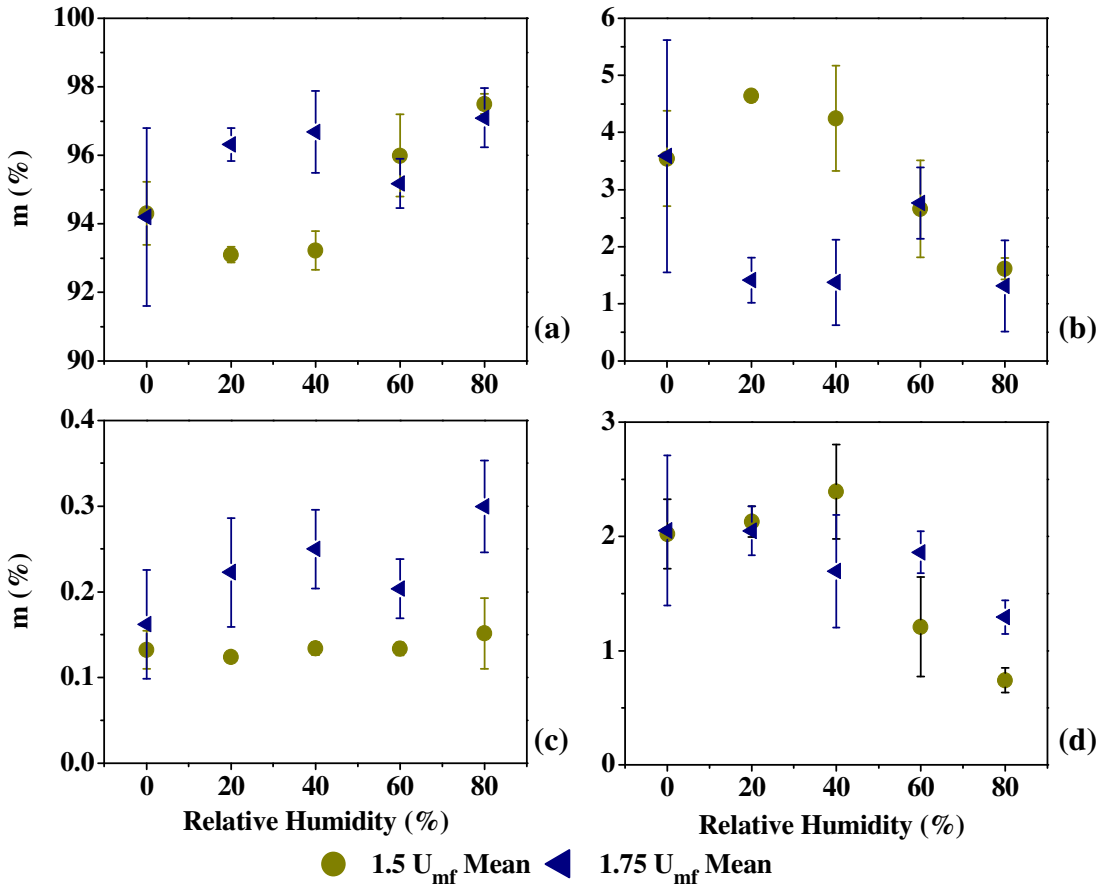

Figure 5-9: Comparison of m% for two velocities in bubbling flow regime: (a) Dropped, (b) Wall, (c) Fines, and (d) Irretrievable.

5.1.3.2. Charge-to-Mass Ratio (q/m)

The initial particles net q/m were similar for all relative humidities for both fluidization gas velocities except at 80% RH where differences were observed. As both of these values were in a similar range to the other RH initial net q/m values and the magnitude in the initial region is less than in the other regions the results for both velocities should still be comparable.

The net q/m for 1.5 and 1.75 U_{mf} was similar for all regions in both trend and magnitude; with the exception of the dropped region for the 20 and 40% RH (Figure 5-10). The difference in these points correlated with a difference in mass collected; however the increased mass for 1.75 U_{mf} at 20% and 40% RH resulted in a decreased net q/m when

compared to the decreased m% collected at 1.5 U_{mf} that resulted in an increased net q/m. Therefore, it is likely that the difference in the net q/m was related to changes in m% and not in charge.

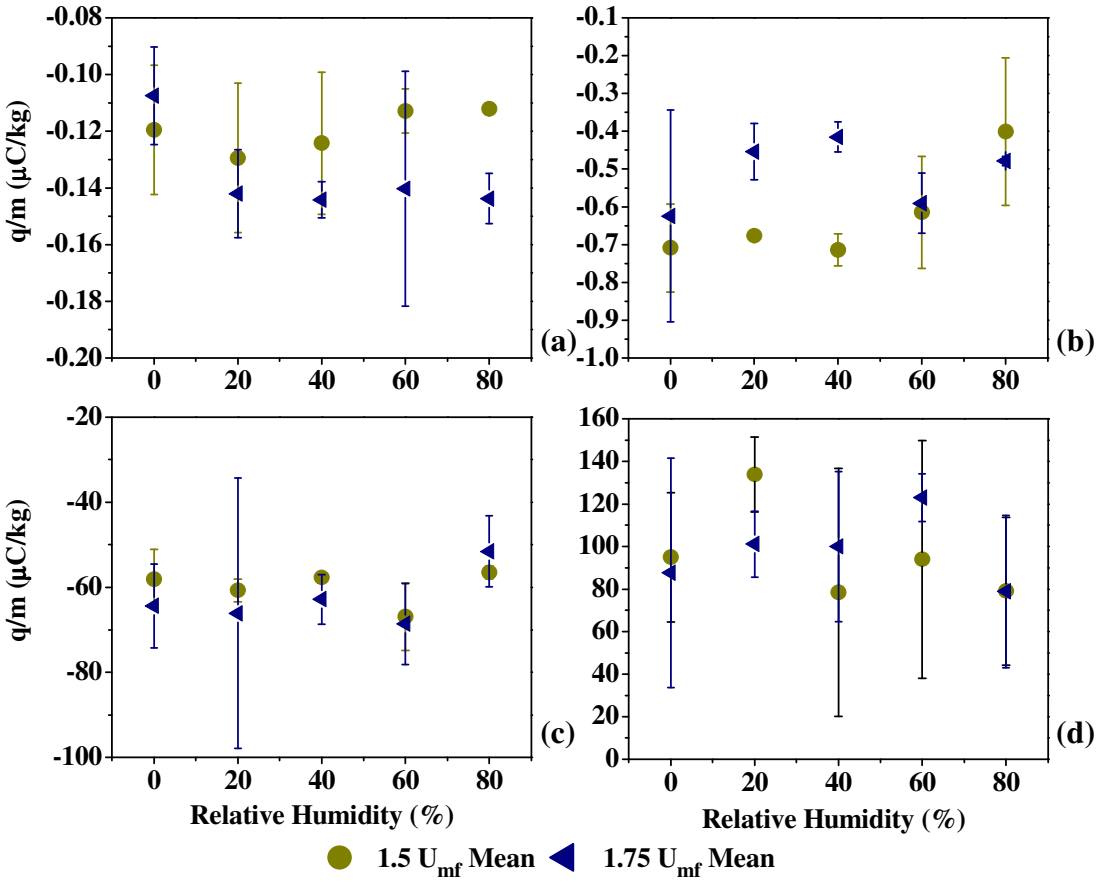

Figure 5-10: Comparison of mean net q/m for two velocities in bubbling flow regime: (a) Initial, (b) Dropped, (c) Wall, and (d) Fines.

5.1.3.3. Particle Size Distribution (PSD)

Similar particle sizes were found for both fluidization gas velocities in all regions for all relative humidities (Figure 5-11). This indicates that the relative humidity did not influence the size range of particles that migrated to each region of the bed in either gas velocity.

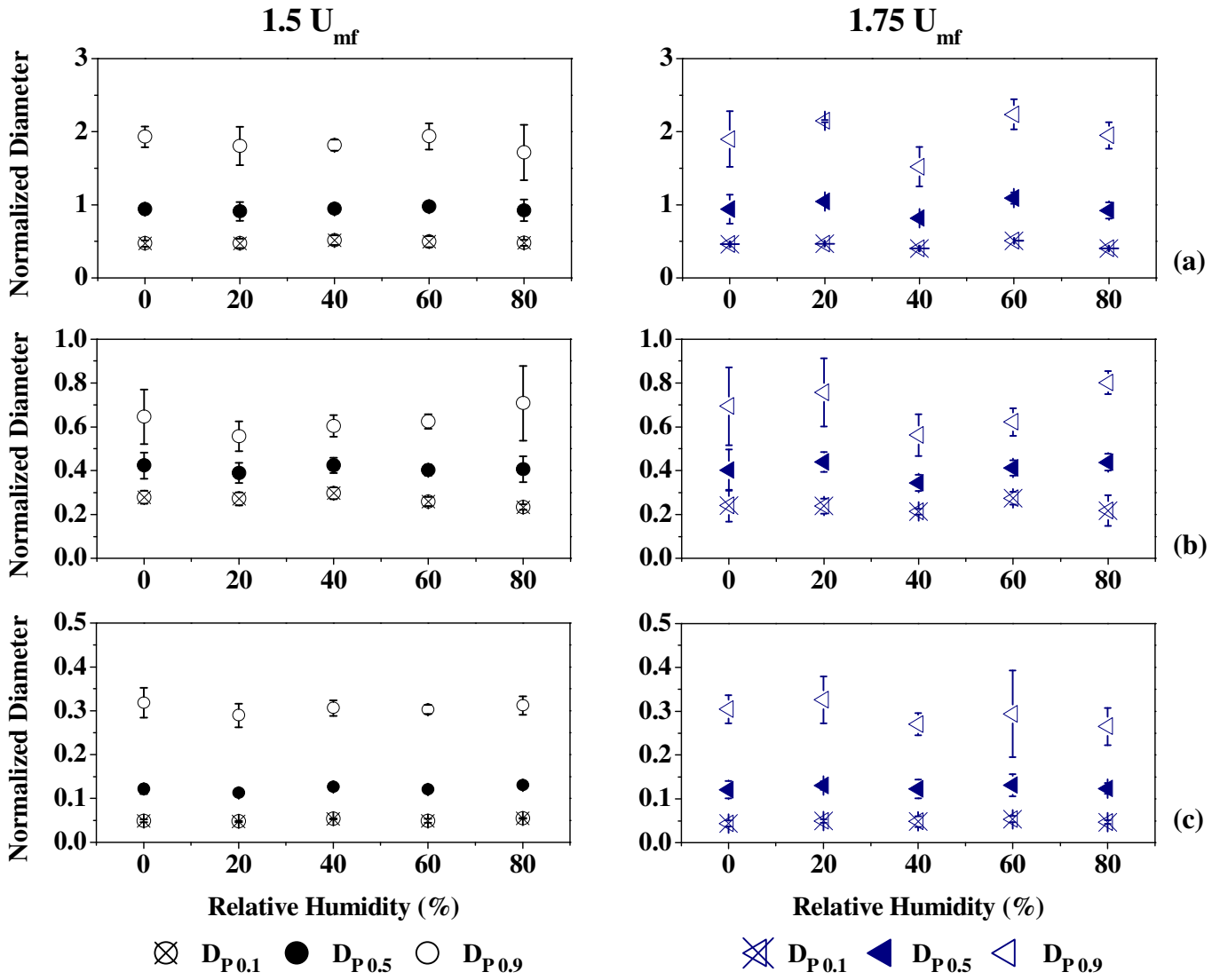

Figure 5-11: Comparison of normalized PSDs for two velocities in bubbling flow regime: (a) Dropped, (b) Wall, and (c) Fines.

5.1.4. Bubbling Flow Summary

Column wall fouling was observed for both velocities, with the 1.5 U_{mf} resulting in a higher magnitude of particle layer coverage. At this velocity, gas relative humidity certainly influenced the particle layer coverage and thickness with a maximum obtained at 40% RH. Increasing relative humidity to 60 and 80% then reduced the fouling significantly. This was mimicked by an increase in charge up to 40% and then a decrease in charge. The change in bed electrification was also observed by Ciborowski and Wlodarski (1962). Although different particles and column materials were used, it could be that these material differences resulted in a different relative humidity turning point. At the higher gas velocity, no apparent variation in the amount of fouling was detected with changing the relative humidity.

5.2. Slugging Flow Regime

In the slugging flow regime, two gas velocities were tested: 3.5 and 4 U_{mf} at five different relative humidities: 0, 20, 40, 60, and 80%. Results are presented for mass collected (m%), charge-to-mass ratio (q/m), particle wall layer and particle size distribution (PSD).

5.2.1. 3.5 U_{mf} Gas Velocity Results and Discussions

The results for the experiments with 3.5 U_{mf} are presented in this section, as well as the associated discussion.

5.2.1.1. Mass Collected (m%)

Figure 5-12 presents the m% results obtained at different gas relative humidities. The dropped particles m% demonstrated no obvious trend with an increase in relative humidity, although there was slight decrease at 60% RH. The wall particles experienced a slight decrease in m% collected from 0 to 20% RH and then remained fairly constant with the

exception of 60% RH where a slight increase was observed, to a level similar to 0% RH. In comparison, results in the dropped and wall regions behaved oppositely with respect to relative humidity. This is an indication of the migration of the particles between these two regions. The fine particles experienced an increase in collection of m% from 0 to 20% RH and then remained at a constant level for all further relative humidities. This indicates that some of the fines that had been attached to the larger particles or the column wall due to the electrostatic charges may have been broken up due to the presence of moisture by increasing the gas relative humidity. However, results show that the amount of separation was not dependent on the moisture content. The amount of mass lost was similar for all trials.

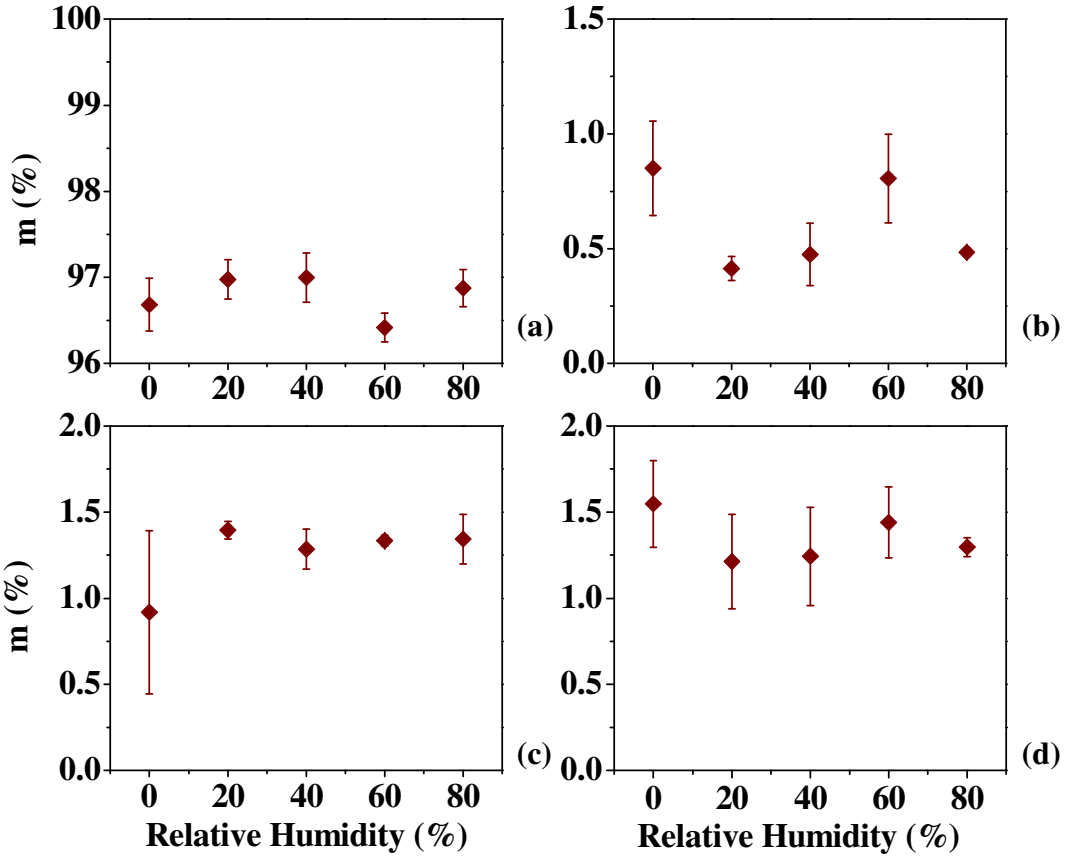

Figure 5-12: Mean m% at 3.5 U_{mf} for different relative humidities: (a) Dropped, (b) Wall, (c) Fines, and (d) Irretrievable.

5.2.1.2. Charge-to-Mass Ratio (q/m)

As seen in Figure 5-13a, the initial net q/m was similar for all experimental trials. The magnitude of the net q/m of the initial particles was the lowest, followed by the dropped particles (-0.3 to -0.6 μC/kg), the fines (5 to 35 μC/kg) and the wall particles (-10 to -60 μC/kg). The polarity of each region was not affected by relative humidity; fine particles were positively charged while dropped and wall particles were negatively charged for all relative humidities.

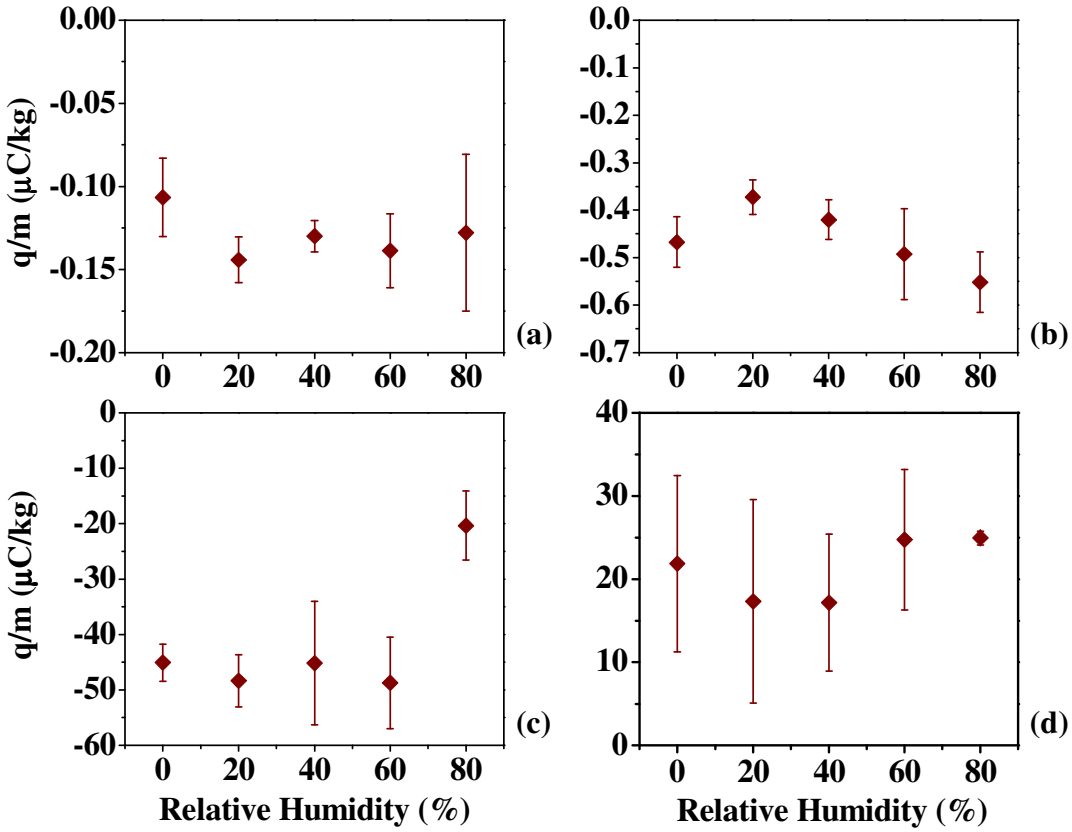

Figure 5-13: Mean net q/m at 3.5 U_{mf} for different relative humidities: (a) Initial, (b) Dropped, (c) Wall, and (d) Fines.

The dropped particles experienced a decrease in net q/m magnitude from 0 to 20% RH and then followed a trend of increasing in magnitude, which resulted in a net q/m at 80% RH that was larger than that at 0% RH (Figure 5-13b). The mass of the dropped particles did not show a trend, except for a fall at 60% RH indicating that initially the charge decreased by 20% RH and then increased as relative humidity increased. At 60% the drop in m% would

account for the larger error bars observed for these trials as a different mass could impact the net q/m recorded.

The wall particles had a relatively constant net q/m from 0 to 60% RH and then decreased sharply in magnitude at 80% RH (Figure 5-13c). Since the mass collected in this region was not much affected by the relative humidity, then particles charge must not have changed to result in a constant q/m for these trials. The amount of net q/m of wall particles decreased at 80% RH, which also indicated that particles charge had must have also decreased at this relative humidity. This could be due to the higher quantity of moisture present in the bed at this condition. As mentioned previously, stainless steel is hydrophilic while polyethylene is hydrophobic; thus it is more likely that a water film may have developed on the surface of the column as opposed to developing on the particles. This water film may promote charge dissipation along the column wall. This may have not been present at lower relative humidities as this was the amount of moisture necessary to provide an amount of dissipation that has become dominant over charge generation.

The net q/m of the fine particles was not impacted by relative humidity as no trend was observed (Figure 5-13d). However, as the m% increased slightly from 0 to 20% RH and then remained constant, the charge must have also increased somewhat between 0 to 20% to maintain a constant net q/m.

5.2.1.3. Wall Particle Layer

Typical examples of the layer of particles adhered to the column wall during fluidization are presented in Figure 5-14. Similar quantities of wall fouling were detected for 0 and 60% RH. At 20, 40, and 80% relative humidities, similar amounts of particles were also found along the wall; however, less particles were observed at these humidities. These results mimic the m% collected from the wall (Figure 5-12)

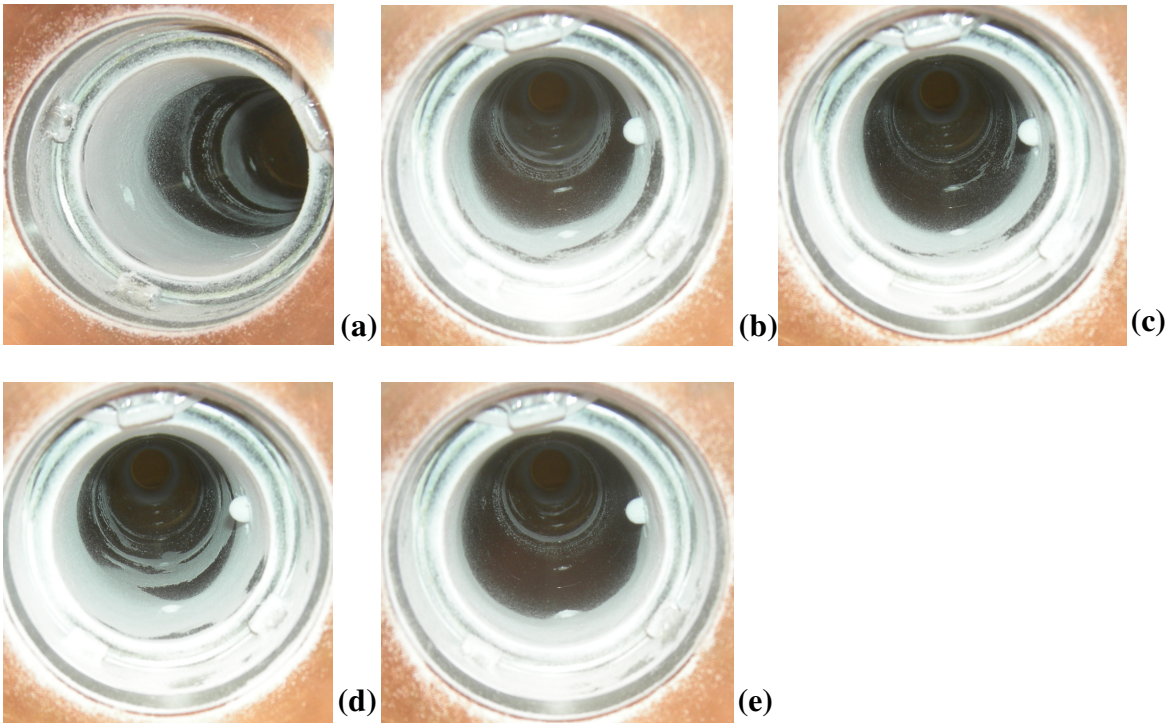

Figure 5-14: Images taken from the particle layer on the column wall at 3.5 U_{mf} for different relative humidities: (a) 0%, (b) 20%, (c) 40%, (d) 60%, and (e) 80%.

5.2.1.4. Particle Size Distribution (PSD)

The normalized particle size distributions were not effected by relative humidity as seen in Figure 5-15 (see Appendix D for more detailed graphs and values for $D_{P\ 0.1}$, $D_{P\ 0.5}$, and $D_{P\ 0.9}$). There was some variation in all trials in most of the regions; this is likely due to the industrial resin having a wide size distribution. The largest particles were found in the initial and dropped regions, as expected as this region was composed of the majority of particles within the bed. The next largest particles were those found adhered to the column wall, in the wall and bottom column regions. There were slightly smaller particles present in the bottom column regions indicating that particles that adhered to the column wall first were slightly smaller than those adhering later (see Table 5-3). The fines and the top column were the smallest particles in the bed. The top column had slightly larger particles than the fines region. This could be due to two reasons: (1) the particles in these areas were able to be entrained from the bed but were too large to be expelled from the column, or the more likely

reason: (2) these particles were slightly larger and were thus more likely to have a slightly negative charge, as it was seen that smaller particles were predominately positively charged, therefore they were adhered to the likely positively charged column.

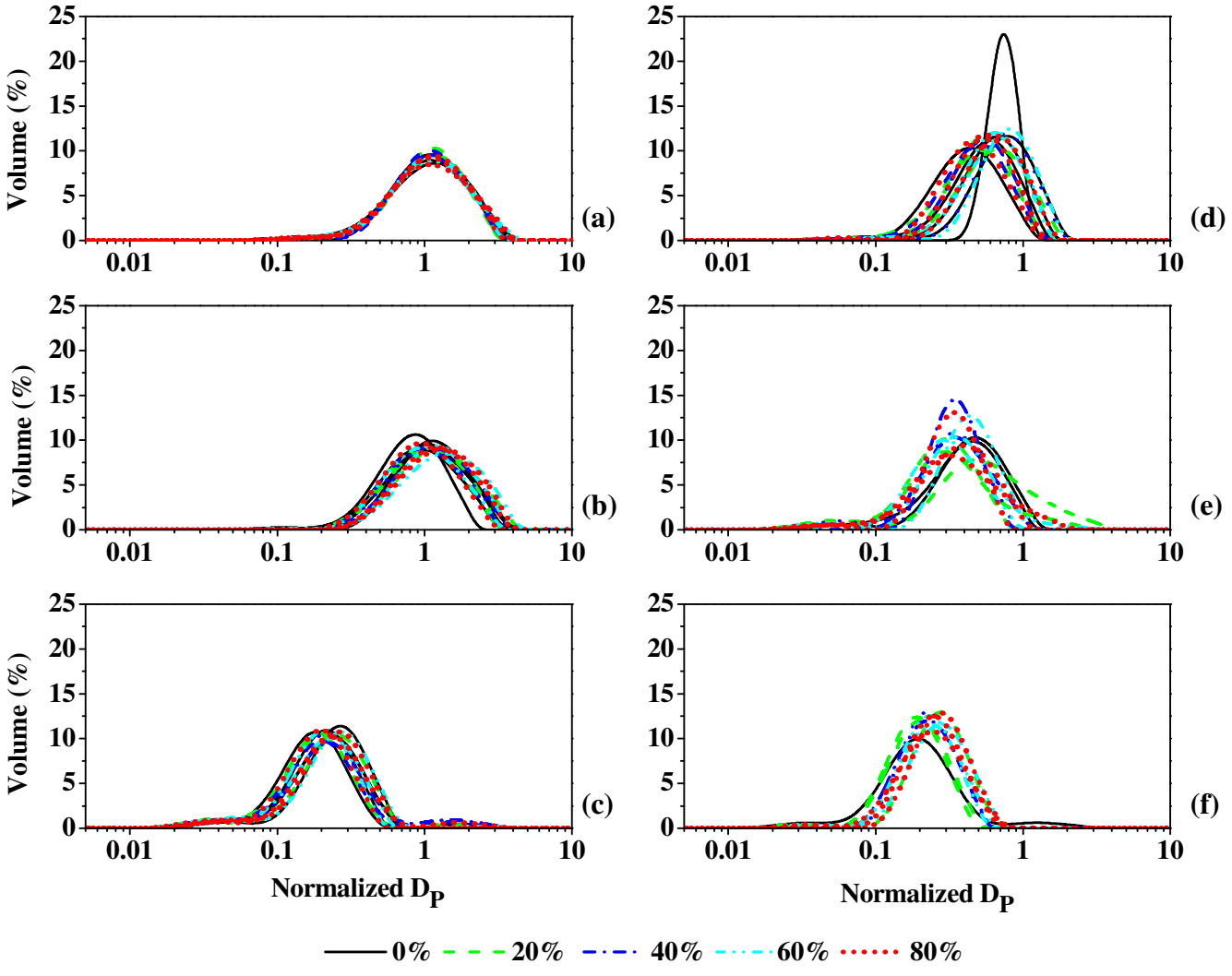

Figure 5-15: Normalized PSDs at 3.5 U_{mf} for different regions of the bed: (a) Initial, (b) Dropped, (c)Fine, (d)Wall, (e) Bottom Column, and (f) Top Column.

5.2.2. 4 U_{mf} Gas Velocity Results and Discussion

The results for the experiments with 4 U_{mf} are presented in this section, as well as the associated discussion.

5.2.2.1. Mass Collected (m%)

As can be seen in Figure 5-16, the m% collected did not seem to be significantly impacted by relative humidity in any region of the bed as no obvious trends with relative humidity were observed. The fines experienced slight increases in m% collected at 20 and 80% RH. Similar amounts of particles were lost from sampling for all trials.

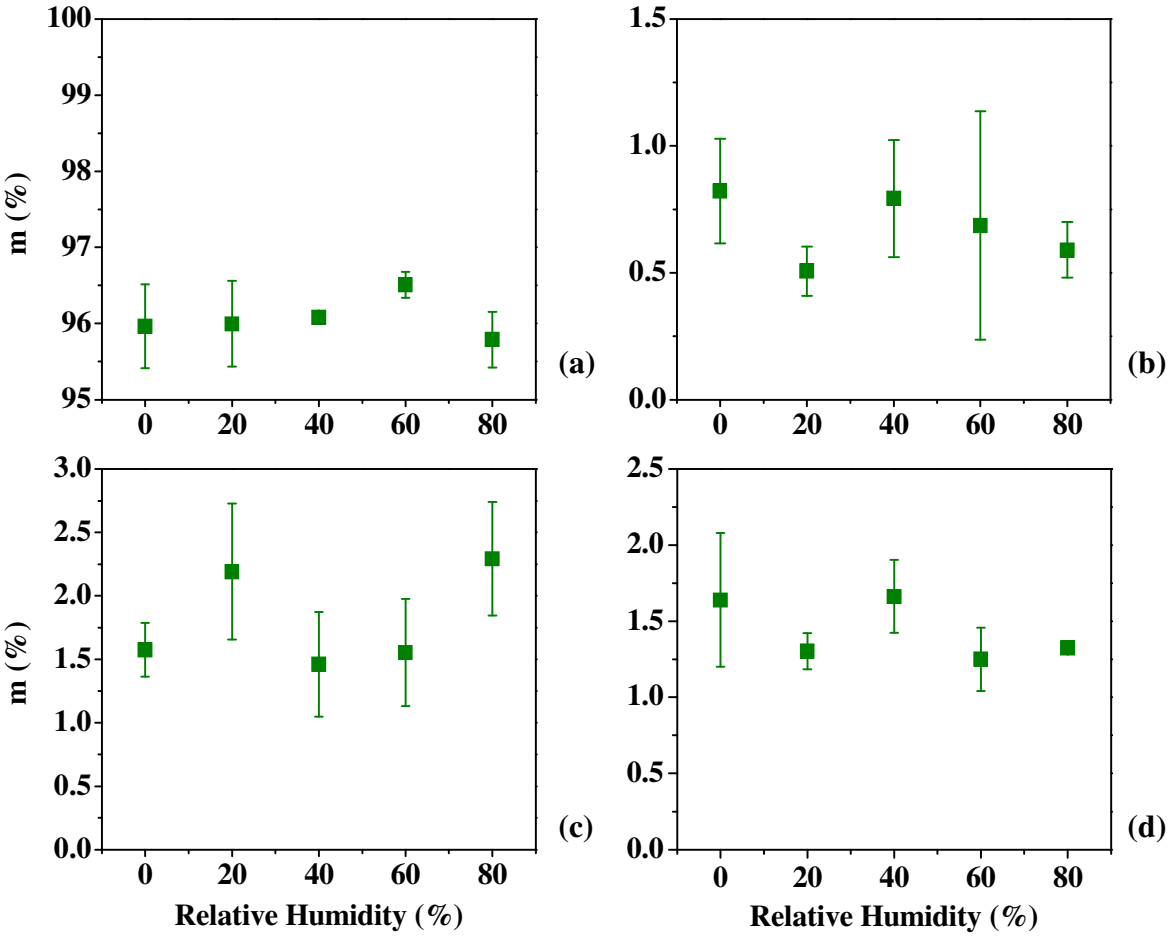

Figure 5-16: Mean m% at 4 U_{mf} for different relative humidities: (a) Dropped, (b) Wall, (c) Fines), and (d) Irretrievable.

5.2.2.2. Charge-to-Mass ratio (q/m)

The particles in each region of the bed had different magnitudes of particle charge generation as can be seen in Figure 5-17. The initial particles had the lowest magnitude net q/m (-0.7 to -0.17 μC/kg), followed by the dropped (-0.4 to -0.6 μC/kg), fines (5 to 55 μC/kg), and finally the wall particles (-10 to -70 μC/kg). The polarity of most of the regions of the bed was negative with the exception of the fine particles which were positively charged. The polarity of each region of the bed was not influenced by relative humidity.

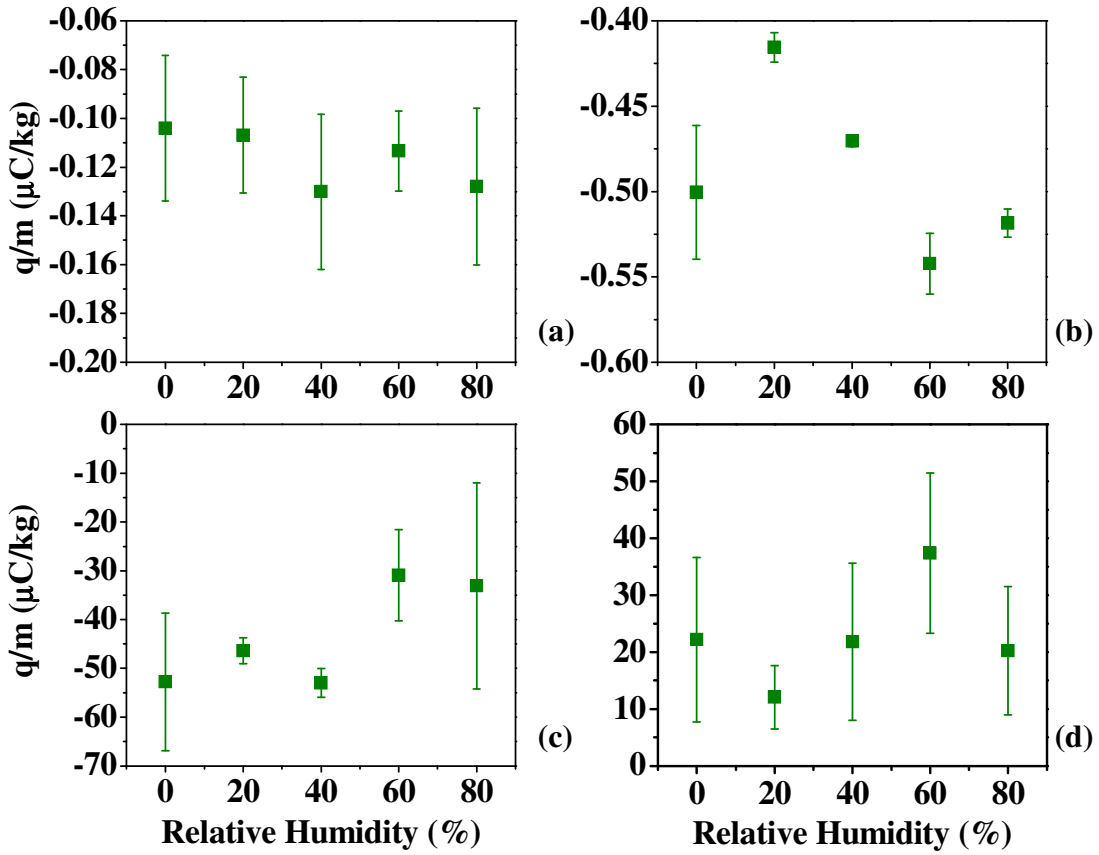

Figure 5-17: Mean q/m at 4 U_{mf} for different relative humidities: (a) Initial, (b) Dropped, (c) Wall, and (d) Fines.

The initial particles had similar net q/m values allowing for comparison for all trials. The dropped particles experienced a slight decrease in net q/m from 0 to 20% and then increased until 60% RH. After which it decreased slightly at 80% to be in the same range as 0% RH. With similar m% collected in all RH trials the charge must have been changing to create different values of net q/m. The net q/m of the wall particles stayed relatively constant from

0 to 40% RH. However, it decreased in magnitude when relative humidity reached 60% and higher. Knowing that the mass of particles collected remained relatively constant, then the particles charge must have declined to result in a lower net q/m at the high gas velocities. Considering the error bars on the net q/m values of the fines, the experimental values did not seem to differ with relative humidity. However, when looking at only the mean values there seemed to be a trend of increasing magnitude between 20 and 60% RH while 0, 40 and 80% RH had similar values.

The net q/m of the wall particles decreased at humidifies higher than 60% indicating that the charge on particles decreased since the mass stayed relatively constant. The effect of high relative humidity, as mentioned previously, is due to the formation of a water film on the inner column wall resulting in less number of contacts between the particles and the stainless column wall, in addition to help in dissipation of charge.

5.2.2.3. Wall Particle Layer

Following the collection of the bulk particles, pictures were taken of the inside of the column to evaluate the particle layer that had built-up along the wall (Figure 5-18). Similar particle layer coverage on the wall can be observed for all relative humidities, with slightly fewer particles found for the 20% RH trial; this correlates with the m% collected as this humidity showed a bit of fluctuation in m% in the wall region. Thus, the layer of particles adhered to the column wall at 4 U_{mf} did not seem to be affected by the gas relative humidity. In slugging flow regime and at such high gas velocity, the gas and particles movement inside the bed are limited to just the large slugs moving up and down the column. Thus, the fluidizing gas would have less chance of contacting the column wall and forming a film of water that would help in less charge generation or more charge dissipation.

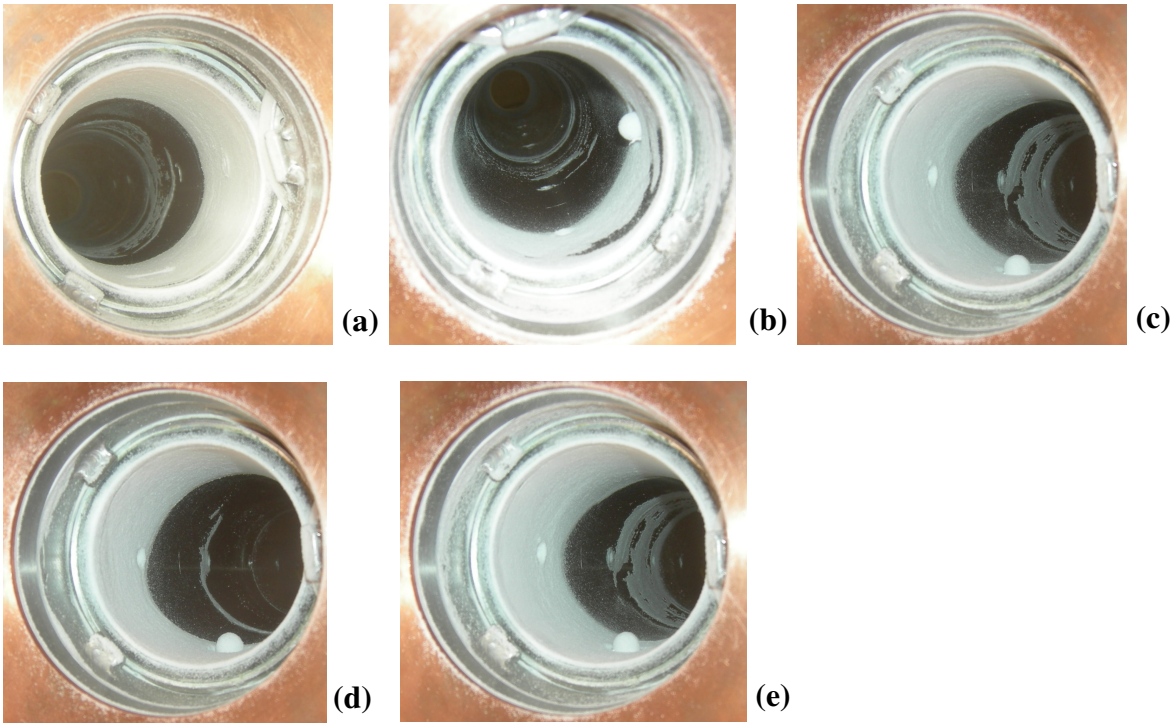

Figure 5-18: Images of particle layer on the column wall at 4 U_{mf} for different relative humidities: (a) 0%, (b) 20%, (c) 40%, (d) 60%, and (e) 80%.

5.2.2.4. Particle Size Distribution (PSD)

Particle size distributions were preformed for all regions of the bed for all relative humidities (Figure 5-19). None of the regions of the bed demonstrated a trend with relative humidity; however all regions experienced some variation in their PSDs. This is likely due to different factors including: initial location of particles, makeup of industrial resin, and sampling.

The initial particles had similar PSDs indicating that although an industrial resin with variable particle sizes had been used, the samples were similar enough to be compared. The largest particles were found in the initial and dropped regions of the bed. These regions had the majority of particles in the bed. The next largest particles were found in the wall and bottom column regions. The wall region had slightly larger particles than those found along the bottom of the column which demonstrated that smaller particles adhered to the column wall first and then got slightly larger further away from the column wall. The fines and top column regions had the smallest particles. In these regions, particles are those with

diameters small enough to have a terminal velocity smaller than the fluidization gas velocity. Slightly smaller particles were found in the fines region. This could be due to slightly larger particles being more likely to have negative charges allowing them to adhere to the positively charged column wall, or were not quite small enough to be elutriated from the bed.

Close inspection of the wall region PSDs shows that at 80% RH the PSD seems to be slightly smaller than that for the 0% RH trials. This can also be seen more clearly in Appendix D by looking at the mean values of $D_{P\ 0.1}$, $D_{P\ 0.5}$, $D_{P\ 0.9}$, and enlarged PSD graphs. However, comparison of the standard deviation shows that the results overlap.

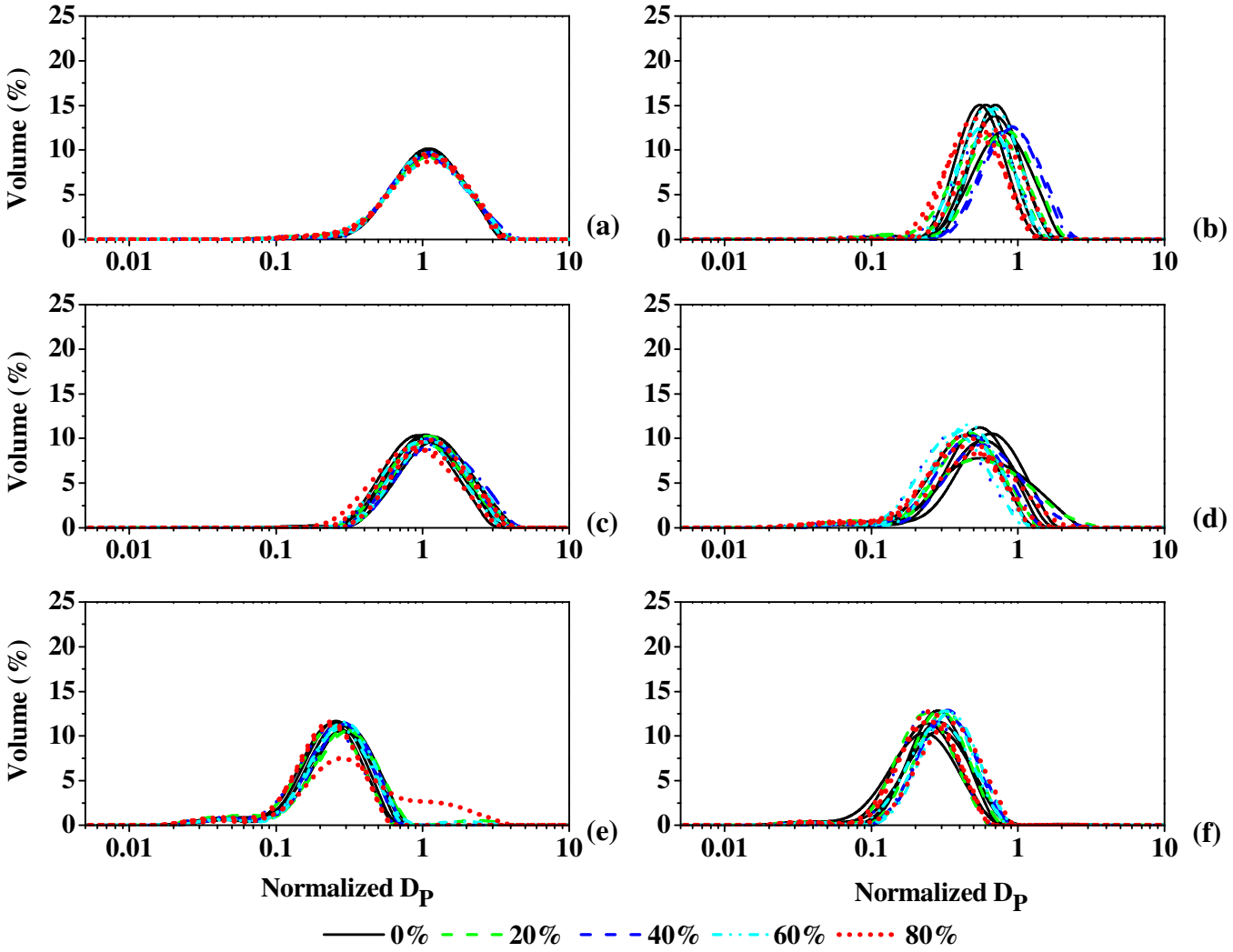

Figure 5-19: Normalized PSDs at 4 U_{mf} for different regions of the bed: (a) Initial, (b) Dropped, (c) Wall, (d) Fines, (e) Bottom Column, and (f) Top Column.

5.2.3. Slugging Flow Regime Comparison

This section compares the results of the 3.5 and 4 U_{mf} gas velocities in the slugging flow regimes. A discussion of the similarities and differences is presented in the following section.

5.2.3.1. Mass Collected (m%)

As seen in Figure 5-20, a larger quantity of mass was collected at the lower gas velocity in the dropped region for all relative humidities with the exception of 60%, where the two gas velocities gave equivalent results; thus, these particles must be migrating to other regions of the bed (i.e., wall or fines). For the cases of 0, 20, and 80% RH, it seems likely that the difference in mass between the two velocities is found in the fines region. The increased number of particles able to be elutriated at the higher velocity results in decreased mass in the dropped region. However, 40 and 60% RH were found to have similar amounts of fines collected for each velocity. The difference in the m% at 40% RH in the dropped region was then likely found in the wall region as additional particles were collected from the wall at this relative humidity at the higher gas velocity. All other relative humidities showed similar quantities of particles collected from the wall suggesting that relative humidity had little influence on the amount of particles adhered to the column wall.

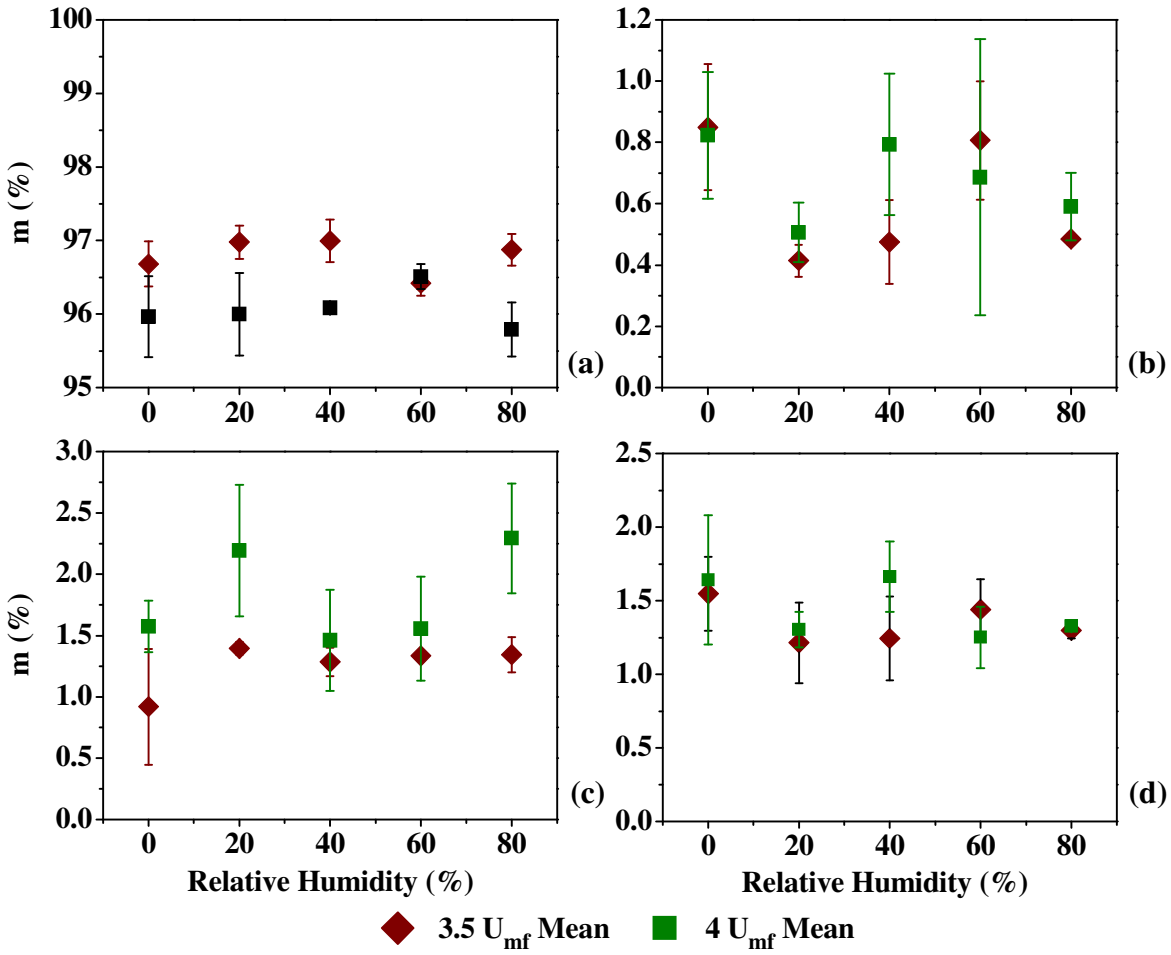

Figure 5-20: Comparison of m% for two velocities in slugging flow regime: (a) Dropped, (b) Wall, (c) Fines, and (d) Irretrievable.

5.2.3.2. Charge-to-Mass Ratio (q/m)

Similar initial net q/m values were recorded for all relative humidities for both velocities allowing for comparison (Figure 5-21). The net q/m in the dropped region resulted in similar trends with relative humidity; a slight decrease in magnitude from 0 to 20% RH and then an increase in magnitude with increasing relative humidities. 80% RH slightly deviates from this trend for 4 U_{mf} with a somewhat lower magnitude, similar to the value of 0% RH. However, this slightly higher value was within the standard deviation of the value obtained at 3.5 U_{mf} so it was difficult to determine whether the increasing magnitude was the trend for both gas velocities or if both velocities had a net q/m that leveled off at 80% RH.

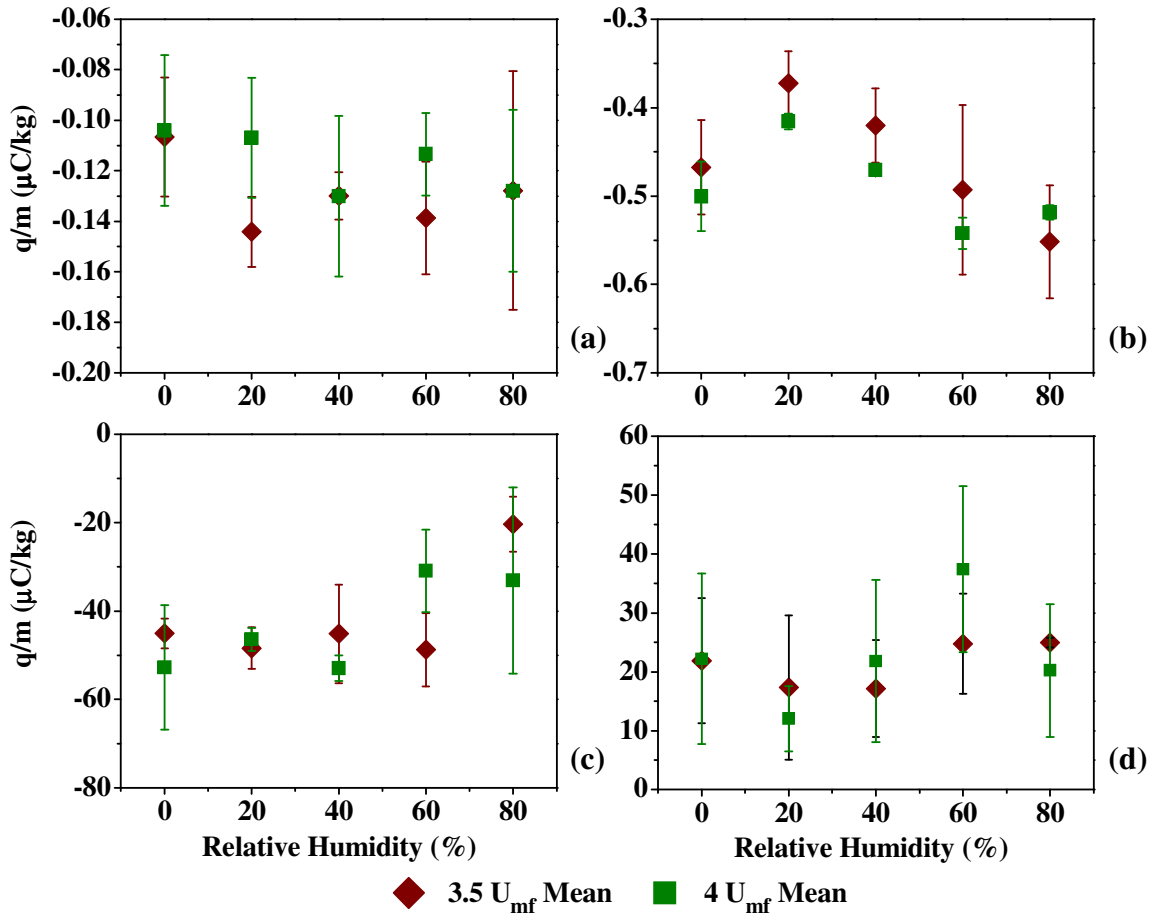

Figure 5-21: Comparison of net q/m for two velocities in the slugging flow regime: (a) Initial, (b) Dropped, (c) Wall, and (d) Fines.

In the wall region, for both velocities, the net q/m decreased with high relative humidities; 3.5 U_{mf} decreased at 80% RH while 4 U_{mf} started to decrease at 60% RH. Since the m% did not change in this region with relative humidity, then it is possible that at high relative humidities in the slugging flow regime less charge is generated on particles that adhere to the column wall. This could be due to the hydrodynamics of the slugging regime. It is likely that due to particles motion in the slugging flow regime, the majority of charging takes place during particle-wall contacting. If a water film developed on the column wall, it would promote charge dissipation on particles through reduction of surface conductivity. In the fines region relative humidity did not seem to affect net q/m for either gas velocity.

5.2.3.3. Particle Size Distribution (PSD)

Similarly sized particles were found in the dropped region for both gas velocities at the different relative humidities tested and no obvious trend with RH was observed for either gas velocity (Figure 5-22). Slightly larger particles were found in the wall region for 4 U_{mf}; however no trend with relative humidity was obtained. Slightly larger particles were elutriated from the bed at 4 U_{mf} in the fines region. This was expected as at a higher fluidizing gas velocity larger particles are entrained.

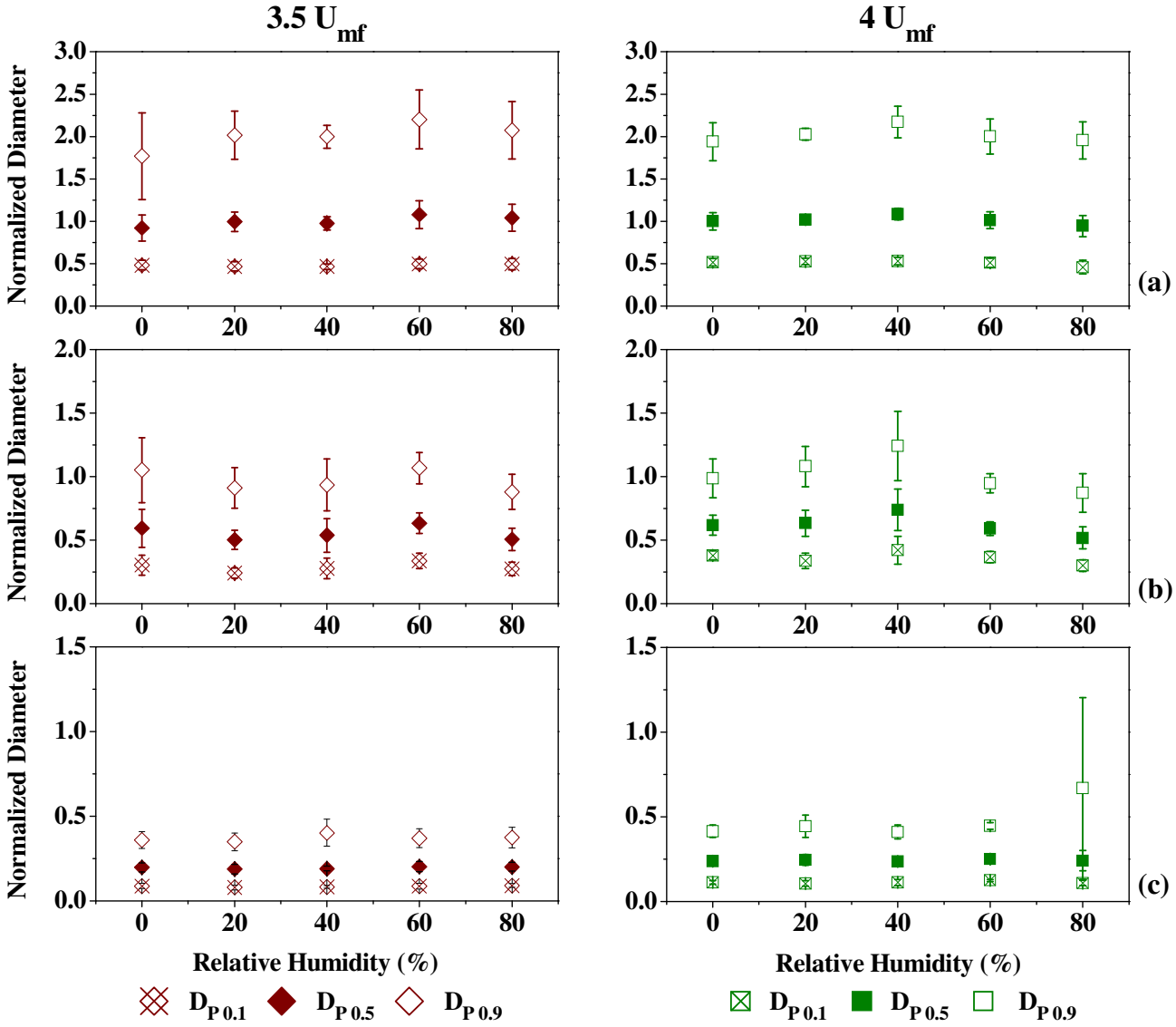

Figure 5-22: Comparison of PSDs for two gas velocities in slugging flow regime: (a) Dropped, (b) Wall, and (c) Fines.

5.2.4. Slugging Flow Regime Summary

Overall, increasing the gas relative humidity did not affect the magnitude of the particle wall fouling in the slugging flow regime as neither the mass of the particles collected, nor images taken from this region showed a trend with relative humidity. This may be due to the manner at which the wall fouling occurs in the slugging flow regime. As concluded in Chapter 3, the wall layer builds onto the column shortly after the onset of fluidization and is not dependent on fluidization time. Therefore, there is less of an opportunity for a water film to form onto the portion of the wall where particles typically adhere. Thus, any influence of relative humidity on the wall fouling would be through the charge on the flux of particles moving from the dropped region to the wall and vice versa.

In the net q/m of the wall region, effects of relative humidity were observed in a decrease in magnitude at 60% for 4 U_{mf} and 80% for 3.5 U_{mf}. The difference in humidities required for an effect to be observed may be due to the amount of moisture necessary as there would be more mass flow rate of water at 4 U_{mf} than 3.5 U_{mf} for the same fluidization time.

Comparison with other studies was not made with respect to charge. This was because previously the effect of relative humidity was only investigated in bubbling flow. Due to the differences in hydrodynamics between the two flow regimes, it is difficult to make adequate comparisons as the predominant charging mechanisms are different.

5.3. Comparison of Results of the Two Flow Regimes

Four gas velocities were tested at different relative humidities ranging from 0 to 80%. Two of these velocities lie within the bubbling flow regime, while the other two in the slugging flow regime. The following sections will compare the two flow regimes with respect to the effects of relative humidity.

5.3.1. Mass Collected (m%)

Table 5-1 summarizes all m% results obtained for all gas relative humidities in both flow regimes. In the dropped region, 1.5 U_{mf} had the least amount of particles collected while 3.5 U_{mf} had the most amounts. Neither flow regimes demonstrated an obvious trend with the increase in relative humidity in the dropped region. In the wall region, the bubbling flow regime had more particles adhered to the column wall and more variance in m% collected than the slugging flow regime. However, neither flow regime depicted any trend with relative humidity in this region with the exception of the 80% RH which resulted in lower m% in the bubbling flow but not much of an effect was observed in the slugging flow. In the fines region, the slugging flow regime resulted in more particles being elutriated from the column than in the bubbling flow regime. There is a clear increase in particle elutriation with an increase in fluidization gas velocity. This is due to larger particles being entrained from the bed with increased gas velocity. However, gas relative humidity did not affect the results.

Table 5-1: Comparison of m% for all gas velocities and relative humidities.

Relative Humidity	Initial				Dropped			
	1.5 U_{mf} m %	1.75 U_{mf} m %	3.5 U_{mf} m %	4 U_{mf} m %	1.5 U_{mf} m %	1.75 U_{mf} m %	3.5 U_{mf} m %	4 U_{mf} m %
0	100.0 ± 0.0	100.0 ± 0.0	100.0 ± 0.0	100.0 ± 0.0	94.30 ± 0.92	94.20 ± 2.60	96.68 ± 0.31	95.96 ± 0.55
20	100.0 ± 0.0	100.0 ± 0.0	100.0 ± 0.0	100.0 ± 0.0	93.10 ± 0.23	96.31 ± 0.49	96.98 ± 0.23	96.00 ± 0.57
40	100.0 ± 0.0	100.0 ± 0.0	100.0 ± 0.0	100.0 ± 0.0	93.23 ± 0.57	96.68 ± 1.20	97.00 ± 0.29	96.08 ± 0.06
60	100.0 ± 0.0	100.0 ± 0.0	100.0 ± 0.0	100.0 ± 0.0	95.99 ± 1.20	95.17 ± 0.72	96.42 ± 0.17	96.51 ± 0.17
80	100.0 ± 0.0	100.0 ± 0.0	100.0 ± 0.0	100.0 ± 0.0	97.50 ± 0.30	97.09 ± 0.87	96.87 ± 0.22	95.79 ± 0.37

Relative Humidity	Wall				Fines			
	1.5 U_{mf} m %	1.75 U_{mf} m %	3.5 U_{mf} m %	4 U_{mf} m %	1.5 U_{mf} m %	1.75 U_{mf} m %	3.5 U_{mf} m %	4 U_{mf} m %
0	3.54 ± 0.84	3.59 ± 2.03	0.85 ± 0.21	0.82 ± 0.21	0.1322 ± 0.02	0.16 ± 0.06	0.92 ± 0.47	1.57 ± 0.21
20	4.64 ± 0.10	1.41 ± 0.40	0.41 ± 0.05	0.51 ± 0.10	0.1242 ± 0.00	0.22 ± 0.06	1.40 ± 0.05	2.19 ± 0.54
40	4.24 ± 0.92	1.38 ± 0.75	0.47 ± 0.14	0.79 ± 0.23	0.1338 ± 0.01	0.25 ± 0.05	1.29 ± 0.12	1.46 ± 0.41
60	2.66 ± 0.85	2.76 ± 0.62	0.81 ± 0.19	0.69 ± 0.45	0.1334 ± 0.01	0.20 ± 0.03	1.33 ± 0.03	1.55 ± 0.42
80	1.61 ± 0.19	1.31 ± 0.80	0.48 ± 0.02	0.59 ± 0.11	0.1515 ± 0.04	0.30 ± 0.05	1.34 ± 0.14	2.29 ± 0.45

5.3.2. Charge-to-Mass Ratio (q/m)

Table 5-2 summarized the net q/m results obtained for all gas relative humidities in both flow regimes. Similar initial net q/m values were recorded for all trials allowing for comparison between them. In the dropped region, the bubbling flow regime seems to have slightly higher magnitudes of net q/m for most relative humidities, with the exception of 1.75 U_{mf} at 40 and 80% RH. Likewise, the bubbling flow regime gas velocities seem to have slightly higher net q/m generated in the wall and substantially higher net q/m than the slugging flow velocities in the fines region. However, neither of these regions demonstrated any trend with relative humidity.

Table 5-2: Comparison of q/m for all gas velocities and relative humidities.

Relative Humidity	Initial				Dropped			
	1.5 U_{mf} q/m	1.75 U_{mf} q/m	3.5 U_{mf} q/m	4 U_{mf} q/m	1.5 U_{mf} q/m	1.75 U_{mf} q/m	3.5 U_{mf} q/m	4 U_{mf} q/m
%	µC/kg	µC/kg	µC/kg	µC/kg	µC/kg	µC/kg	µC/kg	µC/kg
0	-0.120 ± 0.023	-0.107 ± 0.017	-0.107 ± 0.024	-0.104 ± 0.030	-0.709 ± 0.116	-0.625 ± 0.280	-0.467 ± 0.053	-0.501 ± 0.039
20	-0.129 ± 0.026	-0.142 ± 0.015	-0.144 ± 0.014	-0.107 ± 0.024	-0.676 ± 0.008	-0.454 ± 0.074	-0.372 ± 0.036	-0.416 ± 0.009
40	-0.124 ± 0.025	-0.144 ± 0.006	-0.130 ± 0.009	-0.130 ± 0.032	-0.714 ± 0.042	-0.415 ± 0.040	-0.420 ± 0.042	-0.470 ± 0.003
60	-0.113 ± 0.008	-0.140 ± 0.041	-0.139 ± 0.022	-0.113 ± 0.016	-0.615 ± 0.148	-0.591 ± 0.080	-0.493 ± 0.096	-0.542 ± 0.018
80	-0.112 ± 0.000	-0.144 ± 0.009	-0.128 ± 0.047	-0.128 ± 0.032	-0.402 ± 0.195	-0.479 ± 0.012	-0.552 ± 0.064	-0.519 ± 0.008

Relative Humidity	Wall				Fines			
	1.5 U_{mf} q/m	1.75 U_{mf} q/m	3.5 U_{mf} q/m	4 U_{mf} q/m	1.5 U_{mf} q/m	1.75 U_{mf} q/m	3.5 U_{mf} q/m	4 U_{mf} q/m
%	µC/kg	µC/kg	µC/kg	µC/kg	µC/kg	µC/kg	µC/kg	µC/kg
0	-58.1 ± 7.0	-64.4 ± 9.9	-45.1 ± 3.4	-52.8 ± 14.1	94.9 ± 30.4	87.6 ± 53.9	21.9 ± 10.6	22.2 ± 14.5
20	-60.7 ± 2.6	-66.1 ± 31.8	-48.4 ± 4.7	-46.4 ± 2.6	133.9 ± 17.5	101.1 ± 15.5	17.3 ± 12.3	12.0 ± 5.6
40	-57.7 ± 1.3	-62.8 ± 5.8	-45.2 ± 11.2	-53.0 ± 2.9	78.4 ± 58.3	100.0 ± 35.3	17.2 ± 8.2	21.8 ± 13.8
60	-66.9 ± 8.0	-68.6 ± 9.5	-48.7 ± 8.3	-30.9 ± 9.3	93.9 ± 55.9	122.9 ± 11.2	24.8 ± 8.5	37.4 ± 14.1
80	-56.5 ± 1.5	-51.6 ± 8.3	-20.3 ± 6.2	-33.1 ± 21.1	79.0 ± 34.8	78.8 ± 35.7	24.9 ± 0.8	20.2 ± 11.3

5.3.3. Normalized Mean Particle Diameter

Table 5-3 summarizes the normalized particle size distribution results for different gas relative humidities for both flow regimes. Similarly sized particles were found in the dropped region for all gas velocities and relative humidities. Larger particles were found in the slugging flow regime than in the bubbling flow regime in the wall region; however similarly sized particles were found in three out of the four regions, the exception was 4 U_{mf} which had slightly larger particles, along the bottom of the column following wall

collection. This suggested that the initial particle layers built on the column were similarly sized. However, with higher gas velocities larger particles were able to adhere to the outer layers of this layer. This may be due to the particle layer being more likely to build in the radial direction in the slugging flow regime whereas in the bubbling flow regime it is more likely to build in the axial direction. This type of particle layer leads to a more defined layering effect with the addition of positively and negatively particles. The addition of increased quantities of positively charged particles in conjunction with the probably positively charged column wall leads to the ability to attract larger particles that are likely more negatively charged. However, the addition of extra positively charged particles may lead to the observed less negative net q/m in the slugging flow regime. None of the gas velocities demonstrated any change with relative humidity with respect to the wall PSD.

Table 5-3: Normalized mean particle diameters ($D_{P\,0.5}$) for all fluidization gas velocities at different relative humidities.

Relative Humidity %	Dropped				Wall			
	1.5 U_{mf} $D_{P\,0.5}$	1.75 U_{mf} $D_{P\,0.5}$	3.5 U_{mf} $D_{P\,0.5}$	4 U_{mf} $D_{P\,0.5}$	1.5 U_{mf} $d_{P\,(0.5)}$	1.75 U_{mf} $d_{P\,(0.5)}$	3.5 U_{mf} $d_{P\,(0.5)}$	4 U_{mf} $d_{P\,(0.5)}$
0	0.938 ± 0.069	0.939 ± 0.199	0.920 ± 0.153	1.000 ± 0.103	0.423 ± 0.059	0.403 ± 0.094	0.594 ± 0.148	0.618 ± 0.077
20	0.910 ± 0.129	1.046 ± 0.027	0.994 ± 0.115	1.019 ± 0.048	0.389 ± 0.046	0.439 ± 0.045	0.504 ± 0.076	0.633 ± 0.102
40	0.947 ± 0.060	0.815 ± 0.014	0.976 ± 0.077	1.083 ± 0.070	0.424 ± 0.035	0.230 ± 0.201	0.538 ± 0.132	0.738 ± 0.164
60	0.973 ± 0.052	1.089 ± 0.076	1.077 ± 0.165	1.012 ± 0.102	0.403 ± 0.025	0.412 ± 0.035	0.634 ± 0.080	0.590 ± 0.055
80	0.922 ± 0.149	0.925 ± 0.111	1.042 ± 0.160	0.944 ± 0.126	0.407 ± 0.059	0.438 ± 0.038	0.507 ± 0.090	0.518 ± 0.086

Relative Humidity %	Fines				Bottom Column			
	1.5 U_{mf} $D_{P\,0.5}$	1.75 U_{mf} $D_{P\,0.5}$	3.5 U_{mf} $D_{P\,0.5}$	4 U_{mf} $D_{P\,0.5}$	1.5 U_{mf} $D_{P\,0.5}$	1.75 U_{mf} $D_{P\,0.5}$	3.5 U_{mf} $D_{P\,0.5}$	4 U_{mf} $D_{P\,0.5}$
0	0.121 ± 0.011	0.121 ± 0.020	0.198 ± 0.027	0.237 ± 0.019	0.507 -	0.315 -	0.418 -	0.496 ± 0.070
20	0.113 ± 0.006	0.130 ± 0.010	0.188 ± 0.029	0.246 ± 0.032	0.325 ± 0.017	0.319 ± 0.005	0.265 ± 0.253	0.449 ± 0.066
40	0.126 ± 0.009	0.123 ± 0.021	0.192 ± 0.014	0.235 ± 0.027	0.335 ± 0.048	0.390 ± 0.114	0.338 ± 0.048	0.428 ± 0.105
60	0.121 ± 0.004	0.131 ± 0.026	0.205 ± 0.030	0.250 ± 0.007	0.345 ± 0.023	0.290 ± 0.084	0.335 ± 0.064	0.376 ± 0.041
80	0.130 ± 0.004	0.124 ± 0.012	0.202 ± 0.026	0.241 ± 0.060	0.342 ± 0.017	0.313 ± 0.036	0.317 ± 0.012	0.404 ± 0.048

Relative Humidity %	Top Column			
	1.5 U_{mf} $D_{P\,0.5}$	1.75 U_{mf} $D_{P\,0.5}$	3.5 U_{mf} $D_{P\,0.5}$	4 U_{mf} $D_{P\,0.5}$
0	- -	- -	0.180 -	0.242 ± 0.027
20	- -	- -	0.212 ± 0.055	0.258 ± 0.039
40	- -	- -	0.200 ± 0.011	0.277 ± 0.044
60	- -	- -	0.225 ± 0.021	0.582 ± 0.032
80	- -	- -	0.235 ± 0.020	0.253 ± 0.050

In the fines region, larger particles were found in the slugging flow regime with particle size increasing with fluidizing gas velocity. This was expected since the size of particles with a

terminal velocity smaller than the superficial gas velocity, increases as the velocity of the gas increases. The particles adhered to the top of the column are slightly larger than those completely elutriated from the bed. This may be due to these larger particles being slightly more negative, or slightly less positive, allowing for attraction to the positively charged column wall. However, neither the fines nor the top column particles demonstrated a trend of any kind due to relative humidity.

5.4. Overall Summary

Previous works have suggested that humid gas could be used as a method to reduce the amount of electrostatic charging within fluidized beds (Goode et al. 2000; Park et al., 2002). The most obvious of these effects were observed at 1.5 U_{mf}. This velocity could be split into two regions with respect to RH: (a) mid-range: 20 and 40%, and (b) high range: 60 and 80%. At the midrange humidities, wall fouling increased while at the high humidities it decreased. Additionally, at high humidities, the net q/m in the dropped region decreased along with the m% collected in that region. The other gas velocities seemed more likely to experience random variations due to relative humidity. Although, there was a trend in the slugging flow regime where high relative humidities in the wall region resulted in the net q/m to decrease in magnitude.

As stated earlier, some of the previous works have led to the theory that the solid surface layer properties, through the addition of substances that decrease electrical resistance (e.g., water), must be changed in order for electrostatic charge to be dissipated or its formation to be prevented (Bafrnec and Bena, 1972; Chen et al., 2003). The effect of fluidizing gas relative humidity on bed electrification behaviour can be influenced by the affinity of the particles surface for water. Higher affinity for water may lead to sufficient quantities of water molecules to form a film on its surface and thus promote charge dissipation through the reduction of surface resistivity (Boland and Geldart, 1972; Park et al., 2002; Yao et al., 2002). If a material lacks affinity for water, such as in the case of polyethylene, then it is less unlikely that a surface film of moisture will be formed on the particles (Forrest, 1953). Additionally, with an insulating particle, even with a high relative humidity environment,

dissipation may not occur without a conducting path to earth (Boland and Geldart, 1972). However, in this work, experiments were performed in an electrically isolated column.

The boundary between hydrophobic and hydrophilic materials is a contact angle of 90º, with hydrophobic materials having a contact angle of >90º and those of the hydrophilic nature having a contact angle of <90º. Güleç et al. (2006) determined the contact angle of glass, stainless steel and polyethylene, while Sghaier et al. (2006) found those of glass and Plexiglas (Table 5-4). Results of these studies place glass firmly in the hydrophilic region with stainless steel and Plexiglas being less hydrophilic, and polyethylene being hydrophobic. As a result of polyethylene hydrophobicity, it is less likely that a water film would develop on such material. However, the same could not be said with the stainless steel material used in this study for the column wall. A moisture film would likely readily develop on glass while higher humidities may be necessary to develop a moisture film on stainless steel and Plexiglas.

Table 5-4: Contact angles of stainless steel, polyethylene, and glass surfaces

Material	**θ_a (º)**	**Reference**
Stainless Steel 316	78.67 ± 8.71	Güleç et al., 2006
Polyethylene	91.72 ± 5.05	Güleç et al., 2006
Glass	37.39 ± 4.13	Güleç et al., 2006
Glass	39.3 ± 1.4	Sghaier et al., 2006
Plexiglas	81.2 ± 5.0	Sghaier et al., 2006

The formation of water film on different surfaces and their effect on reducing surface electrical resistivity have been discussed in the past where the nature of the material was found to impact the degree of the effect (Ally and Klinzing, 1985; Field, 1946; Kunkel, 1950; Németh et al. 2003; Yao et al., 2002). However, it is important to remember that high quantities of moisture can result in surface effects. Field (1946) reported that for polyethylene, appreciable change in surface electrical resistivity occurs only at 65% relative humidity followed by the equilibrium value changing logarithmically. In that work, no volume adsorption was observed on polyethylene sheets, thus any changes to surface resistivity were concluded to be due to the formation of surface water films. In addition, it has been found that the low surface polarity of polyethylene prevents the formation of stable

water films (Albrecht, 2009; Forrest, 1953). In this work, since the column material was slightly hydrophilic, it was possible that a water film formed on the inner column wall, dissipating charge on those particles nearest to the column which could be responsible for the effect on change of relative humidity. Additionally, it is possible that the random variations, as seen in the 1.75, 3.5 and 4 U_{mf} trials, are due to the formation of instantaneous water films that form and then disappear continuously as fluidization progress. This would result in localized dissipation of charge.

The following sections will deal with the possibility of water film formation on polyethylene surfaces involved in this work.

5.4.1. Additional Experiments

In order to better understand the effect of the presences of moisture in this work, some additional experiments were conducted. The following tests focus on determining whether the polyethylene particles were adsorbing water from the fluidization gas, since the presence of a moisture film was a previous theory found in the literature for observed decreases in electrostatic charge (Ally and Klinzing, 1985; Boland and Geldart, 1971/1972; Field, 1946; Németh et al. 2003; Park et al., 2002; Yao et al., 2002).

5.4.1.1. Bench-scale water adsorption tests

The presence of moisture due to gas relative humidity leading to decreased surface resistance which decreases the particles charge within a fluidized bed is a prevalent theory (Ciborowski and Woldarski, 1961; Katz and Sears, 1969; Park et al., 2002b). To investigate the occurrence of such phenomenon in this work, experiments were conducted to investigate whether moisture was being adsorbed on the polyethylene resins utilized in this study, and to what quantity. A sample of 25 grams of industrial resin was placed in a sieve with a mesh size small enough to prevent any loss of particles. Then humid air, 80% relative humidity, was passed over the resins from the top with a gas velocity of 0.115 m/s, less than the

minimum fluidization velocity of 0.131 m/s, to prevent particle movement. Experiments were conducted for a period of 60 minutes, similar to that of the fluidization runs. However, they were also performed for a shorter period of time of 10 minutes to determine if water adsorption, if any occurred, would increase with time. Results are presented in Table 5-5.

Table 5-5: Water adsorption test results.

Time (min)	Mass of Particles Before (g)	Mass of Particles After (g)
10	25.03 ±0.08	25.03 ±0.06
60	25.07 ±0.02	25.06 ±0.01

In both 10 and 60 min trials, the mass of the particles before and after the humidification were within 0.01 grams with similar standard deviations. This demonstrated that the particles were not adsorbing much, if any water at the highest relative humidity tested during fluidization runs. In other words, this also indicated that it was unlikely that a moisture film developed on the particles, especially at the lower relative humidities. This is to be expected due to the hydrophobic nature of polyethylene (Güleç et al., 2006). However, it is important to note that in these experiments the accuracy of the scales were only ±0.01g which means that trace amounts of water could be present on the polyethylene, but not detectable.

5.4.1.2. Differential pressure fluctuations

Yao et al. (2002) suggested that the standard deviations of the differential pressure fluctuations is related to changes in relative humidity by indicating a change in bubble size which can affect the electrostatic charge generation within the bed. The increase in relative humidity was related to a decrease in bubble size indicating a change in hydrodynamics and mimicked by a decrease in the standard deviation of differential pressure and voltage. As can be seen from Table 5-6, for all trials in the bubbling flow regime, the standard deviation of the pressure fluctuations (σ) did not deviate significantly indicating that the bubble size did not change appreciably as relative humidity increased.

Table 5-6: Standard deviation (σ) of differential pressure fluctuations in psi at different relative humidities for different gas velocities.

Relative Humidity (%)	1.5 U_{mf} σ		1.75 U_{mf} σ		3.5 U_{mf} σ		4 U_{mf} σ	
0	0.009	±0.002	0.015	±0.005	0.060	±0.005	0.069	±0.002
20	0.010	±0.001	0.014	±0.003	0.057	±0.000	0.067	±0.005
40	0.010	±0.000	0.016	±0.003	0.057	±0.001	0.066	±0.002
60	0.008	±0.002	0.014	±0.003	0.058	±0.001	0.067	±0.000
80	0.010	±0.002	0.018	±0.004	0.057	±0.001	0.063	±0.005

5.4.1.3. Humidity probe data

For 10 of the fluidization trials (at 1.75 and 3.5 U_{mf}), the relative humidity of the gas at the outlet of the fluidization column was monitored and compared to that of the gas entering the column by two relative humidity transmitters of the same type (Figure 5-23). This was to evaluate whether any significant quantity of air moisture was lost to condensation or adsorption within the column, either on the particles or on the column wall. The results demonstrated that, when considering the accuracy of the humidity probes and the difference in their calibration (~1%), the water loss was below a quantifiable amount. Therefore, any effects of humidity due to moisture loss would be due to miniscule quantities of water creating layers likely only a few molecules thick.

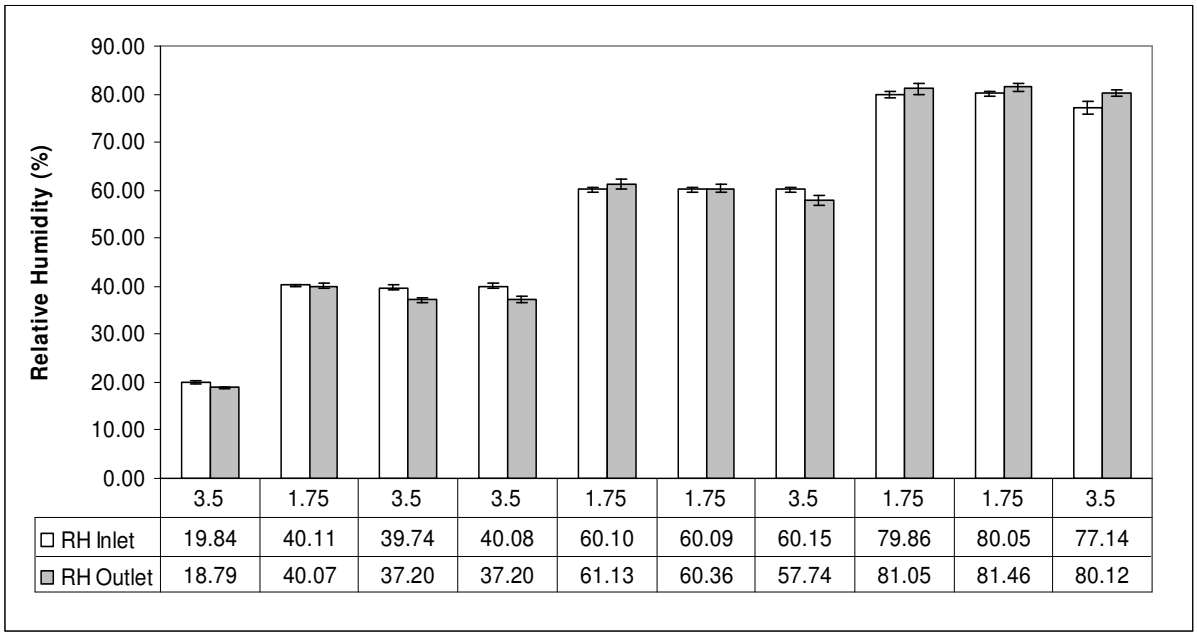

	3.5	1.75	3.5	3.5	1.75	1.75	3.5	1.75	1.75	3.5
RH Inlet	19.84	40.11	39.74	40.08	60.10	60.09	60.15	79.86	80.05	77.14
RH Outlet	18.79	40.07	37.20	37.20	61.13	60.36	57.74	81.05	81.46	80.12

Figure 5-23: Amount of RH (%) lost between inlet and outlet of fluidization column for trials at 1.75 or 3.5 U_{mf}.

5.4.1.4. Thermogravimetric analysis (TGA)

Another method of investigating water adsorption was to employ thermogravimetric analysis, which is used to determine the change in mass of a material by varying temperature through the passage of a specific gas. In this work, this type of analysis was used to determine if a layer of water had formed on polyethylene resins during the humidity trials. Since the humidification system utilized in the fluidization tests could not be directly connected to the TGA unit, which was located in another building, water adsorption tests could not performed. Therefore, desorption tests were conducted by examining the resins that had already been humidified by the fluidization process. If any water had adsorbed on the surface of the resins, in the desorption tests, the water layer would be removed and thus the mass of the test sample would decrease.

A sample of initial polyethylene particles was tested using the TGA along with a sample of the reins, from the dropped region of the bed that had been fluidized using air at 80% RH at a fluidization gas velocity of 1.5 U_{mf}.

Thermogravimetric analysis was conducted using a SD 2960 Simultaneous DSC-TGA (TA Instruments, USA). Pure nitrogen stream with a flow rate of 100 mL/min was used with a heating rate of 1 ºC/min. The sample ran from room temperature up to 85 ºC, below the melting point of polyethylene. The mass of the sample was monitored throughout the run with an accuracy of 0.1 mg. Two repetitions of TGA were performed on each set of particles with new particles used each time (Figure 5-24).

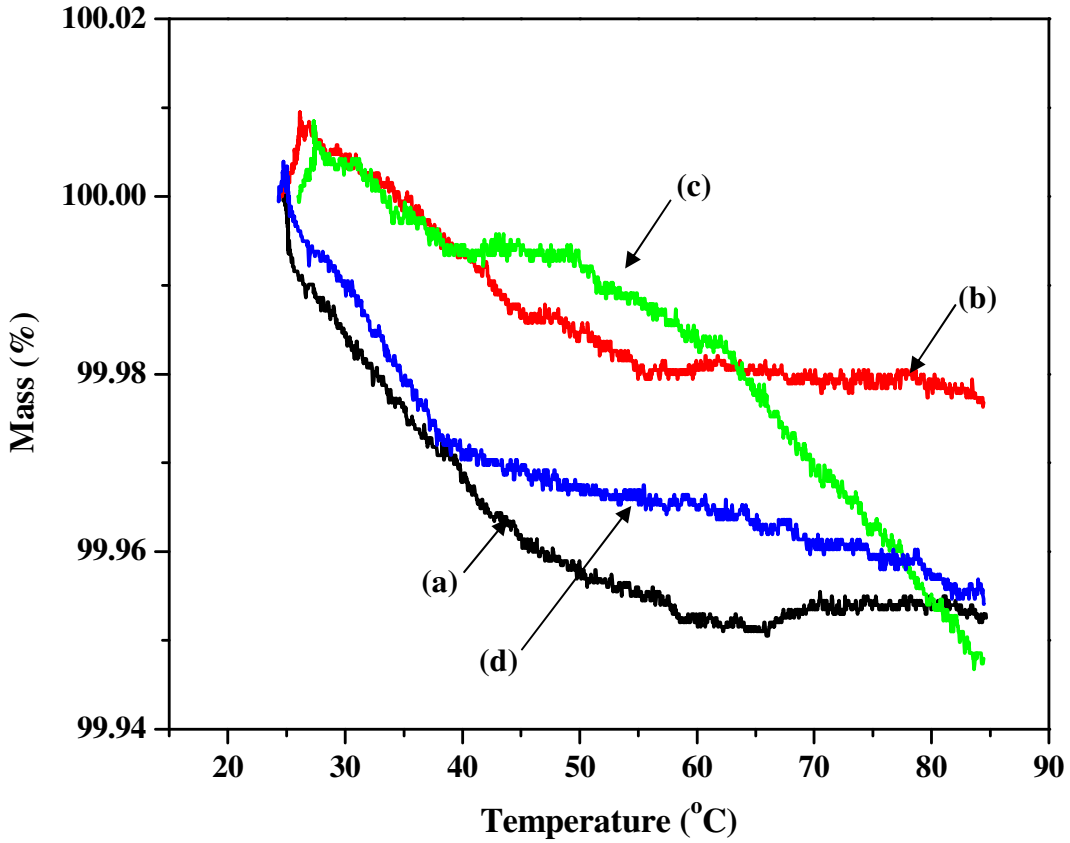

Figure 5-24: Thermogravimetric analysis for m% loss with temperature: (a) & (b) Initial Sample (repetition 1 & 2); (c) & (d) Humidified Sample (repetition 1 & 2).

The results of the TGA are presented in Figure 5-24 where the particles mass lost as temperature increased presented as a percentage of initial mass used for analysis. The amount of mass lost during all of the trials was less than 0.05% of the total mass, which amounts to less than 0.1 mg which is the accuracy of the system. Therefore, it was unlikely that a stable surface film developed on the polyethylene resins in the humid environment.

There is still the possibility that transient surface films developed during fluidization, influencing charge dissipation at instantaneous moments. That would mean that as fluidization progresses, surface films may develop and then disappear on particles throughout the bed creating local spots of increased charge dissipation, which would explain variances in net q/m.

5.5. Conclusions

Although the presence of moisture within a fluidized bed has previously been suggested to reduce electrostatic charge (Ciborowski and Woldarski, 1961; Katz and Sears, 1969; Park et al., 2002b), this was not found for all velocities tested in this thesis. The effect of relative humidity on wall fouling was only obvious at 1.5 U_{mf}; at higher relative humidities no trend was found.

Previously, the presence of a moisture film was suggested to reduce surface electrical resistivity leading to decreased charge (Ally and Klinzing, 1985; Field, 1946; Kunkel, 1950; Németh et al. 2003; Yao et al., 2002) however, in this work different tests such as TGA and bench-scale water adsorption suggested that a water layer was not present on the particles, likely due to the hydrophobic nature of polyethylene. However, it was suggested that an instantaneous water surface film could be present on some particles within the bed at any given time; thus increasing charge dissipation momentarily. Another possibility is that a film may have developed on the column wall, dissipating charge of those particles near the wall, and also reducing the actual contact between polyethylene particles surface and the stainless steel wall, both contributing in the changes in charge observed within the bed.

None of the gas velocities experienced any change in particle size distribution with increased relative humidity. Therefore, relative humidity did not influence the size of particles found within the different regions of the bed.

Chapter 6. Conclusions and Future Work

Electrostatic charge generation poses significant problems in some commercial gas-solid fluidized bed reactors such as those in gas-phase polyolefin production. Understanding the contributing factors to charge generation is important in determining the charge generation mechanisms, leading to the development of methods to reduce or prevent this phenomenon. The first step, essential to exploring and understanding charge generation mechanisms, is having an appropriate measurement technique. A novel online measurement technique has been previously developed in this research group and successfully implemented in a pilot-scale atmospheric gas-solid fluidization system. The second step is then to understand the factors contributing to electrostatic charge generation and their involvement in reactor wall fouling which are of significant importance in developing methods to reduce or prevent the electrostatic phenomenon. Factors contributing to the quantity and the polarity of charge generated on solid particles in fluidized beds include: frequency of contact between particles and between particles and the reactor wall, particle size, shape and surface chemistry, and reactor operating conditions such as fluidization time period, gas velocity and relative humidity, pressure and temperature.

This thesis aimed at investigating the effect of three parameters that might contribute to charge generation and/or dissipation in gas-solid fluidized beds and their significance. The specific objectives were to study the effects of fluidization time (15, 30, 60, 120, 180 and 360 minutes), fluidization column wall material (stainless steel versus carbon steel), and fluidizing gas relative humidity (0%, 20%, 40%, 60% and 80%) on charge distribution within the fluidized bed and reactor wall fouling.

6.1. Conclusions

With all parameters tested, a few general conclusion were drawn based on results obtained. Bipolar charging withing the bed was found for all fluidization times, relative humidities and gas velocities with the small and the large particles being positively and negatively charged, respectively. Typically the fines and the wall regions had higher magnitudes of charge than the bulk region by at least two orders of magnitude. The initial particles charge distribution showed that finer particles were originally likely negatively charged. However, these particles were predominantly positively charged following fluidization. Thus, the change in polarity during fluidization showed that charge generation was taking place.

Reactor wall fouling took place for all parameters tested, at vaying degrees. It was found that the bed hydrodynamics, in this case fluidization flow regime, had significant affects on the magnitude of the particle-reactor wall coverage. In the bubbling flow regime, typically a larger coverage was observed with the particle layer being at a height approximately equal to the static bed height. In the slugging flow regime, the coverage was much shorter; the layer extended from the distributor plate to approximately where slugs became fully formed, after that point the force of the slug prevented the particles from adhering to the wall.

All of the parameters tested resulted in similarly sized particles ending up in the same regions of the bed. Initial and dropped particles were the largest while fines and those adhered to the top of the column were the smallest. Particles from the top column were typically slighly larger than the elutrated fines. The mid-sized particles typically adhered to the column wall with those attached to the bottom of the column and the intermediate wall particles being slightly smaller and larger than the wall region, respectively.

6.1.1. Charging Mechanisms

Particle charging within the fluidized bed is generally dominated by two mechanisms: triboelectrification, predominantly through particle-particle contacts, and frictional charging, predominately through particle-wall interactions. Although both mechanisms may happen

with both types of interaction, one is generally dominant for each type of contact. The possible charging polarity of the particles and that of the column wall are shown in Figure 6-1. In this project it was found that in the case of polyethylene, during particle-particle contacts the smaller particle becomes positively charged while the larger particle becomes negatively charged. During particle-wall contacts between polyethylene resins and stainless steel or carbon steel wall, due to the difference in the materials work function, the resin becomes negatively charged while the metal wall becomes positively charged (Figure 6-1b). It is important to note that similar polarities are unlikely to make contact due to repulsive electrostatic forces.

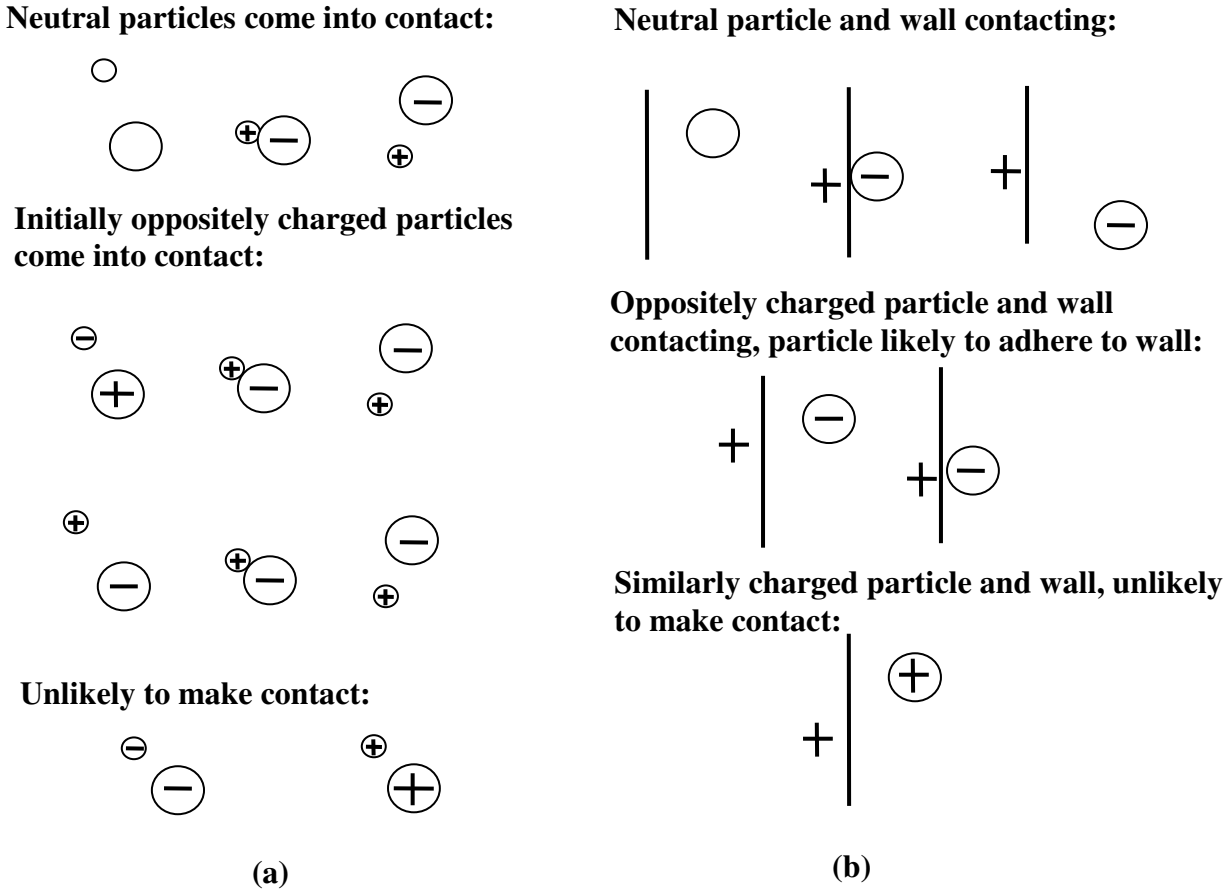

Figure 6-1: Charging mechanisms in stainless steel column with polyethylene particle: (a) Particle-particle contacts, and (b) Particle-wall contacts.

In general, with the majority of experimental trials, it was found that particle migration occurred from the bulk to the wall in the bubbling flow regime, as seen during the fluidization time experiments. This migration was due to a combination of bed hydrodynamics and electrostatic forces. Since the bulk particles were predominantly negatively charged and column wall was positively charged, the electrostatics promoted the movement through either a positive attraction by the wall or a negative repulsion within the bulk, or more likely both (Figure 6-2).

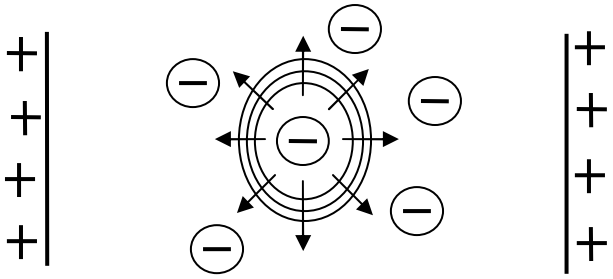

Figure 6-2: Particles movement due to electrostatic forces.

When particles migrate to the wall region, wall fouling occurs when negatively charged particles adhere to the positively charged column wall (Figure 6-3). Then as fluidization progresses, positively charged particles adhere to the negative particle layer to supplement the positive charge already provided by the column. These are followed by larger particles that are more negatively charged. Such layering effect continues until the particles at the outer layer reach a size that the gravitational forces dominate the electrostatic forces.

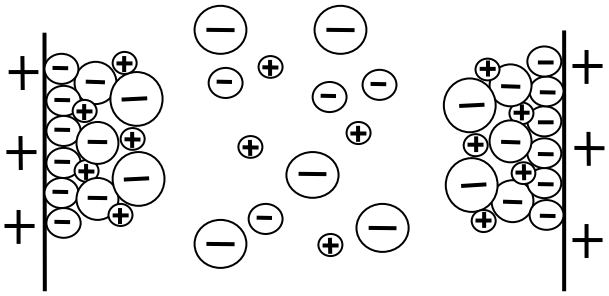

Figure 6-3: Particle wall fouling.

6.1.2. Fluidization Time

The influence of the fluidization time was studied; it was found that the migration of particles increased from the dropped to the wall region during the bubbling flow regime as fluidization time increased. This indicated that the longer particles residence time in a flow regime, where vigorous, in comparison to the slugging flow regime, radial mixing is present, results in more particles charging and thus influences the movement of particles. In the slugging flow regime, there was either little migration between regions or an equilibrium flux was obtained shortly after fluidization began and remained stable for increased fluidization times.

Charge saturation was reached in the bulk and the wall regions within 60 min of fluidization for both flow regimes. Fine particles reach saturation shortly after the onset of fluidization in the slugging flow regime while in the bubbling flow regime they required a longer residence time. The maximum net q/m was calculated and compared to the measured net q/m. In the slugging flow regime, the measured value was lower than the maximum at all fluidization times indicating that air ionization was likely not taking place. However, the bubbling flow regime had some measured values that were greater than the maximum net q/m. Therefore, in this regime many factors, such as particle migration, type and frequency of contact, and potentially air ionization contributed to determining charge saturation.

With respect to wall fouling, the main particle layer was built up during the first 15 minutes in the slugging regime. In contrast, during bubbling regime the particle layer continued to build as fluidization time lengthened.

Similar values of net q/m with increased m% in the wall region during bubbling flow suggested that there was a greater ability to generate charge in this regime than in the slugging regime. This was due to the vigorous mixing in the bubbling regime that resulted in more particle-particle interactions to generate more charge than in the slugging flow regime. With minimal radial mixing in the slugging flow regime, after the formation of the particle layer the amount of particle-wall contacts decrease resulting in less charge being generated as this is the predominant charging mechanism.

6.1.3. Column Material

In the bubbling flow regime it was found that the type of column material does not influence in the magnitude of wall fouling. This was due to particle-particle contacts being the predominant charging mechanism, which would be similar for both columns as all other parameters were kept the same. However, in the slugging flow regime more particles were found on the carbon steel column wall with larger particle layer coverage. This was due to particle-wall contacts and thus frictional charging being the predominant charging mechanism within this flow regime. It was determined that since the carbon steel had a rougher finish, more frictional charge could be generated.

At 1.5 U_{mf}, in the bubbling flow regime, similar net q/m was produced in the dropped region. As the particle layer developed, particle-wall interactions decreased in frequency and particle-particle interactions would likely generated the same amount of charge in each column resulting in similar net q/m. A higher magnitude net q/m was found in the wall region of the carbon steel column, indicating on the higher magnitude of charge on these particles. This was due to these particles becoming more highly charged due to their charge being gained from particle-wall interactions.

At 4 U_{mf}, in the slugging flow regime, both the wall and dropped regions resulted in more charge being generated in the carbon steel column. Again, this is due to the higher charge generated due to the rougher surface finish in the carbon steel column.

6.1.4. Relative Humidity

The effect of relative humidity on wall fouling was studied for two flow regimes of bubbling and slugging. It was found that in bubbling regime, relative humidity of 60% and 80% RH were the most effective reducing the wall fouling. However, in the slugging flow regime, no effect on wall fouling was observed. This was due to the manner at which the particle layer built on the column wall in this regime where wall fouling occurred shortly after the onset of fluidization. Thus, there was little opportunity for a water film to form on the column wall before particles began to adhere.

There was a trend in the slugging flow regime where the net q/m of the wall region decreased for high relative humidities. Other variations in charge were recorded at all velocities with no trend. The effect of relative humidity in this column were likely due to the formation of water films on the column wall or instantaneous water surface films on the particles in the bed or along the wall at any given time. Stable surface films on the particles were unlikely to form due to the hydrophobic nature of the polyethylene, as depicted by additional experiments performed.

6.2. Recommendations for Future Work

The recommendations for future work that have come out of this work are:

- Find ways to accurately quantify the particle layer on the wall for its height and thickness to enable the more accurate investigation of the reactor wall fouling formation and progress under different operating conditions.
- Evaluate a Plexiglas and/or glass column to complete the link between academia and industry in terms of comparing fluidization column wall material.
- Evaluate the effect of relative humidity at shorter fluidization times before charge saturation occurs.
- Investigate transition velocities, those between 1.75 U_{mf} and 3.5 U_{mf}, for all parameters.
- Find ways to measure surface conductivity, resistivity, or permittivity of the particles with changes in gas relative humidity.
- Conduct tests with grounded column wall to determine how charge generation changes with changing the relative humidity.

Bibliography

Adams, C.K., "Nature's Electricity," McGraw-Hill Companies (1986), pp. 160.

Agapiou, A.K., D.M. Glowczwski, Z. Lin, G.D. Mohr, T.A. Powel, M.E. Sieloff, E.F. Smith, K.B. Stavens, K.W. Trapp, M.E. Muhle and D. Hussein, "Methods and devices for polymerization," 12/525,202 (2010).

Albrecht, V., A. Janke, E. Németh, S. Spange, G. Schubert and F. Simon, "Some aspects of the polymers' electrostatic charging effects," J. Electrostatics. 67, 7-11 (2009).

Ali, F.S., M. Adnan Ali, R. Ayesha Ali and I.I. Inculet, "Minority charge separation in falling particles with bipolar charge," J. Electrostatics. 45, 139-155 (1998).

Ali, F.S., I.I. Inculet and A. Tedoldi, "Charging of polymer powder inside a metallic fluidized bed," J. Electrostatics. 45, 199-211 (1999).

Ally, M.R. and G.E. Klinzing, "Inter-relation of electrostatic charging and pressure drops in pneumatic transport," Powder Technol. 44, 85-88 (1985).

Bafrnec, M. and J. Bena, "Quantitative data on the lowering of electrostatic charge in a fluidized bed," Chemical Engineering Science. 27, 1177-1181 (1972).

Baron, T., C.L. Briens, M.A. Bergougnou and J.D. Hazlett, "Electrostatic effects on entrainment from a fluidized bed," Powder Technol. 53, 55-67 (1987).

Bartilucci, M.P., E.R. Davis Jr., B.J. Egan, R.O. Hagerty and P.K. Husby, "Method and apparatus for reducing static charges during polymerization of olefin polymers," 09/802090 (2003).

Bi, H.T., "Electrostatic phenomena in gas-solids fluidized beds," China Particuology. 3, 395-399 (2005).

Blythe, A.R. and D. Bloor, "Electrical properties of polymers," Cambridge University Press, United Kingdom (2005), pp. 480.

Boland, D. and D. Geldart, "Electrostatic charging in gas fluidised beds," Powder Technol. 5, 289-297 (1972).

Cartwright, P., S. Singh, A.G. Bailey and L.J. Rose, "Electrostatic Charging Characteristics of Polyethylene Powder During Pneumatic Conveying," Industry Applications, IEEE Transactions on. IA-21, 541-546 (1985).

Chen, A.H., H.T. Bi and J.R. Grace, "Measurement of particle charge-to-mass ratios in a gas–solids fluidized bed by a collision probe," Powder Technol. 135-136, 181-191 (2003).

Chirillo, J.R., K.C.I. Kimbrough and P.E. McHattie, "Method for reducing sheeting during polymerization of alpha-olefins," 914443 (1989).

Ciborowski, J. and A. Wlodarski, "On electrostatic effects in fluidized beds," Chemical Engineering Science. 17, 23-32 (1962).

Cross, J., "Electrification of Solids and Liquids," in "Electrostatics: Principles, Problems and Applications," Anonymous Adam Hilger, Bristol (1987), pp. 17-85.

De Luca, L., R. Di Felice, P.U. Foscolo and P.P. Boattini, "Slugging behaviour of fluidized beds of large particles," Powder Technol. 69, 171-175 (1992).

Fasso, L., B.T. Chao and S.L. Soo, "Measurement of electrostatic charges and concentration of particles in the freeboard of a fluidized bed," Powder Technology. 33, 211-221 (1982).

Field, R.F., "The formation of ionized water films on dielectrics under conditions of high humidity," J. Appl. Phys. 17, 318-325 (1946).

Forrest, J.S., "Methods of increasing the electrical conductivity of surfaces," British Journal of Applied Physics. 4, S37 (1953).

Fujino, M., S. Ogata and H. Shinohara, "The electric potential distribution profile in a naturally charged fluidized bed and its effects," International Chemical Engineering. 25, 149-159 (1985).

Gallo, C.F. and W.L. Lama, "Some charge exchange phenomena explained by a classical model of the work function," J. Electrostatics. 2, 145-150 (1976).

Geldart, D., "Types of gas fluidization," Powder Technol. 7, 285-292 (1973).

Goode, M.G., C.C. Williams, F.D. Hussein, T.J. McNeil and K.H. Lee, "Static control in olefin polymerization," 224036 (2000).

Grace, J.R., "Fluidized-bed hydrodynamics," in "Handbook of Multiphase Systems," G. Hetsroni, Ed. Hemisphere, Washington (1982).

Guardiola, J., G. Ramos and A. Romero, "Electrostatic behaviour in binary dielectric /conductor fluidized beds," Powder Technol. 73, 11-19 (1992).

Guardiola, J., V. Rojo and G. Ramos, "Influence of particle size, fluidization velocity and relative humidity on fluidized bed electrostatics," J. Electrostatics. 37, 1-20 (1996).

Güleç, H.A., K. Sarıogˇlu and M. Mutlu, "Modification of food contacting surfaces by plasma polymerisation technique. Part I: Determination of hydrophilicity, hydrophobicity and surface free energy by contact angle method," J. Food Eng. 75, 187-195 (2006).

Harper, R.W., "Contact and Frictional Electrification," Oxford University Press, London (1967).

Hendrickson, G., "Electrostatics and gas phase fluidized bed polymerization reactor wall sheeting," Chemical Engineering Science. 61, 1041-1064 (2006).

Hersh, S.P. and D.J. Montgomery, "Static Electrification of Filaments," Textile Research Journal. 25, 279-295 (1955).

Hindermann-Bischoff, M. and F. Ehrburger-Dolle, "Electrical conductivity of carbon black–polyethylene composites: Experimental evidence of the change of cluster connectivity in the PTC effect," Carbon. 39, 375-382 (2001).

Inculet, I.I., G.S. Peter Castle and G. Aartsen, "Generation of bipolar electric fields during industrial handling of powders," Chemical Engineering Science. 61, 2249-2253 (2006).

Jazayeri, B., "Applications for Chemical Production and Processing," in "Handbook of fluidization and fluid-particle systems," W. Yang, Ed. Marcel Dekker, Inc., New York (2003), pp. 421-444.

Katz, H. and J.T. Sears, "Electric Field Phenomena in Fluidized and Fixed Beds," Canadian Journal of Chemical Engineering. 47, 50-53 (1969).

Kisel'nikov, V.N., V.V. Vyalkov and V.M. Filatov, "On the problem of electrostatic phenomena in a fluidized bed," Int. Chem. Eng. 7, 428-431 (1967).

Kunii, D. and O. Levenspiel, "Fluidization Engineering," Butterworth-Heinemann, Newton, USA (1991), pp. 1-478.

Kunkel, W.B., "The static electrification of dust particles on dispersion into a cloud," J. Appl. Phys. 21, 821 (1950).

Leva, M., "Fluidization," McGraw-Hill, New York (1959).

Maryland Metrics, "Surface Roughness Tables," 2010 (2002).

Matsusaka, S., M. Oki and H. Masuda, "Control of electrostatic charge on particles by impact charging," Advanced Powder Technology. 18, 229-244 (2007).

Mehrani, P., H.T. Bi and J.R. Grace, "Electrostatic behavior of different fines added to a Faraday cup fluidized bed," J. Electrostatics. 65, 1-10 (2007).

Miller, C.O. and A.K. Logwinuk, "Fluidization Studies of Solid Particles," Industrial & Engineering Chemistry. 43, 1220-1226 (1951).

Mountain, J.R., M.K. Mazumder, R.A. Sims, D.L. Wankum, T. Chasser and P.H. Pettit, "Triboelectric Charging of Polymer Powders in Fluidization and Transport Processes," IEEE Transactions on Industry Applications. 37, 778-784 (2001).

Murtomaa, M., E. Räsänen, J. Rantanen, A. Bailey, E. Laine, J. Mannermaa and J. Yliruusi, "Electrostatic measurements on a miniaturized fluidized bed," J. Electrostatics. 57, 91-106 (2003).

Németh, E., V. Albrecht, G. Schubert and F. Simon, "Polymer tribo-electric charging: dependence on thermodynamic surface properties and relative humidity," J. Electrostatics. 58, 3-16 (2003).

Ohara, K., "Relationship between frictional electrification and molecular motion of polymers," J. Electrostatics. 9, 107-115 (1980).

Park, A.A., H.T. Bi, J.R. Grace and A. Chen, "Modeling charge transfer and induction in gas–solid fluidized beds," J. Electrostatics. 55, 135-158 (2002a).

Park, A., H. Bi and J.R. Grace, "Reduction of electrostatic charges in gas–solid fluidized beds," Chemical Engineering Science. 57, 153-162 (2002b).

Pfeffer, R. and J.A. Quevedo, "Systems and methods for reducing electrostatic charge in a fluidized bed," 12/142883 (2009).

Pionteck, J. and G. Wypych, Eds., "Handbook of Antistatics," ChemTec Publishing (2007), pp. 417-288.

Pryer, D.W. and P.F. Gale, "Cables," in "Electrical engineer's reference book," M. A. Laughton and D. F. Warne, Eds. Newnes, Oxford (2003), pp. 31/9.

Revel, J., C. Gatumel, J.A. Dodds and J. Taillet, "Generation of static electricity during fluidisation of polyethylene and its elimination by air ionisation," Powder Technol. 135-136, 192-200 (2003).

Rojo, V., J. Guardiola and A. Vian, "A capacitor model to interpret the electric behaviour of fluidized beds. Influence of apparatus geometry," Chemical Engineering Science. 41, 2171-2181 (1986).

Sghaier, N., M. Prat and S. Ben Nasrallah, "On the influence of sodium chloride concentration on equilibrium contact angle," Chem. Eng. J. 122, 47-53 (2006).

Shimizu, S.S., H. Murata and M. Honda, "Electrostatics in Power Transformers," IEEE Trans Power Appar Syst. PAS-98, 1244-1250 (1979).

Siddique, R., "Waste Materials and By-Products in Concrete," Springer-Verlag, Berlin (2007), pp. 413.

Singh, S. and G.L. Hearn, "Development and application of an electrostatic microprobe," J. Electrostatics. 16, 353-361 (1985).

Sowinski, A., L. Miller and P. Mehrani, "Investigation of electrostatic charge distribution in gas–solid fluidized beds," Chemical Engineering Science. 65, 2771-2781 (2010).

Sowinski, A., F. Salama and P. Mehrani, "New technique for electrostatic charge measurement in gas–solid fluidized beds," J. Electrostatics. 67, 568-573 (2009).

Tanoue, K. and H. Masuda, "Electrostatic separation," in "Powder Technology Handbook," H. Masuda, K. Higashitani and H. Yoshida, Eds. Taylor & Francis Group, LLC, Florida (2006), pp. 656.

Tardos, G. and R. Pfeffer, "A method to measure electrostatic charge on a granule in a fluidized bed," Chem Eng Comm. 4, 665-671 (1980).

Thomas, A., K. Saleh, P. Guigon and C. Czechowski, "Characterisation of electrostatic properties of powder coatings in relation with their industrial application," Powder Technol. 190, 230-235 (2009).

Tibtech Innovations, "Properties table of Stainless steel, Metals and other Conductive materials," 2010 (2010).

van Putten, I.C., M. van Sint Annaland and G. Weickert, "Fluidization behavior in a circulating slugging fluidized bed reactor. Part I: Residence time and residence time distribution of polyethylene solids," Chemical Engineering Science. 62, 2522-2534 (2007).

Wolny, A. and W. Kazmierczak, "Triboelectrification in fluidized bed of polystyrene," Chemical Engineering Science. 44, 2607-2610 (1989).

Wolny, A. and I. Opaliǹski, "Electric charge neutralization by addition of fines to a fluidized bed composed of coarse dielectric particles," Journal of Electrostatics. 14, 279-289 (1983).

Yang, W., "Bubbling Fluidized Beds," in "Handbook of Fluidization and Fluid-Particle Systems," W. Yang, Ed. Marcel Dekker, Inc., New York, USA (2003).

Yao, L., H.T. Bi and A. Park, "Characterization of electrostatic charges in freely bubbling fluidized beds with dielectric particles," J. Electrostatics. 56, 183-197 (2002).

Zhao, H., G.S.P. Castle and I.I. Inculet, "The measurement of bipolar charge in polydisperse powders using a vertical array of Faraday pail sensors," J. Electrostatics. 55, 261-278 (2002).

Zhi Chen and Mao-Chang Jin, "An alpha-alumina moisture sensor for relative and absolute humidity measurement," Industry Applications Society Annual Meeting, 1992. , Conference Record of the 1992 IEEE., 1668-1675 vol.2 (1992).

Appendix A. Preliminary Parameters

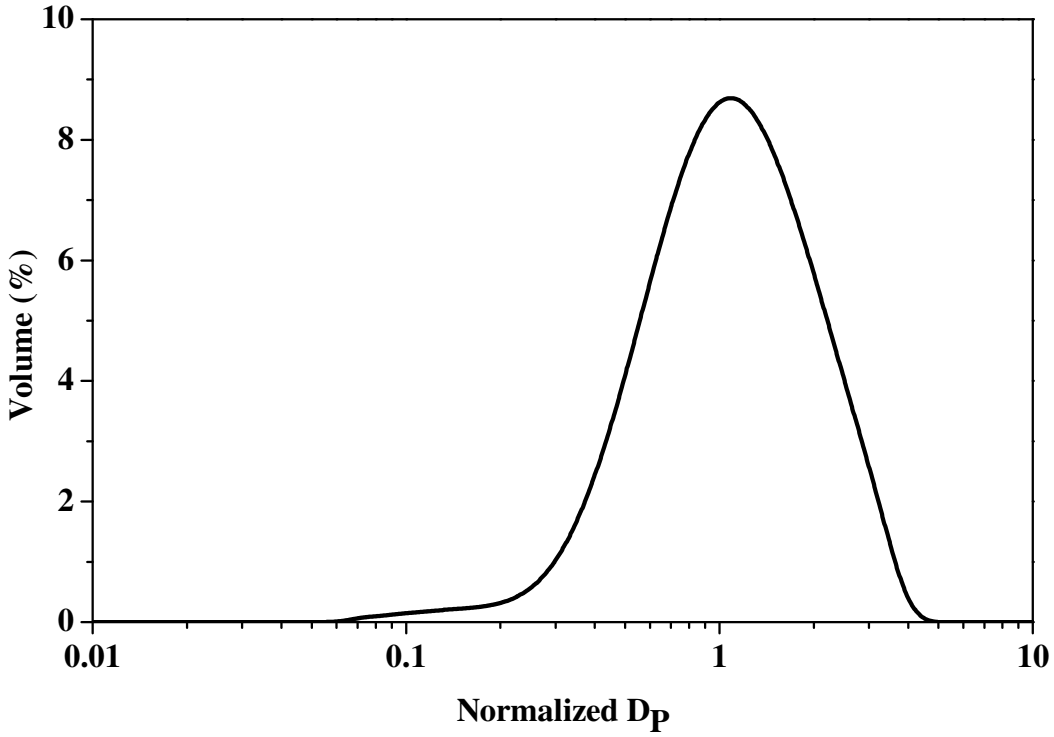

Figure A-1: Typical initial particle size distribution.

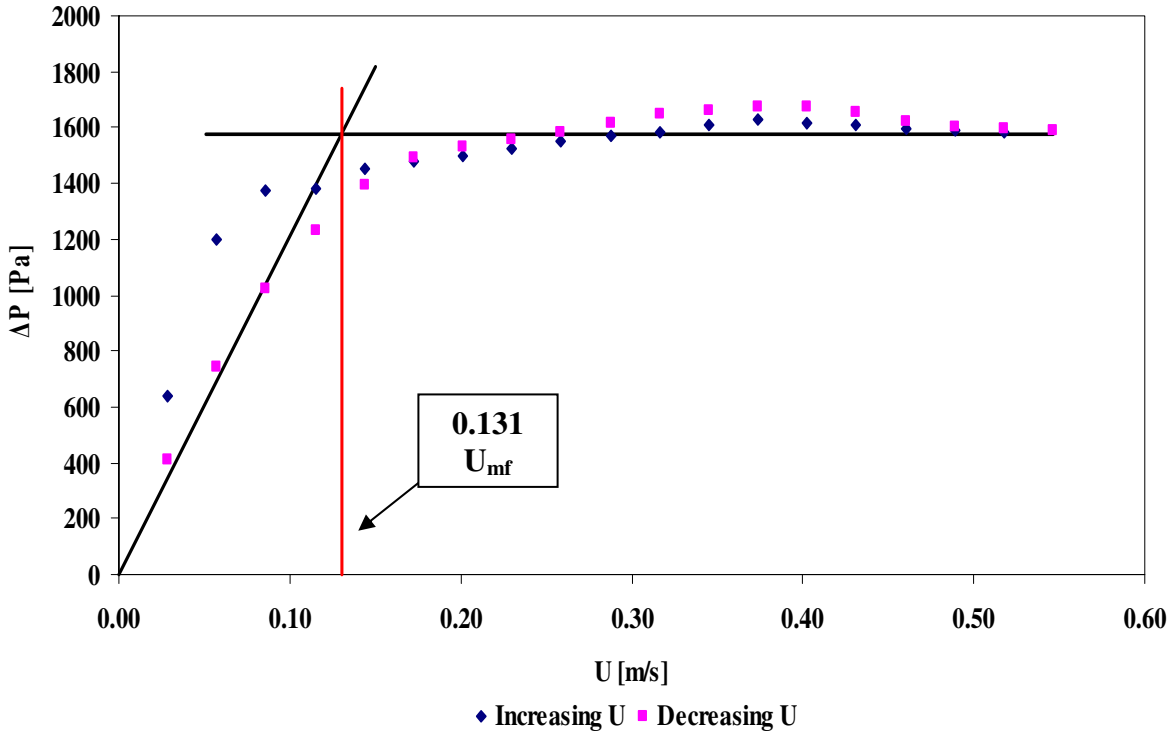

Figure A-2: Experimental determination of U_{mf}.

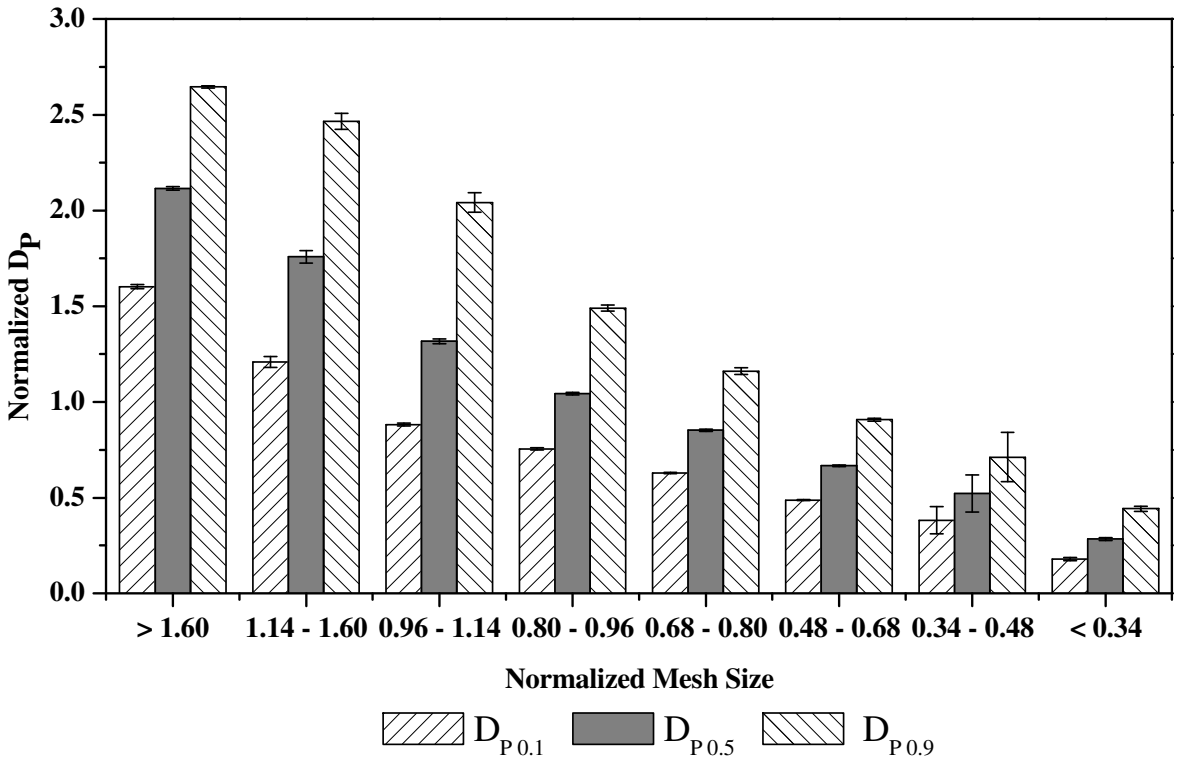

Figure A-3: Mass distribution of initial particles as evaluated by PSD given in $D_{P\,0.1}$, $D_{P\,0.5}$, and $D_{P\,0.9}$.

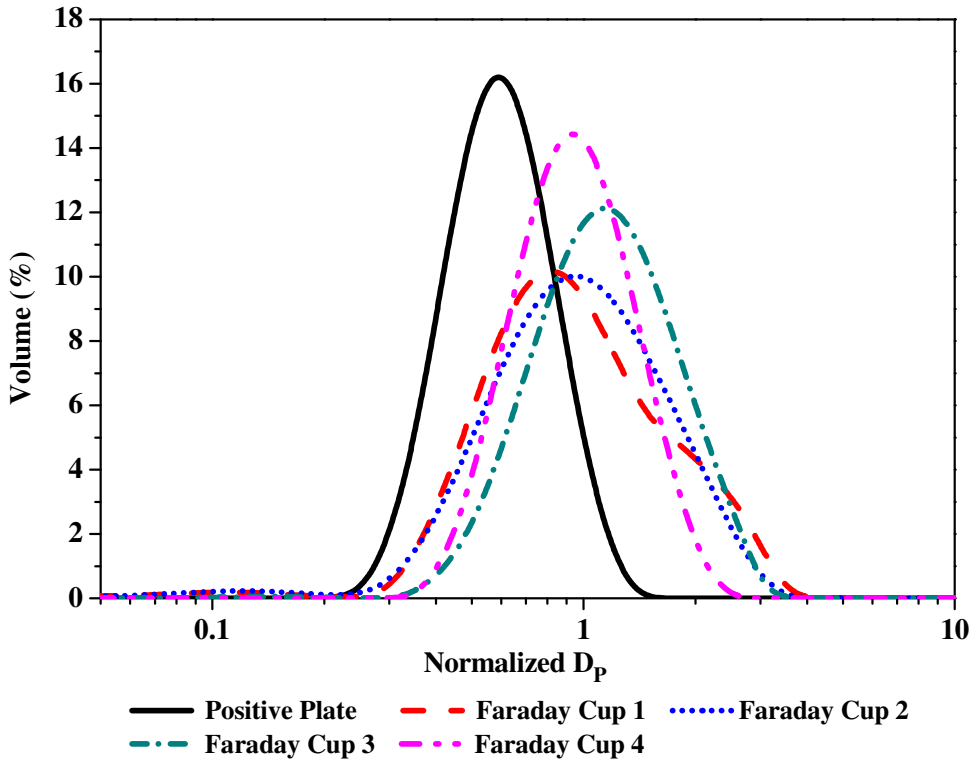

Figure A-4: Average PSDs for charge distribution tests.

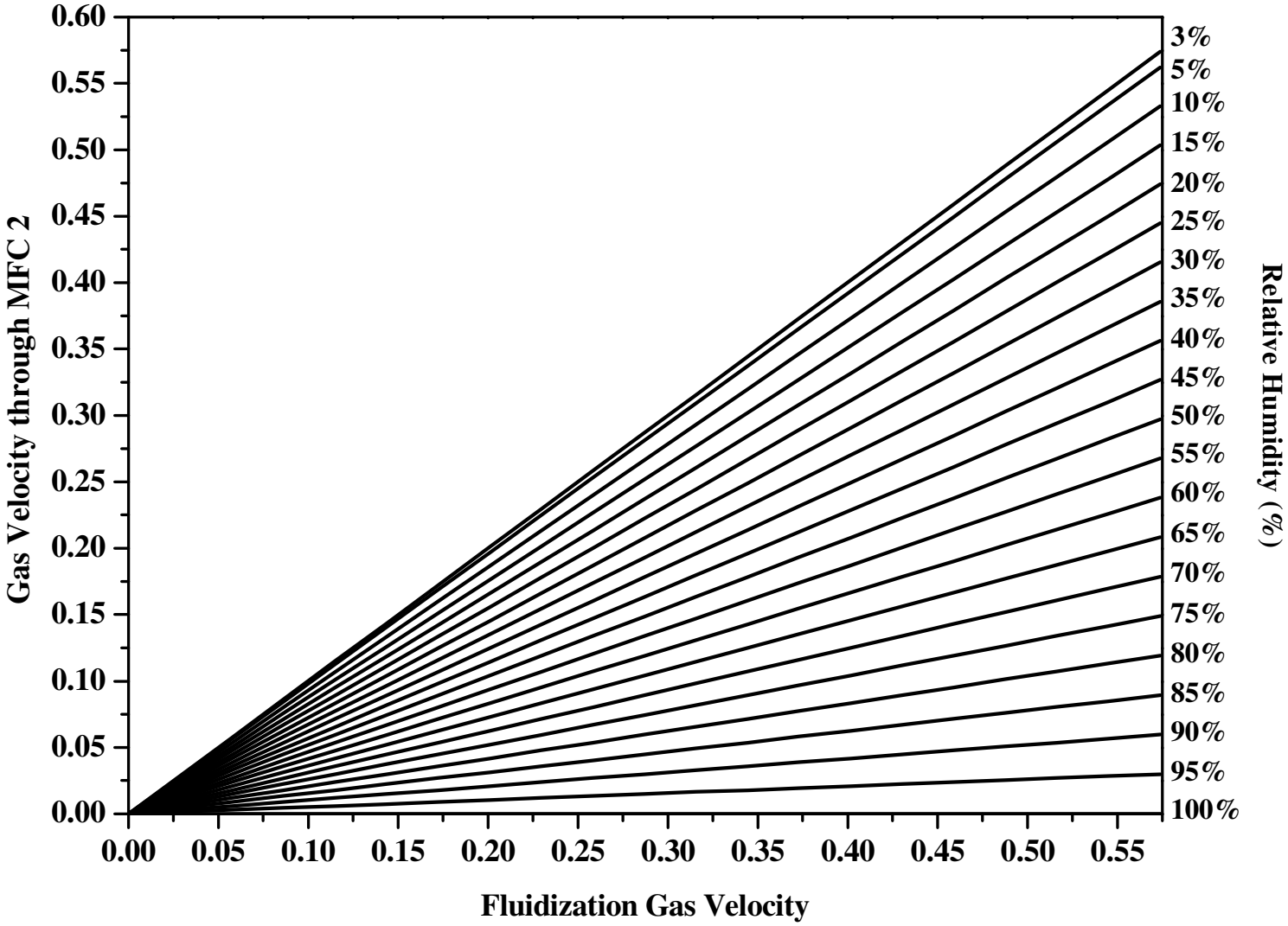

Figure A-5: Humidity reference chart – approximate MFC 2 input values for desired fluidization gas relative humidity and velocity. Note: MFC 1 values were obtained by subtracting MFC 2 from the desired total gas velocity.

Appendix B. Fluidization Time Experimental Data and Additional Graphs

Table B-1: Normalized values for $D_{P\,0.1}$, $D_{P\,0.5}$, and $D_{P\,0.9}$ at 1.5 U_{mf} for all fluidization times.

Fluidization Time min	# of Runs	Initial $D_{P\,0.1}$ µm		Initial $D_{P\,0.5}$ µm		Initial $D_{P\,0.9}$ µm		Fines $D_{P\,0.1}$ µm		Fines $D_{P\,0.5}$ µm		Fines $D_{P\,0.9}$ µm	
15	3	0.46	± 0.01	1.00	± 0.00	2.04	± 0.10	0.05	± 0.01	0.13	± 0.02	0.30	± 0.05
30	3	0.50	± 0.02	1.00	± 0.00	1.94	± 0.07	0.05	± 0.01	0.11	± 0.01	0.24	± 0.03
60	4	0.48	± 0.01	1.00	± 0.00	2.02	± 0.07	0.05	± 0.00	0.12	± 0.01	0.32	± 0.03
120	3	0.49	± 0.00	1.00	± 0.00	1.96	± 0.10	0.05	± 0.01	0.13	± 0.02	0.31	± 0.03
180	3	0.52	± 0.01	1.00	± 0.00	1.86	± 0.05	0.04	± 0.00	0.11	± 0.01	0.27	± 0.02
360	3	0.47	± 0.01	1.00	± 0.00	2.00	± 0.07	0.05	± 0.02	0.13	± 0.02	0.32	± 0.04

Fluidization Time min	# of Runs	Dropped $D_{P\,0.1}$ µm		Dropped $D_{P\,0.5}$ µm		Dropped $D_{P\,0.9}$ µm		Wall $D_{P\,0.1}$ µm		Wall $D_{P\,0.5}$ µm		Wall $D_{P\,0.9}$ µm	
15	3	0.43	± 0.05	0.91	± 0.06	1.87	± 0.10	0.24	± 0.04	0.46	± 0.03	0.84	± 0.02
30	3	0.43	± 0.08	0.88	± 0.09	1.80	± 0.13	0.26	± 0.03	0.40	± 0.02	0.63	± 0.01
60	4	0.47	± 0.04	0.94	± 0.07	1.93	± 0.14	0.28	± 0.03	0.42	± 0.06	0.65	± 0.13
120	3	0.49	± 0.02	0.95	± 0.05	1.88	± 0.07	0.28	± 0.02	0.44	± 0.03	0.66	± 0.05
180	3	0.47	± 0.08	0.87	± 0.11	1.67	± 0.15	0.25	± 0.01	0.37	± 0.02	0.54	± 0.04
360	3	0.51	± 0.03	0.98	± 0.06	1.98	± 0.13	0.29	± 0.01	0.45	± 0.02	0.70	± 0.03

Fluidization Time min	# of Runs	Bottom Column $D_{P\,0.1}$ µm		Bottom Column $D_{P\,0.5}$ µm		Bottom Column $D_{P\,0.9}$ µm		Intermediate Wall $D_{P\,0.1}$ µm		Intermediate Wall $D_{P\,0.5}$ µm		Intermediate Wall $D_{P\,0.9}$ µm	
15	2	0.20	± 0.03	0.38	± 0.03	0.67	± 0.02	-	-	-	-	-	-
30	3	0.17	± 0.01	0.29	± 0.05	0.49	± 0.13	-	-	-	-	-	-
60	1	0.33	-	0.51	-	0.77	-	-	-	-	-	-	-
120	3	0.20	± 0.03	0.34	± 0.05	0.57	± 0.08	0.43	± 0.02	0.61	± 0.04	0.86	± 0.08
180	3	0.19	± 0.02	0.32	± 0.04	0.54	± 0.08	0.41	± 0.02	0.57	± 0.03	0.79	± 0.05
360	3	0.21	± 0.05	0.38	± 0.12	0.67	± 0.25	-	-	-	-	-	-

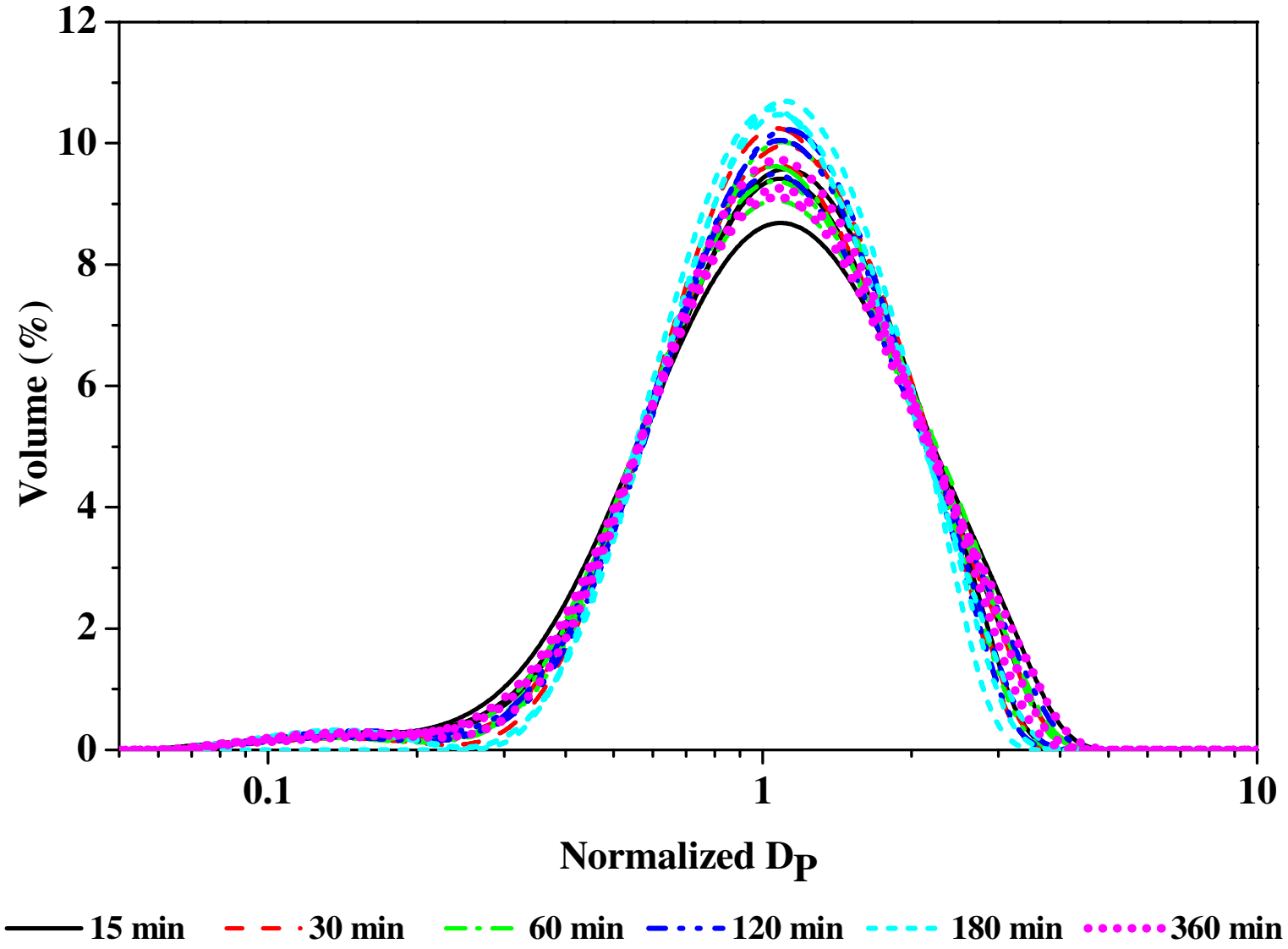

Figure B-1: Normalized PSDs at 1.5 U_{mf} for Initial region for different fluidization times.

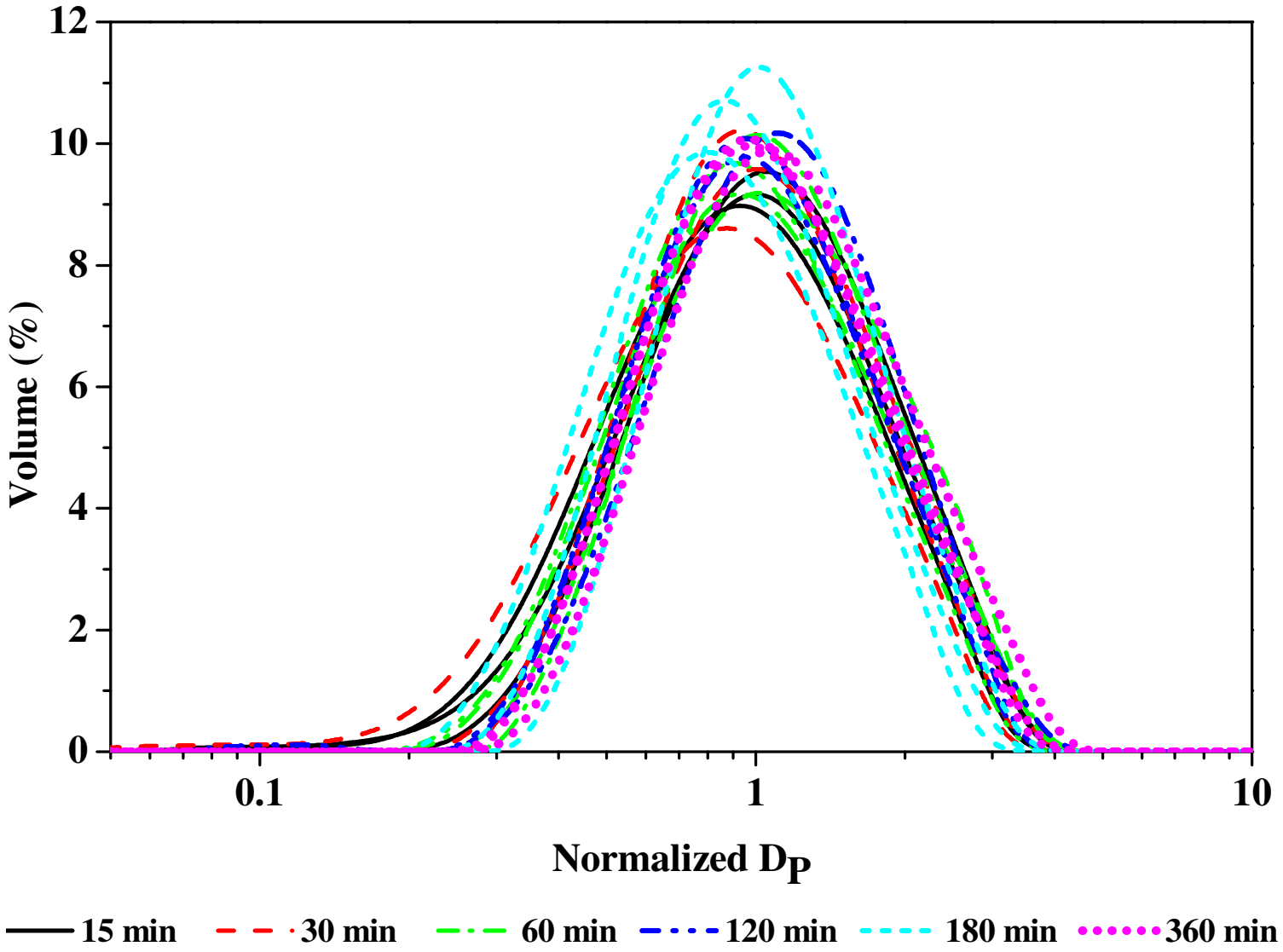

Figure B-2: Normalized PSDs at 1.5 U_{mf} for Dropped region for different fluidization times.

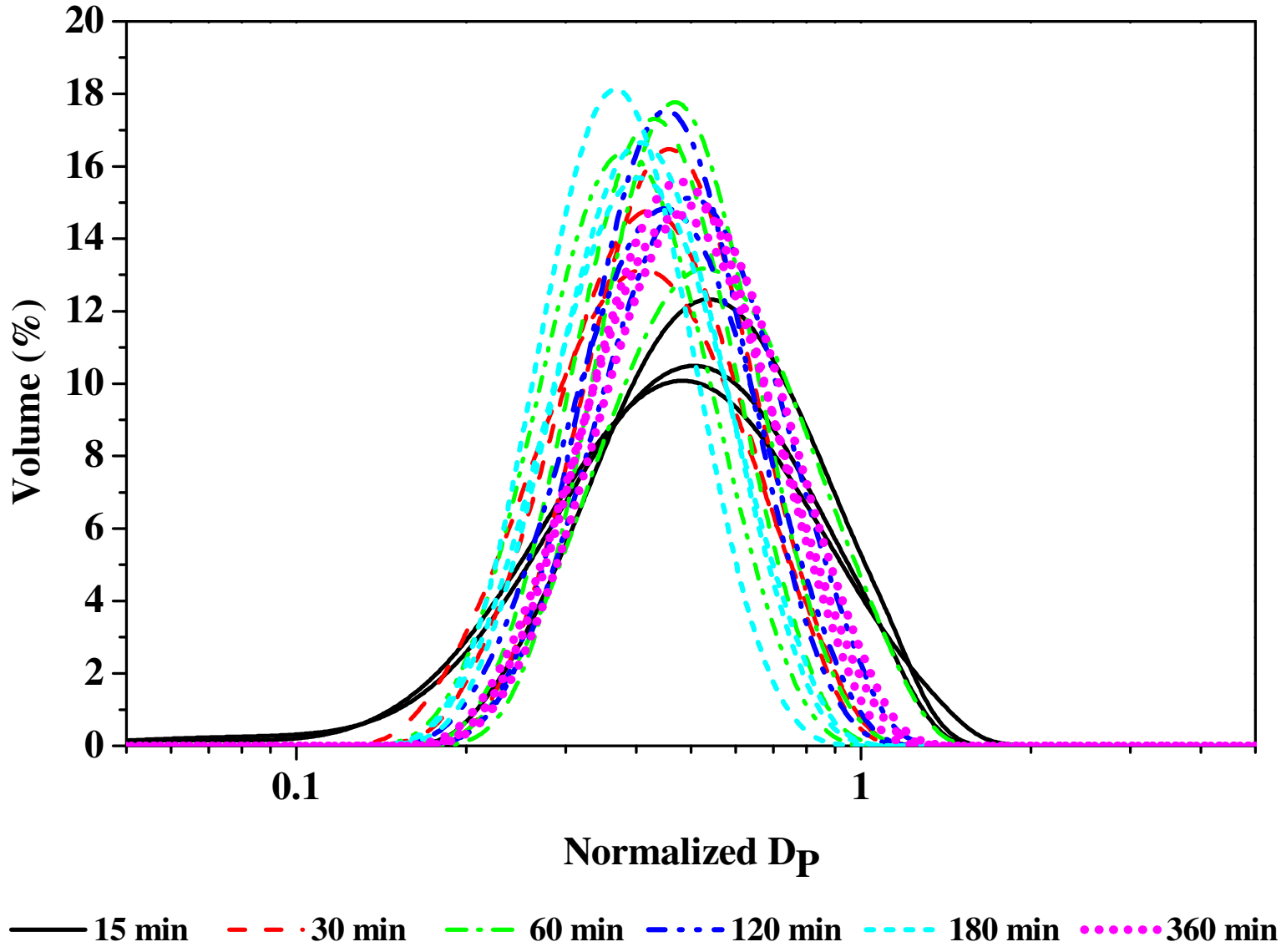

Figure B-3: Normalized PSDs at 1.5 U_{mf} for Wall region for different fluidization times.

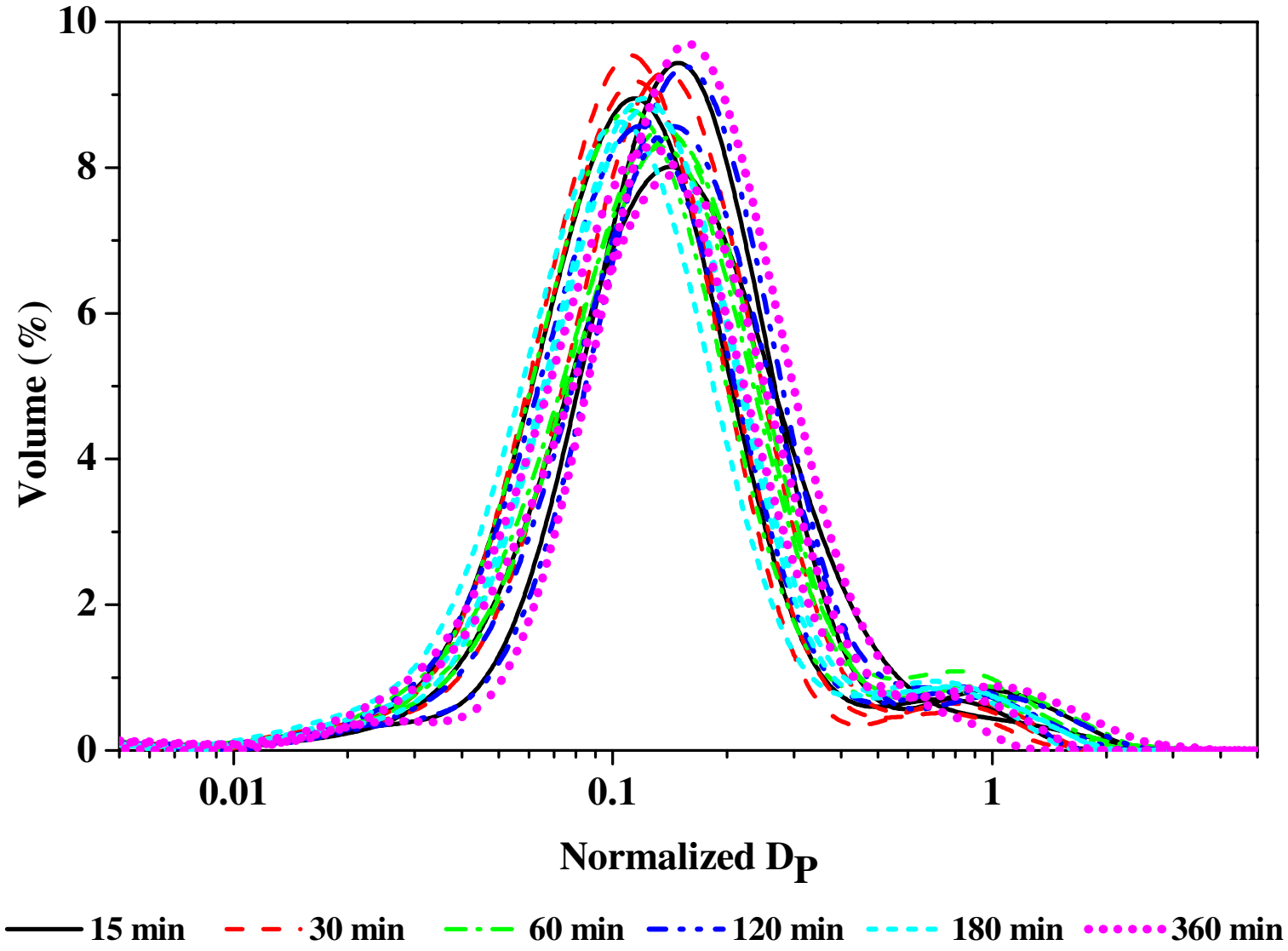

Figure B-4: Normalized PSDs at 1.5 U_{mf} for Fines region for different fluidization times.

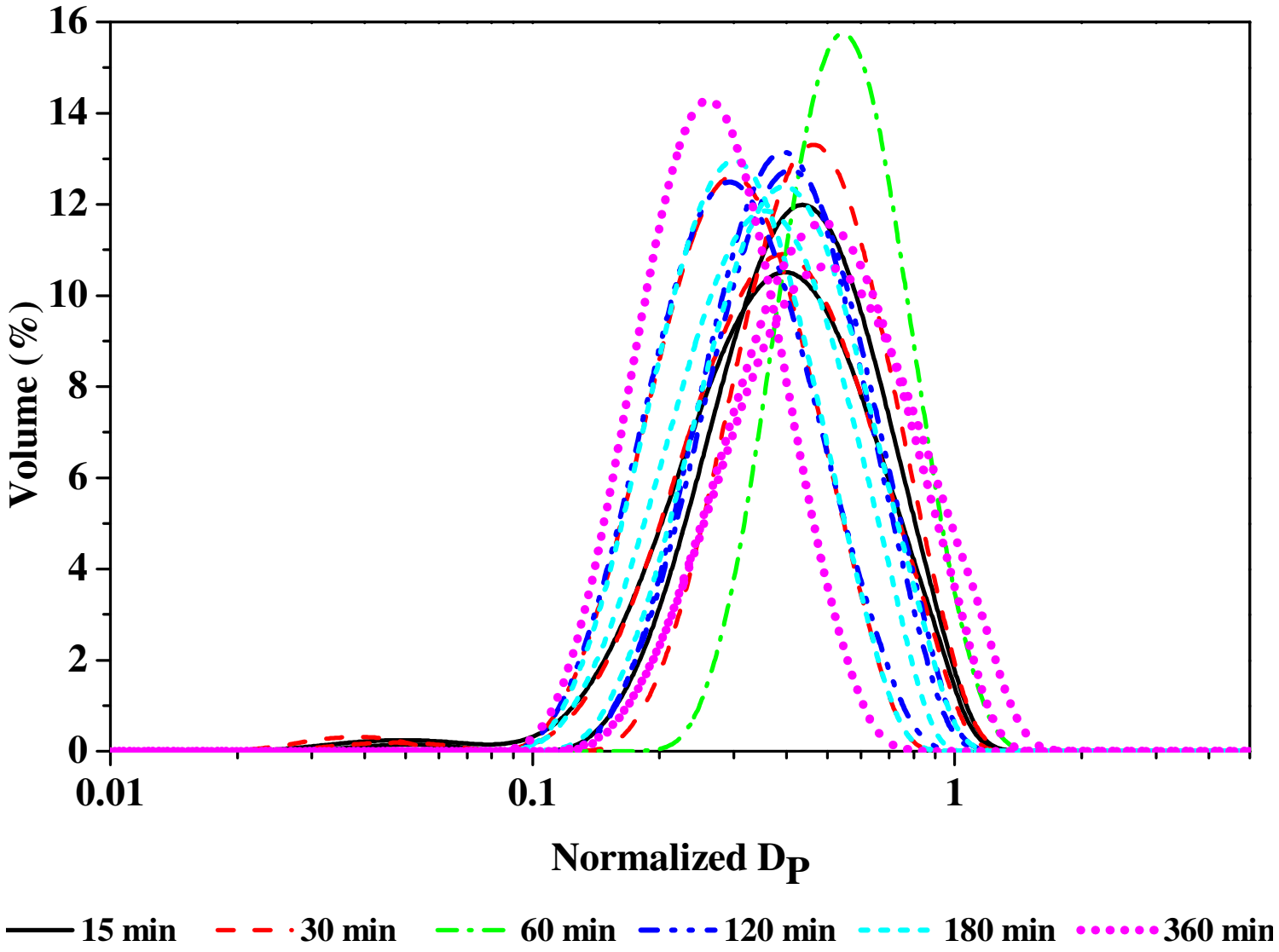

Figure B-5: Normalized PSDs at 1.5 U_{mf} for Bottom Column region for different fluidization times.

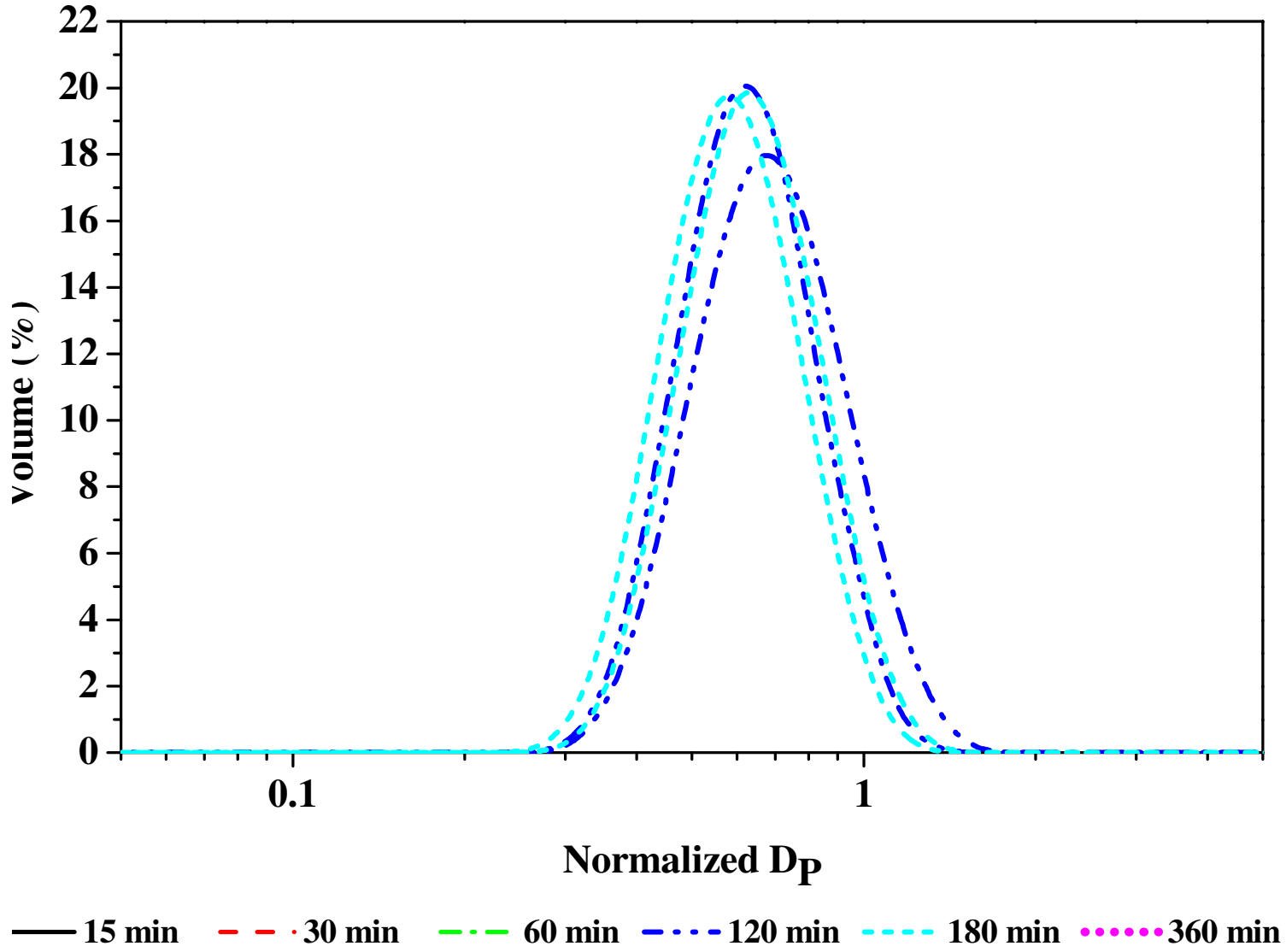

Figure B-6: Normalized PSDs at 1.5 U_{mf} for Intermediate Wall region for different fluidization times.

Table B-2: Normalized values for $D_{P\,0.1}$, $D_{P\,0.5}$, and $D_{P\,0.9}$ at 1.75 U_{mf} for all fluidization times.

Fluidization Time min	# of Runs	Initial $D_{P\,0.1}$ µm		Initial $D_{P\,0.5}$ µm		Initial $D_{P\,0.9}$ µm		Fines $D_{P\,0.1}$ µm		Fines $D_{P\,0.5}$ µm		Fines $D_{P\,0.9}$ µm	
15	3	0.49	± 0.03	1.00	± 0.00	1.90	± 0.18	0.04	± 0.00	0.11	± 0.01	0.29	± 0.01
30	3	0.47	± 0.01	1.00	± 0.00	1.95	± 0.03	0.04	± 0.01	0.11	± 0.02	0.27	± 0.05
60	3	0.48	± 0.04	1.00	± 0.00	1.93	± 0.15	0.05	± 0.01	0.12	± 0.02	0.31	± 0.04
120	3	0.44	± 0.00	1.00	± 0.00	2.07	± 0.03	0.04	± 0.01	0.12	± 0.01	0.29	± 0.02
180	3	0.43	± 0.01	1.00	± 0.00	2.10	± 0.04	0.05	± 0.01	0.14	± 0.01	0.44	± 0.08
360	3	0.45	± 0.02	1.00	± 0.00	2.02	± 0.06	0.04	± 0.00	0.12	± 0.01	0.29	± 0.01

Fluidization Time min	# of Runs	Dropped $D_{P\,0.1}$ µm		Dropped $D_{P\,0.5}$ µm		Dropped $D_{P\,0.9}$ µm		Wall $D_{P\,0.1}$ µm		Wall $D_{P\,0.5}$ µm		Wall $D_{P\,0.9}$ µm	
15	3	0.36	± 0.05	0.82	± 0.12	1.72	± 0.24	0.20	± 0.04	0.37	± 0.06	0.64	± 0.18
30	3	0.42	± 0.02	0.87	± 0.06	1.77	± 0.16	0.23	± 0.05	0.46	± 0.10	0.92	± 0.27
60	3	0.49	± 0.13	0.94	± 0.24	1.85	± 0.46	0.27	± 0.06	0.43	± 0.10	0.69	± 0.22
120	3	0.45	± 0.04	0.93	± 0.03	1.96	± 0.03	0.21	± 0.04	0.37	± 0.02	0.69	± 0.06
180	3	0.53	± 0.06	1.00	± 0.19	1.93	± 0.45	0.26	± 0.03	0.48	± 0.06	0.92	± 0.13
360	3	0.52	± 0.03	1.00	± 0.06	1.96	± 0.13	0.26	± 0.01	0.41	± 0.02	0.65	± 0.04

Fluidization Time min	# of Runs	Bottom Column $D_{P\,0.1}$ µm		Bottom Column $D_{P\,0.5}$ µm		Bottom Column $D_{P\,0.9}$ µm		Intermediate Wall $D_{P\,0.1}$ µm		Intermediate Wall $D_{P\,0.5}$ µm		Intermediate Wall $D_{P\,0.9}$ µm	
15		0.19	± 0.08	0.40	± 0.18	0.73	± 0.31	-	-	-	-	-	-
30		0.21	± 0.06	0.38	± 0.12	0.67	± 0.23	-	-	-	-	-	-
60		0.15	-	0.32	-	0.61	-	-	-	-	-	-	-
120		0.18	± 0.06	0.37	± 0.07	0.72	± 0.11	-	-	-	-	-	-
180		0.20	± 0.04	0.39	± 0.06	0.71	± 0.06	-	-	-	-	-	-
360		0.22	± 0.01	0.41	± 0.01	0.72	± 0.04	0.47	-	0.68	-	0.97	-

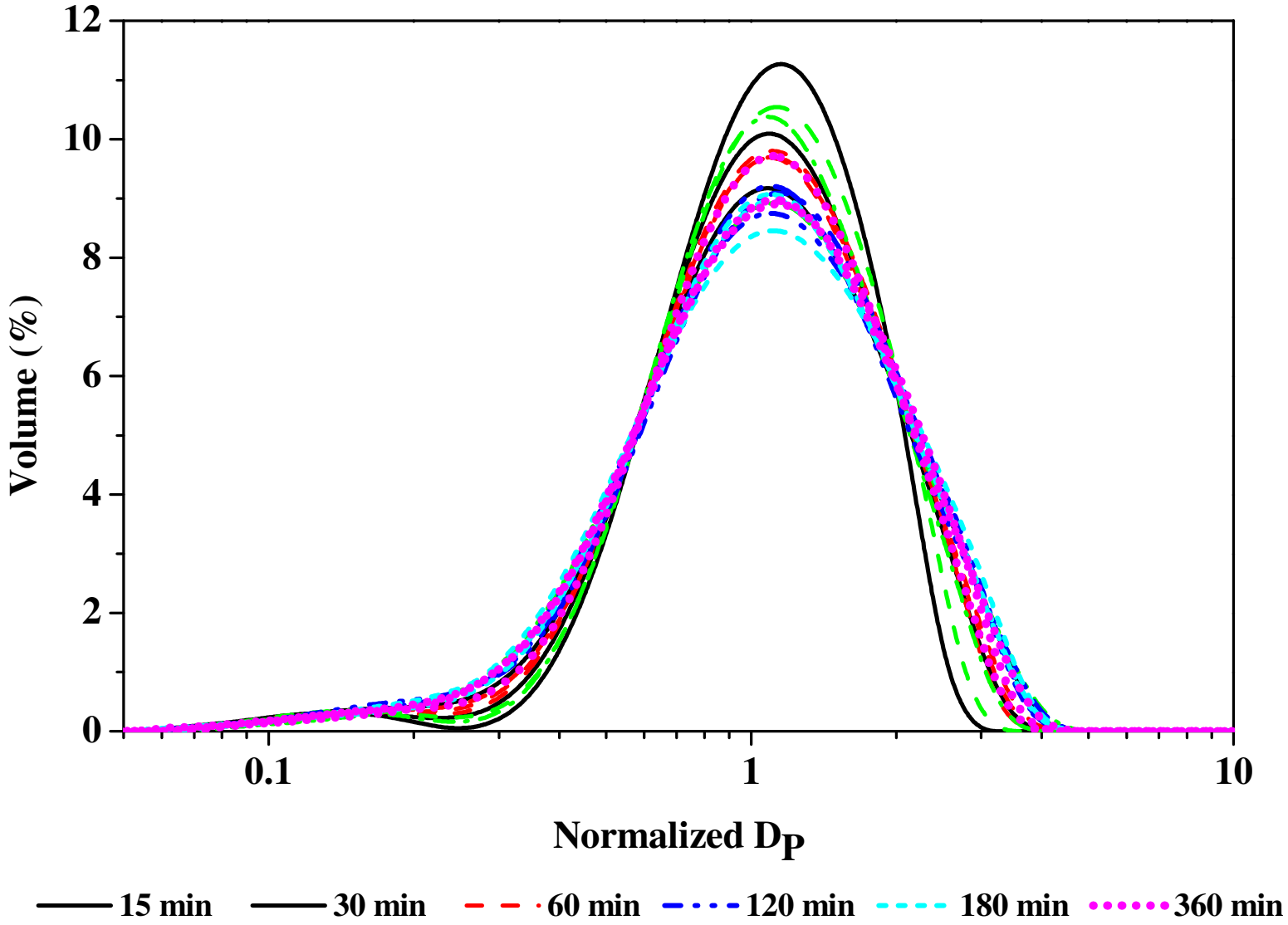

Figure B-7: Normalized PSDs at 1.75 U_{mf} for Initial region for different fluidization times.

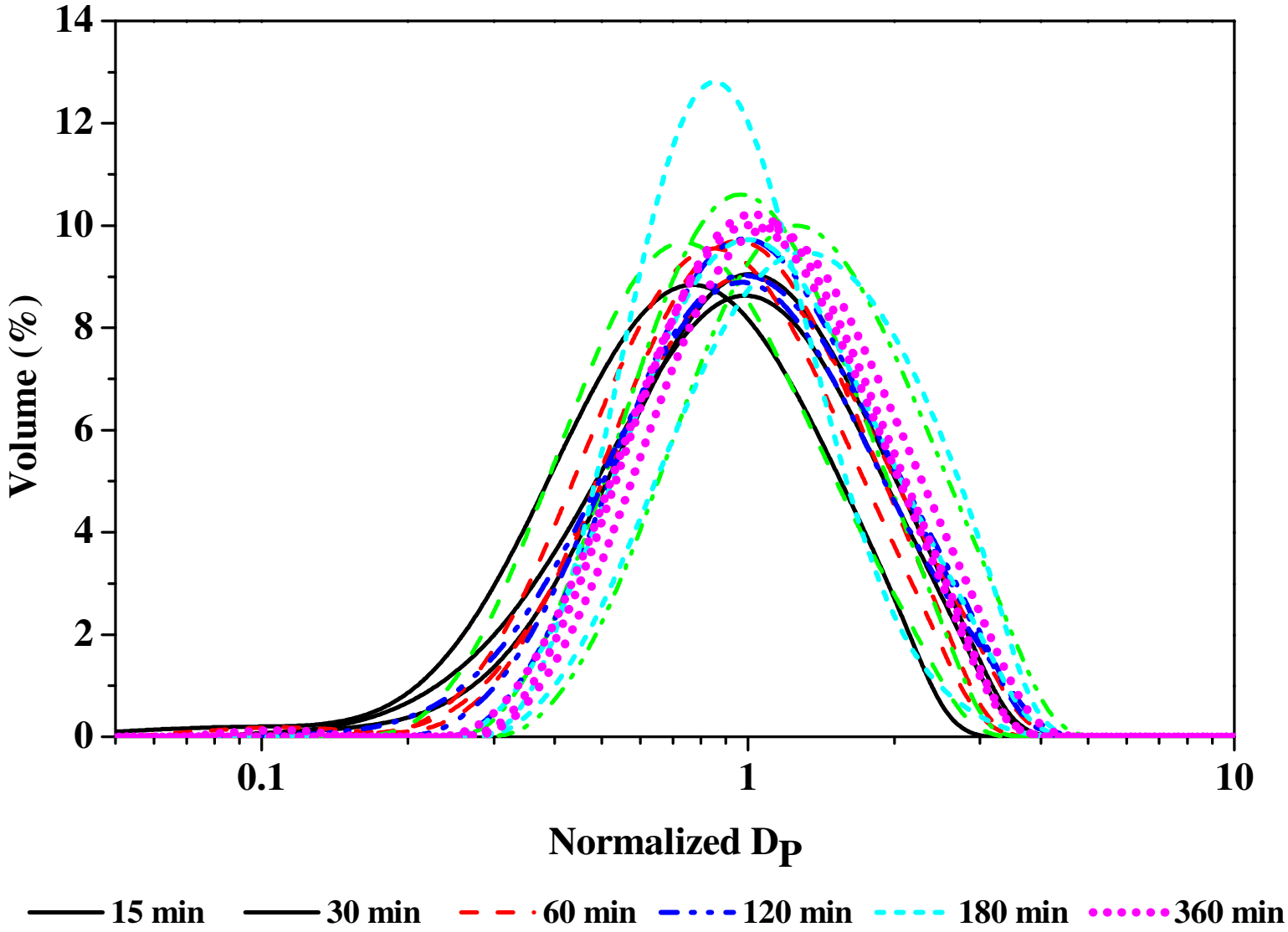

Figure B-8: Normalized PSDs at 1.75 U_{mf} for Dropped region for different fluidization times.

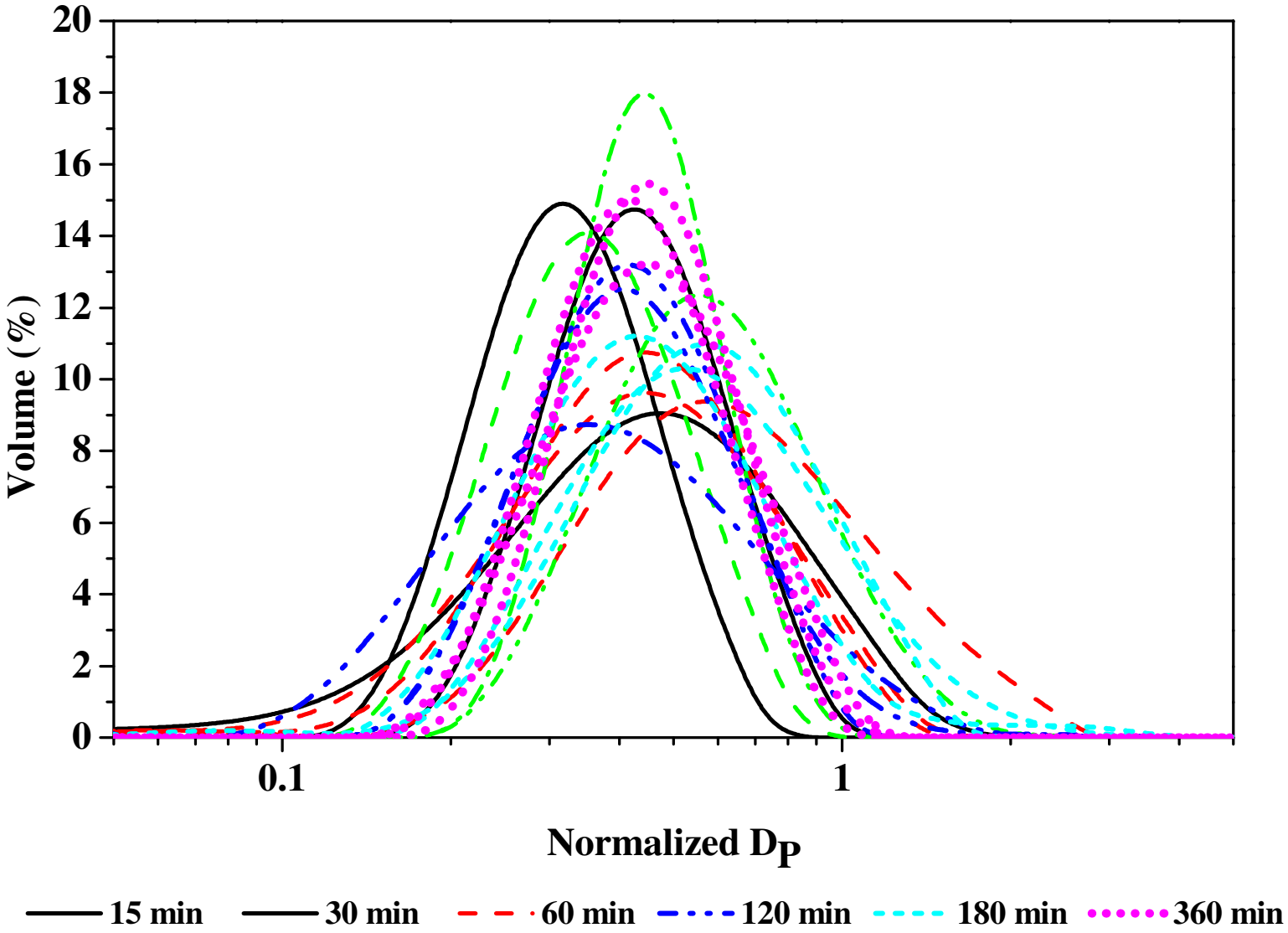

Figure B-9: Normalized PSDs at 1.75 U_{mf} for Wall region for different fluidization times.

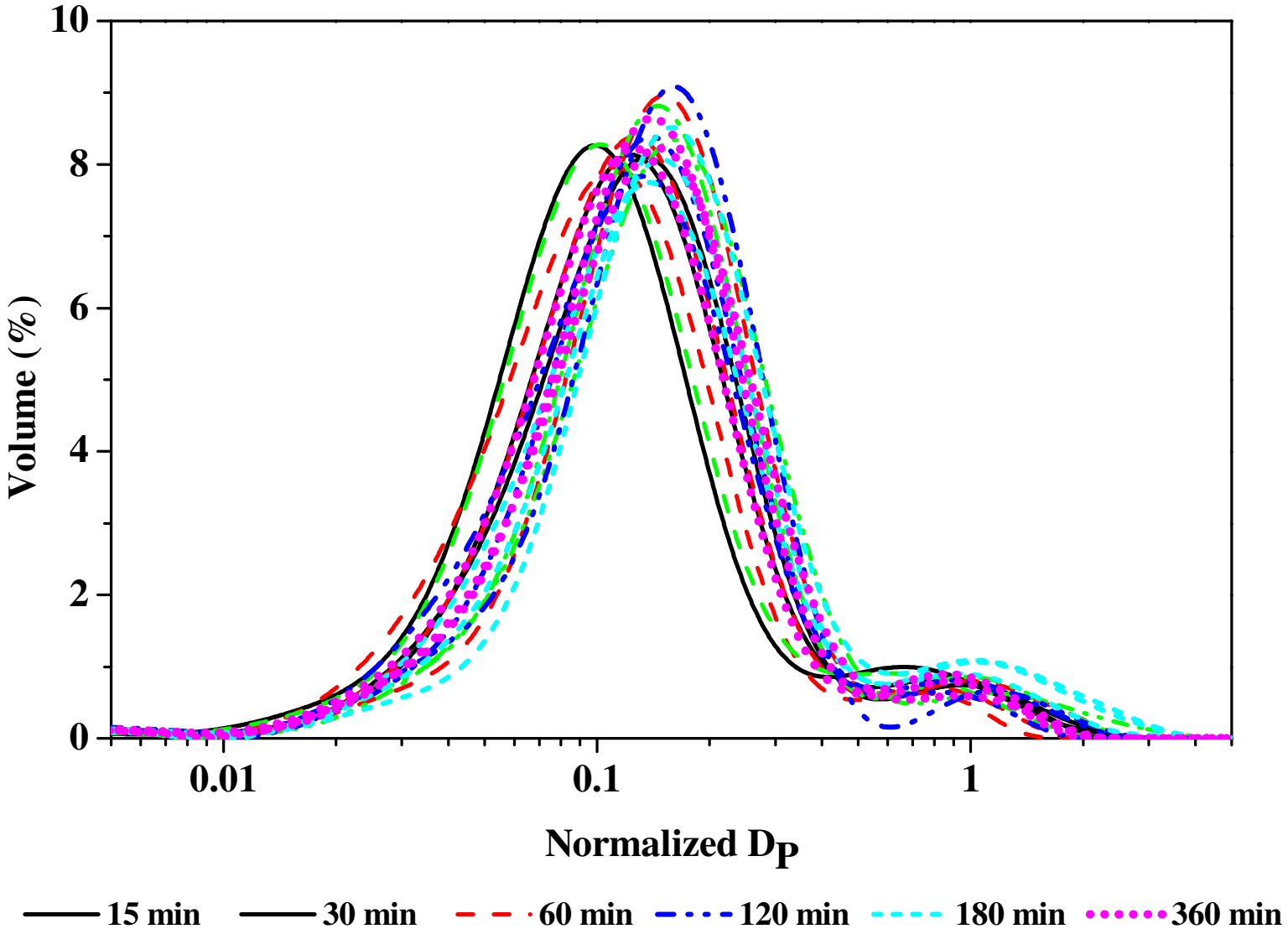

Figure B-10: Normalized PSDs at 1.75 U_{mf} for Fines region for different fluidization times.

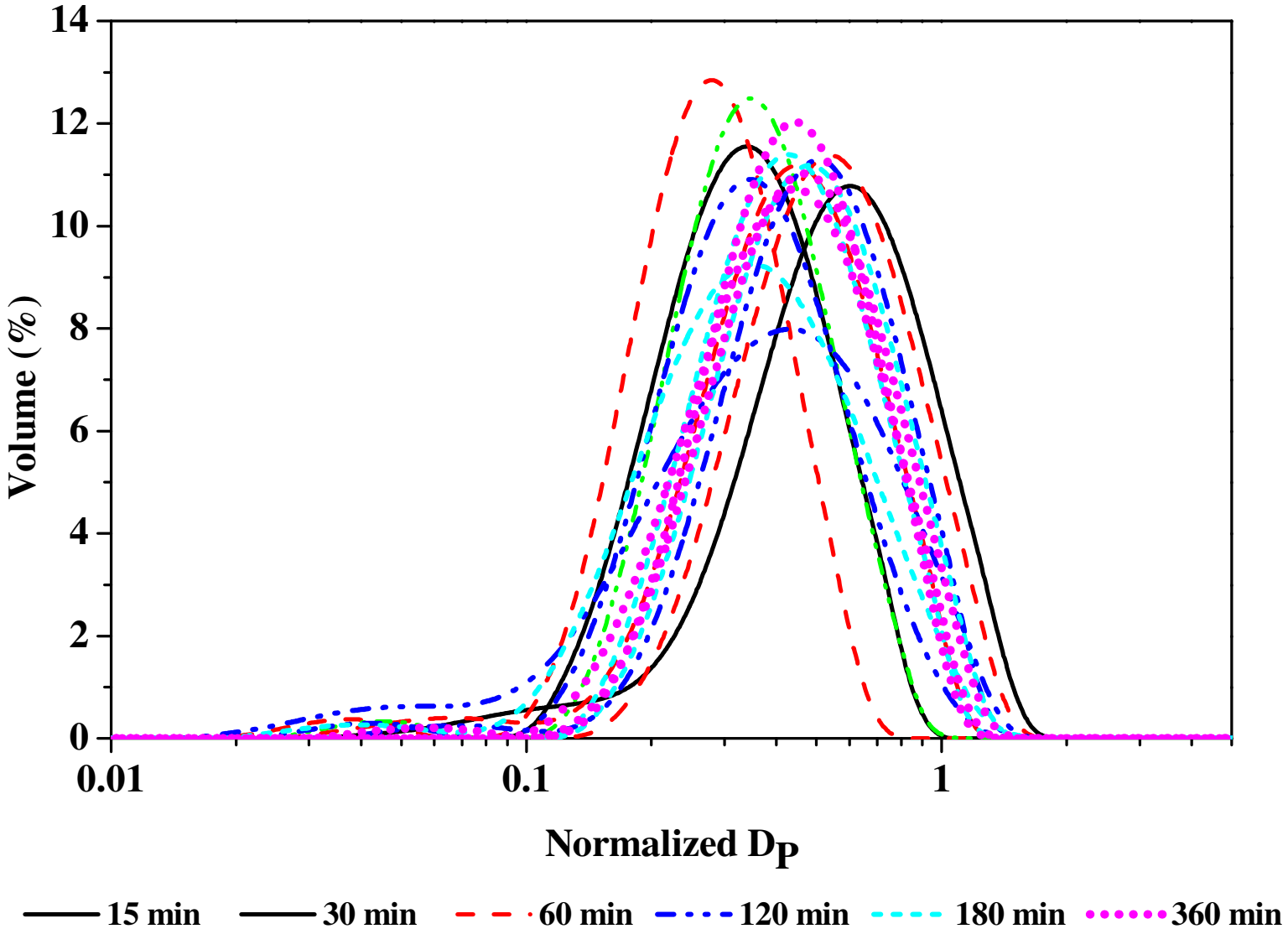

Figure B-11: Normalized PSDs at 1.75 U_{mf} for Bottom Column region for different fluidization times.

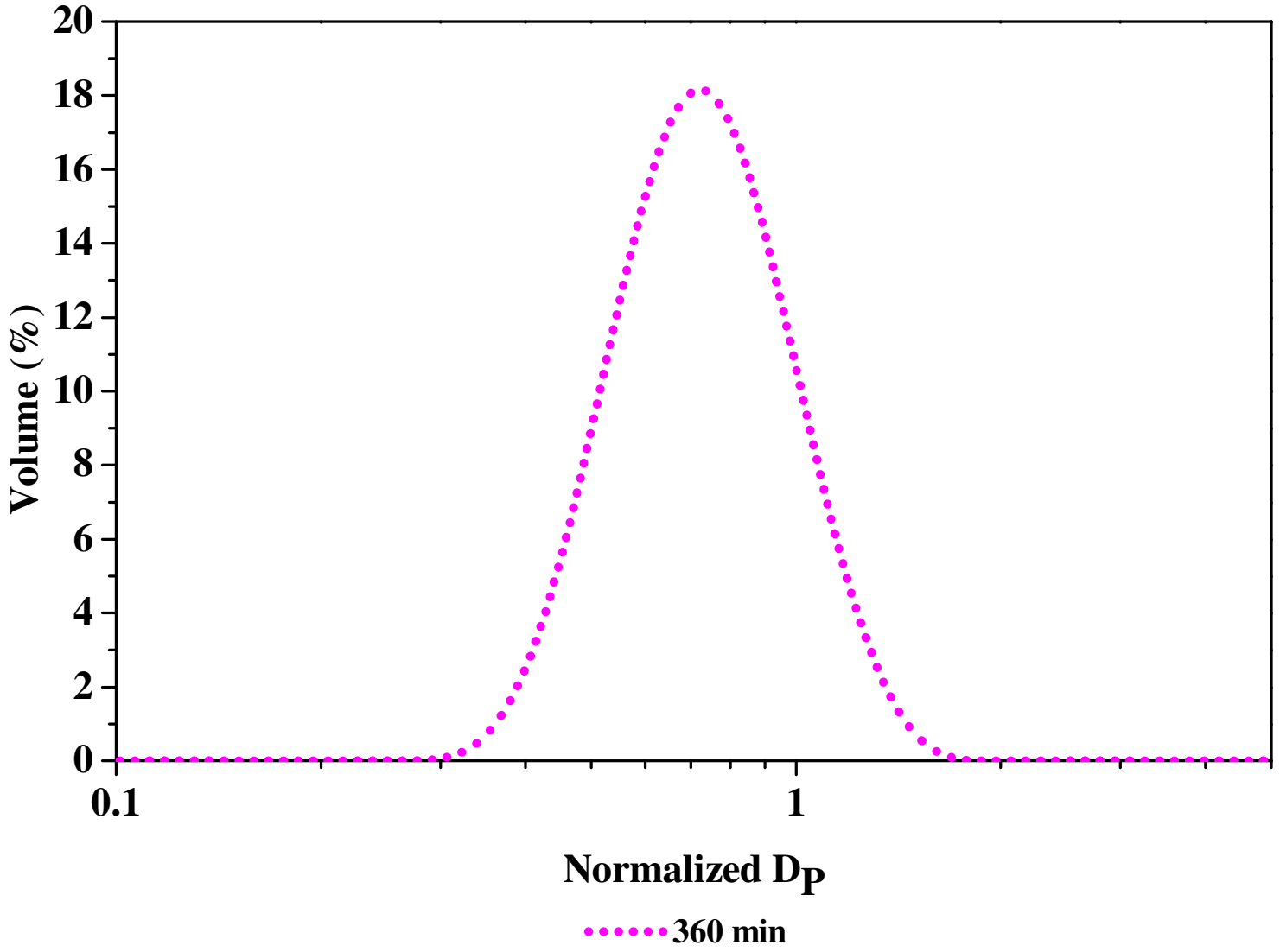

Figure B-12: Normalized PSDs at 1.75 U_{mf} for Intermediate Column region for different fluidization times.

Table B-3: Normalized values for $D_{P\,0.1}$, $D_{P\,0.5}$, and $D_{P\,0.9}$ at 3.5 U_{mf} for all fluidization times.

Fluidization Time min	# of Runs	Initial $D_{P\,0.1}$ µm		Initial $D_{P\,0.5}$ µm		Initial $D_{P\,0.9}$ µm		Fines $D_{P\,0.1}$ µm		Fines $D_{P\,0.5}$ µm		Fines $D_{P\,0.9}$ µm	
15	3	0.43	± 0.03	1.00	± 0.00	2.05	± 0.19	0.09	± 0.03	0.19	± 0.05	0.34	± 0.08
30	3	0.44	± 0.01	1.00	± 0.00	2.04	± 0.11	0.09	± 0.01	0.20	± 0.02	0.35	± 0.04
60	3	0.45	± 0.02	1.00	± 0.00	2.10	± 0.08	0.10	± 0.02	0.21	± 0.02	0.39	± 0.02
120	3	0.46	± 0.02	1.00	± 0.00	2.01	± 0.04	0.09	± 0.00	0.19	± 0.00	0.35	± 0.02
180	3	0.44	± 0.04	1.00	± 0.00	2.08	± 0.10	0.10	± 0.01	0.21	± 0.02	0.38	± 0.04
360	3	0.42	± 0.04	1.00	± 0.00	2.01	± 0.09	0.10	± 0.01	0.20	± 0.02	0.35	± 0.03

Fluidization Time min	# of Runs	Dropped $D_{P\,0.1}$ µm		Dropped $D_{P\,0.5}$ µm		Dropped $D_{P\,0.9}$ µm		Wall $D_{P\,0.1}$ µm		Wall $D_{P\,0.5}$ µm		Wall $D_{P\,0.9}$ µm	
15	3	0.42	± 0.13	0.91	± 0.23	1.93	± 0.47	0.19	± 0.04	0.44	± 0.14	0.92	± 0.30
30	3	0.45	± 0.07	0.98	± 0.13	2.04	± 0.25	0.29	± 0.07	0.57	± 0.06	1.01	± 0.10
60	3	0.48	± 0.09	0.95	± 0.17	1.86	± 0.42	0.40	± 0.10	0.66	± 0.06	1.04	± 0.17
120	3	0.39	± 0.07	0.91	± 0.11	1.92	± 0.17	0.22	± 0.03	0.44	± 0.07	0.80	± 0.12
180	3	0.49	± 0.03	1.03	± 0.07	2.11	± 0.19	0.29	± 0.06	0.54	± 0.07	0.94	± 0.10
360	3	0.40	± 0.17	0.96	± 0.19	1.98	± 0.28	0.28	± 0.05	0.54	± 0.08	0.98	± 0.14

Fluidization Time min	# of Runs	Bottom Column $D_{P\,0.1}$ µm		Bottom Column $D_{P\,0.5}$ µm		Bottom Column $D_{P\,0.9}$ µm		Top Column $D_{P\,0.1}$ µm		Top Column $D_{P\,0.5}$ µm		Top Column $D_{P\,0.9}$ µm	
15	3	0.19	± 0.04	0.45	± 0.13	0.97	± 0.26	0.11	± 0.03	0.20	± 0.05	0.34	± 0.07
30	3	0.16	± 0.04	0.36	± 0.10	0.69	± 0.21	0.11	± 0.02	0.21	± 0.03	0.36	± 0.06
60	1	0.20	-	0.42	-	0.78	-	0.08	-	0.18	-	0.38	-
120	3	0.15	± 0.02	0.38	± 0.06	0.73	± 0.09	0.09	± 0.00	0.20	± 0.01	0.38	± 0.02
180	3	0.14	± 0.01	0.34	± 0.02	0.63	± 0.07	0.13	± 0.03	0.23	± 0.04	0.39	± 0.04
360	3	0.19	± 0.04	0.40	± 0.06	0.73	± 0.12	0.11	± 0.02	0.21	± 0.02	0.38	± 0.05

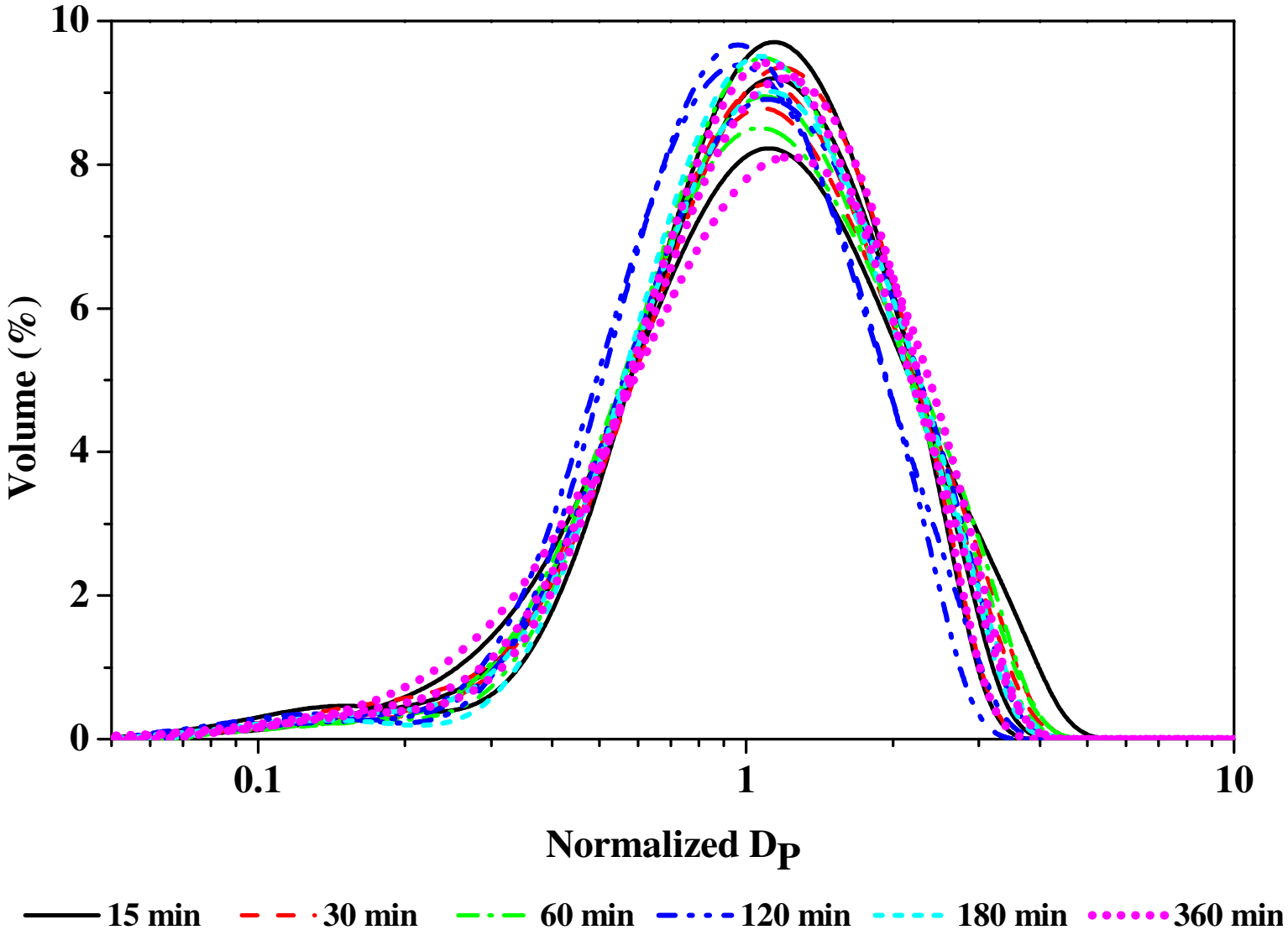

Figure B-13: Normalized PSDs at 3.5 U_{mf} for Initial region for different fluidization times.

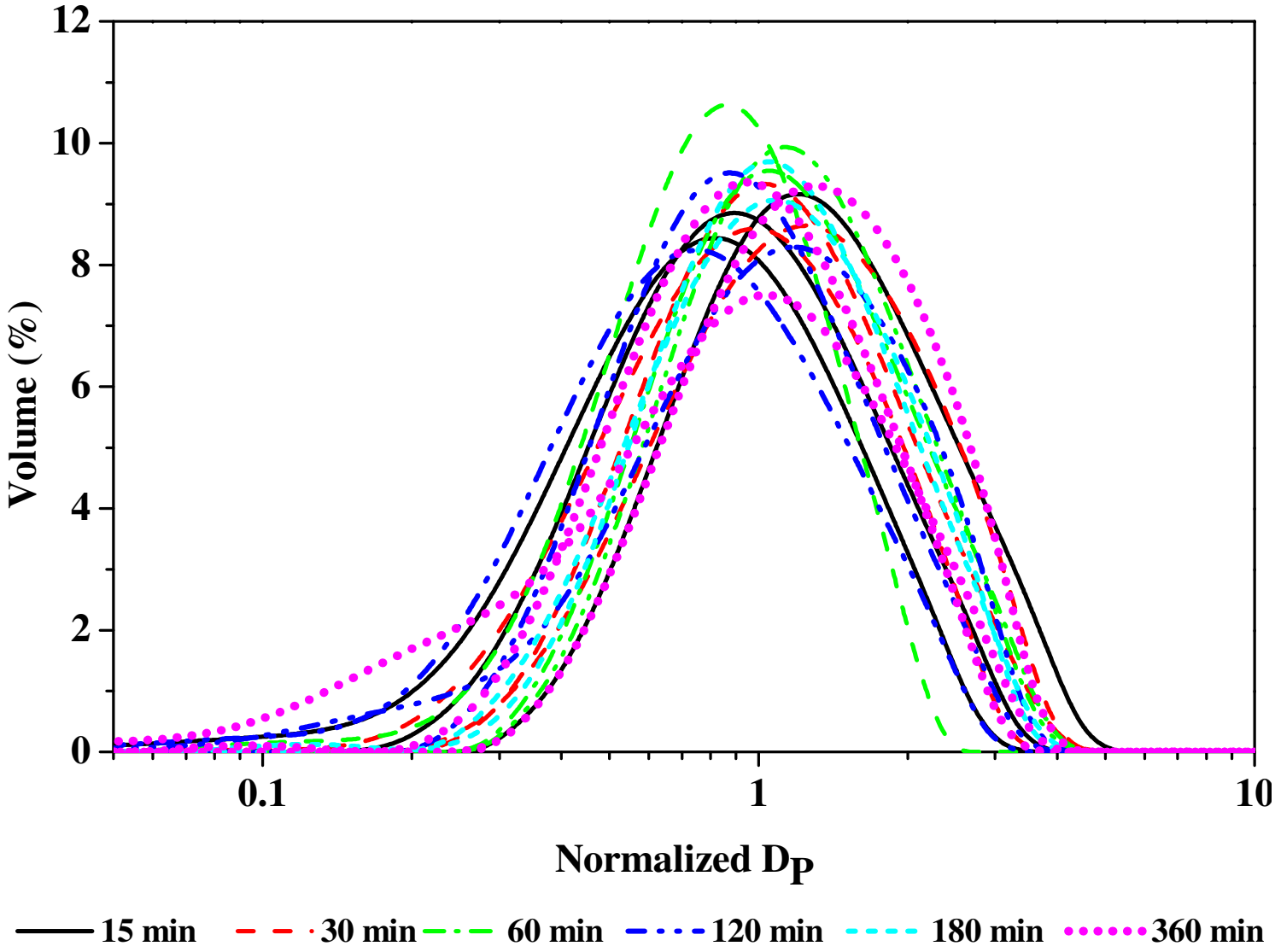

Figure B-14: Normalized PSDs at 3.5 U_{mf} for Dropped region for different fluidization times.

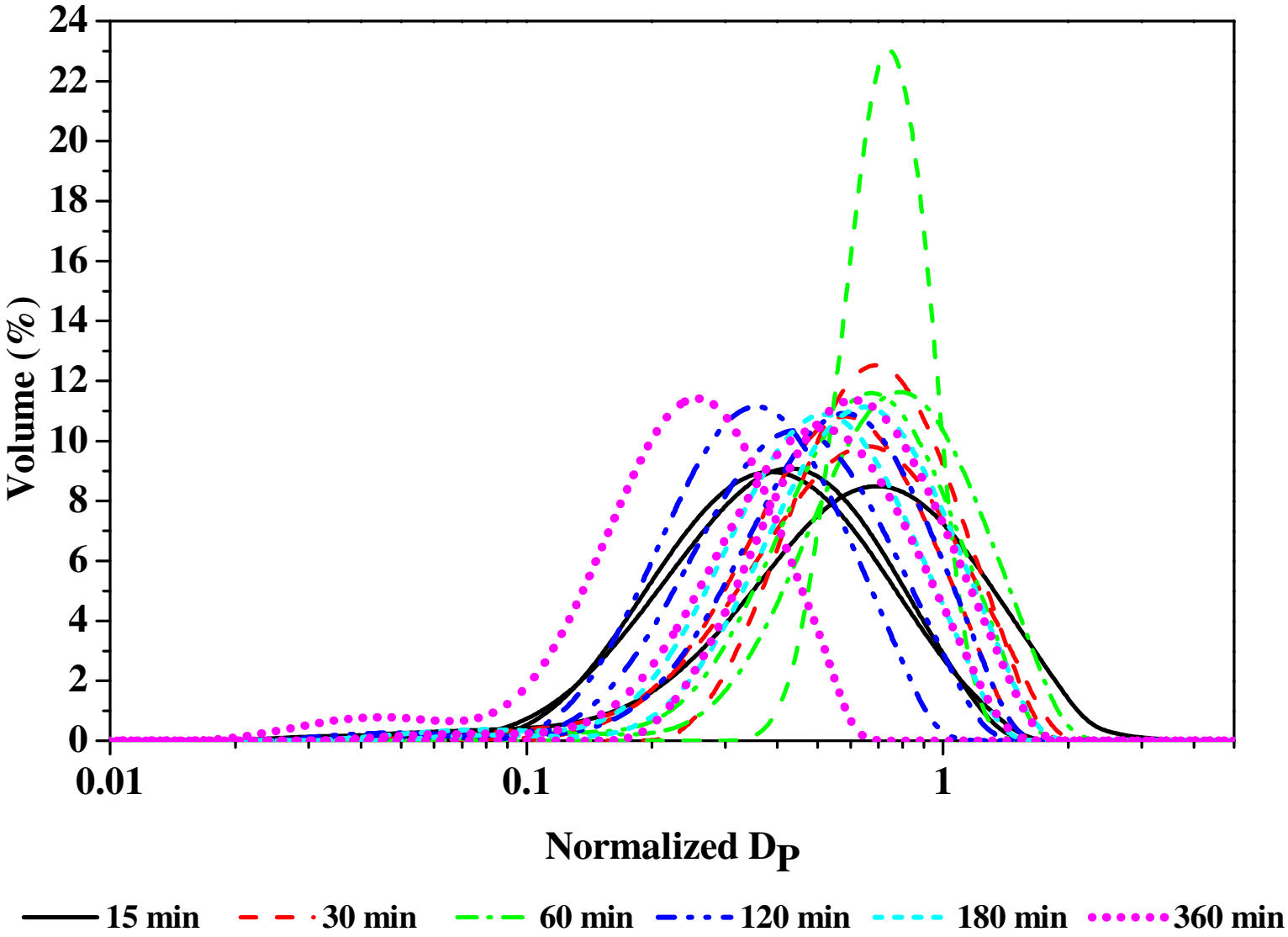

Figure B-15: Normalized PSDs at 3.5 U_{mf} for Wall region for different fluidization times.

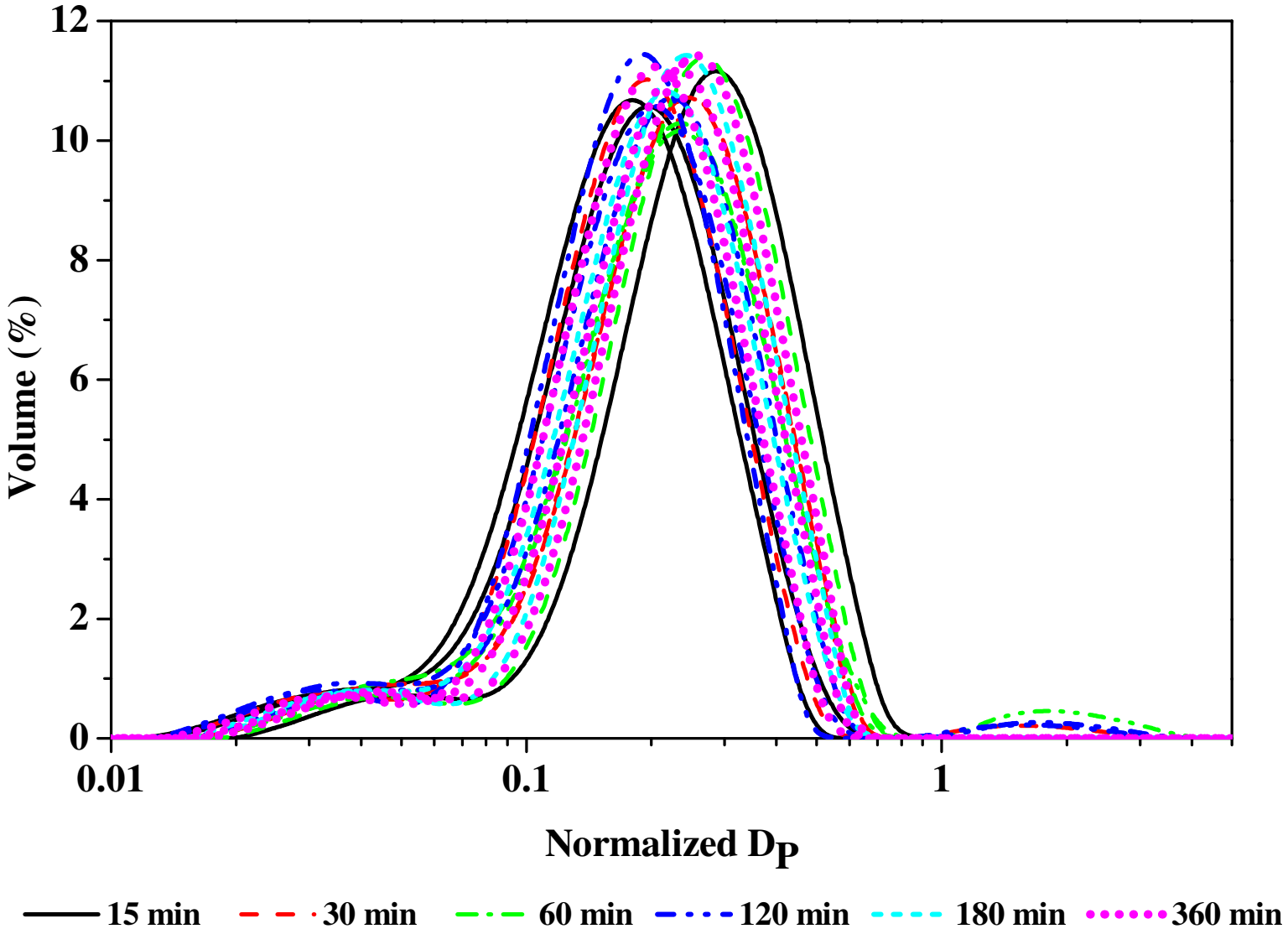

Figure B-16: Normalized PSDs at 3.5 U_{mf} for Fines region for different fluidization times.

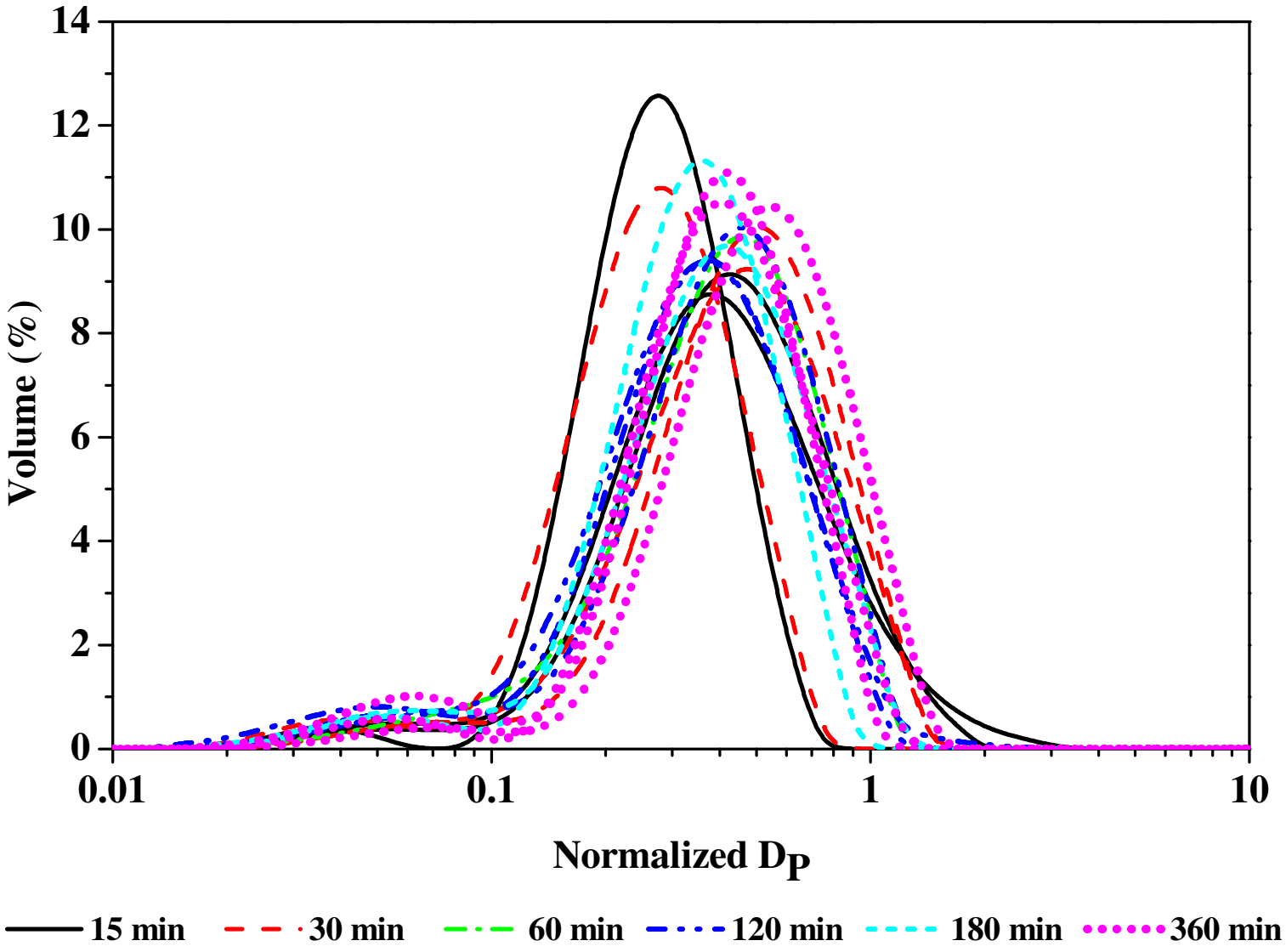

Figure B-17: Normalized PSDs at 3.5 U_{mf} for Bottom Column region for different fluidization times.

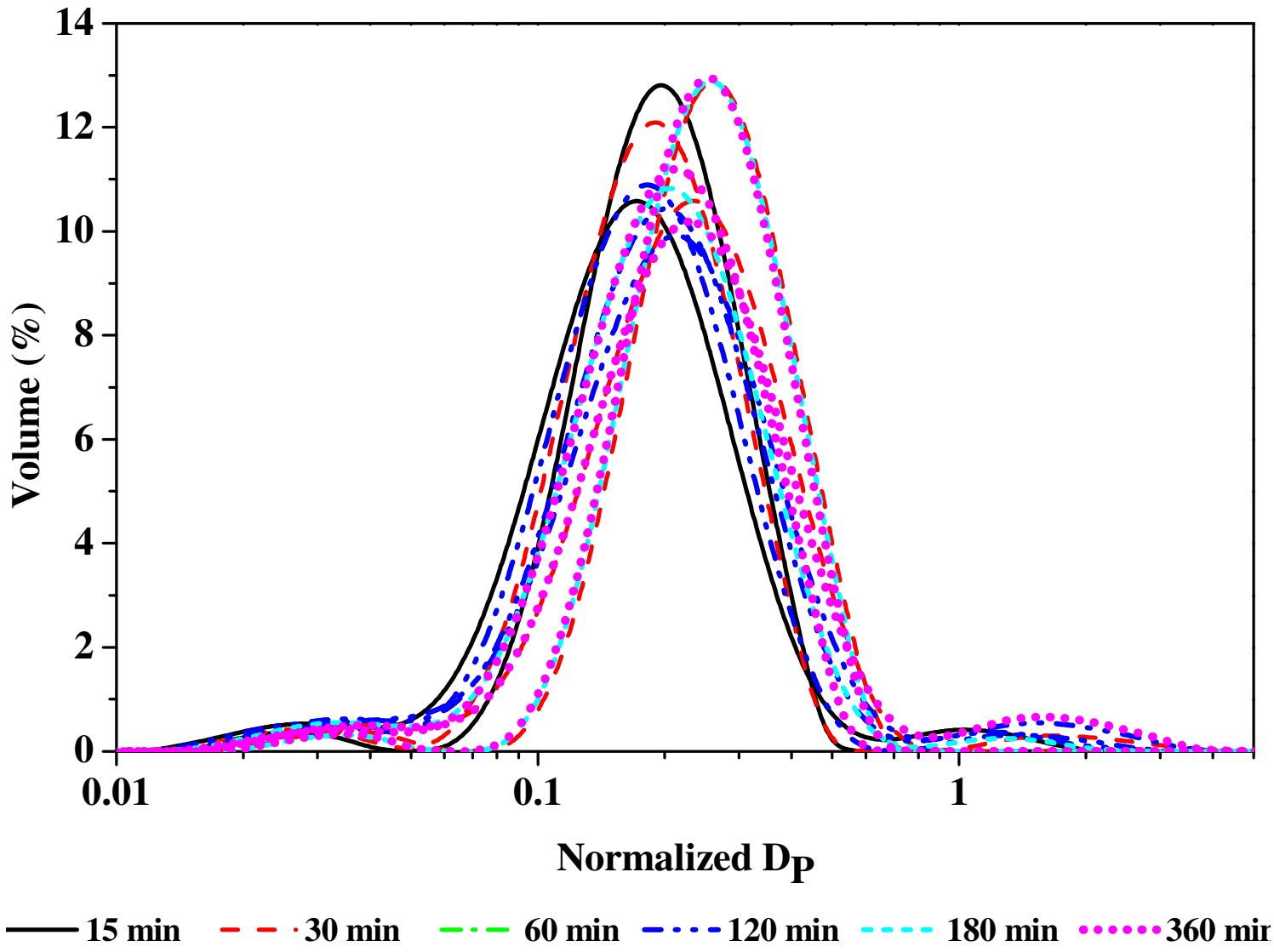

Figure B-18: Normalized PSDs at 3.5 U_{mf} for Top Column region for different fluidization times.

Table B-4: Normalized values for $D_{P\,0.1}$, $D_{P\,0.5}$, and $D_{P\,0.9}$ at 4 U_{mf} for all fluidization times.

Fluidization Time min	# of Runs	Initial $D_{P\,0.1}$ µm		Initial $D_{P\,0.5}$ µm		Initial $D_{P\,0.9}$ µm		Fines $D_{P\,0.1}$ µm		Fines $D_{P\,0.5}$ µm		Fines $D_{P\,0.9}$ µm	
15	3	0.47	± 0.02	1.00	± 0.00	1.98	± 0.05	0.10	± 0.01	0.22	± 0.02	0.39	± 0.03
30	3	0.45	± 0.01	1.00	± 0.00	1.99	± 0.05	0.10	± 0.01	0.22	± 0.01	0.38	± 0.02
60	3	0.48	± 0.01	1.00	± 0.00	1.97	± 0.03	0.12	± 0.01	0.24	± 0.02	0.41	± 0.04
120	5	0.47	± 0.02	1.00	± 0.00	1.94	± 0.10	0.11	± 0.03	0.23	± 0.05	0.40	± 0.09
180	3	0.48	± 0.02	1.00	± 0.00	1.96	± 0.04	0.12	± 0.01	0.24	± 0.02	0.47	± 0.11
360	3	0.48	± 0.02	1.00	± 0.00	1.94	± 0.10	0.11	± 0.01	0.22	± 0.02	0.39	± 0.04

Fluidization Time min	# of Runs	Dropped $D_{P\,0.1}$ µm		Dropped $D_{P\,0.5}$ µm		Dropped $D_{P\,0.9}$ µm		Wall $D_{P\,0.1}$ µm		Wall $D_{P\,0.5}$ µm		Wall $D_{P\,0.9}$ µm	
15	3	0.51	± 0.03	1.01	± 0.02	1.97	± 0.09	0.34	± 0.03	0.63	± 0.04	1.10	± 0.07
30	3	0.44	± 0.10	0.93	± 0.07	1.85	± 0.05	0.34	± 0.06	0.58	± 0.06	0.98	± 0.07
60	5	0.51	± 0.05	1.01	± 0.12	1.96	± 0.25	0.38	± 0.04	0.61	± 0.09	0.97	± 0.18
120	3	0.47	± 0.13	0.97	± 0.23	1.91	± 0.45	0.35	± 0.10	0.60	± 0.17	1.00	± 0.27
180	3	0.49	± 0.02	0.95	± 0.04	1.88	± 0.07	0.37	± 0.03	0.57	± 0.03	0.88	± 0.11
360	3	0.43	± 0.08	0.89	± 0.14	1.80	± 0.23	0.36	± 0.06	0.57	± 0.10	0.88	± 0.16

Fluidization Time min	# of Runs	Bottom Column $D_{P\,0.1}$ µm		Bottom Column $D_{P\,0.5}$ µm		Bottom Column $D_{P\,0.9}$ µm		Top Column $D_{P\,0.1}$ µm		Top Column $D_{P\,0.5}$ µm		Top Column $D_{P\,0.9}$ µm	
15	3	0.24	± 0.04	0.47	± 0.04	0.85	± 0.06	0.12	± 0.01	0.22	± 0.01	0.41	± 0.06
30	3	0.19	± 0.09	0.40	± 0.15	0.73	± 0.23	0.12	± 0.00	0.22	± 0.01	0.40	± 0.05
60	5	0.22	± 0.03	0.50	± 0.07	0.96	± 0.21	0.13	± 0.02	0.24	± 0.03	0.43	± 0.04
120	3	0.15	± 0.05	0.32	± 0.07	0.58	± 0.12	0.13	± 0.03	0.24	± 0.06	0.42	± 0.11
180	3	0.16	± 0.04	0.34	± 0.09	0.62	± 0.15	0.13	± 0.00	0.24	± 0.02	0.42	± 0.05
360	3	0.18	± 0.03	0.37	± 0.05	0.64	± 0.09	0.12	± 0.02	0.23	± 0.03	0.40	± 0.05

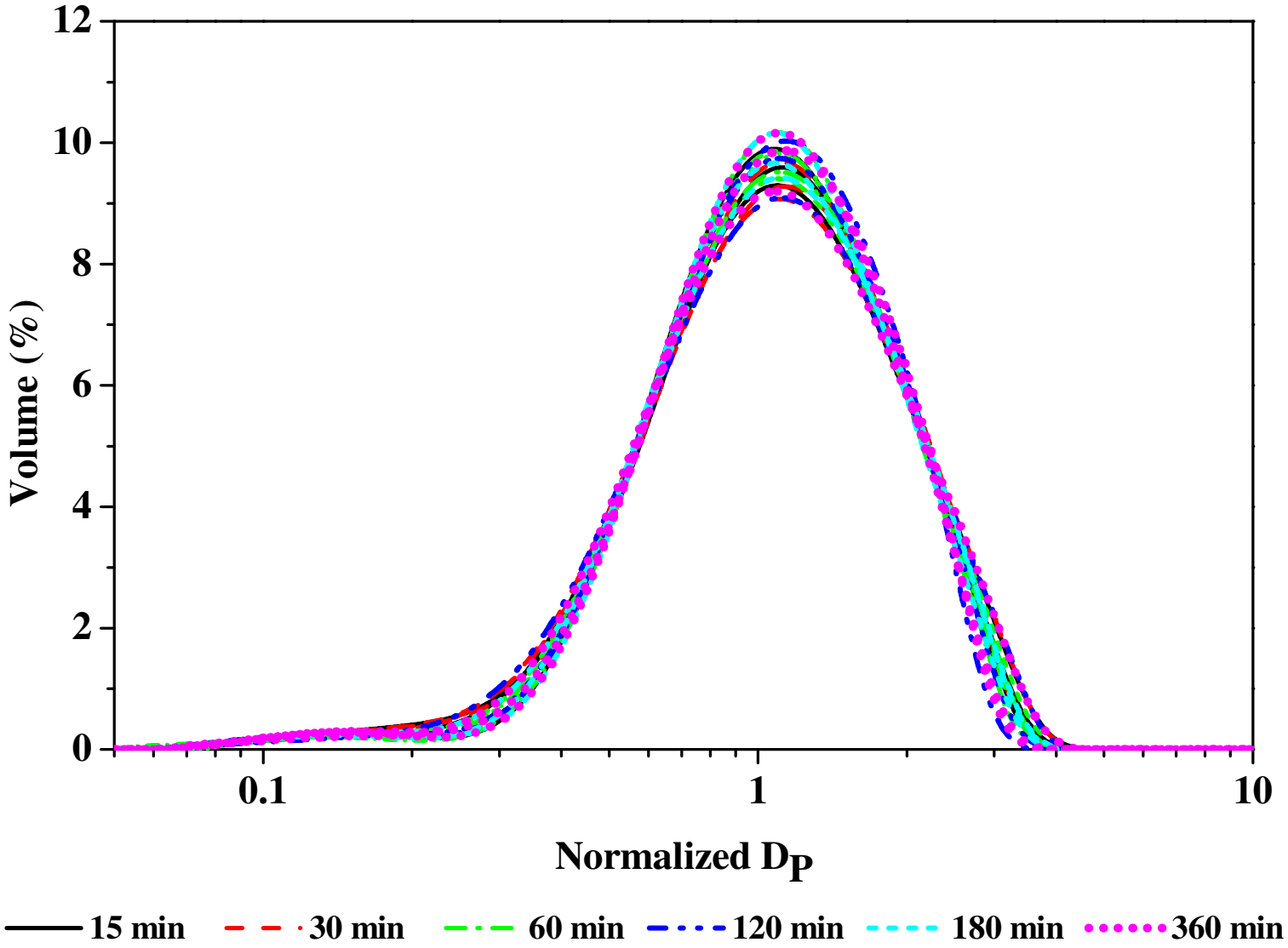

Figure B-19: Normalized PSDs at 4 U_{mf} for Initial region for different fluidization times.

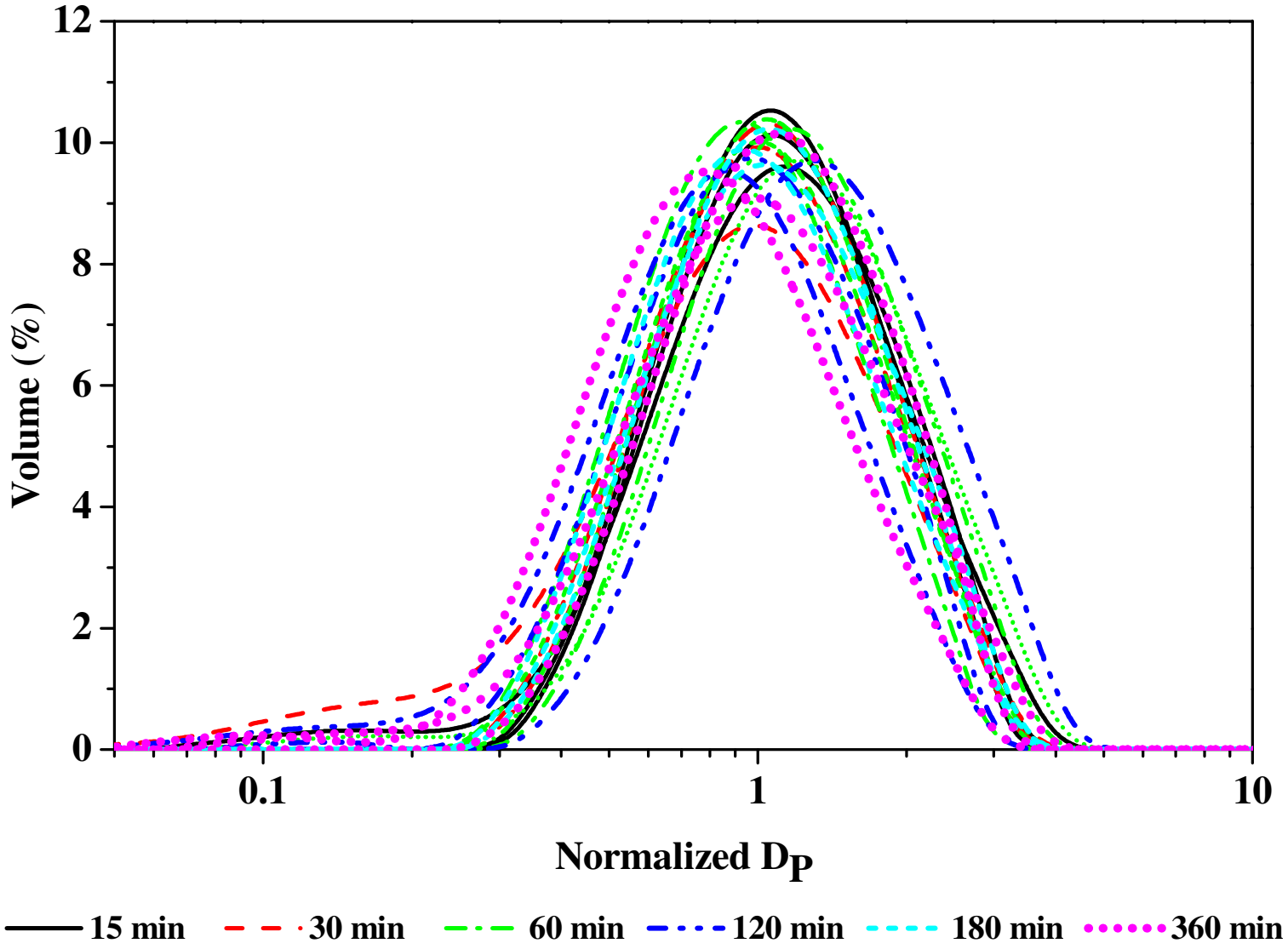

Figure B-20: Normalized PSDs at 4 U_{mf} for Dropped region for different fluidization times.

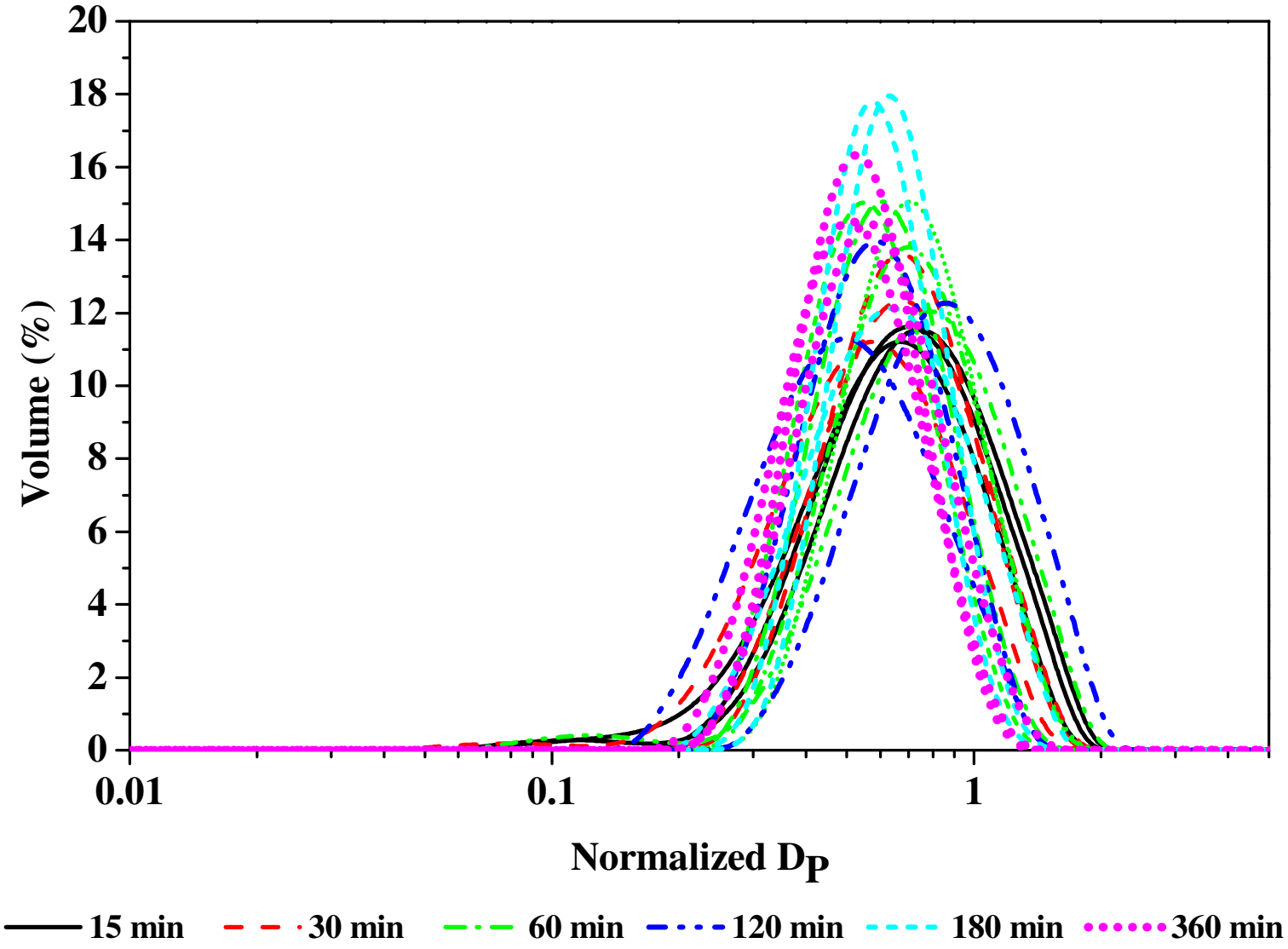

Figure B-21: Normalized PSDs at 4 U_{mf} for Wall region for different fluidization times.

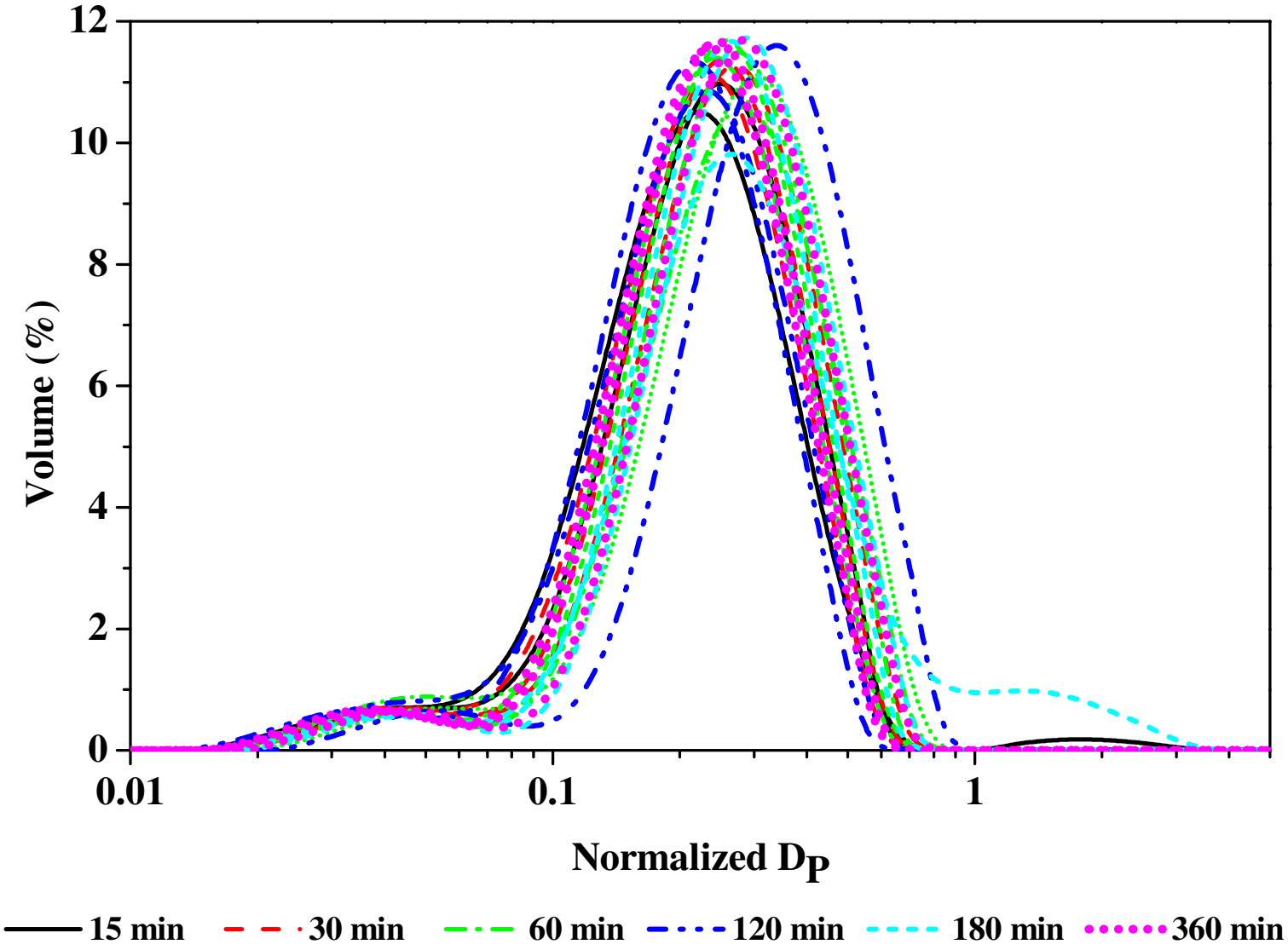

Figure B-22: Normalized PSDs at 4 U_{mf} for Fines region for different fluidization times.

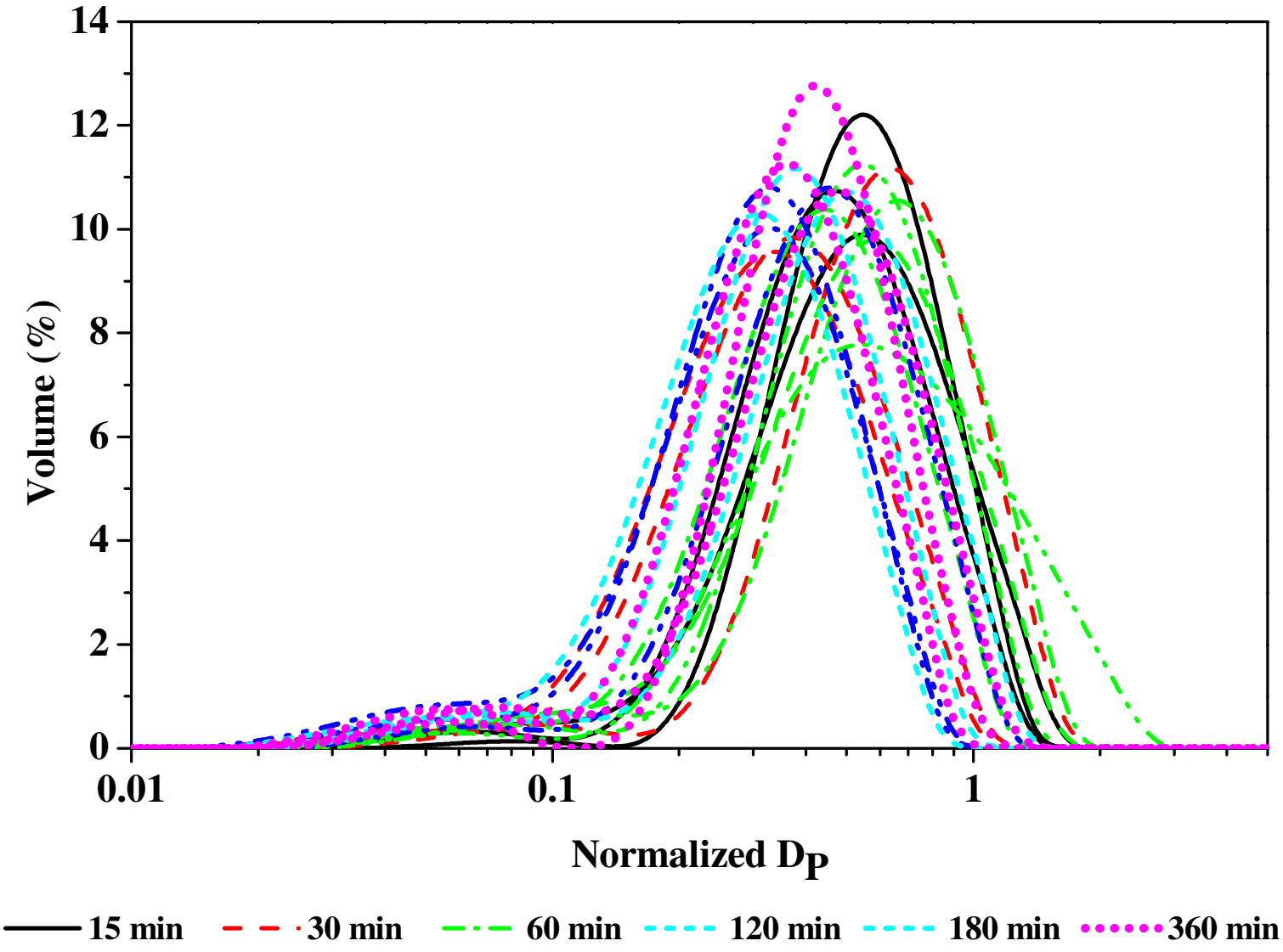

Figure B-23: Normalized PSDs at 4 U_{mf} for Bottom Column region for different fluidization times.

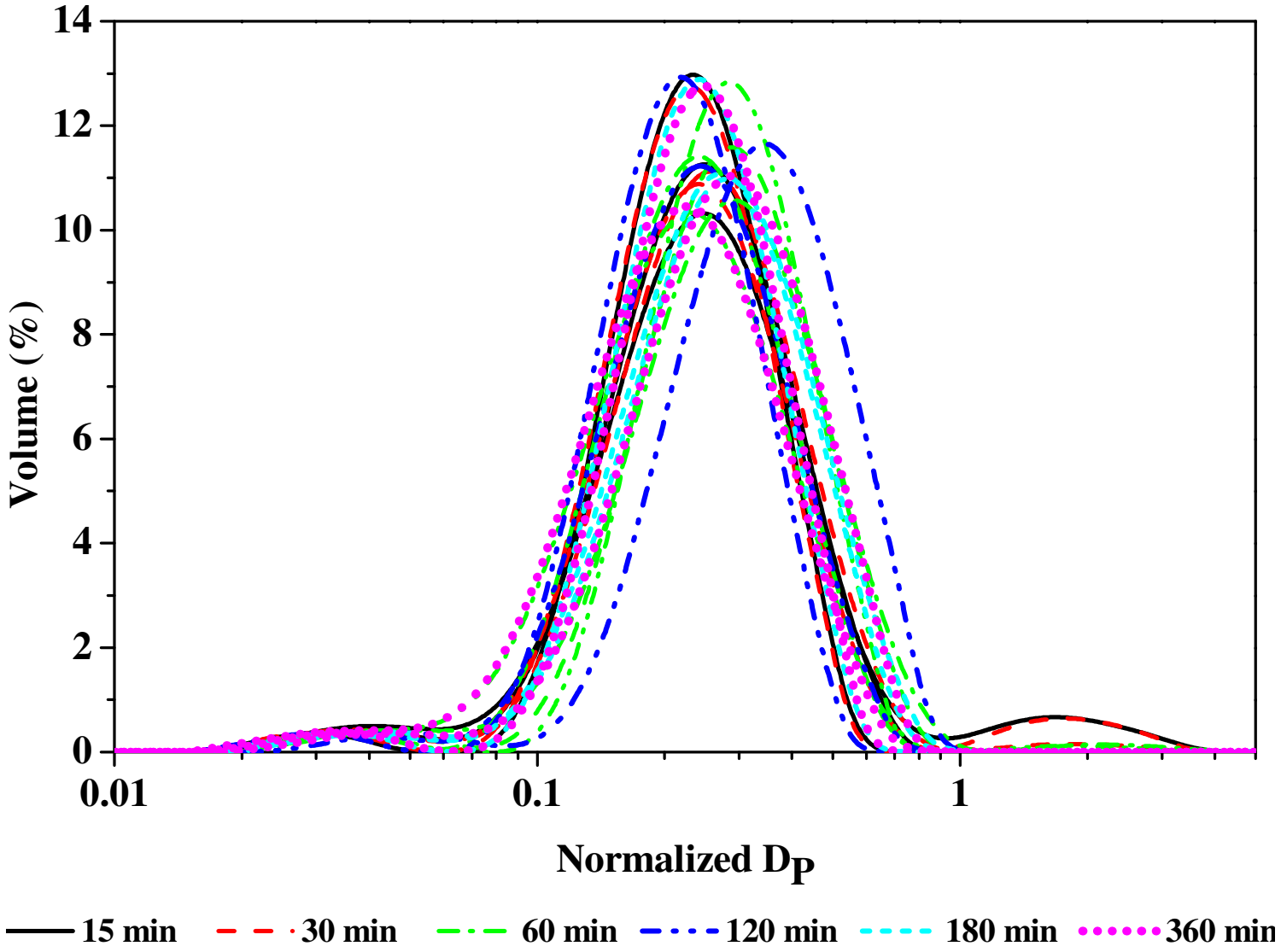

Figure B-24: Normalized PSDs at 4 U_{mf} for Top Column region for different fluidization times.

Appendix C. Relative Humidity Experimental Data and Additional Graphs

Table C - 1: Normalized values for $D_{P\,0.1}$, $D_{P\,0.5}$, and $D_{P\,0.9}$ at 1.5 U_{mf} for all relative humidities.

Relative Humidity %	# of Runs	Initial $D_{P\,0.1}$ µm	Initial $D_{P\,0.5}$ µm	Initial $D_{P\,0.9}$ µm	Fines $D_{P\,0.1}$ µm	Fines $D_{P\,0.5}$ µm	Fines $D_{P\,0.9}$ µm
0	4	0.48 ± 0.01	1.00 ± 0.00	2.02 ± 0.07	0.05 ± 0.00	0.12 ± 0.01	0.32 ± 0.03
20	3	0.46 ± 0.01	1.00 ± 0.00	1.96 ± 0.10	0.05 ± 0.00	0.11 ± 0.01	0.29 ± 0.03
40	3	0.49 ± 0.02	1.00 ± 0.00	1.96 ± 0.08	0.05 ± 0.00	0.13 ± 0.01	0.31 ± 0.02
60	3	0.48 ± 0.01	1.00 ± 0.00	1.99 ± 0.06	0.05 ± 0.00	0.12 ± 0.00	0.30 ± 0.01
80	3	0.48 ± 0.02	1.00 ± 0.00	1.91 ± 0.04	0.05 ± 0.00	0.13 ± 0.00	0.31 ± 0.02

Relative Humidity %	# of Runs	Dropped $D_{P\,0.1}$ µm	Dropped $D_{P\,0.5}$ µm	Dropped $D_{P\,0.9}$ µm	Wall $D_{P\,0.1}$ µm	Wall $D_{P\,0.5}$ µm	Wall $D_{P\,0.9}$ µm
0	4	0.47 ± 0.04	0.94 ± 0.07	1.93 ± 0.14	0.28 ± 0.03	0.42 ± 0.06	0.65 ± 0.13
20	3	0.47 ± 0.06	0.91 ± 0.13	1.80 ± 0.26	0.27 ± 0.03	0.39 ± 0.05	0.56 ± 0.07
40	3	0.52 ± 0.07	0.95 ± 0.06	1.81 ± 0.08	0.30 ± 0.03	0.42 ± 0.03	0.60 ± 0.05
60	3	0.50 ± 0.07	0.97 ± 0.05	1.94 ± 0.18	0.26 ± 0.02	0.40 ± 0.02	0.62 ± 0.03
80	3	0.48 ± 0.04	0.92 ± 0.15	1.72 ± 0.38	0.23 ± 0.01	0.41 ± 0.06	0.71 ± 0.17

Relative Humidity %	# of Runs	Bottom Column $D_{P\,0.1}$ µm	Bottom Column $D_{P\,0.5}$ µm	Bottom Column $D_{P\,0.9}$ µm
0	1	0.33 -	0.51 -	0.77 -
20	3	0.20 ± 0.00	0.32 ± 0.02	0.54 ± 0.05
40	3	0.21 ± 0.03	0.33 ± 0.05	0.53 ± 0.08
60	3	0.19 ± 0.02	0.35 ± 0.02	0.60 ± 0.02
80	3	0.16 ± 0.03	0.34 ± 0.02	0.64 ± 0.01

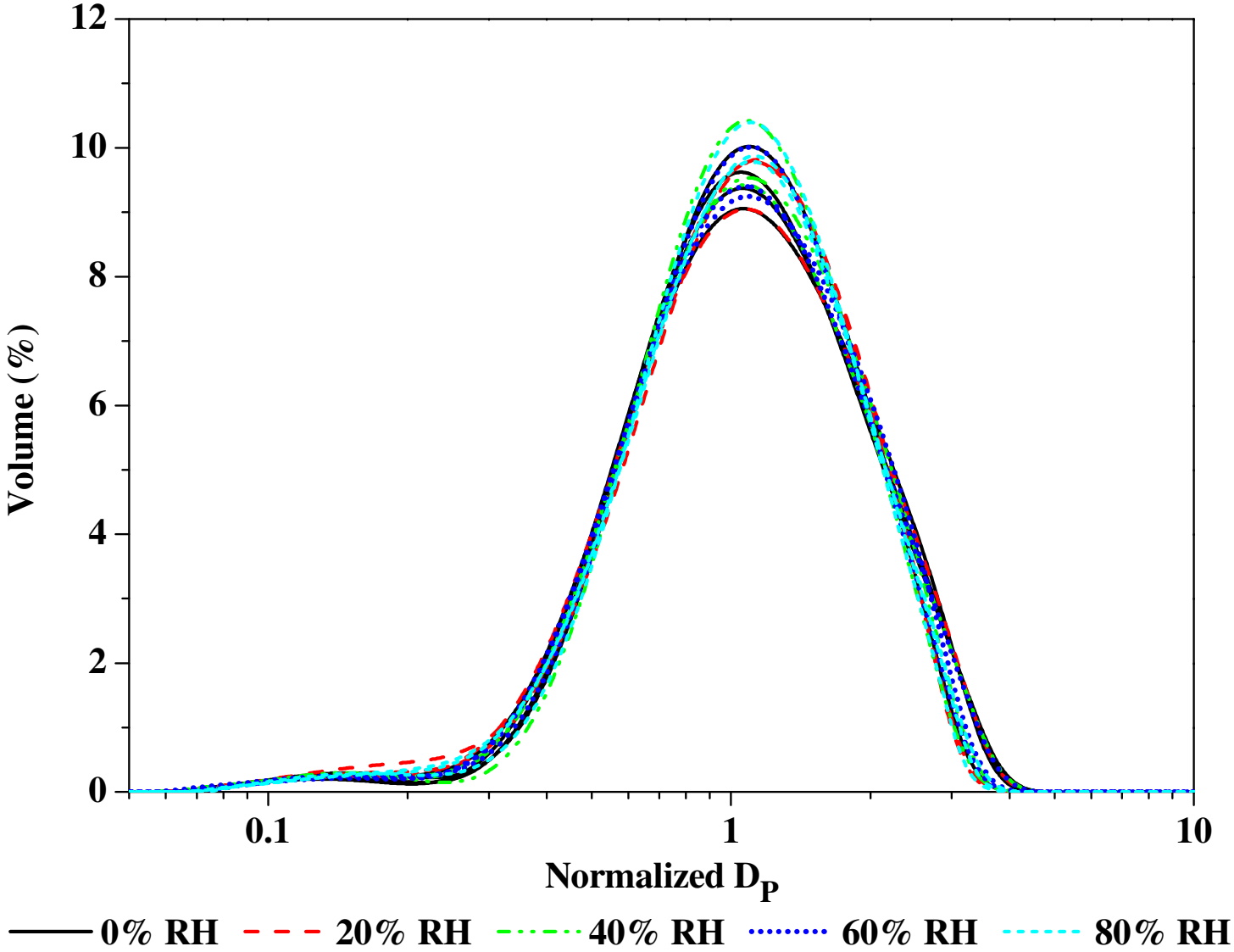

Figure C - 1: Normalized PSD at 1.5 U_{mf} in the Initial region for different relative humidity.

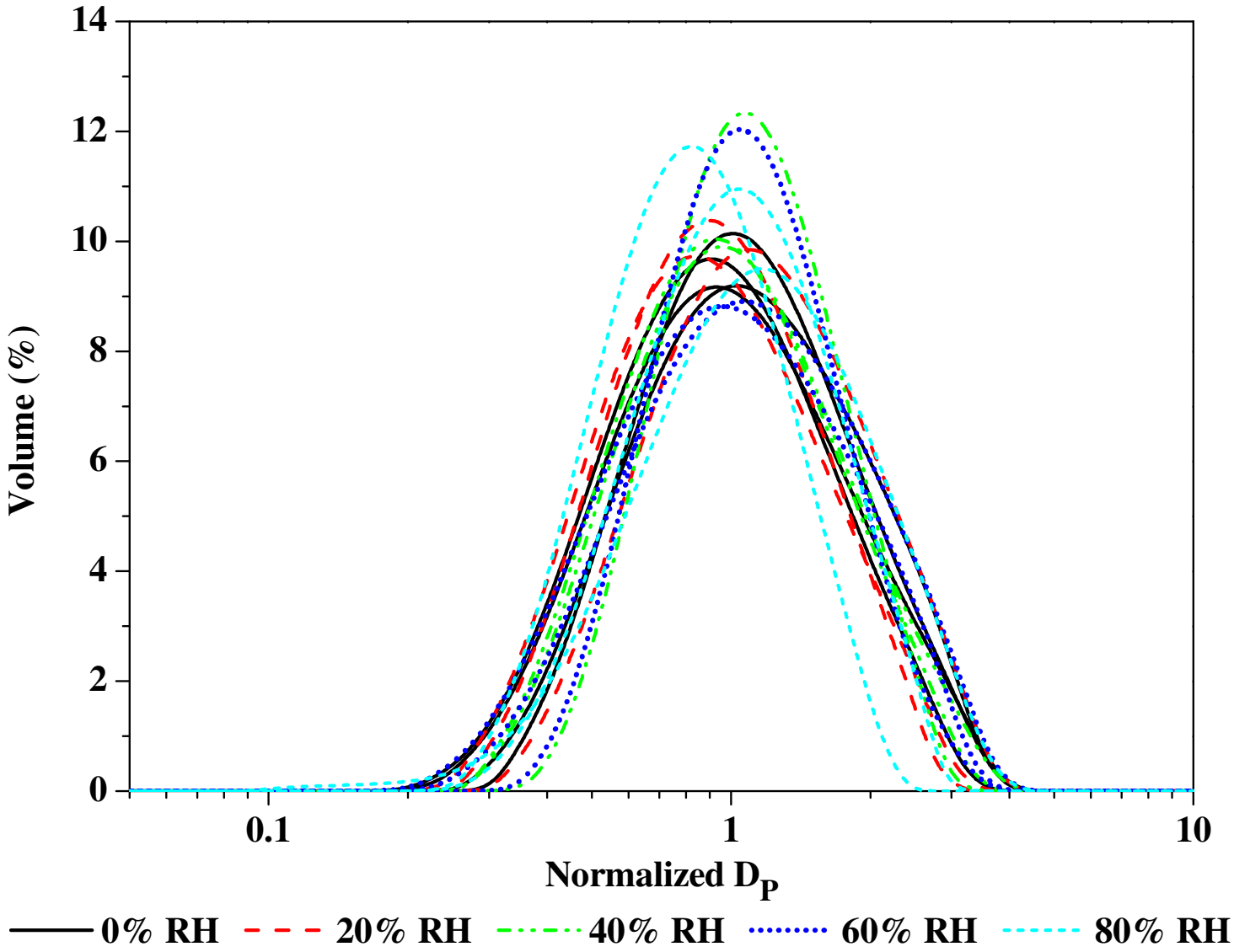

Figure C - 2: Normalized PSD at 1.5 U_{mf} in the Dropped region for different relative humidity.

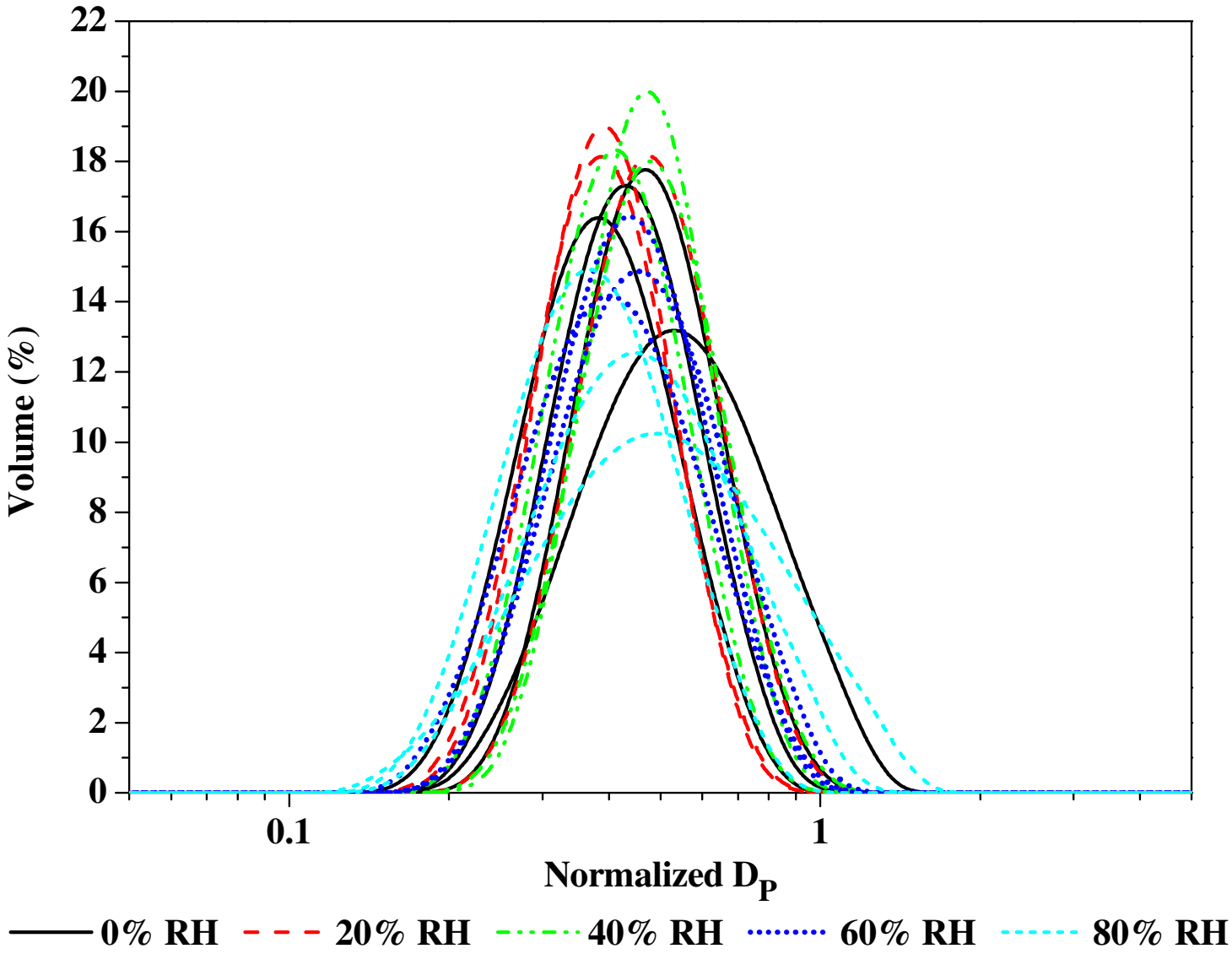

Figure C - 3: Normalized PSD at 1.5 U_{mf} in the Wall region for different relative humidity.

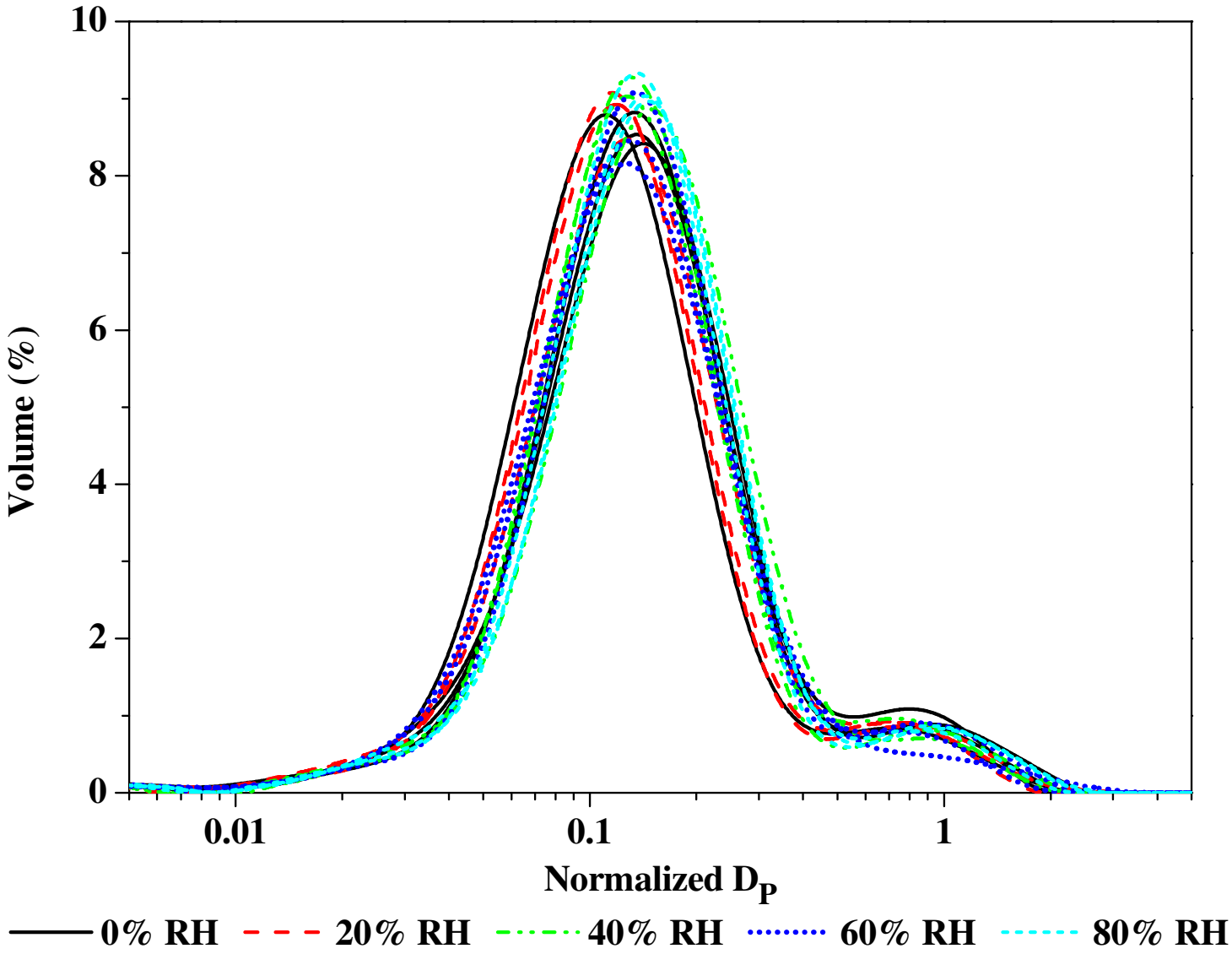

Figure C - 4: Normalized PSD at 1.5 U_{mf} in the Fines region for different relative humidity.

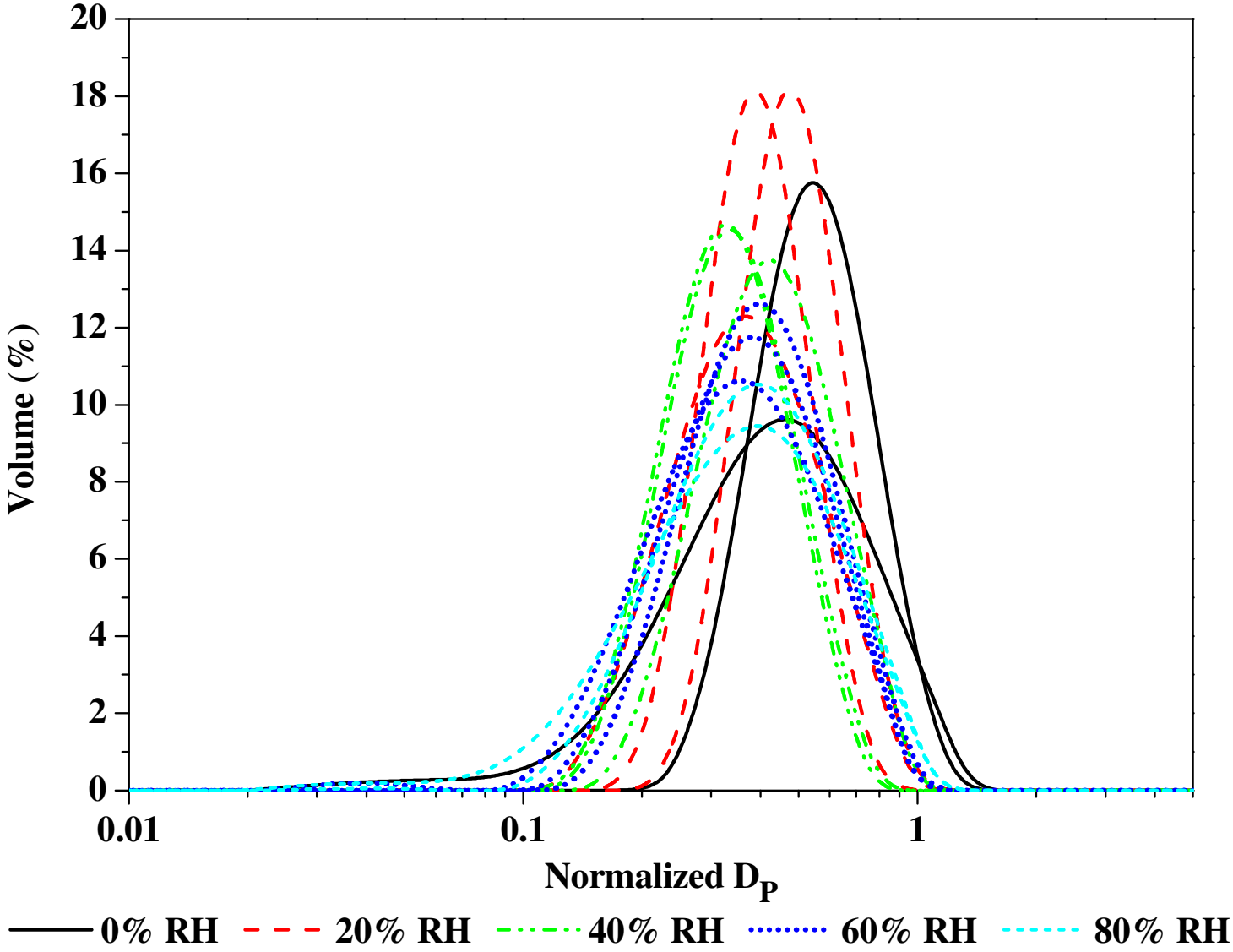

Figure C - 5: Normalized PSD at 1.5 U_{mf} in the Bottom Column region for different relative humidity.

Table C - 2: Normalized values for $D_{P\,0.1}$, $D_{P\,0.5}$, and $D_{P\,0.9}$ at 1.75 U_{mf} for all relative humidities.

Relative Humidity %	# of Runs	Initial $D_{P\,0.1}$ µm	Initial $D_{P\,0.5}$ µm	Initial $D_{P\,0.9}$ µm	Fines $D_{P\,0.1}$ µm	Fines $D_{P\,0.5}$ µm	Fines $D_{P\,0.9}$ µm
0	4	0.46 ± 0.05	1.00 ± 0.00	1.97 ± 0.15	0.04 ± 0.01	0.12 ± 0.02	0.30 ± 0.03
20	3	0.45 ± 0.02	1.00 ± 0.00	2.04 ± 0.07	0.05 ± 0.00	0.13 ± 0.01	0.33 ± 0.05
40	3	0.45 ± 0.03	1.00 ± 0.00	1.99 ± 0.21	0.05 ± 0.01	0.12 ± 0.02	0.27 ± 0.03
60	3	0.46 ± 0.01	1.00 ± 0.00	1.99 ± 0.14	0.05 ± 0.01	0.13 ± 0.03	0.29 ± 0.10
80	3	0.45 ± 0.01	1.00 ± 0.00	1.99 ± 0.06	0.05 ± 0.00	0.12 ± 0.01	0.27 ± 0.04

Relative Humidity %	# of Runs	Dropped $D_{P\,0.1}$ µm	Dropped $D_{P\,0.5}$ µm	Dropped $D_{P\,0.9}$ µm	Wall $D_{P\,0.1}$ µm	Wall $D_{P\,0.5}$ µm	Wall $D_{P\,0.9}$ µm
0	4	0.46 ± 0.12	0.94 ± 0.20	1.90 ± 0.38	0.24 ± 0.07	0.40 ± 0.09	0.69 ± 0.18
20	3	0.46 ± 0.04	1.05 ± 0.03	2.15 ± 0.02	0.24 ± 0.03	0.44 ± 0.04	0.76 ± 0.16
40	3	0.40 ± 0.05	0.82 ± 0.01	1.52 ± 0.27	0.14 ± 0.12	0.23 ± 0.20	0.37 ± 0.33
60	3	0.51 ± 0.02	1.09 ± 0.08	2.24 ± 0.21	0.27 ± 0.03	0.41 ± 0.04	0.62 ± 0.06
80	3	0.40 ± 0.05	0.92 ± 0.11	1.95 ± 0.18	0.22 ± 0.07	0.44 ± 0.04	0.80 ± 0.05

Relative Humidity %	# of Runs	Bottom Column $D_{P\,0.1}$ µm	Bottom Column $D_{P\,0.5}$ µm	Bottom Column $D_{P\,0.9}$ µm
0	1	0.15 -	0.32 -	0.61 -
20	2	0.09 ± 0.00	0.32 ± 0.00	0.41 ± 0.01
40	3	0.18 ± 0.06	0.39 ± 0.11	0.74 ± 0.24
60	3	0.13 ± 0.07	0.29 ± 0.08	0.55 ± 0.13
80	3	0.14 ± 0.05	0.31 ± 0.04	0.60 ± 0.06

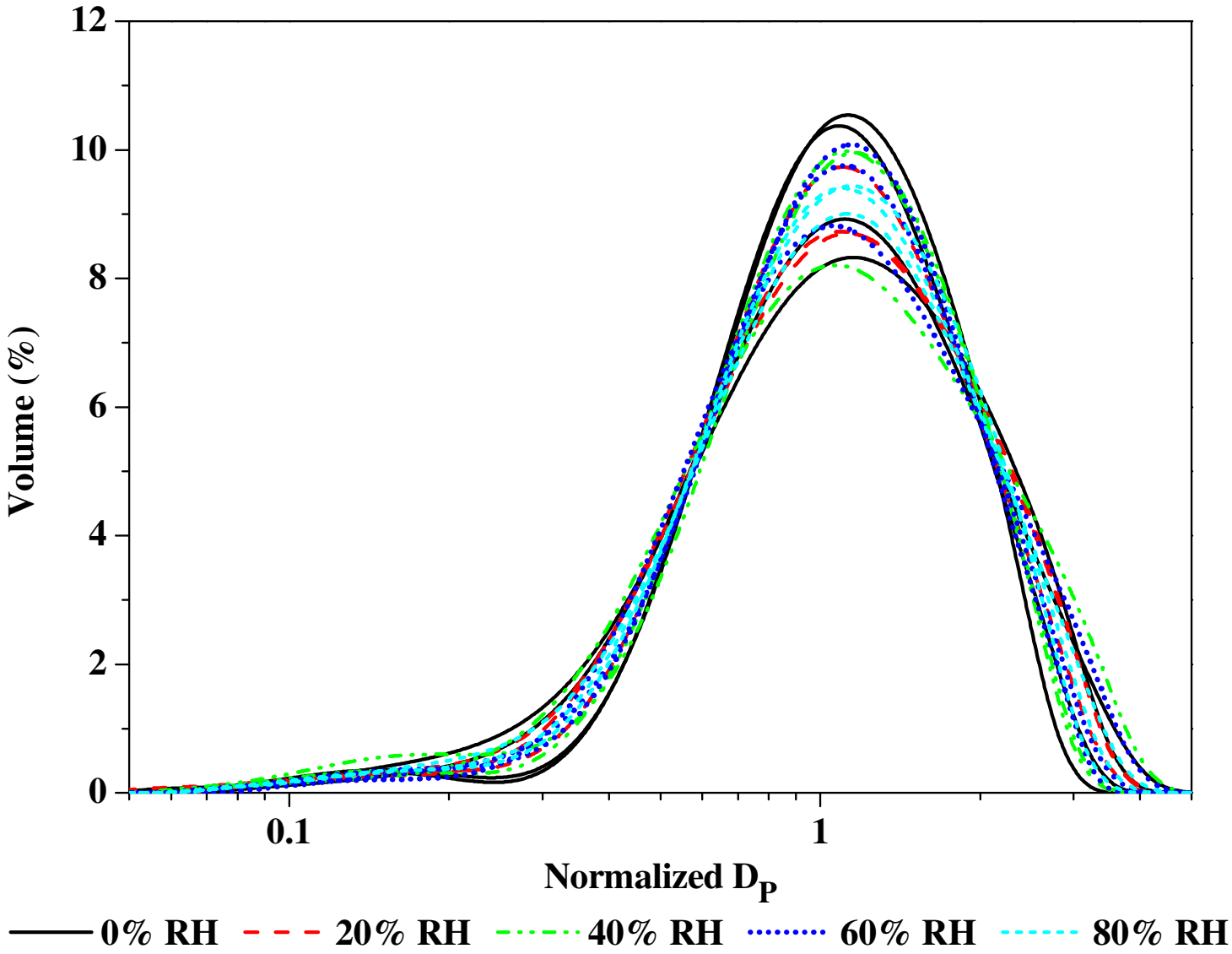

Figure C - 6: Normalized PSD at 1.75 U_{mf} in the Initial region for different relative humidity.

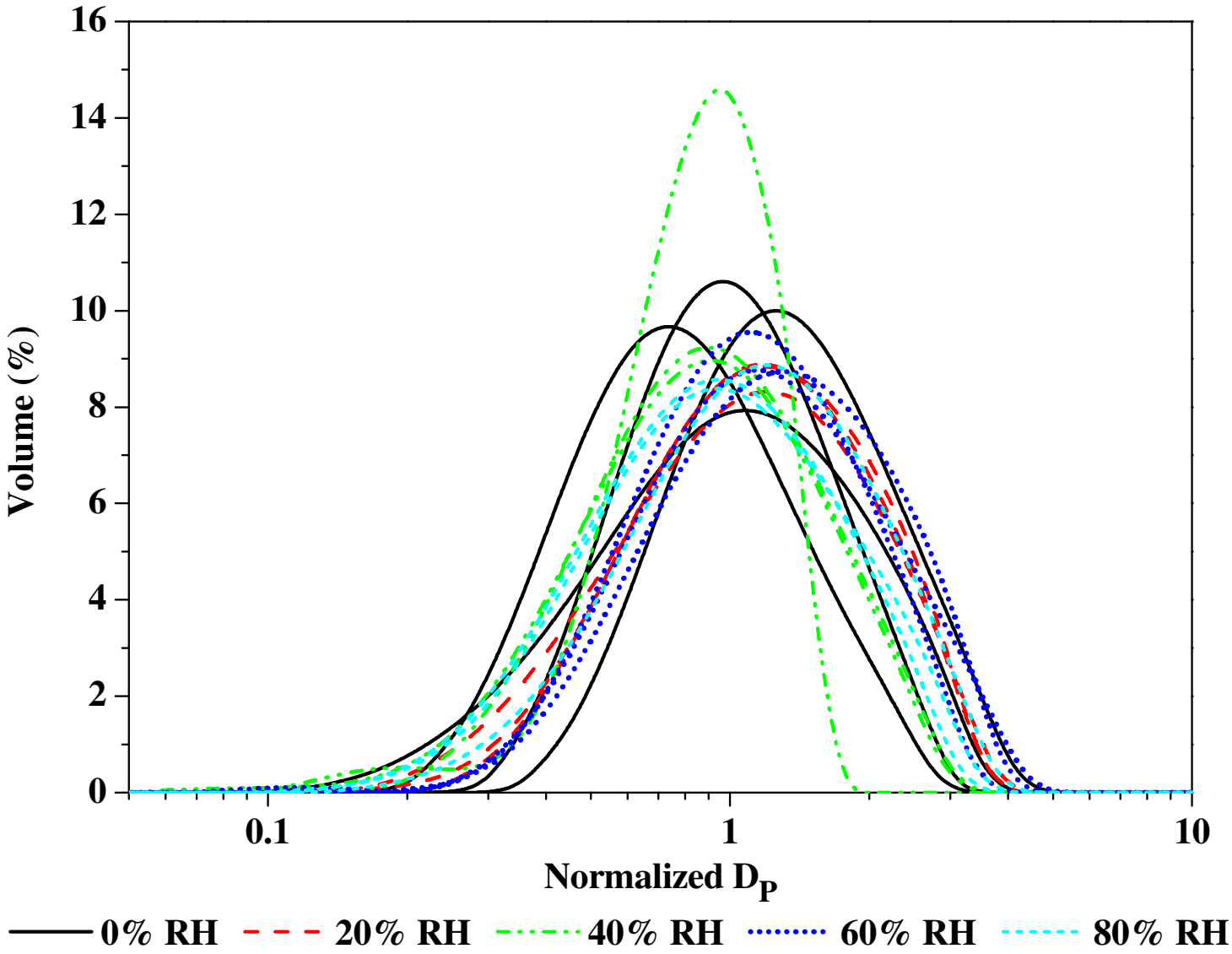

Figure C - 7: Normalized PSD at 1.75 U_{mf} in the Dropped region for different relative humidity.

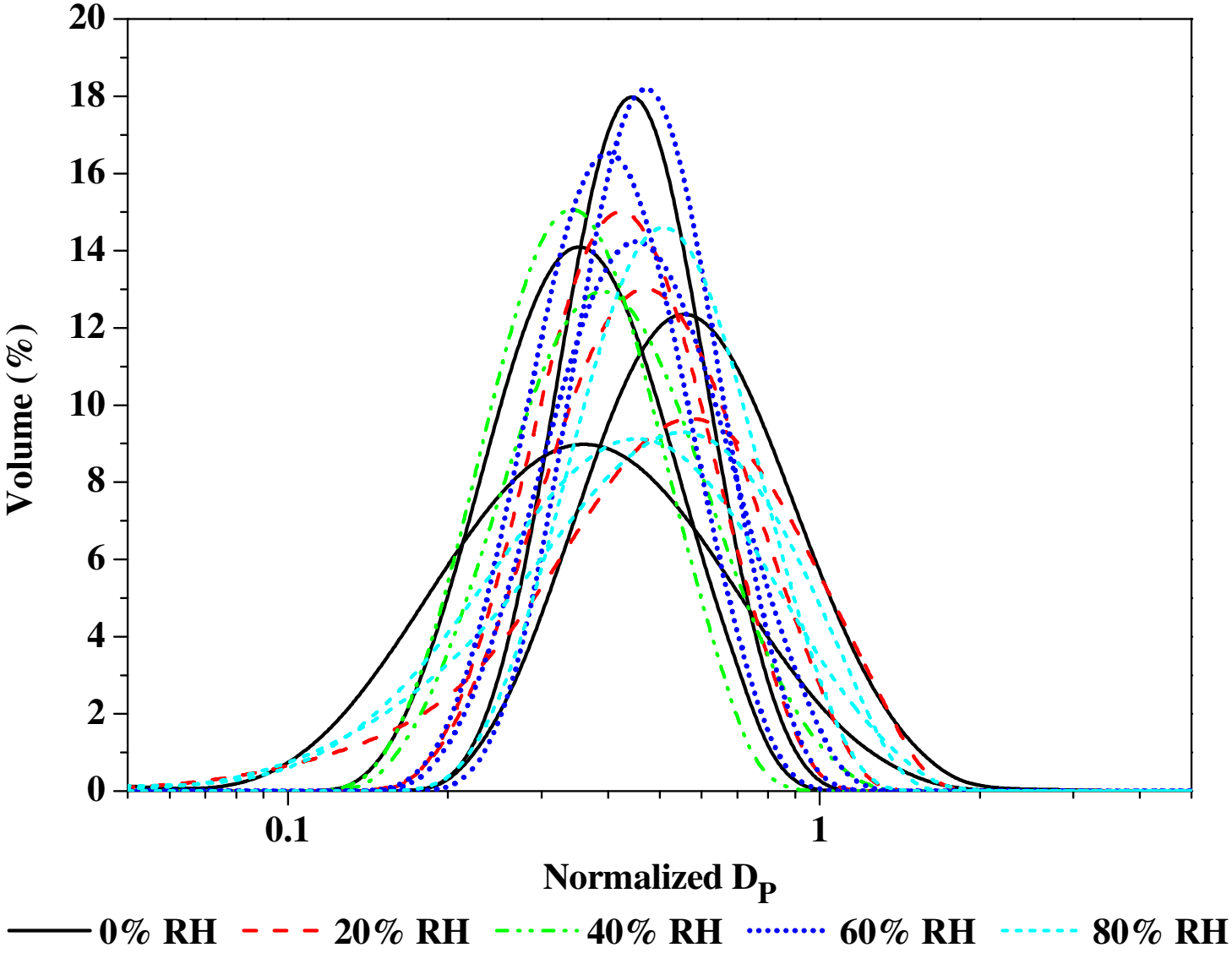

Figure C - 8: Normalized PSD at 1.75 U_{mf} in the Wall region for different relative humidity.

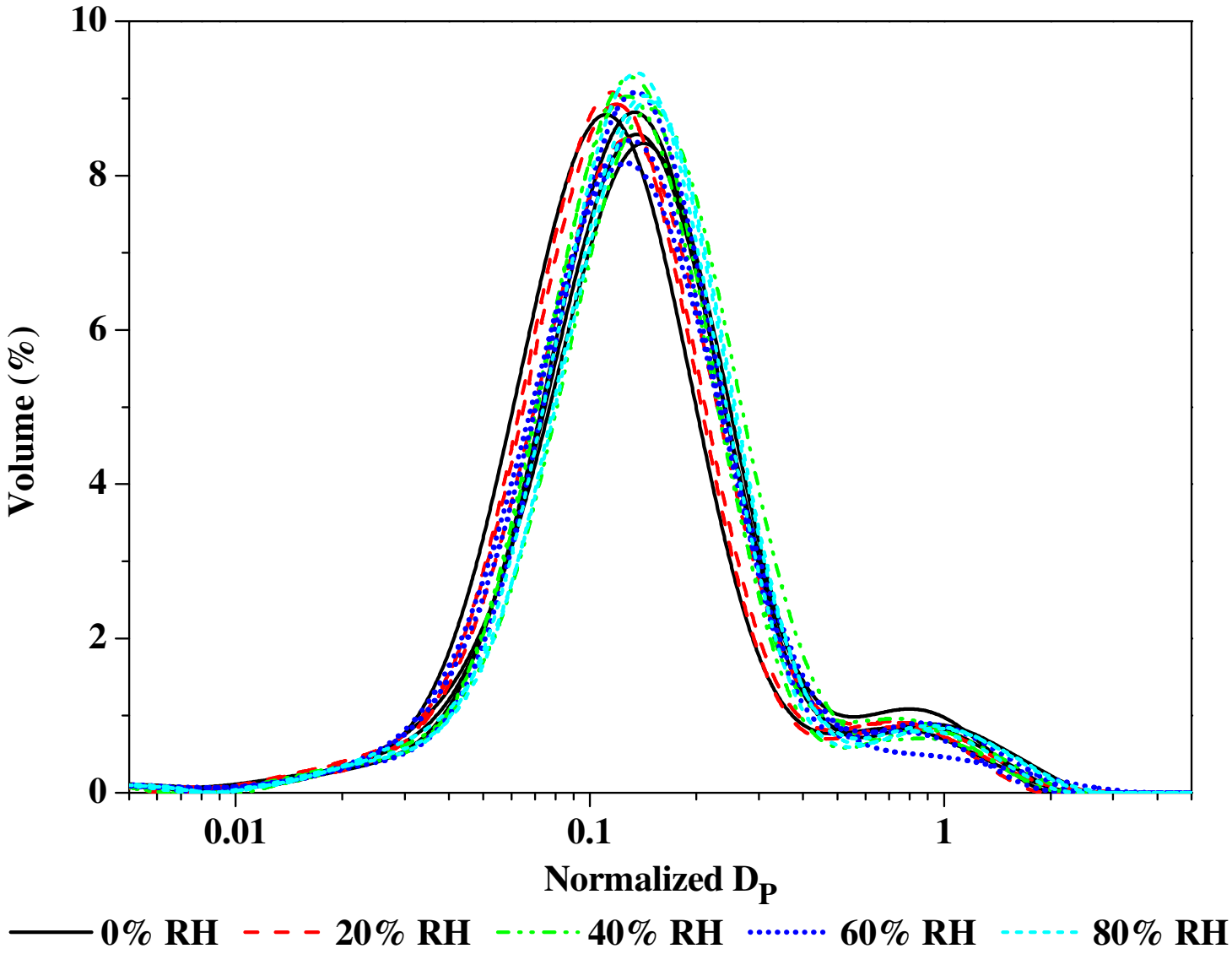

Figure C - 9: Normalized PSD at 1.75 U_{mf} in the Fines region for different relative humidity.

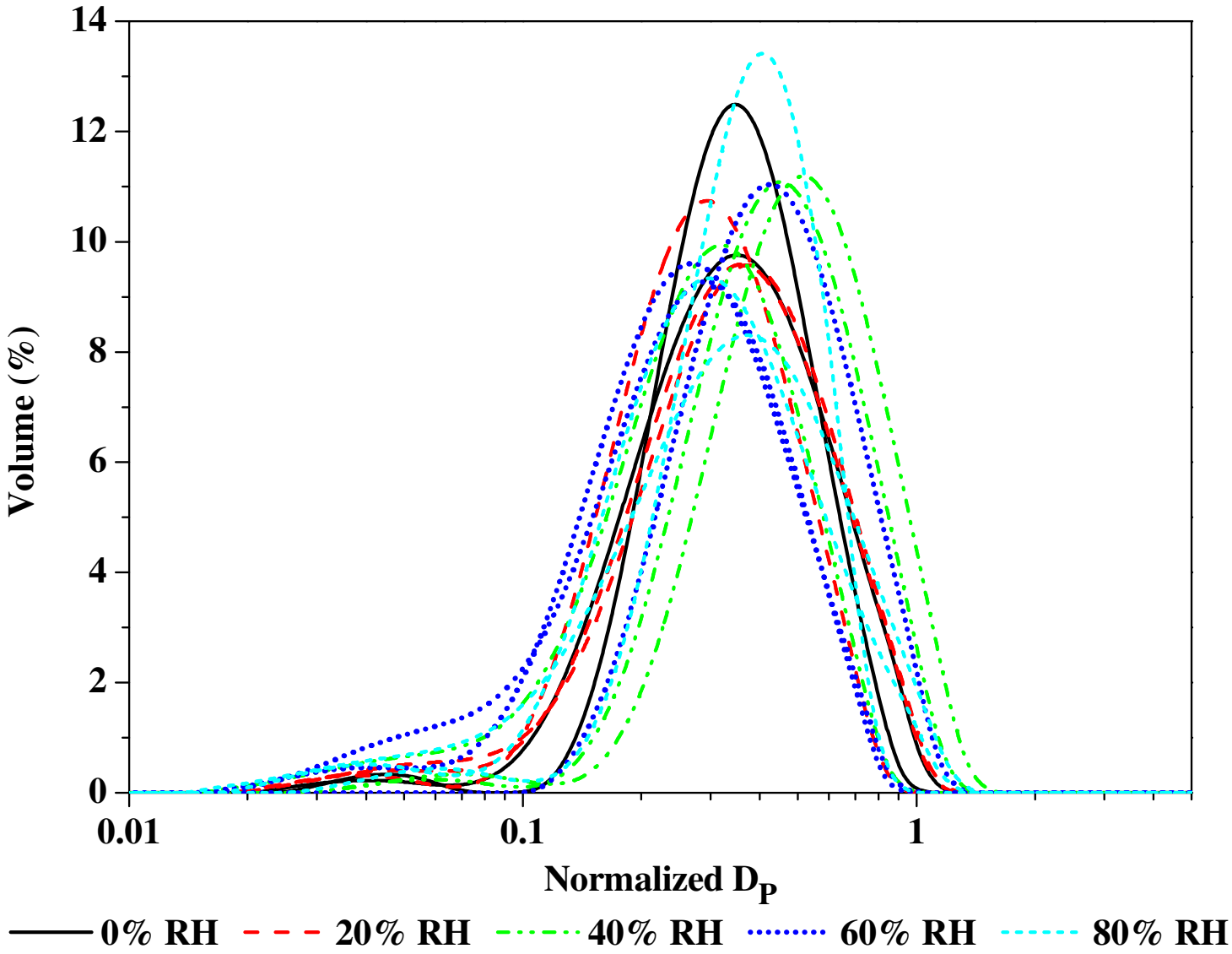

Figure C - 10: Normalized PSD at 1.75 U_{mf} in the Bottom Column region for different relative humidity.

Table C - 3: Normalized values for $D_{P\,0.1}$, $D_{P\,0.5}$, and $D_{P\,0.9}$ at 3.5 U_{mf} for all relative humidities.

Relative Humidity %	# of Runs	Initial $D_{P\,0.1}$ µm	Initial $D_{P\,0.5}$ µm	Initial $D_{P\,0.9}$ µm	Fines $D_{P\,0.1}$ µm	Fines $D_{P\,0.5}$ µm	Fines $D_{P\,0.9}$ µm
0	5	0.45 ± 0.03	1.00 ± 0.00	2.05 ± 0.09	0.09 ± 0.02	0.20 ± 0.03	0.36 ± 0.05
20	3	0.46 ± 0.01	1.00 ± 0.00	1.90 ± 0.04	0.08 ± 0.01	0.19 ± 0.03	0.35 ± 0.05
40	3	0.48 ± 0.01	1.00 ± 0.00	1.97 ± 0.05	0.08 ± 0.01	0.19 ± 0.01	0.40 ± 0.08
60	3	0.44 ± 0.02	1.00 ± 0.00	2.04 ± 0.08	0.09 ± 0.02	0.20 ± 0.03	0.37 ± 0.06
80	3	0.44 ± 0.02	1.00 ± 0.00	2.04 ± 0.11	0.09 ± 0.01	0.20 ± 0.03	0.38 ± 0.06

Relative Humidity %	# of Runs	Dropped $D_{P\,0.1}$ µm	Dropped $D_{P\,0.5}$ µm	Dropped $D_{P\,0.9}$ µm	Wall $D_{P\,0.1}$ µm	Wall $D_{P\,0.5}$ µm	Wall $D_{P\,0.9}$ µm
0	5	0.48 ± 0.06	0.92 ± 0.15	1.77 ± 0.51	0.30 ± 0.08	0.59 ± 0.15	1.05 ± 0.26
20	3	0.47 ± 0.06	0.99 ± 0.11	2.02 ± 0.28	0.24 ± 0.04	0.50 ± 0.08	0.91 ± 0.16
40	3	0.46 ± 0.03	0.98 ± 0.08	2.00 ± 0.13	0.28 ± 0.08	0.54 ± 0.13	0.94 ± 0.21
60	3	0.50 ± 0.05	1.08 ± 0.16	2.20 ± 0.35	0.34 ± 0.06	0.63 ± 0.08	1.07 ± 0.12
80	3	0.49 ± 0.07	1.04 ± 0.16	2.07 ± 0.34	0.27 ± 0.05	0.51 ± 0.09	0.88 ± 0.14

Relative Humidity %	# of Runs	Bottom Column $D_{P\,0.1}$ µm	Bottom Column $D_{P\,0.5}$ µm	Bottom Column $D_{P\,0.9}$ µm	Top Column $D_{P\,0.1}$ µm	Top Column $D_{P\,0.5}$ µm	Top Column $D_{P\,0.9}$ µm
0	1	0.20 -	0.42 -	0.78 -	0.08 -	0.18 -	0.38 -
20	3	0.11 ± 0.11	0.26 ± 0.25	0.74 ± 0.71	0.12 ± 0.03	0.21 ± 0.05	0.35 ± 0.09
40	3	0.16 ± 0.02	0.34 ± 0.05	0.69 ± 0.19	0.11 ± 0.01	0.20 ± 0.01	0.34 ± 0.02
60	3	0.17 ± 0.05	0.34 ± 0.06	0.63 ± 0.10	0.12 ± 0.01	0.23 ± 0.02	0.39 ± 0.04
80	3	0.15 ± 0.03	0.32 ± 0.01	0.65 ± 0.15	0.13 ± 0.02	0.24 ± 0.02	0.41 ± 0.02

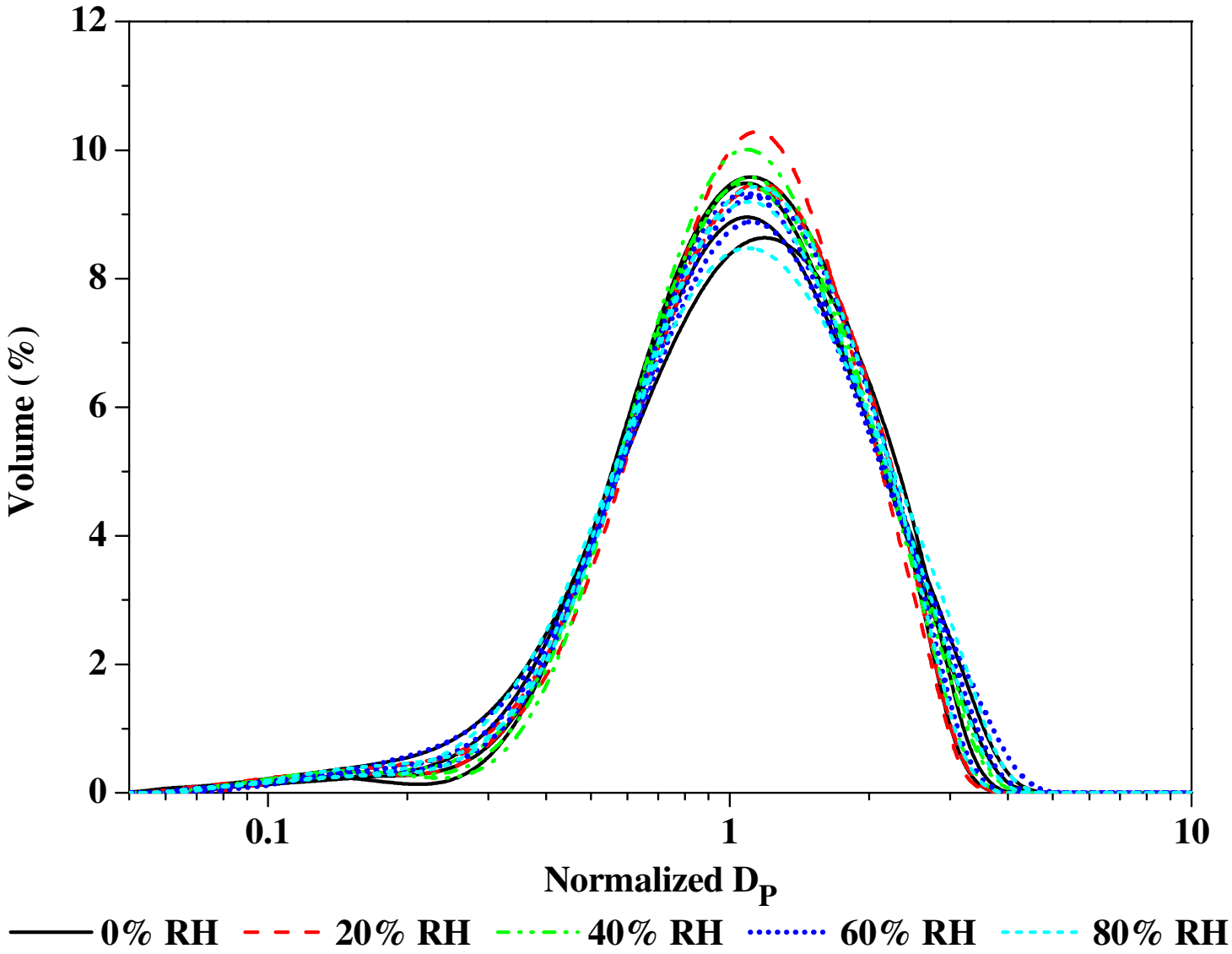

Figure C - 11: Normalized PSD at 3.5 U_{mf} in the Initial region for different relative humidity.

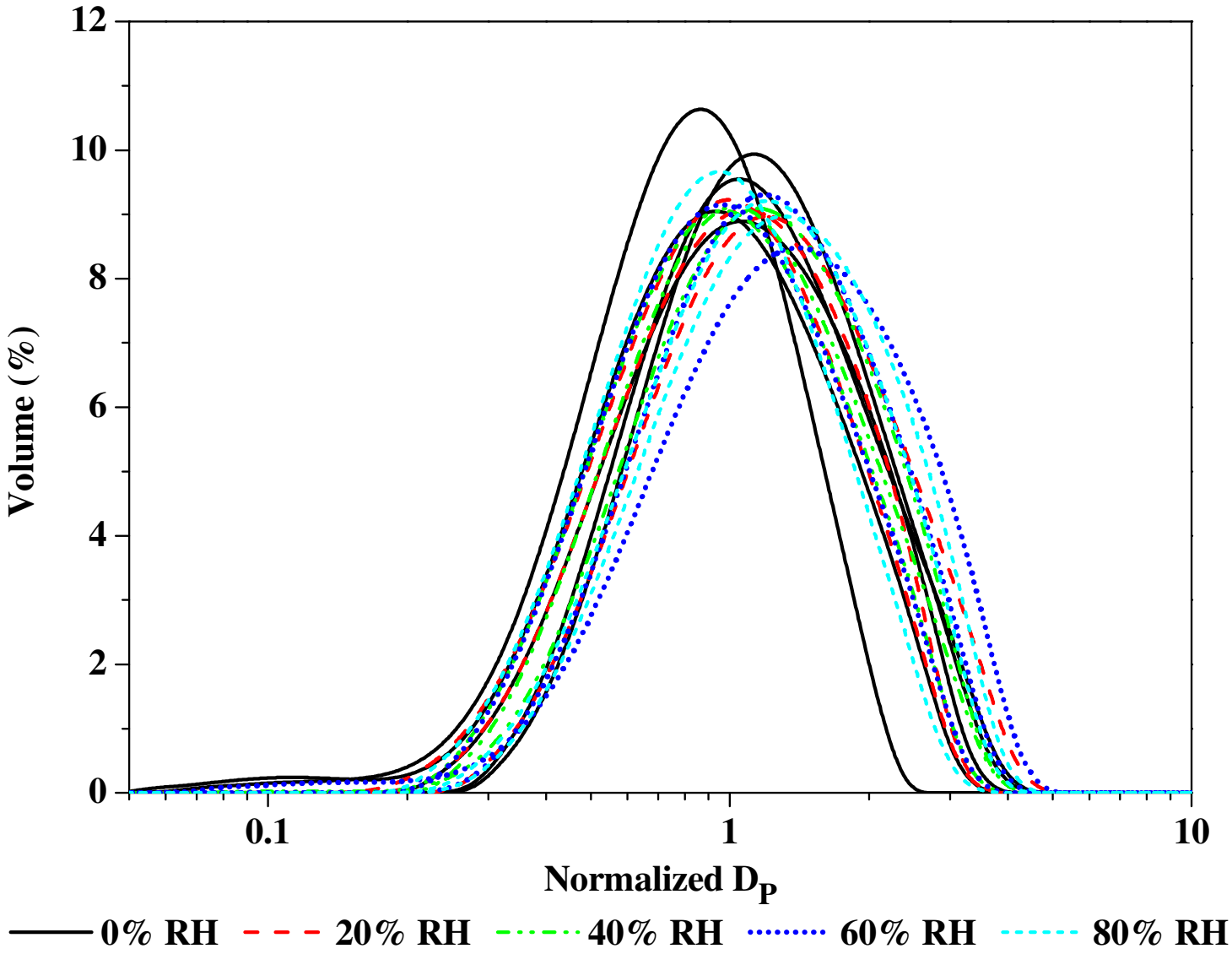

Figure C - 12: Normalized PSD at 3.5 U_{mf} in the Dropped region for different relative humidity.

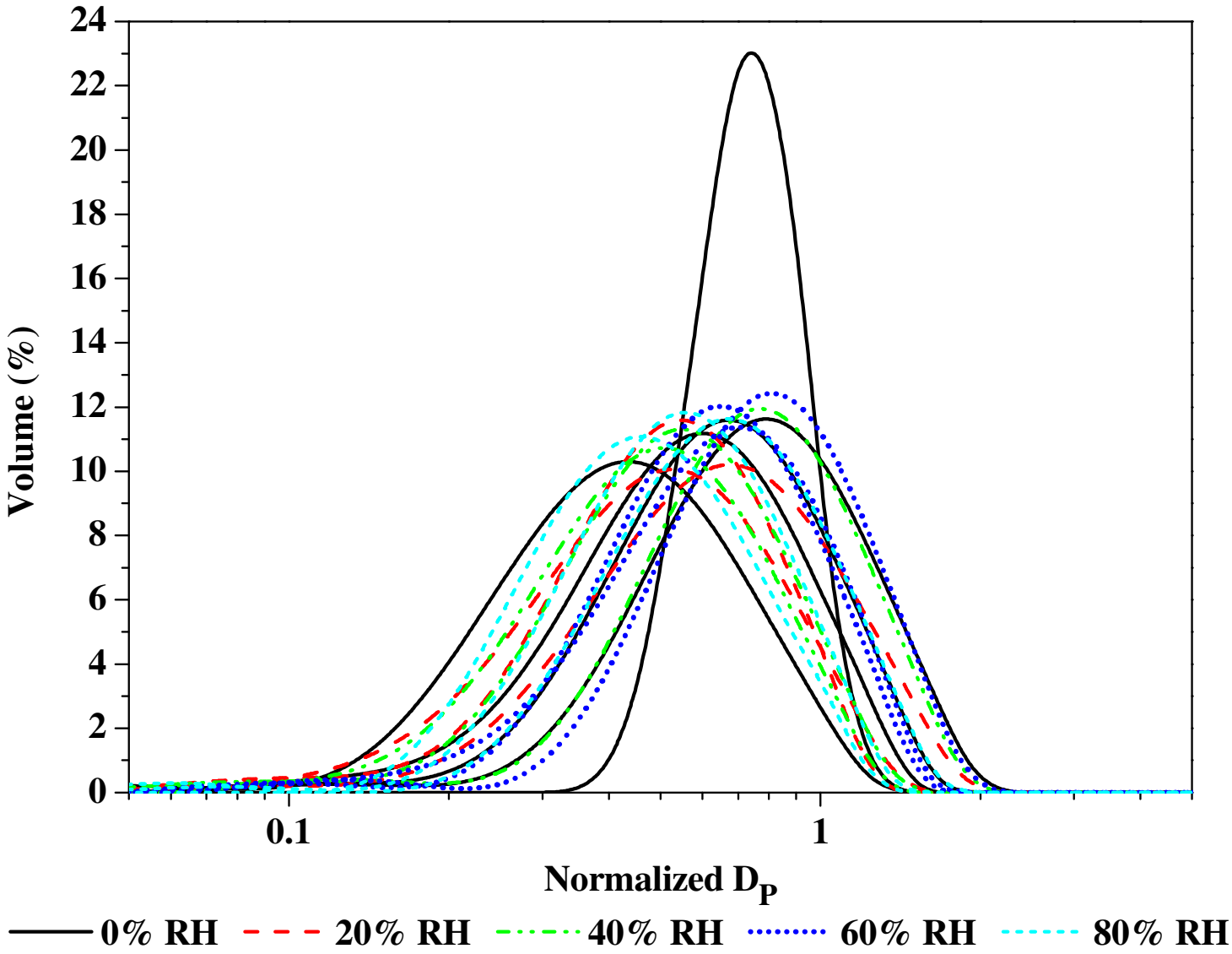

Figure C - 13: Normalized PSD at 3.5 U_{mf} in the Wall region for different relative humidity.

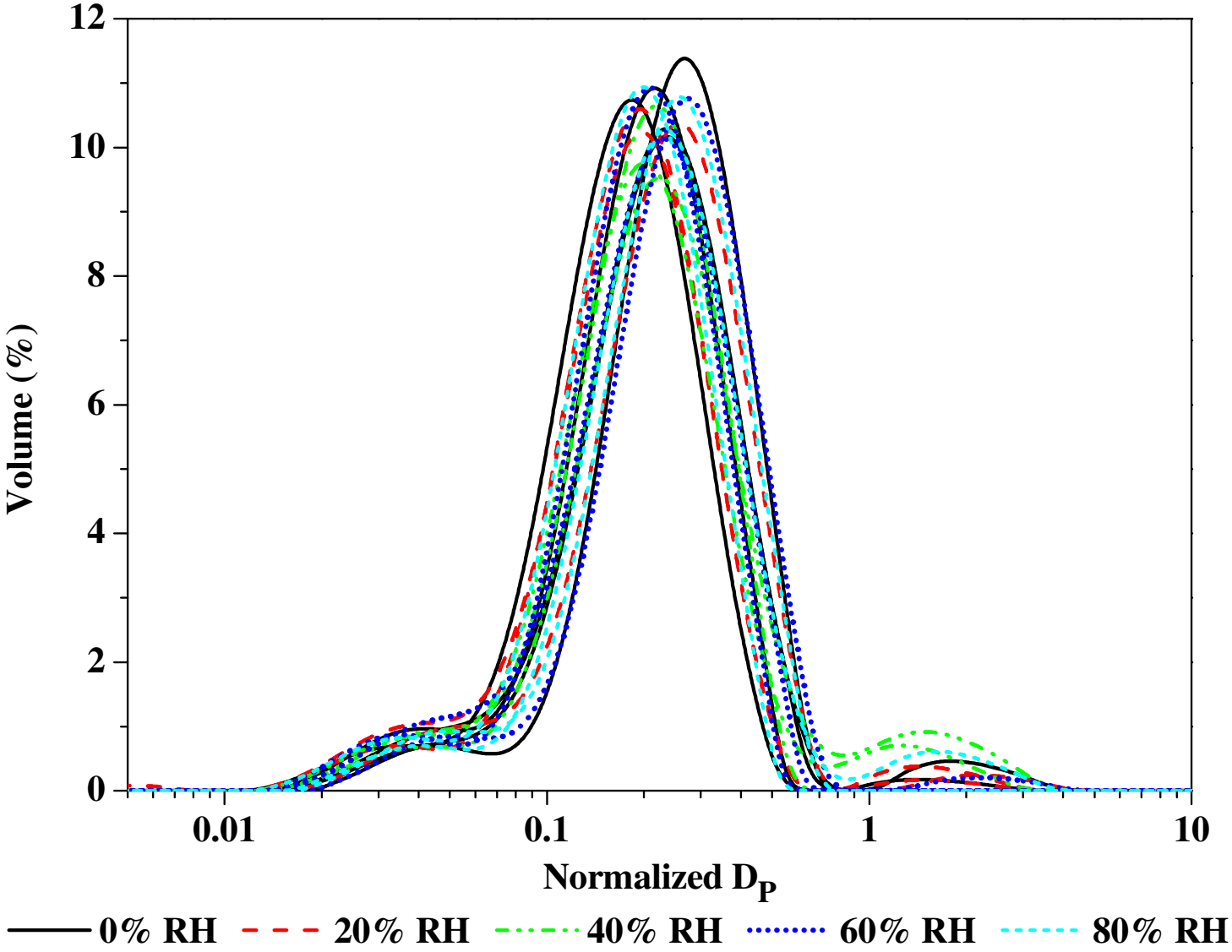

Figure C - 14: Normalized PSD at 3.5 U_{mf} in the Fines region for different relative humidity.

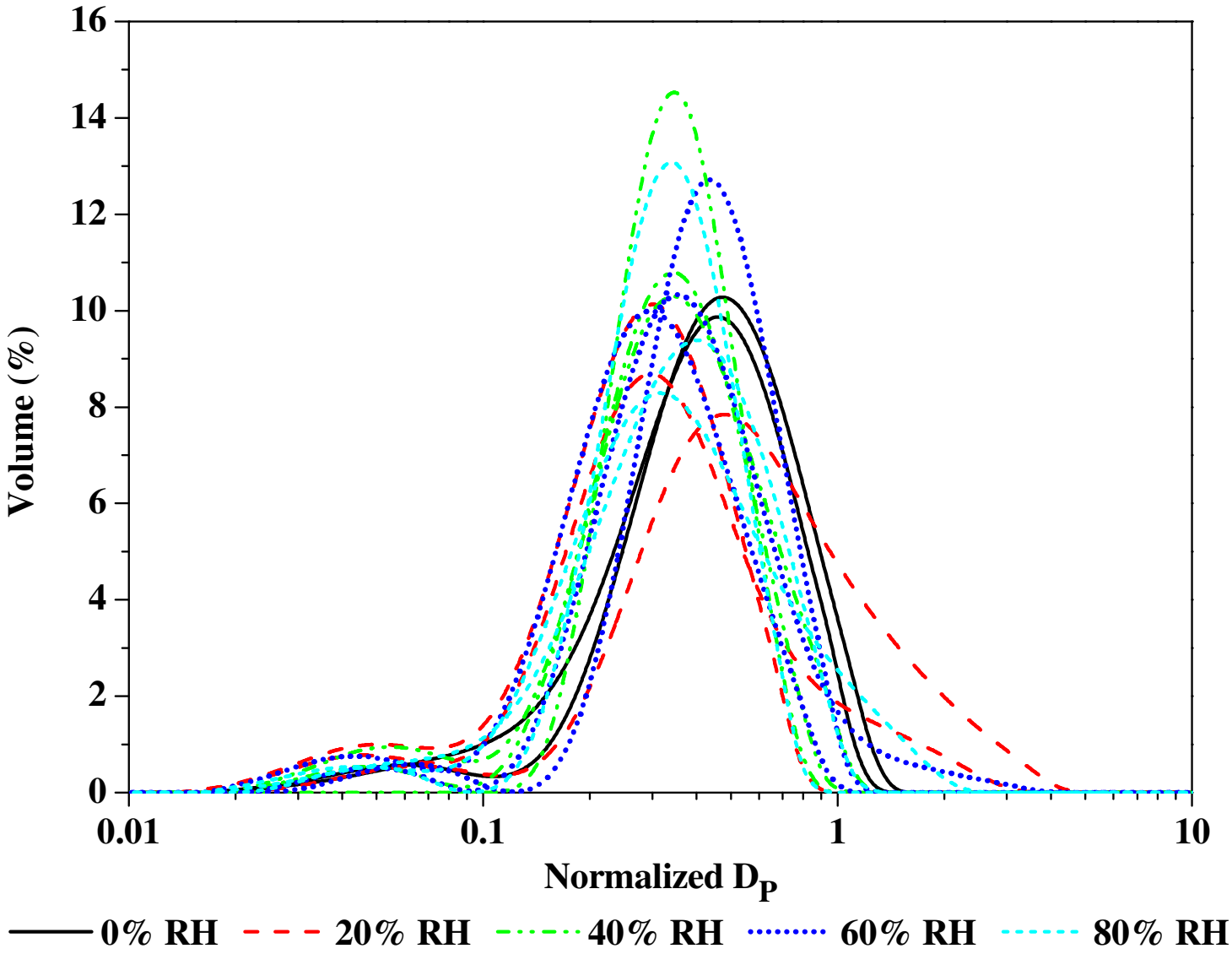

Figure C - 15: Normalized PSD at 3.5 U_{mf} in the Bottom Column region for different relative humidity.

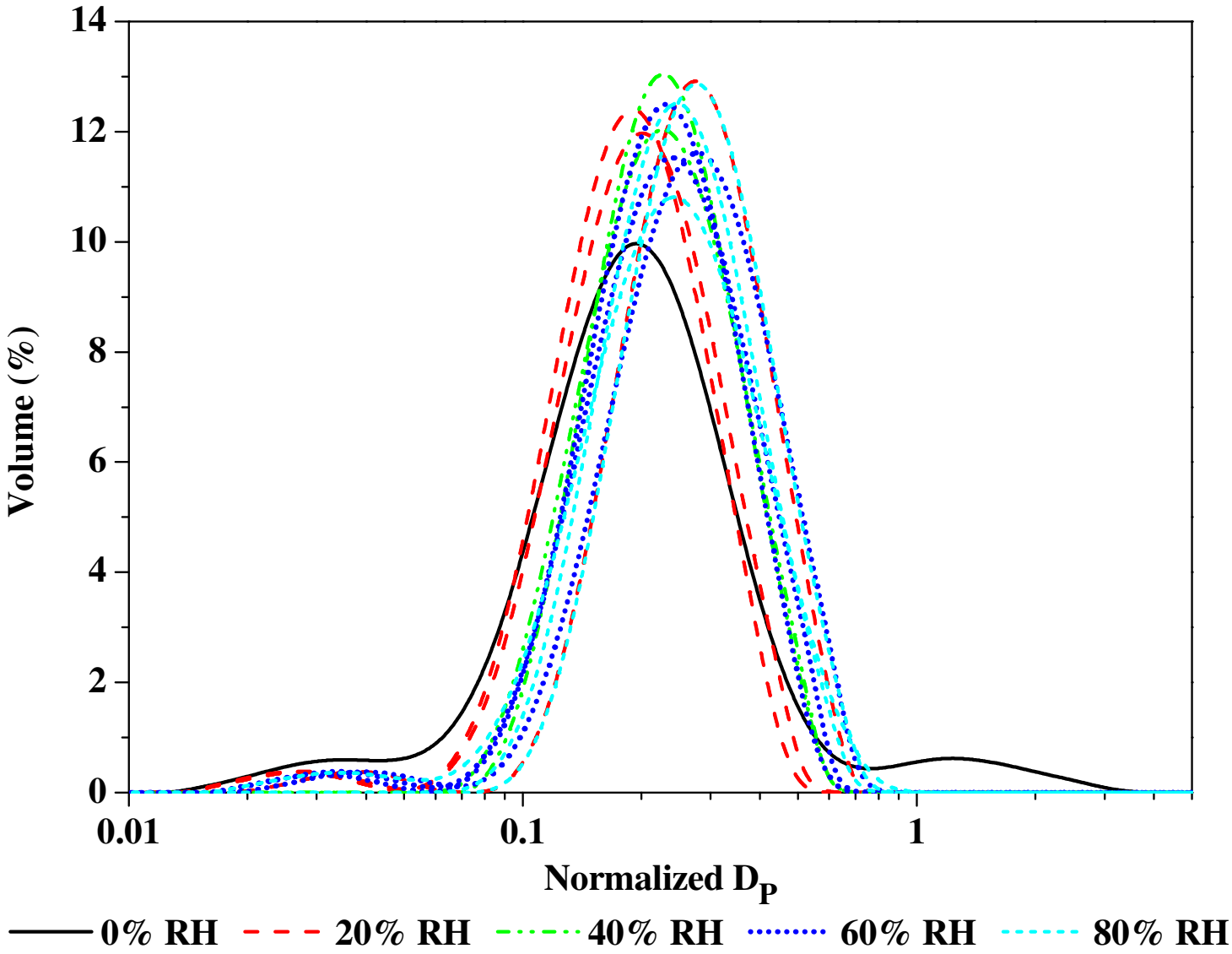

Figure C - 16: Normalized PSD at 3.5 U_{mf} in the Top Column region for different relative humidity.

Table C - 4: Normalized values for $D_{P\,0.1}$, $D_{P\,0.5}$, and $D_{P\,0.9}$ at 4 U_{mf} for all relative humidities.

Relative Humidity %	# of Runs	Initial $D_{P\,0.1}$ µm	Initial $D_{P\,0.5}$ µm	Initial $D_{P\,0.9}$ µm	Fines $D_{P\,0.1}$ µm	Fines $D_{P\,0.5}$ µm	Fines $D_{P\,0.9}$ µm
0	5	0.48 ± 0.01	1.00 ± 0.00	1.95 ± 0.04	0.11 ± 0.01	0.24 ± 0.02	0.41 ± 0.04
20	3	0.45 ± 0.01	1.00 ± 0.00	2.04 ± 0.01	0.11 ± 0.02	0.25 ± 0.03	0.44 ± 0.07
40	3	0.48 ± 0.00	1.00 ± 0.00	2.03 ± 0.07	0.11 ± 0.02	0.24 ± 0.03	0.41 ± 0.04
60	3	0.46 ± 0.04	1.00 ± 0.00	2.02 ± 0.06	0.12 ± 0.01	0.25 ± 0.01	0.45 ± 0.02
80	3	0.44 ± 0.03	1.00 ± 0.00	1.99 ± 0.06	0.11 ± 0.02	0.24 ± 0.06	0.67 ± 0.54

Relative Humidity %	# of Runs	Dropped $D_{P\,0.1}$ µm	Dropped $D_{P\,0.5}$ µm	Dropped $D_{P\,0.9}$ µm	Wall $D_{P\,0.1}$ µm	Wall $D_{P\,0.5}$ µm	Wall $D_{P\,0.9}$ µm
0	5	0.51 ± 0.04	1.00 ± 0.10	1.94 ± 0.22	0.38 ± 0.03	0.62 ± 0.08	0.99 ± 0.15
20	3	0.53 ± 0.04	1.02 ± 0.05	2.03 ± 0.07	0.34 ± 0.06	0.63 ± 0.10	1.08 ± 0.16
40	3	0.53 ± 0.04	1.08 ± 0.07	2.17 ± 0.19	0.42 ± 0.11	0.74 ± 0.16	1.24 ± 0.27
60	3	0.51 ± 0.05	1.01 ± 0.10	2.00 ± 0.21	0.37 ± 0.05	0.59 ± 0.05	0.95 ± 0.08
80	3	0.46 ± 0.08	0.94 ± 0.13	1.95 ± 0.22	0.30 ± 0.05	0.52 ± 0.09	0.87 ± 0.15

Relative Humidity %	# of Runs	Bottom Column $D_{P\,0.1}$ µm	Bottom Column $D_{P\,0.5}$ µm	Bottom Column $D_{P\,0.9}$ µm	Top Column $D_{P\,0.1}$ µm	Top Column $D_{P\,0.5}$ µm	Top Column $D_{P\,0.9}$ µm
0	5	0.22 ± 0.03	0.50 ± 0.07	0.96 ± 0.21	0.13 ± 0.02	0.24 ± 0.03	0.43 ± 0.04
20	3	0.19 ± 0.02	0.45 ± 0.07	0.94 ± 0.30	0.15 ± 0.02	0.26 ± 0.04	0.43 ± 0.06
40	3	0.20 ± 0.05	0.43 ± 0.11	0.84 ± 0.26	0.16 ± 0.02	0.28 ± 0.04	0.46 ± 0.08
60	3	0.19 ± 0.03	0.38 ± 0.04	0.67 ± 0.05	0.32 ± 0.02	0.58 ± 0.03	1.00 ± 0.04
80	3	0.16 ± 0.01	0.40 ± 0.05	0.82 ± 0.16	0.14 ± 0.02	0.25 ± 0.05	0.43 ± 0.09

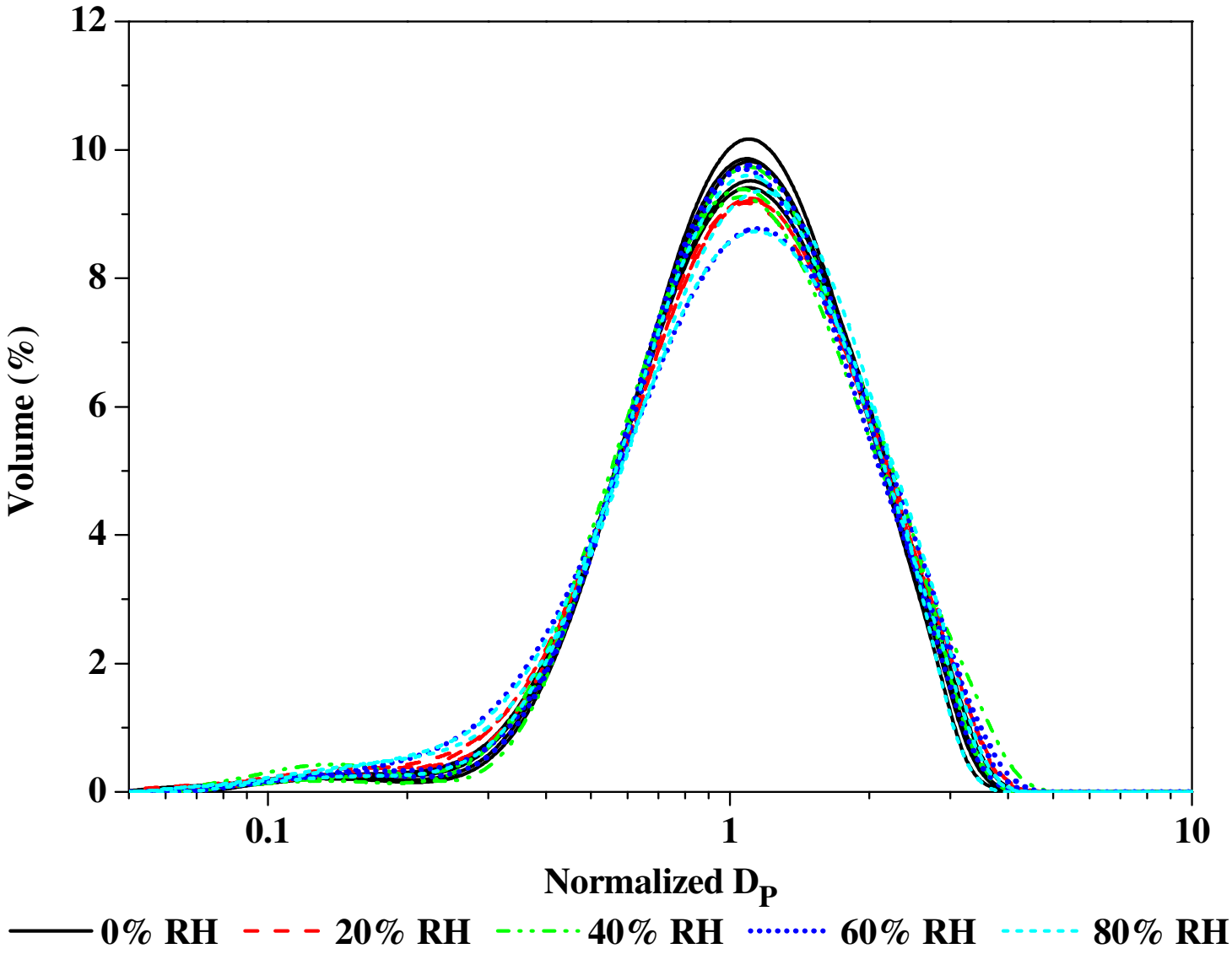

Figure C - 17: Normalized PSD at 4 U_{mf} in the Initial region for different relative humidity.

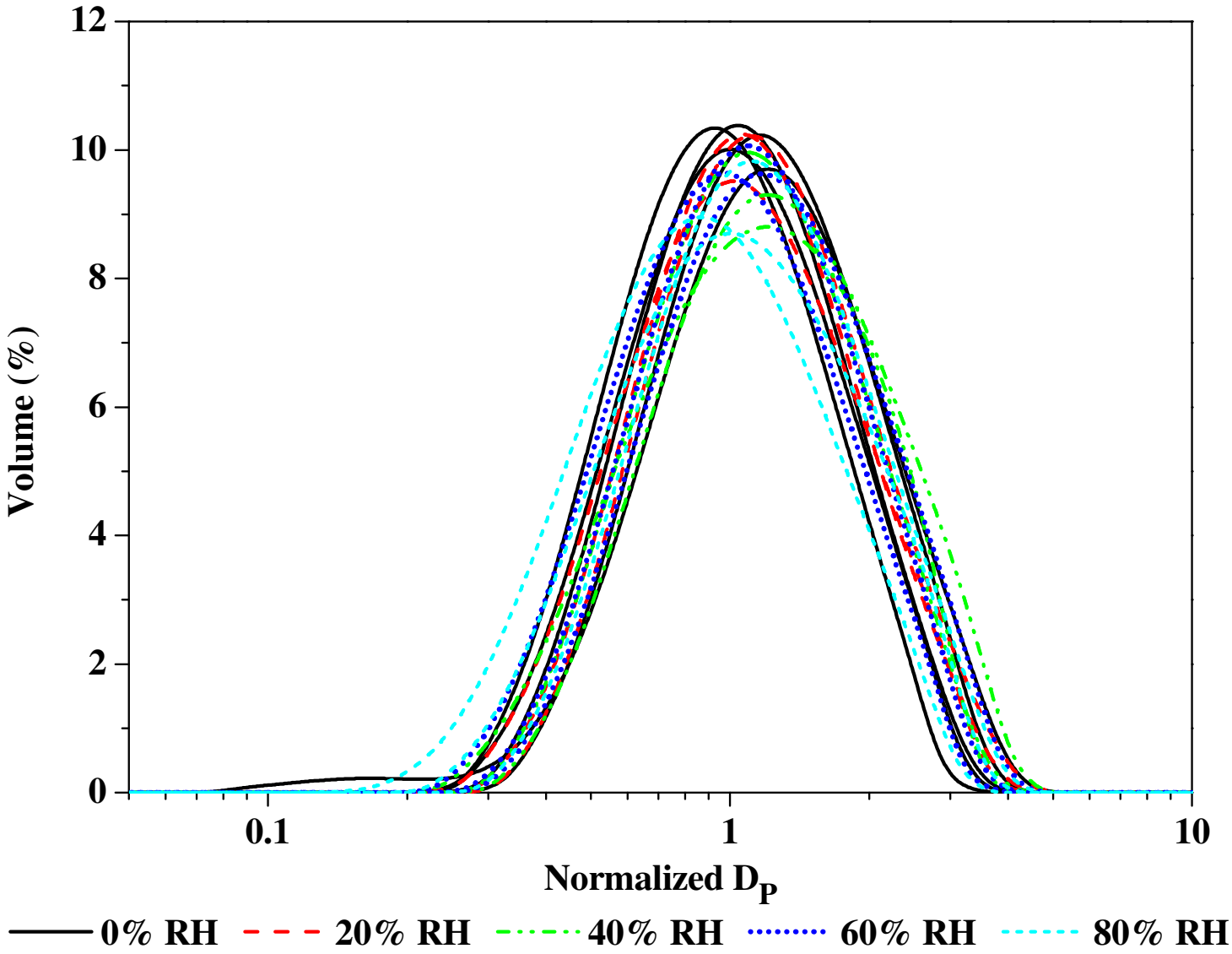

Figure C - 18: Normalized PSD at 4 U_{mf} in the Dropped region for different relative humidity.

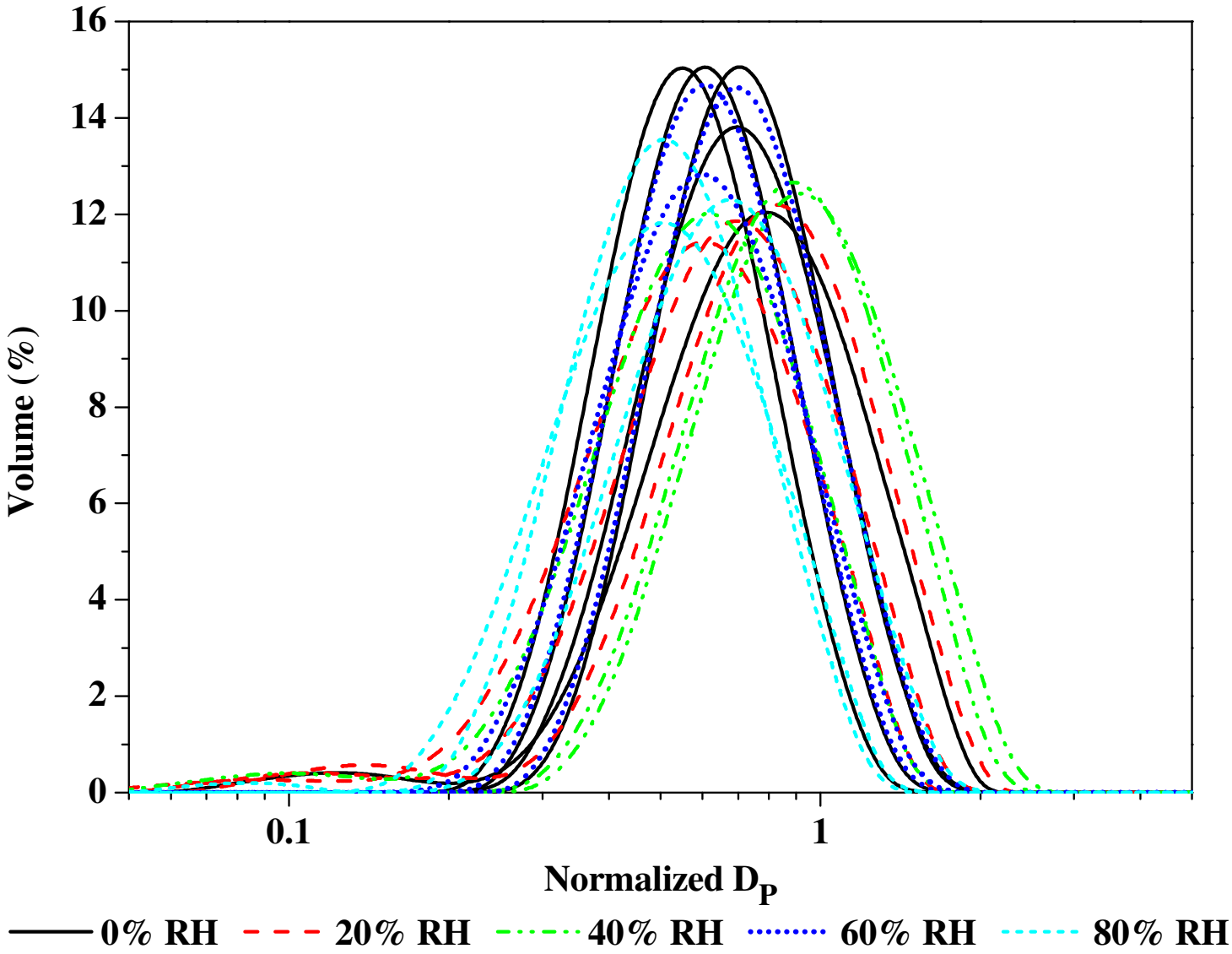

Figure C - 19: Normalized PSD at 4 U_{mf} in the Wall region for different relative humidity.

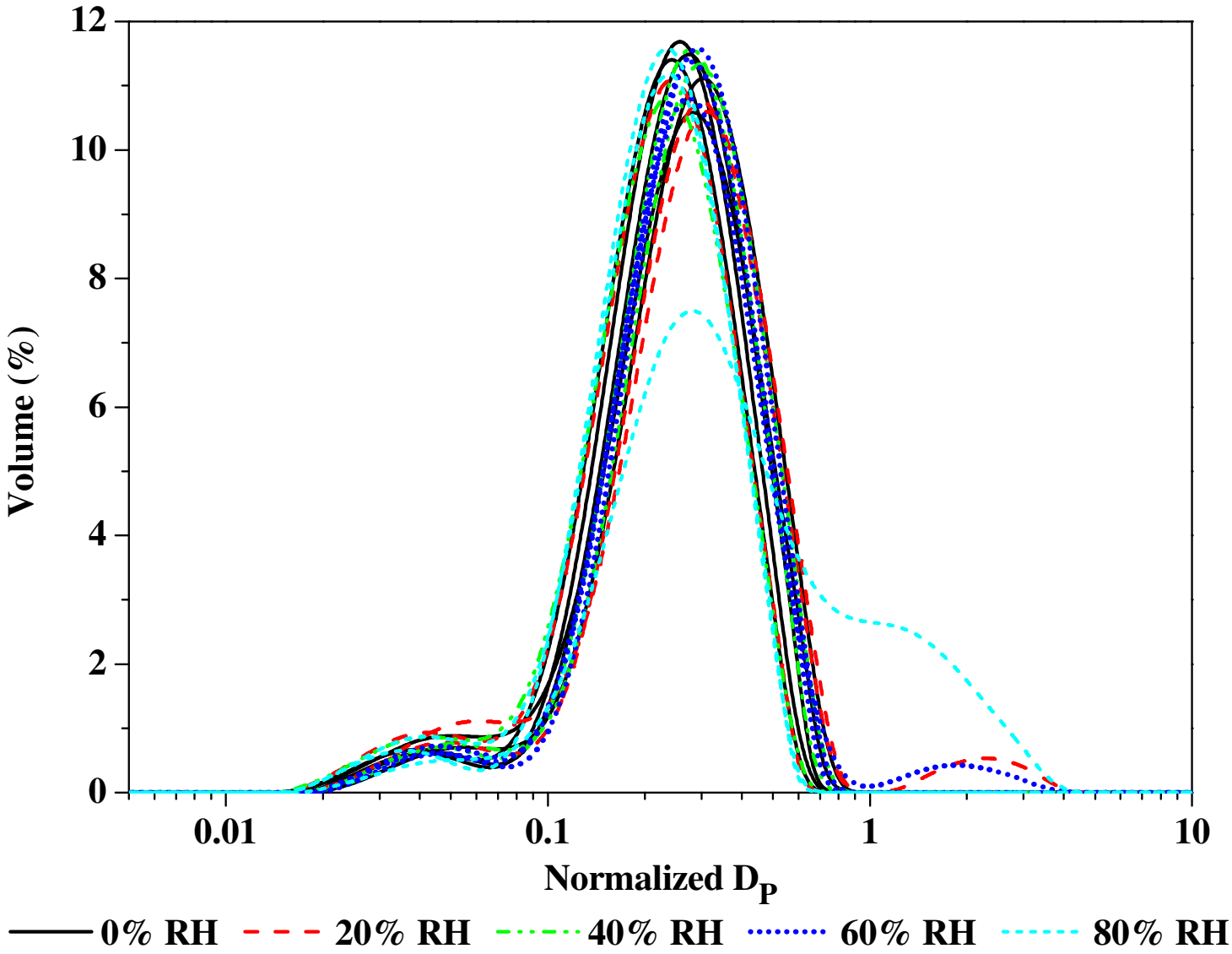

Figure C - 20: Normalized PSD at 4 U_{mf} in the Fines region for different relative humidity.

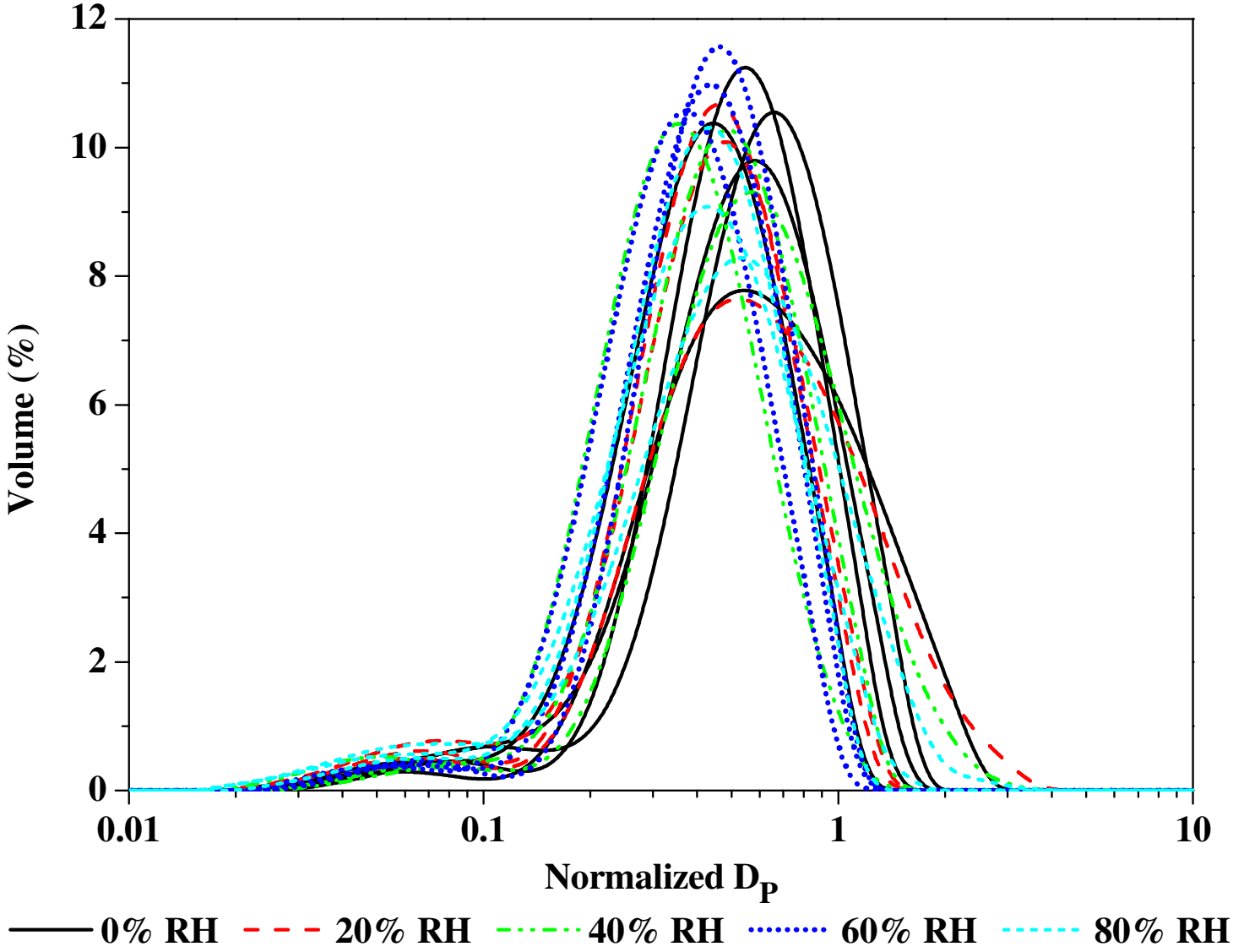

Figure C - 21: Normalized PSD at 4 U_{mf} in the Bottom Column region for different relative humidity.

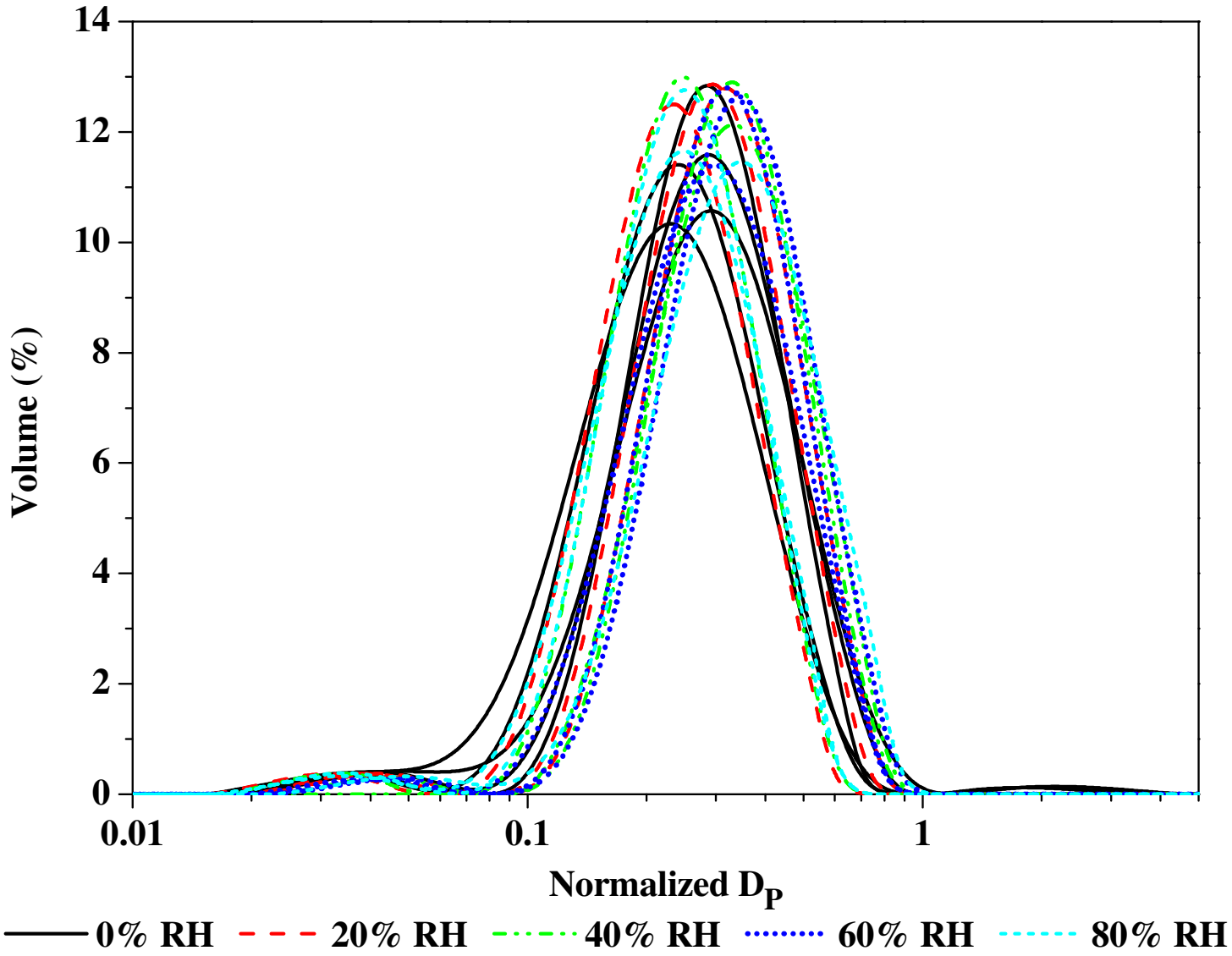

Figure C - 22: Normalized PSD at 4 U_{mf} in the Top Column region for different relative humidity.